DISSERTATION

DEVELOPMENT OF A MICROCHIP ELECTROPHORESIS SYSTEM FOR ONLINE MONITORING OF ATMOSPHERIC AEROSOL COMPOSITION

Submitted by

Scott D. Noblitt

Department of Chemistry

In partial fulfillment of the requirements

For the Degree of Doctor of Philosophy

Colorado State University

Fort Collins, Colorado

Spring 2011

Doctoral Committee:

Advisor: Charles S. Henry

C. Michael Elliott
Steven H. Strauss
Dawn Rickey
Jeffrey L. Collett, Jr.

ABSTRACT

DEVELOPMENT OF A MICROCHIP ELECTROPHORESIS SYSTEM FOR ONLINE MONITORING OF ATMOSPHERIC AEROSOL COMPOSITION

Atmospheric aerosols are solid or liquid particles that remain suspended in the environment for an extended time because of their size. Due to their high number concentration, low mass concentration, unique size range, and high temporal and spatial variability, atmospheric aerosols represent a significant unknown in both environmental impact and human health. Despite the importance of aerosols, current instrumentation for monitoring their chemical composition is often limited by poor temporal resolution, inadequate detection limits, lack of chemical speciation, and/or high cost. To help address these shortcomings, microchip electrophoresis (MCE) has been introduced for the semi-continuous monitoring of water-soluble aerosol composition. The MCE instrument was coupled to a water condensation particle collector (growth tube), and the integrated system is termed Aerosol Chip Electrophoresis (ACE). ACE is capable of measuring particle composition with temporal resolution of 1 min and detection limits of ~100 ng m^{-3}. This dissertation covers the development process of the prototype ACE instrument, including the novel separation chemistry, necessary modifications to traditional microfluidic devices, and the interface between the growth tube and the microchip.

ACKNOWLEDGEMENTS

The research described in this dissertation was funded from a variety of sources. The author was funded in 2009 and 2010 under STAR Research Assistance Agreement No. F08B10308 awarded by the U.S. Environmental Protection Agency. This work has not been formally reviewed by the EPA. The views expressed in this document are solely those of the author, and EPA does not endorse any products or commercial services mentioned in this publication. The research was also funded through U.S. Department of Energy STTR Phase II Grant No. DE-FG02-04ER-86179, U.S. National Science Foundation Grant No. ATM-0737201, and U.S. Environmental Protection Agency SBIR Phase II Project EP-D-05-058.

The research shown in this dissertation would not have been possible without the contributions of many individuals who otherwise would not get credit for their contributions. These individuals and brief descriptions of their contributions are given here.

Aerosol Dynamics, Inc. (ADI): The employees at ADI developed the growth tube aerosol collection system used in this work for coupling to the microchip. There were several contributors to the growth tube work. Most of the work was performed by Susanne Hering, followed by Greg Lewis. Alex Teng and Steven Spielman also contributed to the growth tube development. Also, Armond Gauthier helped with improving the LabView virtual instrument I developed to control and collect data with the ACE system.

Jeffrey Collett Lab: Several individuals in the Jeffrey Collett lab in the Atmospheric Science department at Colorado State University aided with my research. In particular, professor Collett himself was a valuable aid in nearly every aerosol-related issue I addressed. Ashley R. Evanoski, a student, helped to do initial testing of some of the modifications made to the ACE prototype after its publication. Other contributors from the lab include Lynn R. Mazzoleni, Jennifer Cox, Florian M. Schwandner, Amy P. Sullivan, Taehyoung Lee, Stephen Holcomb, and Yan Liu.

Charles Henry Lab: I performed the majority of my work in the Charles Henry lab and some members of this lab contributed to my work. Specifically, Jaimie M. VanBuren and James R. Kraly contributed to development of the inclusion of membranes into microfluidic devices. Rachel M. Speights performed most of the experiments for measuring binding constants between protonated diamine moieties and anions (this work is still in progress so the data is not given in this dissertation). Brian M. Murphy and Ryan E. Holcomb also provided useful insight and discussion on a variety of topics throughout the course of my graduate work.

My advisor, Charles S. Henry, deserved special acknowledgement for his contribution to my graduate research. He guided my research throughout the entire process and was given the difficult task of determining when to have a hands-on approach and when to stay hands-off. I think we both have learned a great deal throughout the process.

Finally, I want to acknowledge my wife Jennifer Noblitt for all her love and support throughout my time as a graduate student. She's had to listen to a lot from me, both complaints and excitement.

The majority of the material presented in this dissertation were collected and analyzed by me. However, some of the samples and data were collected by other individuals, and help from other people was sometimes obtained in the method development. Specific contributions are listed below, organized by chapter.

Chapter 2: Lynn R. Mazzoleni collected the aerosol samples. She also performed some initial testing on the background electrolyte surfactant concentration.

Chapter 3: Jamie M. VanBuren helped with initial method development for the membrane inclusion process. James R. Kraly collected, analyzed, and formatted the data for Figures 3.6 and 3.8.

Chapter 5: Florian M. Schwandner collected the filter samples and analyzed them with ion chromatography.

Chapter 6: Most of the growth tube development was performed by Susanne V. Hering and Gregory S. Lewis of ADI. Greg Lewis also prepared Figure 6.1. Alex Teng (ADI) collected the data for Figure 6.5. The PILS-IC data shown in Figure 6.13 was collected by Yan Liu, and Taehyoung Lee assisted in analyzing the PILS-IC data.

Chapter 8: The PILS-IC data shown in Figure 8.1 was collected and analyzed by Kaitlyn Suski (University of California, San Diego, UCSD) with help from Amy P. Sullivan. The data shown in Figure 8.3 was collected on a microchip constructed by Ashley R. Evanoski. The data shown in Figure 8.5 was collected with the aid of Gregory C. Roberts. The prototype detectors tested in chapter 8 were developed in conjunction with Allen White and George Kassabian (UCSD).

TABLE OF CONTENTS

CHAPTER 1. DEVELOPMENT OF AEROSOL CHIP ELECTROPHORESIS, A NEW TECHNIQUE FOR ONLINE MONITORING OF ATMOSPHERIC AEROSOL CHEMICAL COMPOSITION: AN INTRODUCTION

Atmospheric aerosols are small particles that remain suspended in the environment because of their small size. Typically the size range of aerosols is defined as between about 1 nm and 100 μm in diameter.[1] Smaller particles approach the size of single molecules, and larger particles rapidly settle. Aerosols come from a variety of sources and can be solid, liquid, or a mixture of the two. Due to their ubiquity, size range, high spatial and temporal variability, and/or large surface area, aerosols play important roles in both human health and the environment. Although some effects of size on aerosol behavior have been elucidated, the role of chemistry in aerosol functionality is less understood. The small total mass of aerosols coupled with their high compositional diversity and instability of some constituents makes measuring aerosol chemistry challenging. Current techniques for measuring aerosol composition include a variety of online and offline methods. However, current approaches can be limited by sampling artifacts, insufficient time resolution, inadequate detection limits, high cost, low portability, and the inability to distinguish specific chemical components. To address these issues, my research has focused on developing an online aerosol-monitoring instrument utilizing microchip electrophoresis for chemical speciation.

AEROSOL ORIGINS, SIGNIFICANCE, AND CHARACTERISTICS

Atmospheric aerosols originate from a wide range of sources and can undergo many reaction processes, contributing to their high variability and diversity.[2] General classes of aerosol sources include biogenic sources such as natural plant and animal processes, anthropogenic sources such as manmade combustion, and geogenic sources including volcanism and sea spray. Primary aerosols are those emitted directly into the atmosphere in particulate form, while secondary aerosols form in the atmosphere from physical or chemical reactions such as condensation or oxidation reactions that form larger or more polar molecules. Whether primary or secondary, the aerosol components themselves undergo further reactions, termed aging, and these reactions change the size, morphology, and/or chemical composition of the aerosol. The large surface area of aerosols can allow them to promote or catalyze reactions, and it also makes aerosols act as condensational nuclei. The combination of so many sources, initial compositions, oxidation reactions, available reactants, and morphology results in a chemical mixture with many different classes of species. Some of those species will be discussed here, but this is not an exhaustive list. Three broad classifications of the aerosol constituents are elemental carbon, inorganic species, and organic carbon. Note that although water is often a primary component of aerosols, it is not considered here because water content is often dictated by the size of the aerosol, its chemical composition, the ambient temperature, and the relative humidity. Elemental carbon is primarily emitted as primary aerosol during incomplete combustion processes. It is insoluble in practically all solvents and is often synonymous with soot, black carbon, and graphite.[3] Inorganic species include inorganic cations and anions, zero valent metals and alloys, and heavy metal ions and

salts. Typically, the mass fraction contributed by heavy metals is small. However, this portion can be important because of its catalytic ability and its usefulness to serve as tracer or marker species for specific aerosol sources. Also, metals such as iron, aluminum, and zinc can sometimes contribute significantly to the mass fraction of aerosols, particularly when they come from crustal sources.[3] The main components to the inorganic fraction are the salts of atmospheric acids and bases. Ammonia is the dominant gas phase base in the atmosphere (which is typically acidic) and acts as a neutralizing agent in the atmosphere, forming ammonium salts. Gas phase nitrogen oxides come from a variety of biogenic and anthropogenic sources and gas phase reactions and act as atmospheric acids, eventually forming nitrate salts in the particle phase. Finally, sulfuric acid, typically derived from sulfur dioxide in the gas phase, forms sulfate salts with ammonium or other cations. Combined, ammonium, nitrate, and sulfate represent a significant portion of the water-soluble aerosol mass, often reaching 50% or higher of the water-soluble mass fraction.[1] Other inorganic ions, including chloride, nitrite, phosphate, sodium, potassium, calcium, and magnesium are also prevalent in aerosols and can indicate specific origins. For instance, chloride originates from sea salt and potassium is a marker for biomass burning.

The final broad category of aerosol composition is the organic carbon fraction, which can be split into water-insoluble species and water-soluble organic carbon (termed WSOC). The insoluble fraction contains both aliphatic and aromatic species. Because the insoluble organics have few or no polar functional groups, the compounds in aerosols are typically larger molecules that avoid volatilization to the gas phase. These species come

from a variety of sources, and some individual components can be used as tracers for source apportionment. The water-soluble organic fraction is also of interest. Because these species are more polar than those in the insoluble fraction, they are often found in secondary aerosols or older primary aerosols that have undergone considerable oxidation. Representative molecules include alcohols, aldehydes, ketones, carboxylic acids, and carbohydrates.[4] Transient or intermediate species such as organonitrates and organosulfates have also been observed.[5-7] Carbohydrates are often produced via biomass burning, and the molecule levoglucosan is particularly important as a marker for biomass burning source apportionment.[8] Organic acids (carboxylates) typically comprise a much smaller fraction of the total aerosol than the inorganic acids sulfate and nitrate.[9] However, their acidic functionalities can still contribute significantly to the acidity of the aerosol, making them important in pH-dependent reactions in secondary aerosol. Recently, organic amines have drawn some interest as well because their presence has been detected in aerosols and they represent additional basic functionality in the atmosphere beyond ammonia.[10-12] Unlike organic acids, which are less acidic than the inorganic acids and therefore won't contribute additional acidity in highly acidic aerosols, organic amines are often more basic than ammonia, which may be important in environments with neutral or basic aerosols. It should be noted no aerosol classification scheme is completely objective or unambiguous, as there are always species that do not fit into a category or overlap multiple categories. For example, bioaerosols do not fit into one of the aforementioned divisions. Proteins might loosely be considered WSOC, but their behavior is quite different than most water-soluble organics. Larger bioaerosols such as viruses and bacteria have unique characteristics. Some small molecules overlap

multiple classifications. As an example, oxalate is often considered WSOC in the aerosol community because the mechanisms for its formation are similar to other soluble organics. However, it could be argued that its chemical characteristics are more similar to inorganic anions because of its low pKa and higher diffusion constants. Additionally, its metal binding properties give it some characteristics of neither group. The behavior of many species also depends on the other compounds present. For example, if considerable barium ion were present in an aerosol, the sulfate in that aerosol would not be soluble because it would be in the form of barium sulfate. This matrix effect would also likely lead to an inaccurate report of the sulfate content in the aerosol because most techniques only measure soluble sulfate. In summary, the large number of compounds present, their diversity, and matrix effects make aerosol composition very complex. This complexity increases the difficulty in making compositional measurements and in attributing health and environmental effects to specific aerosol chemistry.

Better understanding of aerosol chemistry is needed because of the potential implications of aerosol composition on human health.[1,13-16] Aerosols represent a unique health risk because they cover the size range that allows them to penetrate into the human lung, whereas both smaller and larger species are removed prior to entering the lung. Entering the lung potentially allows access to the bloodstream across the blood-air barrier. Also, aerosols present a large surface area that can induce or catalyze potentially harmful reactions. Mortality is the most studied and most serious health effect due to aerosol exposure,[15] and it obtained considerable focus after the London smog episode of 1952. Cardiovascular mortality, in particular, strongly correlates to aerosol exposure, typically

measured as total aerosol mass below a given size cutpoint (for instance, PM_{10} is the total particulate matter with an aerodynamic diameter below 10 μm).[17] More important than the total mass, however, is the size of the aerosol particles being breathed, as this determines the deposition region in the body. Inertial behavior dominates larger particles, leading to deposition in the upper airways. Very small particles also preferentially deposit in the upper airways due to their higher diffusion constants. Thus, particles between 3 and 100 nm in diameter have the highest probability of reaching alveoli in the lungs.[18] For instance, deposition modeling indicates that up to 90% of the mass fraction of inhaled $PM_{0.1}$ deposits in the human respiratory tract, with about 50% of that in the alveolar region.[18] The aerosol size also affects toxicity, and ultrafine particles (< 100 nm) have been shown to cause more inflammation than equivalent masses of larger particles,[19] which may be due to easier penetration into cells.[20] While aerosol size dictates the deposition fraction and location and also affects toxicity, the shape of the aerosol is also a major factor in toxicity. The best example of the shape dependence on toxicity comes from carbon nanotubes and their comparison to asbestos fibers.[18] However, toxicity dependence on shape is not well understood. Similarly, the impact of aerosol composition on the toxicity is also unclear. Aerosols with reactive surface chemistry have been shown to be more toxic than those with inert surface chemistry, but studies on specific chemistries are not common.

Atmospheric aerosols also have a significant impact on the environment, particularly in their effect on climate through direct and indirect radiative forcing.[1,21] The direct effect includes radiation absorption and scattering. Absorption leads to localized heating,

whereas scatter reduces the amount of radiation reaching the surface, resulting in net cooling. Indirect effects include the ability of aerosols to act as cloud condensation nuclei (CCN) and ice nuclei (IN).[22] The absorption, scatter, and nuclei characteristics of aerosols are governed by particle size, structure, and chemistry.[23] However, because many of the factors governing the particle size and structure, including hygroscopicity, partitioning coefficients, and growth rates, are determined by chemical composition, the chemistry of the primary aerosol and its surrounding environment play a central role in the net effects of aerosols in climate. Overall, aerosols exhibit a net cooling effect on the earth's climate, but the magnitude of this effect and even its sign are dependent upon the chemistry of the aerosol.[1,22] In addition to its climatological impact, aerosols are related to other environmental phenomena. One example is that of acid deposition, which includes the more specific and well-known acid rain.

ANALYTICAL CHEMISTRY OF AEROSOLS

Although the demand for improved chemical analysis of aerosols is high in the areas of environmental monitoring and human health, the same characteristics of aerosols that make them of interest in these areas also make them a daunting analytical challenge. These aspects include their small size, high diversity, low accumulated mass, spatial and temporal variability, and the high reactivity or volatility of some species. As an example, a typical urban aerosol might contain 50 000 particles cm^{-3} with a mass of 30 $\mu g\ m^{-3}$. This implies an average aerosol mass of 600 ag, for an average aerosol diameter of 41 nm (assuming a particle specific gravity of 1.7, similar to the value for ammonium sulfate). In reality, the size distribution is not uniform, so most of the aerosol mass is present in

the larger particles, most of the aerosol number is in the smaller particles, and the average numbers given above are at best approximate. However, they make clear the difficulty in performing chemical measurement on aerosols. If half of the aerosol mass is fully neutralized ammonium, sulfate, and nitrate, and the two anions were present in equal molar levels, these species would be present at levels of 3.8, 4.4, and 6.8 μg m^{-3}, respectively. For 5 min of air sampling at the standard rate of 16.7 L min^{-1}, respective masses of 320, 370, and 570 ng would be collected. Though handling of these masses can be difficult, the quantities are relatively easy to measure with modern instrumentation (i.e., concentrations of 6-18 μM if dissolved in 1 mL of solution), although achieving this level of time resolution while avoiding significant sampling artifacts is not as straightforward. If the remainder of the aerosol were equally composed of elemental and organic carbon, then the organic carbon fraction would represent 7.5 μg m^{-3}, representing thousands of different compounds. Even the most prevalent of those species would be present in only a fraction of the mass of the inorganic ions, and unambiguous detection of individual components represents a daunting task. Thus, this example (which represents a heavily polluted environment) clearly illustrates the need for instrumentation that is capable of multicomponent compositional monitoring with high time resolution and the ability to handle small masses in the form of microscopic particulate matter.

Over the past several decades, great strides have been made in the development of instrumentation for monitoring aerosol composition.[24] The traditional approach to analyzing atmospheric aerosols has been to collect them using filtering or inertial impaction methods. The aerosols can then be measured offline using standard chemical

instrumentation with little or no adaptation. More recently, the advent of online instruments that permit semi-continuous and real-time data acquisition has revolutionized the field. These instruments can be split into two categories, those that measure the composition of an ensemble of aerosols, acquiring bulk speciation data, and those that measure the composition of individual aerosol particles and are capable of obtaining mixing state information.

Offline monitoring methods are the traditional technique for monitoring aerosol composition and are still in wide use today. Collection methods include filters, inertial impaction, and diffusion methods. After collection, aerosols can be directly analyzed from the surface through a variety of techniques. Some of these are spectroscopic techniques such as infrared reflectance and scanning electron microscopy. Thermal gravimetric analysis can also be used to obtain bulk composition information. However, the majority of offline methods do not analyze the directly deposited aerosols; instead, the aerosols are extracted into solution and then analyzed. This approach prevents analysis of individual aerosol particle composition, adds a dilution step, and can cause unwanted side reactions to occur, but it allows for a host of additional analyses to be done. Solution phase analyses can be as simple as a pH measurement. A wide range of spectroscopic techniques can be used, including infrared absorbance, UV/Vis absorbance, fluorescence, and nuclear magnetic resonance (NMR) methods. Because of the large number of chemical species present in aerosols, separation methods are commonly employed and can provide much more information than is possible without a separation technique, particularly when mass spectrometric (MS) detection is employed. Typical

separation methods are gas chromatography (GC), liquid chromatography (LC), and capillary electrophoresis (CE). GC has the advantages of high peak capacity (up to 200 analytes analyzed in a single one-dimensional analysis), mature instrumentation, and little or no use of liquids (meaning that aerosol samples can be analyzed directly from a surface through volatilization without the need to prepare a solution). Its primary disadvantage is the requirement of volatile samples or sample compounds that can be derivatized to a volatile product. Its use of elevated temperatures precludes the analysis of unstable species. Because it employs compressed gas sources and oven, it has a large physical footprint that makes its use in the field difficult. LC provides several benefits over GC, primarily that it does not require volatile analytes or (usually) derivatization. Though the analyses are of similar length to those in GC (a few minutes to several hours), the peak capacity in LC is typically lower. Although LC avoids using large compressed gas sources, this benefit is a tradeoff because LC requires relatively large volumes of mobile phase (~1-2 mL min^{-1}). A major disadvantage to LC is its requirement of relatively large sample, which can be as high as 500 μL. One major subset of LC is ion chromatography (IC). IC has become a standard method for measuring the ionic composition of dissolved particulate matter, especially for the inorganic fraction but also for ionic WSOC. Its detection limits (< 10 nM is possible) are more than adequate for most of the inorganic aerosol fraction and are even acceptable for the organic ions. However, its relatively poor peak capacity severely limits its applicability in organic analysis. CE is a relatively new instrumental technique that exhibits intermediate peak capacity. It has several benefits, including small sample consumption and short analysis times. Because it consumes low reagent quantities and does not require pumps, it is

attractive for field deployment. However, CE's major drawbacks are its lack of concentration sensitivity and poor reproducibility. Concentration detection limits are often 1-2 orders of magnitude higher than those of LC, although CE's mass detection limits are often better than LC's because of its very small injection volumes. CE's irreproducibilities are both qualitative and quantitative. Qualitatively, peak migration times can shift due to poor stability of the capillary surface, and quantitative irreproducibilities are caused by both the capillary surface and poor control over injection volumes. Specifically, difficulties with capillary surface stability include changes to the protonation state of the surface due to operation at non-equilibrium conditions,[25] accumulation of macromolecules from the sample through nonspecific binding,[26] and changes in the charge state of the surface from trace metal ion contamination in the background electrolyte (BGE).[27] Thus, CE is promising for the speciation of organics in aerosols because of its fast analysis times and high peak capacity, but its poor concentration sensitivity and reproducibility keep it from being embraced as the primary instrumental method for the analysis of WSOC.

Despite the maturity and success of offline aerosol analyses, they still possess several drawbacks. One of these is the lack of real-time feedback. Often, optimal sampling intervals require approximate knowledge of the aerosol composition being sampled. With offline methods, this is limited to educated guessing. With real-time feedback, improved results can be attained via appropriate sampling frequency. Another major drawback of offline sampling is its susceptibility to artifacts.[28] For example, particles collected on a filter can undergo reactions that do not occur when suspended and

dispersed in the atmosphere, yielding compounds that otherwise would not be present. Gas phase species passing through the filter can also react with or condense on the aerosols, although some of these reactions can be avoided by flowing the air through a denuder prior to filter collection. The opposite behavior, volatilization of the collected aerosols, can also be problematic. Many of these artifacts increase in severity with increasing collection time; consequently, the demand for online monitoring systems has increased, as these systems will not suffer from many of the described artifacts.

The recent development of online systems for monitoring aerosol composition has permitted the collection of new information that was impossible to obtain with offline methods.[29] Early online systems did not utilize separation techniques and measured one selected component in the bulk aerosol. Huntzicker et al. produced one of the earliest of these devices, which measured sulfate in aerosols via flame photometry.[30] Stolzenburg and Hering developed a nitrate-specific online system that worked by flash vaporization and chemiluminescent detection and was capable of unattended operation for days.[31] The instrument exhibited a detection limit of 0.4 μg m^{-3}, and a similar instrument was developed for sulfate using a SO_2 pulsed fluorescence analyzer. However, multianalyte monitoring is crucial for many analyses. One approach to monitoring multiple aerosol components simultaneously with a single instrument is via single particle mass spectrometry.[32,33] Separate instruments have been developed for this purpose, specifically the Aerosol Mass Spectrometer (AMS)[34,35] and the Aerosol Time of Flight Mass Spectrometer (ATOFMS).[36-38] The AMS has the ability to monitor particle size, bulk composition, and individual particle composition. Measuring the composition of

individual particles allows determination of the mixing state of the aerosol particles, which is impossible to do with bulk composition methods. Additionally, because the aerosols are not placed in solution, the possibility of one source of unwanted side reactions is eliminated. Reported detection limits for the AMS with 10 min sampling are in the 0.01-0.09 μg m^{-3} range for inorganic anions, 0.11-0.49 μg m^{-3} for ammonium, and 0.15-0.73 μg m^{-3} for organics.[35] However, the quantitative capability of the AMS is limited due to variable ionization efficiencies, and calibration versus another instrument is often needed. Without frequent calibration against another instrument, accuracy to within 25% can be expected.[35] However, even with calibration, quantitative errors can still occur due to differences in ionization efficiency between different forms of the same species (i.e. sulfuric acid versus ammonium sulfate). Additionally, the ability of AMS systems to quantify specific species is limited to only a few compounds that have unique mass-to-charge ratios, such as inorganic ions. Consequently, quantification and even identification of individual organic compounds is difficult or impossible with the exception of some notable compounds such as poly-aromatic hydrocarbons (PAHs).[39] Another drawback to the AMS is its large physical footprint, which can make transport difficult and space requirements in the field high. Perhaps the biggest disadvantage of the AMS is its high cost, which is at least 5-10 times higher than most aerosol bulk composition analysis instrumentation. The ATOFMS systems spearheaded by the Prather research group are another class of mass spectrometric instruments.[36-38] These instruments have focused on single particle monitoring, providing qualitative aerosol composition and mixing state information. However, quantitative data from the ATOFMS is limited and requires input data from at least one other instrument and/or

multivariate analysis.[40-42] The ATOFMS possesses an even larger physical footprint than the AMS system and also has larger power requirements and produces more heat, complicating field deployment. In contrast to mass spectrometric instruments, other online speciation methods are limited to bulk measurements of aerosol composition. One recently developed instrument is the Thermal desorption Aerosol Gas chromatograph (TAG).[43] This instrument works by coupling traditional GC-MS (or GC-FID) instrumentation to an in situ aerosol collector via thermal desorption. TAG is limited to volatile compounds of low polarity, provides one-hour time resolution, and is capable of quantitation.[44] A two-dimensional version of TAG has also been developed for increased peak capacity.[45] Perhaps the most common approach to online aerosol collection is to condense a solvent, typically water, on sampled aerosols, increasing their mass, and then inertially impact them into a solution stream or reservoir. Once dissolved, the aerosols can be analyzed with any of a variety of methods, including spectroscopy, electrochemistry, and separation methods. Note that this approach requires the aerosol components of interest to be soluble in the chosen solvent. Also, to avoid contamination from gas phase species partitioning into the solution, the sampled air stream needs to be passed through denuders before the condensational step. Simon and Dasgupta pioneered the condensational approach for aerosol collection in online monitoring of aerosol composition measurement.[46] Their system, the steam collector, sampled air at 10 L min^{-1} and deposited the enlarged particles onto a wetted wall parallel plate diffusion denuder. The sampled aerosol was then chemically analyzed using IC, and detection limits of 0.6-5.1 ng m^{-3} were achieved for inorganic anions with 8 min time resolution. This general collection approach has been utilized by other researchers, and a large number of similar

instruments have been developed.[46-53] The most widespread of these instruments in the United States is the particle-into-liquid-sampler (PILS), which was developed by Weber and co-workers and has undergone several refinements since the original publication.[52,53] The PILS is frequently coupled to IC for chemical speciation, and the combined PILS-IC system is capable of analysis times as fast as 2.5 min with detection limits in the 1-300 ng m^{-3} range, with longer analysis time and higher detection limits for organic species.[53,54] However, the time resolution for all of the steam collection instruments is limited by the inherent speed of the separation and/or detection method. Additionally, the other limitations of LC/IC mentioned earlier apply for online instrumentation too, and the chromatography system is a major contributor to the cost of the coupled instrument. To work around this, some efforts have attempted to couple ion selective electrodes and UV/Vis absorbance detectors (with a liquid waveguide capillary cell and complexation chemistry) to the PILS.[55] However, these detection approaches are limited relative to separation approaches because each sensor can only monitor a single species. Accurate volume correction for dilution in the PILS requires an internal standard, so an additional sensor is needed for the non-separation detection methods.

The current status of instrumentation for aerosol composition monitoring indicates that offline methods suffer from improper or excessively long sampling intervals, systematic sampling artifacts, and/or excessive manual handling. Recently developed online instruments address many of these issues but have their own drawbacks, including high cost, large physical footprints, difficulty in maintaining extended operation, insufficient time resolution, large sample volume requirements, or sampling artifacts. One method

that can potentially alleviate many of these issues is CE. CE is a separation method that has the advantages of small sample consumption, relatively high peak capacity, operation without mechanical pumps, and fast analyses. As mentioned earlier, CE has been employed for the offline analysis of aerosols. Much of the original work with CE for aerosol compositional analysis was performed by Dabek-Zlotorzynska and coworkers, and they developed CE protocols for a wide variety of aerosol components, including inorganic anions,[56-58] inorganic cations,[59] heavy metals,[60,61] hydroxymethanesulfonic acid (HMSA),[62] and organic acids.[56,63-65] Other authors have developed methods for the analysis of inorganic species in aerosols,[66-71] although more focus has been given to organic acids.[69-77] Despite the effort put into these methods, they have not been broadly embraced because the majority of the separations employ indirect UV absorbance detection, which typically yields detection limits in the 1-10 μM range. While limits of detection (LOD) in this range are acceptable for most inorganic species, the majority of organic ions are present at levels 2-3 orders of magnitude below the dominant inorganic ions and will not be detected with these methods without long collection times. Consequently, while CE's high peak capacity is amenable to organic ion analysis, its detection limits are typically too high to make the CE methods useful, which is the opposite situation as that of IC. Valsecchi et al. utilized traditional CE instrumentation with a conductivity detector to obtain detection limits of 20-60 nM for inorganic anions in rainwater,[68] which is a significant improvement over methods with indirect UV detection. These LODs would be suitable for organic ions in aerosols, but conductivity detectors for CE have only been intermittently commercially available, and no traditional CE methods for organic ions in aerosols have been developed for use with conductivity

detectors. Additionally, the commercially available detectors employ contactless conductivity detection and are thus less sensitive than the detection approach used by Valsecchi. In terms of online analysis, coupling traditional CE instruments to an automated aerosol collector is not straightforward. However, several interfaces between CE and flowing liquid streams have been developed,[78-80] and presumably similar approaches could be employed to couple CE to an aerosol sampler such as the PILS. This approach has not been successfully pursued, in part because of the limitations of CE with regards to detection limits, extended and continuous operation, and reproducibility. Additionally, many of the benefits of traditional CE have been eclipsed by the success of MicroChip Electrophoresis (MCE).[81,82] MCE is part of the larger field of microfluidics, which promises small devices capable of fast and highly integrated analyses packaged in a "Micro Total Analysis System".[83-89] MCE and traditional CE share many of the same attributes but are distinct enough to often be reviewed separately.[90-93] MCE has several advantages over traditional CE, including smaller instrument footprint, lower reagent consumption, ability to analyze smaller sample volumes, facile coupling to pre- or post-separation treatments, lower energy consumption, and increased portability. However, MCE has its own share of drawbacks, many of which were covered in the review by Revermann et al.[93] These include poor reproducibility because of the less well understood capillary surface chemistry, difficulty in achieving reproducible injections because of the small volumes involved, increased joule heating due to lower heat transfer coefficients, and short operational times before BGE replenishment is required due to electrolysis and the small BGE volumes. Also, some detection methods, such as absorbance detection, are more difficult to integrate with MCE. Very little aerosol

analysis has been accomplished with MCE. Garcia et al. were the first to report an aerosol composition analysis method with MCE.[94] The method utilized MCE with pulsed amperometric detection to analyze levoglucosan and other carbohydrates from biomass combustion aerosols. Detection limits ranged from 17 μM for levoglucosan to 260 μM for galactosan, and the total analysis time was about 1.5 min. The only other reported MCE analysis of aerosols was by Liu et al. for nitrate and sulfate.[95] Detection limits were reported as 1 μM in a total analysis time of about 2 min. However, it should be noted that neither of these papers considered potential interfering compounds with similar migration times as the analytes. Also, accurate and reproducible quantitation in electrophoresis typically requires the use of internal standards to account for fluctuations in injection volume and/or capillary surface condition, and neither of these methods utilized internal standards. Thus, these publications represent a proof-of-concept of the idea of offline aerosol analysis by MCE, but the methods have not been utilized for routine measurement.

Ambient atmospheric aerosols demonstrate high spatial and temporal variability, and monitoring of this variability is important for monitoring health and environmental effects as well as determining aerosol sources and reaction chemistry. Measurement of the physical characteristics of the aerosol such as size and number are useful, but better knowledge of the aerosol composition is needed for more complete understanding in the above areas. Offline methods for composition are often insufficient for elucidating the necessary chemical information due to poor temporal resolution and potential sampling artifacts. Recently developed online instrumentation addresses some of the limitations of

offline techniques, and knowledge of aerosol chemistry has significantly increased. However, current online instruments often suffer from insufficient temporal resolution, inadequate sensitivity, inability to quantify species, and limited resolving of mixtures and identification of specific compounds. Even when these shortcomings are not an issue, current instrumentation is often too costly for routine use and widespread deployment into observation networks. Instead, these instruments are typically relegated to laboratories or small field sites during relatively short-term field campaigns.

IMPROVING MONITORING OF AEROSOL COMPOSITION

To address the need for improved online aerosol composition instrumentation, my research has focused on developing an instrument that overcomes many of the shortcomings of current online methods. The main advantage of this instrument will be its use of MCE as a separation method for chemical speciation. MCE can dramatically improve time resolution for bulk aerosol speciation by performing separations in under a minute compared to 2.5 min to 1 h for IC and even longer for GC methods. Required sample mass should be much lower than with existing techniques because MCE can analyze samples in the low μL range using injection volumes around 1 nL, whereas IC requires 10-100 times the sample of MCE and consumes the entire sample for a single injection. Reagent consumption is an even bigger advantage for MCE, as 1 L of BGE could theoretically operate the device for over a year, while an IC uses 1 L of mobile phase in less than a day. Because the microchip itself has a footprint of less than 100 cm^2 and does not require a pump, it is much more portable and field-ready than other instruments. Finally, the most important advantage of employing MCE for aerosol

analysis is its low cost. Costing hundreds or thousands of times less than GC or IC instruments, a network of MCE devices could be deployed for high resolution spatial monitoring of aerosols or throughout a much larger grid of sites, such as the Interagency Monitoring of Protected Visual Environments (IMPROVE) program. However, development of an online MCE instrument for measuring aerosol composition is not straightforward. Part of the difficulty is due to compatibility issues between aerosol samplers and MCE devices. The high voltages used in MCE can potentially couple to the aerosol collector, resulting in arcing and damage to either or both instruments. Most online aerosol collectors generate a flowing aqueous stream, and these hydrodynamic flows can be difficult to couple to MCE. Several designs for incorporating hydrodynamic flow into MCE have been successful,[96-105] but each of these is method-specific and would therefore not be applicable for aerosol monitoring without additional modification. Also, continuous flow interfacing with MCE typically analyzes only a fraction of the total solution flow, resulting in a large amount of wasted sample that undergoes excessive dilution. The difficulties introduced by the aerosol sampler are minor relative to the shortcomings of existing MCE methods. Operational times between BGE replacements, for instance, are very low with MCE, and are sometimes as short as just a few minutes. Reproducibility is often poor due to several factors, including BGE changes due to electrolysis, unstable capillary surface conditions, unwanted hydrodynamic flow from head height differences or meniscus pressures, sample matrix effects, large uncertainties in injection volumes, and ion depletion of the sample. Existing separations for MCE are unsuitable for online aerosol separations. Very few operate at steady state; instead, they rely on preconditioning rinses that change the capillary surface conditions, thus

performing the separation at a transient condition. Preconditioning rinses can be difficult to automate for MCE and also result in fragmented temporal series. Most current separations suffer from late migrating "system zone" peaks or interfering peaks from unimportant ions in the sample. Because the bulk flow in the system travels from the sample into the microfluidic network, the capillaries can become clogged from insoluble particulate matter or the capillaries can be coated by unanticipated species in the sample. Perhaps the biggest difficulty in implementing MCE into online aerosol instrumentation is finding an adequate detection approach. While MCE is often touted for having high sensitivity, this is often only true when using fluorescent or chemiluminescent detection. Other detection methods typically give poor concentration LODs that are orders of magnitude higher than with those two optical techniques. Because many of the important aerosol species are ionic, conductivity detection is an obvious choice for many MCE aerosol separations. The dominant conductivity detection approach for MCE is contactless conductivity detection.[106-110] However, this technique yields broader peaks than other methods because of the relatively long detection window. Also, despite a decade of optimization with capillary electrophoresis, this technique still provides unacceptably high detection limits for most aerosol analyses. Typical reported detection limits for high mobility inorganic ions are 1-10 μM. Even the most optimized systems did not achieve detection limits below 0.15 μM, and achieving those lower levels required a special electrode configuration, heavy electronic shielding, and very thin microfluidic substrates (they severely limit BGE volumes unless additional measures are taken).[111] The environmental conditions in field campaigns often exhibit more electronic interference than pristine labs. Online monitoring also places additional demands on the

microchip geometry that make sensitive contactless detection difficult. Thus, it is probable that detection limits below 1 μM cannot be achieved for this application. Instead, it is likely that another detection option would need to be pursued.

In this dissertation, I describe the development process of the first online monitoring system for aerosol composition using microchip electrophoresis. Much of the effort involved in this task was in overcoming the many shortcomings of MCE and potential obstacles when coupling MCE to an aerosol collector as listed above. Chapter 2 discusses the creation of a separation method for both inorganic and organic anions using traditional CE.[112] This separation was not employed in the online MCE instrument, but some of the binding chemistry discovered when developing this method was extensively employed throughout the rest of my research. Chapter 3 describes the inclusion of filtering membranes into MCE devices with the additional benefit of suppressing undesirable hydrodynamic flow.[113] Although the membrane approach was abandoned later, the methodology may be included at a later date to reduce interference from insoluble particulate matter during online aerosol sampling. In chapter 4, the development of a novel bubble cell detection zone for improving contact conductivity detection in MCE is described.[114] The bubble cell reduces unwanted electrochemical reactions on the detection electrode surface, permitting detection limits several times better than those achievable with contactless conductivity detection. Chapter 5 shows the separation chemistry employed for monitoring inorganic anions and oxalate in atmospheric aerosols.[115] The chemistry was specifically designed for online monitoring and is superior to previous methods because of its lower detection limits, faster analysis

times, elimination of all system peaks, employment of an internal standard, avoidance of transient rinsing protocols, and analysis longevity without BGE replenishment. The chosen aerosol collector for online monitoring was the water condensation particle collector (WCPC),[116] also called a growth tube, and chapter 6 describes the interfacing of the WCPC with MCE technology to create the first online MCE aerosol composition monitoring system.[117] Initial testing of the instrument was for a period of over one day of semi-continuous monitoring. Chapter 7 takes several of the unique approaches to MCE utilized in chapters 5 and 6 and generalizes them for a broader audience. Explicit detail is given on how to maximize the performance of MCE in extended monitoring applications, whereas this information was only briefly discussed in prior chapters because those chapters focused on more specific issues. Finally, chapter 8 shows the recent improvements to the techniques discussed in earlier chapters, as well as the extensions of the progress made in my research into other areas. Overall, the research described in this dissertation might have a significant impact on the field of MCE by increasing the detection performance and by illustrating how to design methods with practical applicability for real samples. The impact on the aerosol community is harder to predict. At one extreme, it is possible that this technology will not be embraced because of its departure from existing techniques and will instead remain a novelty approach that is seldom employed. On the other extreme, this technology may be rapidly improved and deployed in routine monitoring networks throughout the world. Much of the technology's future course depends on the needs of aerosol scientists in environmental and health fields.

REFERENCES

1. Poschl, U., *Angew. Chem. Int. Ed.* **2005,** *44*, 7520-7540.
2. Raes, F.; Van Dingenen, R.; Vignati, E.; Wilson, J.; Putaud, J. P.; Seinfeld, J. H.; Adams, P., *Atmos. Environ.* **2000,** *34*, 4215-4240.
3. Pandis, S. N.; Wexler, A. S.; Seinfeld, J. H., *J. Phys. Chem.* **1995,** *99*, 9646-9659.
4. Saxena, P.; Hildemann, L. M., *J. Atmos. Chem.* **1996,** *24*, 57-109.
5. Farmer, D. K.; Matsunaga, A.; Docherty, K. S.; Surratt, J. D.; Seinfeld, J. H.; Ziemann, P. J.; Jimenez, J. L., *Proc. Natl. Acad. Sci. U.S.A.* **2010,** *107*, 6670-6675.
6. Zaveri, R. A.; Berkowitz, C. M.; Brechtel, F. J.; Gilles, M. K.; Hubbe, J. M.; Jayne, J. T.; Kleinman, L. I.; Laskin, A.; Madronich, S.; Onasch, T. B.; Pekour, M. S.; Springston, S. R.; Thornton, J. A.; Tivanski, A. V.; Worsnop, D. R., *J. Geophys. Res-Atmos.* **2010,** *115*.
7. Surratt, J. D.; Gomez-Gonzalez, Y.; Chan, A. W. H.; Vermeylen, R.; Shahgholi, M.; Kleindienst, T. E.; Edney, E. O.; Offenberg, J. H.; Lewandowski, M.; Jaoui, M.; Maenhaut, W.; Claeys, M.; Flagan, R. C.; Seinfeld, J. H., *J. Phys. Chem. A* **2008,** *112*, 8345-8378.
8. Simoneit, B. R. T.; Schauer, J. J.; Nolte, C. G.; Oros, D. R.; Elias, V. O.; Fraser, M. P.; Rogge, W. F.; Cass, G. R., *Atmos. Environ.* **1999,** *33*, 173-182.
9. Chebbi, A.; Carlier, P., *Atmos. Environ.* **1996,** *30*, 4233-4249.
10. Pratt, K. A.; Hatch, L. E.; Prather, K. A., *Environ. Sci. Technol.* **2009,** *43*, 5276-5281.
11. Murphy, S. M.; Sorooshian, A.; Kroll, J. H.; Ng, N. L.; Chhabra, P.; Tong, C.; Surratt, J. D.; Knipping, E.; Flagan, R. C.; Seinfeld, J. H., *Atmos. Chem. Phys.* **2007,** *7*, 2313-2337.
12. Herckes, P.; Leenheer, J. A.; Collett, J. L., *Environ. Sci. Technol.* **2007,** *41*, 393-399.
13. Bernstein, J. A.; Alexis, N.; Barnes, C.; Bernstein, I. L.; Bernstein, J. A.; Nel, A.; Peden, D.; Diaz-Sanchez, D.; Tarlo, S. M.; Williams, P. B., *J. Allergy Clin. Immunol.* **2004,** *114*, 1116-1123.
14. Ren, C.; Tong, S., *Environ. Health* **2008,** *7*, 1-10.
15. Anderson, H. R., *Atmos. Environ.* **2009,** *43*, 142-152.
16. Russell, A. G.; Brunekreef, B., *Environ. Sci. Technol.* **2009,** *43*, 4620-4625.
17. Sun, Q. H.; Hong, X. R.; Wold, L. E., *Circulation* **2010,** *121*, 2755-2765.
18. Maynard, A. D.; Kuempel, E. D., *J. Nanopart. Res.* **2005,** *7*, 587-614.
19. Oberdorster, G.; Ferin, J.; Gelein, R.; Soderholm, S. C.; Finkelstein, J., *Environ. Health Perspect.* **1992,** *97*, 193-199.
20. Li, N.; Sioutas, C.; Cho, A.; Schmitz, D.; Misra, C.; Sempf, J.; Wang, M. Y.; Oberley, T.; Froines, J.; Nel, A., *Environ. Health Perspect.* **2003,** *111*, 455-460.
21. Kanakidou, M.; Seinfeld, J. H.; Pandis, S. N.; Barnes, I.; Dentener, F. J.; Facchini, M. C.; Van Dingenen, R.; Ervens, B.; Nenes, A.; Nielsen, C. J.; Swietlicki, E.; Putaud, J. P.; Balkanski, Y.; Fuzzi, S.; Horth, J.; Moortgat, G. K.; Winterhalter, R.; Myhre, C. E. L.; Tsigaridis, K.; Vignati, E.; Stephanou, E. G.; Wilson, J., *Atmos. Chem. Phys.* **2005,** *5*, 1053-1123.
22. Lohmann, U.; Feichter, J., *Atmos. Chem. Phys.* **2005,** *5*, 715-737.

23. McFiggans, G.; Artaxo, P.; Baltensperger, U.; Coe, H.; Facchini, M. C.; Feingold, G.; Fuzzi, S.; Gysel, M.; Laaksonen, A.; Lohmann, U.; Mentel, T. F.; Murphy, D. M.; O'Dowd, C. D.; Snider, J. R.; Weingartner, E., *Atmos. Chem. Phys.* **2006,** *6*, 2593-2649.
24. Sipin, M. F.; Guazzotti, S. A.; Prather, K. A., *Anal. Chem.* **2003,** *75*, 2929-2940.
25. Melanson, J. E.; Baryla, N. E.; Lucy, C. A., *TrAC-Trend. Anal. Chem.* **2001,** *20*, 365-374.
26. Liu, J. K.; Lee, M. L., *Electrophoresis* **2006,** *27*, 3533-3546.
27. Gassner, B.; Friedl, W.; Kenndler, E., *J. Chromatogr. A* **1994,** *680*, 25-31.
28. Appel, B. R.; Tokiwa, Y.; Haik, M.; Kothny, E. L., *Atmos. Environ.* **1984,** *18*, 409-416.
29. Sullivan, R. C.; Prather, K. A., *Anal. Chem.* **2005,** *77*, 3861-3885.
30. Huntzicker, J. J.; Hoffman, R. S.; Ling, C. S., *Atmos. Environ.* **1978,** *12*, 83-88.
31. Stolzenburg, M. R.; Hering, S. V., *Environ. Sci. Technol.* **2000,** *34*, 907-914.
32. Suess, D. T.; Prather, K. A., *Chem. Rev.* **1999,** *99*, 3007-3035.
33. Noble, C. A.; Prather, K. A., *Mass Spectrom. Rev.* **2000,** *19*, 248-274.
34. Jayne, J. T.; Leard, D. C.; Zhang, X. F.; Davidovits, P.; Smith, K. A.; Kolb, C. E.; Worsnop, D. R., *Aerosol Sci. Technol.* **2000,** *33*, 49-70.
35. Canagaratna, M. R.; Jayne, J. T.; Jimenez, J. L.; Allan, J. D.; Alfarra, M. R.; Zhang, Q.; Onasch, T. B.; Drewnick, F.; Coe, H.; Middlebrook, A.; Delia, A.; Williams, L. R.; Trimborn, A. M.; Northway, M. J.; DeCarlo, P. F.; Kolb, C. E.; Davidovits, P.; Worsnop, D. R., *Mass Spectrom. Rev.* **2007,** *26*, 185-222.
36. Prather, K. A.; Nordmeyer, T.; Salt, K., *Anal. Chem.* **1994,** *66*, 1403-1407.
37. Nordmeyer, T.; Prather, K. A., *Anal. Chem.* **1994,** *66*, 3540-3542.
38. Gard, E.; Mayer, J. E.; Morrical, B. D.; Dienes, T.; Fergenson, D. P.; Prather, K. A., *Anal. Chem.* **1997,** *69*, 4083-4091.
39. Dzepina, K.; Arey, J.; Marr, L. C.; Worsnop, D. R.; Salcedo, D.; Zhang, Q.; Onasch, T. B.; Molina, L. T.; Molina, M. J.; Jimenez, J. L., *Int. J. Mass Spectrom.* **2007,** *263*, 152-170.
40. Fergenson, D. P.; Song, X. H.; Ramadan, Z.; Allen, J. O.; Hughes, L. S.; Cass, G. R.; Hopke, P. K.; Prather, K. A., *Anal. Chem.* **2001,** *73*, 3535-3541.
41. Qin, X. Y.; Bhave, P. V.; Prather, K. A., *Anal. Chem.* **2006,** *78*, 6169-6178.
42. Zhao, W. X.; Hopke, P. K.; Qin, X. Y.; Prather, K. A., *Anal. Chim. Acta* **2005,** *549*, 179-187.
43. Williams, B. J.; Goldstein, A. H.; Kreisberg, N. M.; Hering, S. V., *Aerosol Sci. Technol.* **2006,** *40*, 627-638.
44. Kreisberg, N. M.; Hering, S. V.; Williams, B. J.; Worton, D. R.; Goldstein, A. H., *Aerosol Sci. Technol.* **2009,** *43*, 38-52.
45. Goldstein, A. H.; Worton, D. R.; Williams, B. J.; Hering, S. V.; Kreisberg, N. M.; Panic, O.; Gorecki, T., *J. Chromatogr. A* **2008,** *1186*, 340-347.
46. Simon, P. K.; Dasgupta, P. K., *Anal. Chem.* **1995,** *67*, 71-78.
47. Simon, P. K.; Dasgupta, P. K., *Environ. Sci. Technol.* **1995,** *29*, 1534-1541.
48. Khlystov, A.; Wyers, G. P.; Slanina, J., *Atmos. Environ.* **1995,** *29*, 2229-2234.
49. Zellweger, C.; Ammann, M.; Hofer, P.; Baltensperger, U., *Atmos. Environ.* **1999,** *33*, 1131-1140.
50. Loflund, M.; Kasper-Giebl, A.; Tscherwenka, W.; Schmid, M.; Giebl, H.; Hitzenberger, R.; Reischl, G.; Puxbaum, H., *Atmos. Environ.* **2001,** *35*, 2861-2869.

51. Slanina, J.; ten Brink, H. M.; Otjes, R. P.; Even, A.; Jongejan, P.; Khlystov, A.; Waijers-Ijpelaan, A.; Hu, M., *Atmos. Environ.* **2001,** *35*, 2319-2330.
52. Weber, R. J.; Orsini, D.; Daun, Y.; Lee, Y. N.; Klotz, P. J.; Brechtel, F., *Aerosol Sci. Technol.* **2001,** *35*, 718-727.
53. Orsini, D. A.; Ma, Y. L.; Sullivan, A.; Sierau, B.; Baumann, K.; Weber, R. J., *Atmos. Environ.* **2003,** *37*, 1243-1259.
54. Peltier, R. E.; Sullivan, A. P.; Weber, R. J.; Brock, C. A.; Wollny, A. G.; Holloway, J. S.; de Gouw, J. A.; Warneke, C., *Atmos. Chem. Phys.* **2007,** *7*, 3231-3247.
55. Rastogi, N.; Oakes, M. M.; Schauer, J. J.; Shafer, M. M.; Majestic, B. J.; Weber, R. J., *Environ. Sci. Technol.* **2009,** *43*, 2425-2430.
56. Dabekzlotorzynska, E.; Dlouhy, J. F., *J. Chromatogr. A* **1994,** *671*, 389-395.
57. Dabekzlotorzynska, E.; Dlouhy, J. F.; Houle, N.; Piechowski, M.; Ritchie, S., *J. Chromatogr. A* **1995,** *706*, 469-478.
58. DabekZlotorzynska, E.; Piechowski, M.; Liu, F.; Kennedy, S.; Dlouhy, J. F., *J. Chromatogr. A* **1997,** *770*, 349-359.
59. Dabekzlotorzynska, E.; Dlouhy, J. F., *J. Chromatogr. A* **1995,** *706*, 527-534.
60. Dabek-Zlotorzynska, E.; Kelly, M.; Chen, H. D.; Chakrabarti, C. L., *Chemosphere* **2005,** *58*, 1365-1376.
61. Dabek-Zlotorzynska, E.; Aranda-Rodriguez, R.; Buykx, S. E. J., *Anal. Bioanal. Chem.* **2002,** *372*, 467-472.
62. Dabek-Zlotorzynska, E.; Piechowski, M.; Keppel-Jones, K.; Aranda-Rodriguez, R., *J. Sep. Sci.* **2002,** *25*, 1123-1128.
63. Dabek-Zlotorzynska, E.; Piechowski, M.; McGrath, M.; Lai, E. P. C., *J. Chromatogr. A* **2001,** *910*, 331-345.
64. Dabek-Zlotorzynska, E.; Aranda-Rodriguez, R.; Graham, L., *J. Sep. Sci.* **2005,** *28*, 1520-1528.
65. Dabekzlotorzynska, E.; Dlouhy, J. F., *J. Chromatogr. A* **1994,** *685*, 145-153.
66. Deng, Y. W., *Water Res.* **1998,** *32*, 2249-2256.
67. Garcia, S. T.; Valenzuela, M. I. A.; Gil, E. P., *Talanta* **2008,** *75*, 748-752.
68. Valsecchi, S.; Tartari, G.; Polesello, S., *J. Chromatogr. A* **1997,** *760*, 326-332.
69. Krivacsy, Z.; Molnar, A.; Tarjanyi, E.; Gelencser, A.; Kiss, G.; Hlavay, J., *J. Chromatogr. A* **1997,** *781*, 223-231.
70. Tam, W. F. C.; Tanner, P. A.; Law, P. T. R.; Bachmann, K.; Potzsch, S., *Anal. Chim. Acta* **2001,** *427*, 259-269.
71. Tenberken, B.; Bachmann, K., *J. Chromatogr. A* **1997,** *775*, 372-377.
72. Adler, H.; Siren, H.; Kulmala, M.; Riekkola, M. L., *J. Chromatogr. A* **2003,** *990*, 133-141.
73. Blanco-Heras, G. A.; Turnes-Carou, M. I.; Lopez-Mahia, P.; Muniategui-Lorenzo, S.; Prada-Rodriguez, D.; Fernandez-Fernandez, E., *Electrophoresis* **2008,** *29*, 1347-1354.
74. Gao, S. D.; Rudolph, J., *J. Chromatogr. Sci.* **2004,** *42*, 323-328.
75. Iinuma, Y.; Herrmann, H., *J. Chromatogr. A* **2003,** *1018*, 105-115.
76. Souza, S. R.; Vasconcellos, P. C.; Carvalho, L. R. F., *Atmos. Environ.* **1999,** *33*, 2563-2574.
77. van Pinxteren, D.; Herrmann, H., *J. Chromatogr. A* **2007,** *1171*, 112-123.
78. Chen, X. G.; Fan, L. Y.; Hu, Z., *Electrophoresis* **2004,** *25*, 3962-3969.

79. Kuban, P.; Karlberg, B., *Anal. Chim. Acta* **2009,** *648*, 129-145.
80. Kuban, P.; Karlberg, B., *TrAC-Trend. Anal. Chem.* **1998,** *17*, 34-41.
81. Manz, A.; Harrison, D. J.; Verpoorte, E. M. J.; Fettinger, J. C.; Paulus, A.; Ludi, H.; Widmer, H. M., *J. Chromatogr.* **1992,** *593*, 253-258.
82. Harrison, D. J.; Manz, A.; Fan, Z. H.; Ludi, H.; Widmer, H. M., *Anal. Chem.* **1992,** *64*, 1926-1932.
83. Manz, A.; Graber, N.; Widmer, H. M., *Sensor. Actuat. B-Chem.* **1990,** *1*, 244-248.
84. Reyes, D. R.; Iossifidis, D.; Auroux, P. A.; Manz, A., *Anal. Chem.* **2002,** *74*, 2623-2636.
85. Auroux, P. A.; Iossifidis, D.; Reyes, D. R.; Manz, A., *Anal. Chem.* **2002,** *74*, 2637-2652.
86. Vilkner, T.; Janasek, D.; Manz, A., *Anal. Chem.* **2004,** *76*, 3373-3385.
87. Dittrich, P. S.; Tachikawa, K.; Manz, A., *Anal. Chem.* **2006,** *78*, 3887-3907.
88. West, J.; Becker, M.; Tombrink, S.; Manz, A., *Anal. Chem.* **2008,** *80*, 4403-4419.
89. Arora, A.; Simone, G.; Salieb-Beugelaar, G. B.; Kim, J. T.; Manz, A., *Anal. Chem.* **2010,** *82*, 4830-4847.
90. Dolnik, V.; Liu, S. R.; Jovanovich, S., *Electrophoresis* **2000,** *21*, 41-54.
91. Dolnik, V.; Liu, S. R., *J. Sep. Sci.* **2005,** *28*, 1994-2009.
92. Wu, D. P.; Qin, J. H.; Lin, B. C., *J. Chromatogr. A* **2008,** *1184*, 542-559.
93. Revermann, T.; Gotz, S.; Kunnemeyer, J.; Karst, U., *Analyst* **2008,** *133*, 167-174.
94. Garcia, C. D.; Engling, G.; Herckes, P.; Collett, J. L.; Henry, C. S., *Environ. Sci. Technol.* **2005,** *39*, 618-623.
95. Liu, Y.; MacDonald, D. A.; Yu, X. Y.; Hering, S. V.; Collett, J. L.; Henry, C. S., *Analyst* **2006,** *131*, 1226-1231.
96. Attiya, S.; Jemere, A. B.; Tang, T.; Fitzpatrick, G.; Seiler, K.; Chiem, N.; Harrison, D. J., *Electrophoresis* **2001,** *22*, 318-327.
97. Fang, Z. L.; Fang, Q., *Fresenius J. Anal. Chem.* **2001,** *370*, 978-983.
98. Lin, Y. H.; Lee, G. B.; Li, C. W.; Huang, G. R.; Chen, S. H., *J. Chromatogr. A* **2001,** *937*, 115-125.
99. Chen, S. H.; Lin, Y. H.; Wang, L. Y.; Lin, C. C.; Lee, G. B., *Anal. Chem.* **2002,** *74*, 5146-5153.
100. Fang, Q.; Xu, G. M.; Fang, Z. L., *Anal. Chem.* **2002,** *74*, 1223-1231.
101. Buttgenbach, S.; Wilke, R., *Anal. Bioanal. Chem.* **2005,** *383*, 733-737.
102. Li, M. W.; Huynh, B. H.; Hulvey, M. K.; Lunte, S. M.; Martin, R. S., *Anal. Chem.* **2006,** *78*, 1042-1051.
103. Mecker, L. C.; Martin, R. S., *Anal. Chem.* **2008,** *80*, 9257-9264.
104. Reschke, B. R.; Luo, H.; Schiffbauer, J.; Edwards, B. F.; Timperman, A. T., *Lab Chip* **2009,** *9*, 2203-2211.
105. Reschke, B. R.; Schiffbauer, J.; Edwards, B. F.; Timperman, A. T., *Analyst* **2010,** *135*, 1351-1359.
106. Guijt, R. M.; Evenhuis, C. J.; Macka, M.; Haddad, P. R., *Electrophoresis* **2004,** *25*, 4032-4057.
107. Kuban, P.; Hauser, P. C., *Electroanalysis* **2004,** *16*, 2009-2021.
108. Solinova, V.; Kasicka, V., *J. Sep. Sci.* **2006,** *29*, 1743-1762.
109. Kuban, P.; Hauser, P. C., *Electrophoresis* **2009,** *30*, 176-188.
110. Felhofer, J. L.; Blanes, L.; Garcia, C. D., *Electrophoresis* **2010,** *31*, 2469-2486.

111. Mahabadi, K. A.; Rodriguez, I.; Lim, C. Y.; Maurya, D. K.; Hauser, P. C.; de Rooij, N. F., *Electrophoresis* **2010,** *31*, 1063-1070.
112. Noblitt, S. D.; Mazzoleni, L. R.; Hering, S. V.; Collett, J. L.; Henry, C. S., *J. Chromatogr. A* **2007,** *1154*, 400-406.
113. Noblitt, S. D.; Kraly, J. R.; VanBuren, J. M.; Hering, S. V.; Collett, J. L.; Henry, C. S., *Anal. Chem.* **2007,** *79*, 6249-6254.
114. Noblitt, S. D.; Henry, C. S., *Anal. Chem.* **2008,** *80*, 7624-7630.
115. Noblitt, S. D.; Schwandner, F. M.; Hering, S. V.; Collett, J. L.; Henry, C. S., *J. Chromatogr. A* **2009,** *1216*, 1503-1510.
116. Hering, S. V.; Stolzenburg, M. R.; Quant, F. R.; Oberreit, D. R.; Keady, P. B., *Aerosol Sci. Technol.* **2005,** *39*, 659-672.
117. Noblitt, S. D.; Lewis, G. S.; Liu, Y.; Hering, S. V.; Collett, J. L.; Henry, C. S., *Anal. Chem.* **2009,** *81*, 10029-10037.

CHAPTER 2. SEPARATION OF COMMON ORGANIC AND INORGANIC ANIONS IN ATMOSPHERIC AEROSOLS USING A PIPERAZINE BUFFER AND CAPILLARY ELECTROPHORESIS

CHAPTER OVERVIEW

The overall goal of the research described in this dissertation is the development of a microchip electrophoresis system for the routine online monitoring of aerosol chemical composition. A major portion of that is the development of robust separation chemistry and protocols for the analytes of interest. As a first step towards acceptable separation chemistry, a procedure for the separation of organic acids in aerosols was developed for traditional (non-microchip) capillary electrophoresis. This work was published in *The Journal of Chromatography A*,[2] and is given here. The developed method has not been directly used in my research since its completion, when I transitioned to microchip electrophoresis analysis. However, some of this work established part of the foundation for the development of the online system. In particular, the discovery of the interaction between sulfate and protonated diamines was a cornerstone in the separation chemistry used for anions in aerosols. This interaction permitted the resolution of chloride, sulfate, and nitrate at the low ionic strength needed for conductivity detection in microchip electrophoresis (described in chapter 5).

ABSTRACT

The ability to monitor and quantify anionic components of aerosols is important for developing a better fundamental understanding of temporal and spatial variations in aerosol composition. Of the many methods that can be used to detect anions, capillary electrophoresis is among the most attractive because of its high separation efficiency, high resolving power for ionic compounds, and ability to be miniaturized for in-field monitoring. Here we present a method to baseline resolve common aerosol components nitrate, sulfate, chloride, and over two dozen organic acids in a single separation. A capillary electrophoresis separation utilizing a pH 5.78 piperazine buffer with 1,5-naphthalenedisulfonic acid as a probe for indirect UV absorbance detection was developed for this analysis. Previously, two different buffers were required to adequately separate all of these compounds. Electrophoretic mobilities, limits of detection, and migration time reproducibilities were measured for 38 organic and 8 inorganic anions. For solutions of low conductivity, detection limits for electrokinetic injections were found to be up to two orders of magnitude lower (0.2-0.4 μM) than those for pressure injection (1-45 μM). This separation was optimized and used for routine analysis of aqueous extracts of ambient atmospheric aerosols, but may be extended to other samples containing similar mixtures of anions.

INTRODUCTION

Routine analysis of complex organic and inorganic anion mixtures in aqueous samples is important in several fields, including atmospheric aerosol characterization.[3-8] Improved analytical separation and sensitivity are especially needed to increase understanding of

the effects of aerosol composition on human health, visibility and cloud-aerosol dynamics.[9,10] Aerosol components can come from a variety of biogenic and anthropogenic sources and may undergo a variety of photochemical and oxidation reactions.[11-17] The resulting aerosol compositions are consequently highly diverse with significant variations due to location, climate, season, and time of day.[7,12-14] The compositional differences may in turn affect the ability of aerosol particles to scatter visible radiation, influencing visibility and climate forcing, and to act as cloud condensation nuclei, which indirectly influences climate.[18,19] Improving characterization of the water-soluble fraction of aerosol particles is a major research interest in atmospheric chemistry. The anion contribution to this fraction is usually dominated by sulfate and nitrate (chloride can be important at coastal sites), with important contributions also coming from a large number of mono- and dicarboxylic acids. These highly varied mixtures benefit from a chemical separation method to help decode the composition. Complex mixtures of up to dozens of organic acids can be present in aqueous aerosol extracts with inorganic anions having concentrations over an order of magnitude higher than those of most organic acids.[3,5-7,12-14] The result is a set of compounds with low molar absorptivities above 200 nm that need to be analyzed with a method that is selective, can detect low concentrations (nM-μM), analyze μL-level volumes, and not be disrupted by the relatively high concentration of inorganic anions. Furthermore, it would be ideal to be able to simultaneously quantify the inorganic anions.

Currently, gas chromatography and/or ion chromatography are commonly used for the analysis of organic acids and inorganic anions in aerosols and beverages.[3,8,20-25] Both

approaches, however, have limitations. Gas chromatography requires the use of organic solvents and often employs derivatization to improve volatility and thermal stability, a process that can lead to sample artifacts and also significantly increases costs of sample analysis. Ion chromatography needs samples of >20 μL, requiring relatively long atmospheric sampling times to ensure adequate detection limits when ambient concentrations are low. Furthermore, separation efficiency and resolution can be low, leading to peak co-elution and ambiguous peak identification, especially for organic acids. Both techniques require long analysis times (30-90 min) relative to modern electrophoretic separations (less than 10 min).

To help overcome these limitations, several protocols for aerosol analysis have been developed using capillary electrophoresis (CE). CE allows for the rapid analysis of samples with high peak resolution from very small volumes while maintaining low (nM-μM) limits of detection.[3,4,26-29] Aerosol cation analyses have been published several times, both for transition metals and other cations.[30-34] CE protocols for neutral aerosol combustion products have also been developed.[35,36] Inorganic anions in aerosols were also measured with CE.[31,37] Organic acid aerosol CE analysis has been shown considerable attention since the number of analytes potentially in a sample is so large and peak co-elution can be problematic with liquid chromatography methods. Several groups have developed CE separations for organic acids and successfully tested these against other methods, but most of these separations had inorganic anion comigration.[3,13,26-29,38-42] Krivácsy et al. developed a separation with both the inorganic and organic anion portions of aerosols but was limited to higher mobility organic acids.[31] Masár et al. demonstrated

improved inorganic anion separation in CE using cyclodextrins for selectivity.[43] Virtanen et al. also showed successful CE separation of the inorganic species that may be present in atmospheric aerosols.[44] Despite the success of these methods, there is still considerable need for improvement, particularly for the simultaneous analysis of both inorganic and organic anions.

Here we present a new running buffer system for capillary electrophoresis (CE) that allows for simultaneous separation of many common organic and inorganic anions that are present in ambient atmospheric aerosols. An aqueous buffer consisting of piperazine, 1,5-naphthalenedisulfonic acid, and tetradecyltrimethylammonium bromide was found to separate chloride, nitrate, and sulfate, three common inorganic ions in aerosols, as well as a plethora of organic acids potentially present in ambient aerosol samples. Migration times for all analyzed compounds were under 8.5 minutes, intraday migration times had relative standard deviations (RSDs) of 0.07-1.8%, and interday RSDs were 1.14-3.56%. Hydrodynamic limits of detection ranged from 1-45 μM, whereas electrokinetic injections gave detection limits of 0.2-0.4 μM. Finally, two different atmospheric samples were analyzed using the method and found to contain significant amounts of both organic acids and inorganic anions.

EXPERIMENTAL

Instrumentation

CE experiments were performed with a Beckman Coulter P/ACE MDQ Capillary Electrophoresis System and data analyzed using 32 Karat (7.0) software (Fullerton, CA,

USA). Fused silica capillaries (Polymicro Technologies, Phoenix, AZ, USA) with an internal diameter of 50 μm and an outer diameter of 360 μm were used in all experiments. Electropherograms were obtained with detection by indirect absorbance at 280 nm with a data acquisition rate of 4 Hz. An Agilent 8453 UV-visible spectrophotometer was used to acquire UV absorbance spectra.

Chemicals and Standards

The organic acid analytes were purchased as either the free acid or sodium or potassium salts from Fisher Scientific (Fair Lawn, NJ, USA), Aldrich (Milwaukee, WI, USA), Acros Organics (New Jersey, USA), or JT Baker Chemical Co. (Phillipsburg, NJ, USA), 1,5-naphthalenedisulfonic acid tetrahydrate and tetradecyltrimethylammonium bromide (TTAB) were purchased from Aldrich. Cetyltrimethylammonium hydroxide (CTAOH) was obtained from Fisher. Piperazine was purchased from Acros Organics. Most stock analyte solutions were made in 18 MΩ cm deionized water, with some longer-chain carboxylic acids being prepared in dilute sodium hydroxide solution to increase their aqueous solubility. All chemicals were used as received without further purification.

Electrophoretic Procedures

New capillaries were first hydrated with deionized water then rinsed with 0.1-M NaOH (60 min), water (5 min), 0.1-M HCl (20 min), water (5 min), methanol (20 min), water (5 min), and the background electrolyte (30 min). At the start of each day, the capillary was rinsed with 0.1-M NaOH (5 min), 0.1-M HCl (5 min), water (5 min), and background electrolyte (10 min). Application of –20 kV (3 min) was also applied prior to the first

separation of the day to improve baseline stability. Between trials, the capillary was rinsed with background electrolyte (2 min). All rinsing was performed using hydrodynamic flow at a pressure of 20 psi. When used, all polyelectrolyte coatings were applied by flushing the capillary with 0.1-M NaOH for 5 min, followed by a 30 min exposure to a 0.5% (w/v) aqueous solution of the polyelectrolyte.

CE operating conditions varied depending upon experiments. The pH optimization was performed using a 60-cm capillary (50-cm effective length.) For all other experiments, the capillary length was increased to 75-cm total (65-cm effective) to increase resolution between closely migrating compounds. Separations were performed in constant voltage mode using reverse polarity. During the pH optimization process with 60-cm capillaries, a –20 kV separation potential was utilized. In the other experiments, –30kV was used. Injection conditions also varied during optimization experiments. After optimization, hydrodynamic injections were done at 0.5 psi for 16 s, and electrokinetic injections were performed at –3 kV for 16 s.

Real Sample Preparation

Laboratory generated wood combustion aerosol particles were collected using a Thermo Anderson (Smyrna, GA) high-volume collector. The sampler was equipped with an impactor to give a nominal upper cutoff of 2.5-mm aerodynamic particle diameter. Samples were collected on pre-fired Whatman quartz fiber filters at a flow rate of 1130 L min^{-1}. A portion of the quartz filter was then extracted by ultrasonic agitation for 30 min with high purity deionized water (>18MΩ cm). Cloud water samples were collected in

Steamboat Springs, CO with a stainless steel version of the Caltech Active Strand cloud collector which collects cloud droplets by inertial impaction on a bank of stainless steel strands.[45] The version of the collector used here operates at a flow rate of approximately 40 m^3 min^{-1} and provides a lower size cut for drop collection of approximately 4 μm. All samples (aerosol extracts and cloud water) were filtered using 0.2-μm syringe filters (Pall Life Sciences Acrodisk LC13 PVDF) and were then analyzed without alteration or pre-concentration. 10-μM *trans*-cinnamic acid was added just prior to analysis to serve as an internal standard for quantization and mobility.

RESULTS AND DISCUSSION

Background Electrolyte (BGE) Development

Buffer Selection

Much of the previous work performed in the separation of organic acids by CE with indirect absorbance detection utilized bis(2-hydroxyethyl)iminotris(hydroxymethyl)methane (bis-tris) to buffer the background electrolyte (BGE), due to its cationic nature.[3,27,28] When titrated to the proper pH with the free-acid form of the indirect probe, the resulting BGE yields no system peaks in electropherograms, making resolution of more compounds possible. The pK_a of bis-tris is 6.46. Since the majority of the analytes have pK_a values in the 4.2-5.6 range, it was believed that the optimum separation pH might be below the buffering range of bis-tris. Thus, another buffer was sought. System peaks in indirect detection are well-known to be caused by BGE ions with the same charge as the indirect probe[46-52] To prevent the formation of interfering system peaks in this separation, potential buffers were therefore

limited to cationic buffers[27,53,54] and ampholytic buffers operating at their pI.[54-56] Common CE buffers that met these requirements were limited, so a BGE utilizing piperazine (1,4-diethylenediamine, pK_a = 5.33) was selected. With piperazine, sulfate was found to migrate slower than in other BGE's, allowing for excellent separation from nitrate. We suspect this behavior is due to complexation between sulfate and the diamine in piperazine. Others have reported interactions between sulfate-containing surfactants and multiple amine-containing macromolecules, supporting this hypothesis.[57,58] To the authors' knowledge, this is the first use of piperazine as a buffer in CE and improves the resolution between some inorganic anions.

Indirect Probe

Previous work found 2,6-naphthalenedicarboxylic acid (NDC) to be a suitable indirect absorbance probe for organic acids due to its high molar absorptivity and an electrophoretic mobility that closely matches many of the organic acid analytes.[3,27,28,38,39,42] At lower pH, partial protonation of NDC results in a reduced aqueous solubility, limiting the background electrolyte to a pH above 6. As mentioned earlier, a lower pH would likely improve resolution between many of the target organic acids. 1,5-naphthalenedisulfonic (NDS) acid has already been shown to be a useful indirect probe in CE,[53,59] and its sulfonic acid groups remain deprotonated at low pH values, increasing solubility. Otherwise, its properties are similar to NDC. Experimentally, NDS was found to have a mobility between malate and maleate, as determined by peak shapes of analytes. This mobility was about -4.2×10^{-4} cm^2 V^{-1} s^{-1}, near the middle of the range of the analytes, helping to reduce band broadening due to mobility differences between

analytes and probe.[46,60,61] NDS was stable in the piperazine buffer at the pH tested, so it was chosen as the indirect probe. A molar absorptivity spectrum for NDS in the 205-330 nm range is given in Figure 2.1.

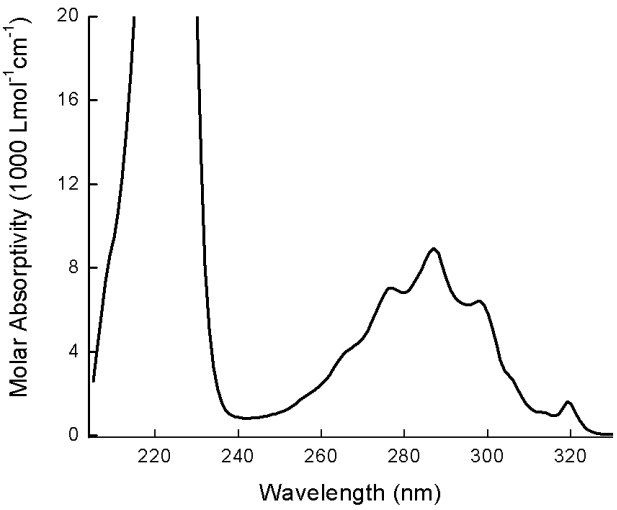

Figure 2.1. Molar absorption spectrum of NDS. Conditions: 10-μM NDS in water; water spectrum subtracted as blank.

Maxima are observed at 226 nm (56,400 L mol^{-1} cm^{-1}) and 287 nm (8,900 L mol^{-1} cm^{-1}). The separation was designed to be used on instruments utilizing typical UV filter sets (200, 214, 254, or 280 nm), so monitoring at 226 nm was not chosen. Although monitoring at 214 nm (17,200 L mol^{-1} cm^{-1}) gives higher signal-to-noise ratios for saturated carboxylic acids, 280 nm (6,800 L mol^{-1} cm^{-1}) was chosen instead since it allowed for better detection of some UV-absorbing compounds of interest, including nitrate, benzoate, phthalate, and maleate. For instruments utilizing photodiode arrays, monitoring at 226 nm or 287 nm would give best results, but the NDS concentration might need to be modified to give optimal results.

Electroosmotic Flow Reversal

Reversal of the electroosmotic flow (EOF) was desired to shorten analysis time of the target anions. Both wall-coating polyelectrolytes and cationic surfactants were considered for EOF reversal based on previous literature in the field.[62-65] Poly(ethyleneimine), poly(diallyl-dimethylammonium chloride), and hexadimethrine bromide (polybrene) cationic polyelectrolytes were tested to determine their effectiveness at providing a stable reversed EOF. Polyelectrolyte coatings were tested first because they require a less complex run buffer relative to dynamic coatings done with surfactants. None of the three coatings were found to stably and reproducibly reverse the EOF at the buffer conditions used, limiting EOF reversal to surfactants.

Two cationic surfactants were examined for EOF reversal, tetradecyltrimethylammonium bromide (TTAB) and cetyltrimethylammonium hydroxide (CTAOH). EOF reversal was found to be successful and similar for the two compounds. One significant difference between the two is that buffers containing TTAB yielded a positive peak immediately adjacent to the (expected) negative peak for quickly migrating ions such as chloride and bromide. This "double peak" interfered with quantification due to the abnormal peak shape. This feature was also seen in electropherograms of similar separations utilizing surfactants with bromide counterions,[3,26,27] but was not observed when using CTAOH. We conclude that this unwanted peak feature was caused by the competitive displacement of bromide over NDS for anions with mobilities very similar to bromide. Unfortunately, CTAOH was found to form a precipitate over a period of several hours when added to

piperazine buffers, as observed by others for some buffer systems.[66] As a result, TTAB was chosen over CTAOH for further studies.

The concentration of surfactant was also tested to determine its effect on separation performance. Results showed no significant difference in either separation efficiency or signal-to-noise ratio for BGE's with TTAB concentrations in the tested range of 0.1–0.3 mM (higher concentrations were not tested since increases in bromide concentration in the BGE were undesirable). However, at surfactant concentrations of 0.05 mM, the EOF behaved erratically, indicating that a higher concentration was needed for stable EOF reversal. To ensure a more stable EOF than observed at low concentrations and to minimize preferential bromide displacement at high concentrations, 0.15 mM TTAB was chosen for the final BGE.

Optimization of Separation Conditions

Background Electrolyte pH

To prepare BGE's of varying pH, the NDS concentration was held constant while the piperazine concentration was varied. Values from 5.2 to 6 were tested, and the mobilities of the analytes of interest were measured in this range. At the low end of this pH range, it was found that the decreased mobility of the analytes caused considerable tailing for many of the analytes because their mobilities were significantly slower than that of the pH insensitive NDS probe. A pH of 5.78 ± 0.01 was chosen since it was found to be sufficient for separating many of the major components in cloud water and wood smoke aerosol samples and exhibited far less tailing for slower migrating compounds than

observed at lower pH values. Higher pH yielded even less tailing in lower mobility compounds but was not used because more analytes co-migrated. To obtain the pH accuracy needed, the desired amount of NDS was titrated with a piperazine solution until pH 5.78 was attained since pH precision was deemed more important than concentrations due to the pH sensitivity of the separation.

Indirect Probe Concentration

The NDS concentration was optimized by varying the BGE concentration while maintaining a constant pH of 5.78 and monitoring both the separation efficiency and the signal-to-noise ratio of nitrate, malate, and benzoate (using a 60-μM mixture). The results are shown in Figures 2.2 and 2.3.

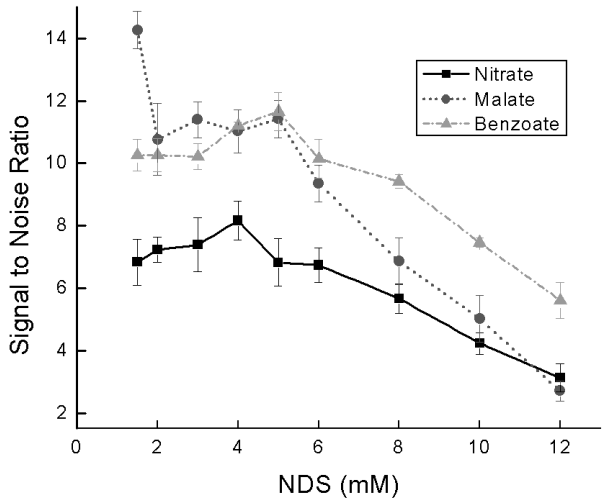

Figure 2.2. Effect of NDS concentration on signal-to-noise ratio of 60-μM analytes. Conditions: 75-cm capillary; –30-kV potential; 0.5-psi/16-s injection. pH 5.78 BGE containing 0.15-mM TTAB, given amount of NDS, and concentration of piperazine for desired pH.

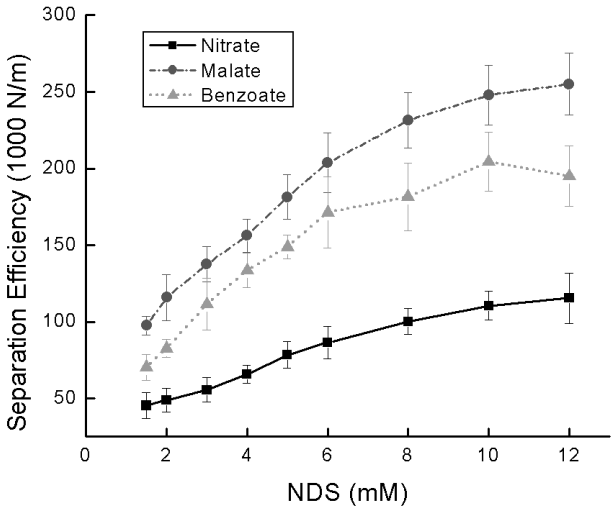

Figure 2.3. Effect of NDS concentration on separation efficiency of 60-μM analytes. 75-cm capillary; –30-kV potential; 0.5-psi/16-s inj. Conditions: Same as Figure 2.

As observed previously, increasing the probe concentration was found to increase the separation efficiency[66] while decreasing signal-to-noise ratio.[46] As shown in Figure 2.2, signal-to-noise ratio is nearly constant at lower concentrations of NDS before beginning to drop off significantly between 5- and 6-mM NDS. In Figure 2.3, we observe that separation efficiency increases considerably with probe concentration at low concentrations, but this effect lessens at high NDS values. Since both limit of detection (LOD) and resolution between analytes are important in ambient atmospheric aerosol analyses, a NDS concentration of 5.5 mM was chosen for the best compromise between high separation efficiency and high signal-to-noise ratio. This NDS concentration required a piperazine concentration of about 7.8 mM to obtain the desired pH.

Reproducibility and Electrophoretic Mobility

Analytes were analyzed with the optimized separation method six times per day for six days in order to find intra-day and inter-day relative standard deviations (RSD) of their migration times. Intraday values were in the 0.1-1.8% range. Interday RSD's were determined to be 1.1-3.6%. The majority of these variations resulted from changes in the EOF, causing slower anions to have higher RSD's than faster anions. The EOF mobility was determined to be $-1.27*10^{-4}$ cm^2 V^{-1} s^{-1} with a relatively high interday RSD of 7.7%. EOF monitoring was accomplished with the use of *trans*-cinnamic acid as an internal standard. *Trans*-cinnamic acid was used as an internal standard because it gave a noticeable positive peak and is not expected to be present in real samples. Using an internal standard allowed calculation of the electrophoretic mobilities of the analytes, which varied considerably less than migration times. Interday mobility RSD values were in the 0.3-1.7% range, with an average of 0.6%. The mobilities for all 46 analytes are given in Table 2.1.

Table 2.1. Electrophoretic Mobilities and Pressure Injection Limits of Detection Conditions: 75-cm capillary (65 cm to detection), –30-kV separation voltage, pH 5.78 NDS/piperazine/TTAB at room temperature, 0.5-psi/16-s pressure injection.

Inorganic Anions	**Mobility (10^{-4} cm^2 V^{-1} s^{-1})**	**LOD (μM)**
Bromide	–7.23	28
Iodide	–7.15	10
Chloride	–7.11	9
Nitrite	–6.69	18
Nitrate	–6.66	14
Perchlorate	–6.04	12
Sulfate	–5.46	7
Phosphate	–3.01	13
Organic Acids		
Oxalate	–5.24	45
Formate	–5.12	8
Fumarate	–4.76	4
Tartrate	–4.46	12
Malonate	–4.37	12
Methane sulfonate	–4.32	8
Malate	–4.32	8
Maleate	–3.96	7
Succinate	–3.95	6
Pyruvate	–3.87	27
Glutarate	–3.85	5
Glycolate	–3.77	8
Adipate	–3.62	3
Citrate	–3.61	38
Acetate	–3.50	5
Pimelate	–3.42	3
Norpinate	–3.35	4
Phthalate	–3.30	2
Lactate	–3.29	8
Suberate	–3.28	4
Trichloroacetate	–3.25	7
Pinate	–3.23	5
Azeliate	–3.14	4
Sebacate	–3.02	4
2-hydroxybutyrate	–3.01	8
Propionate	–2.98	7
Benzoate	–2.93	7
3-hydroxybutyrate	–2.78	10
Butyrate	–2.73	3
3-hydroxybenzoate	–2.68	11
Valerate	–2.54	3
4-hydroxybutyrate	–2.54	7
Ascorbate	–2.41	24
Trans-cinnamate (IS)	–2.40	1
Vanillate	–2.38	13
Gluconate	–2.33	4
Homovanillate	–2.28	9
Pinonate	–2.18	3

Detection Limits

Limits of detection (LOD), defined as signal-to-noise ratio of 3, were measured by analyzing successively lower concentrations of analytes and monitoring peak height divided by the peak-to-peak baseline noise. Measurements were performed for both electrokinetic and hydrodynamic (pressure) injection. Hydrodynamic LODs are given in Table 2.1 and ranged from 1-45 μM. Oxalate had the highest LOD, which was believed to be caused by its tendency to adsorb to impurities present in the batch of capillary used during the experiment. LODs for electrokinetic injection were obtained using the same method as with hydrodynamic injection, with the exception that all standards were prepared in 50-μM $NaNO_3$ to simulate the presence of inorganic salts that are present in much higher concentration than organic acids.[3,6,13,27] Results for some analytes are summarized in Table 2.2.

Table 2.2. Comparison of Pressure and Electrokinetic LODs for Some Analytes
Conditions: 75-cm capillary (65 cm to detection), –30-kV separation voltage, pH 5.78 NDS/piperazine/TTAB at room temperature, 0.5-psi/16-s pressure injection, –3-kV/16-s electrokinetic injection

Compound	Pressure LOD (μM)	Electrokinetic LOD (μM)	Improvement Factor
Perchlorate	12	0.3	40
Oxalate	45	0.4	110
Malate	8	0.2	40
Glutarate	5	0.2	25
Benzoate	7	0.3	23
Trans-cinnamate	1	0.3	3
Pinonate	3	0.4	7

As expected, electrokinetic injection gave lower LODs for all analytes in low-conductivity samples than pressure injection due to field-effect stacking.[67] Electrokinetic injection biasing is also apparent, as anions with higher mobilities showed a larger improvement over pressure injection than slower anions. The pressure LODs were

similar to some indirect detection methods[26] but could not match the sub-micromolar results of others.[27-29] The electrokinetic LODs were below those of Gao and Rudolph,[28] but could not match those measured by Dabek-Zlotorzynska et al.[27] The sub-micromolar detection limits of electrokinetic injection are very encouraging for analysis of trace organic acids in cloud water and wood smoke aerosol samples as these compounds are often present at roughly the micromolar level.

Atmospheric Aerosol Analysis

Once optimized, the separation method was tested by analyzing aqueous aerosol filter extracts and ambient cloud water samples. Electrokinetic injection was utilized since the anticipated organic acid concentrations were sub-micromolar. A mixture of 3 inorganic anions and 15 organic acids was prepared as a calibration standard. An example electropherogram for the mixture is shown in Figure 2.4. Even at a concentration of 5 μM, the analytes have a high signal to noise ratio and are easily quantified. Both cloud water and wood combustion-generated aerosol samples were analyzed and representative electropherograms are shown in Figures 2.5 and 2.6, respectively.

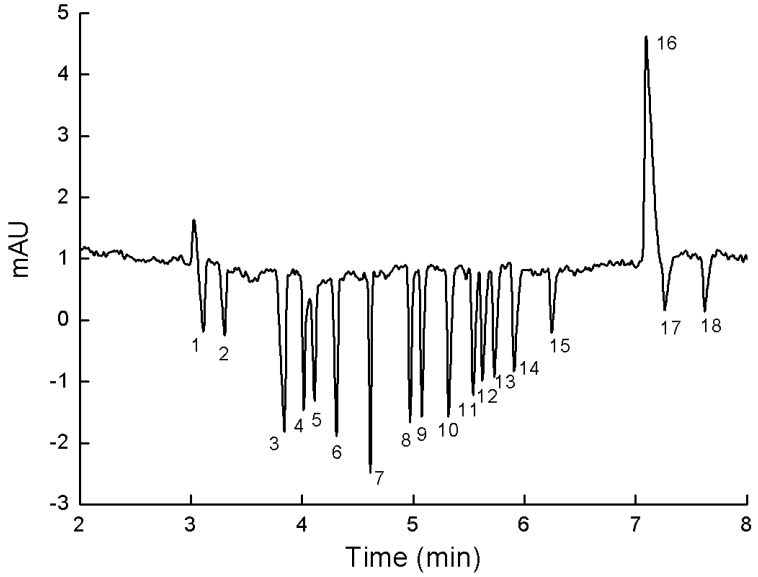

Figure 2.4. Analysis of 5-μM lab mixture with 10-μM internal standard: chloride, 1; nitrate, 2; sulfate, 3; oxalate, 4; formate, 5; fumarate, 6; malonate, 7; succinate, 8; glutarate, 9; adipate, 10; pimelate, 11; norpinate, 12; suberate, 13; azeliate, 14; benzoate, 15; *trans*-cinnamate (IS), 16; gluconate, 17; pinonate, 18. Conditions: 75 cm capillary (65 cm to detection), –30-kV separation voltage, pH 5.78 NDS/piperazine/TTAB at room temperature, –3-kV/16-s electrokinetic injection.

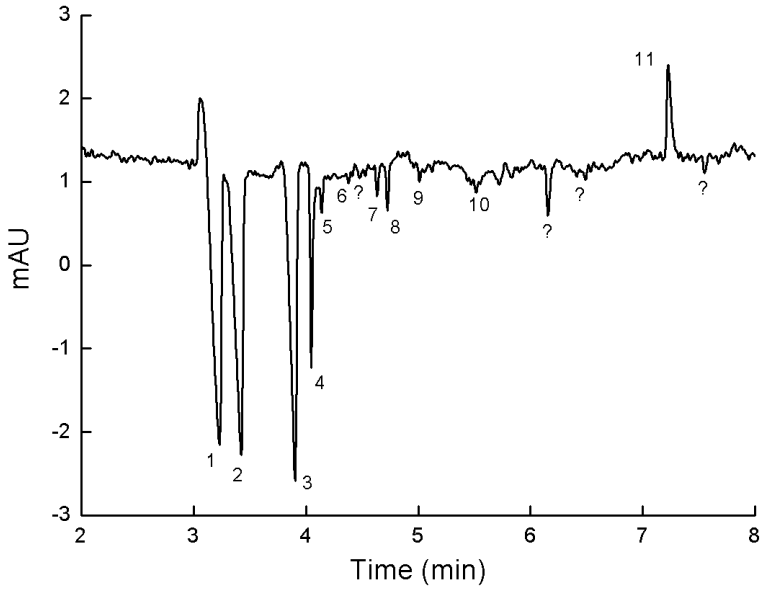

Figure 2.5. Analysis of Steamboat Springs Cloud Water Sample with 10-μM Internal Standard and Suspected Peak Assignments: chloride, 1; nitrate, 2; sulfate, 3; oxalate, 4; formate, 5; fumarate, 6; tartrate, 7; malate, 8; maleate, 9; acetate, 10; *trans*-cinnamate (IS), 11. Conditions: Same as Figure 2.4.

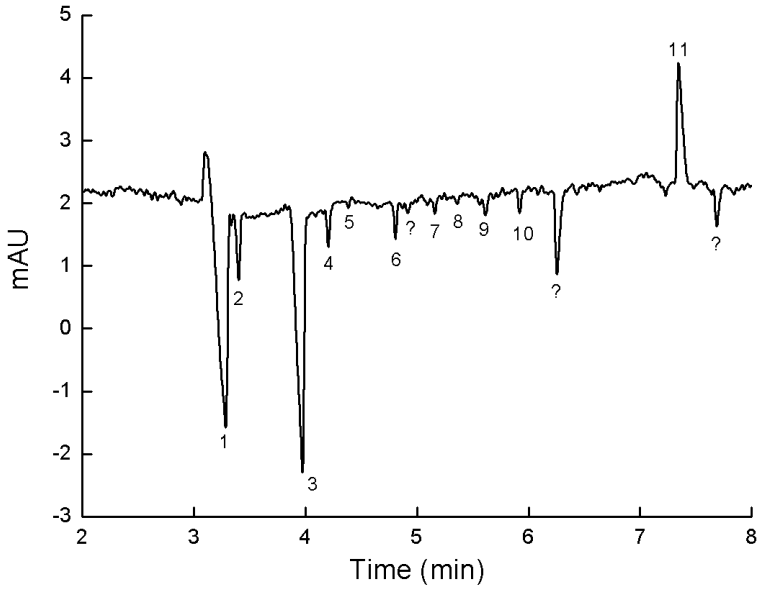

Figure 2.6. Analysis of chamise biomass combustion aerosol sample with 10-μM internal standard and suspected peak assignments: chloride, 1; nitrate, 2; sulfate, 3; formate, 4; fumarate, 5; malate, 6; succinate, 7; glycolate, 8; acetate, 9; lactate, 10; *trans*-cinnamate (IS), 11. Conditions are the same as Figure 2.4.

Both samples contained significant quantities of inorganic anions, but these anions did not interfere with the organic acid analysis. Both samples contained multiple quantifiable mono- and dicarboxylic acids. Also, *trans*-cinnamic acid is shown to be a successful internal standard since no other strong positive peaks were observed. As expected, the natural samples exhibited a noisier baseline than did samples generated from stock solutions. This additional noise interferes with detection of compounds present near the limit of detection. Both samples also contained a relatively strong peak near 6 min that did not match the mobility of any of the analytes from Table 2.1. Experiments are currently underway to determine the identity of this compound.

CONCLUSIONS

A capillary electrophoresis method was developed for the separation and quantification of anions, specifically organic acids, in extracts from atmospheric aerosols. A unique buffer system utilizing piperazine, 1,5-naphthalenedisulfonic acid, and tetradecyltrimethylammonium bromide allowed for simultaneous monitoring of inorganic anions and organic acids using indirect absorbance detection at 280 nm. *Trans*-cinnamic acid was utilized as an internal standard for both migration time and quantification. The effectiveness of the method was verified through analysis of real atmospheric samples. While developed for analysis of atmospheric samples, the method should be generally applicable to the analysis of inorganic and organic anions in a variety of situations, including food and beverage and industrial wastewater applications.

CLOSING COMMENTS

The method developed here was never used extensively because my research turned exclusively to microchip electrophoresis for the online monitoring of atmospheric aerosols. The transition to the microchip was chosen for a variety of reasons, including smaller and less expensive instrumentation, lower required sample quantities, faster analysis times, and easier incorporation into pseudo steady-state online monitoring systems. The most important finding from this work was the identification of the interaction between sulfate and the protonated diamine moiety. Though not shown in the original publication because it was developed after the original study, the propensity for this moiety to bind sulfate can be seen in Figure 2.7, which compares the experimental results to a simulation using PeakMaster,[1] which assumes no binding.

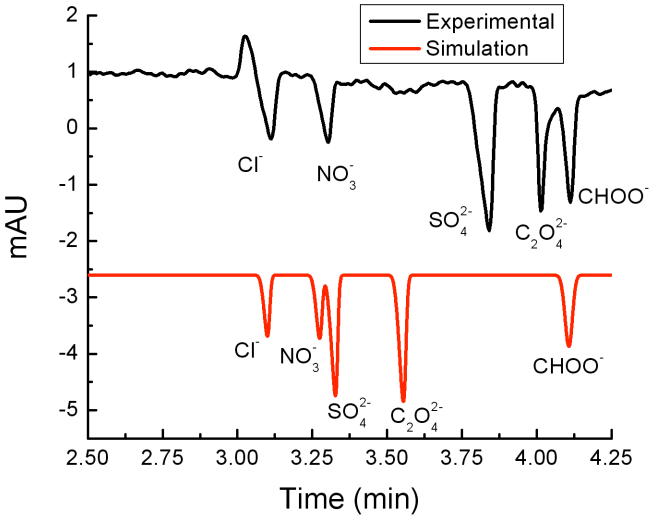

Figure 2.7. Comparison of the experimental results from this work to a PeakMaster[1] simulation at the same conditions. The experimental results show slower migration times for sulfate and oxalate than predicted, indicating binding between these dianions and the protonated diamine functionality in piperazine.

Both sulfate and oxalate are found to migrate significantly slower in reality than predicted by the simulation. This observation is strong evidence for binding between the dianions and the piperazine buffer. However, the binding constants of protonated piperazine to these ions have not been measured. In ongoing work, the binding constants of other protonated diamines to a variety of dianions have been measured by affinity capillary electrophoresis. Initial studies estimate the respective binding constants of sulfate and oxalate to protonated ethylenediamine at 58.2 and 49.2 M^{-1} at an ionic strength of 15 mM. The binding was confirmed to only be significant for the diprotonated species and is therefore heavily pH dependent. Switching to a 1,3-diamine, specifically bis-tris propane, changes the affinity considerably with only a small change in selectivity, and the measured binding constants are 17.2 and 15.7 M^{-1}, respectively. The interaction of this protonated moiety with dianions was exploited in the microchip

separation chemistry described in chapter 5 and is critical to resolving chloride, sulfate, and nitrate at low ionic strength. Ongoing research is being performed to measure binding constants of these species to dianions and to determine any selectivity trends.

REFERENCES

1. Jaros, M.; Hruska, V.; Stedry, M.; Zuskova, I.; Gas, B., *Electrophoresis* **2004,** *25*, 3080-3085.
2. Noblitt, S. D.; Mazzoleni, L. R.; Hering, S. V.; Collett, J. L.; Henry, C. S., *J. Chromatogr. A* **2007,** *1154*, 400-406.
3. Dabek-Zlotorzynska, E.; Aranda-Rodriguez, R.; Graham, L., *J. Sep. Sci.* **2005,** *28*, 1520-1528.
4. Galli, V.; Garcia, A.; Saavedra, L.; Barbas, C., *Electrophoresis* **2003,** *24*, 1951-1981.
5. Harrison, R. M.; Jones, A. M.; Lawrence, R. G., *Atmos. Environ.* **2004,** *38*, 4531-4538.
6. Karthikeyan, S.; Balasubramanian, R., *Microchem. J.* **2006,** *82*, 49-55.
7. Kawamura, K.; Yasui, O., *Atmos. Environ.* **2005,** *39*, 1945-1960.
8. Mato, I.; Suarez-Luque, S.; Huidobro, J. F., *Food Res. Int.* **2005,** *38*, 1175-1188.
9. Saxena, P.; Hildemann, L. M.; McMurry, P. H.; Seinfeld, J. H., *J. Geophys. Res-Atmos.* **1995,** *100*, 18755-18770.
10. Seaton, A.; Macnee, W.; Donaldson, K.; Godden, D., *Lancet* **1995,** *345*, 176-178.
11. Chebbi, A.; Carlier, P., *Atmos. Environ.* **1996,** *30*, 4233-4249.
12. Fisseha, R.; Dommen, J.; Gaeggeler, K.; Weingartner, E.; Samburova, V.; Kalberer, M.; Baltensperger, U., *J. Geophys. Res-Atmos.* **2006,** *111*.
13. Lee, P. K. H.; Brook, J. R.; Dabek-Zlotorzynska, E.; Mabury, S. A., *Environ. Sci. Technol.* **2003,** *37*, 4831-4840.
14. Mochida, M.; Kawabata, A.; Kawamura, K.; Hatsushika, H.; Yamazaki, K., *J. Geophys. Res-Atmos.* **2003,** *108*.
15. Seinfeld, J. H.; Pandis, S. N., *Atmospheric Chemistry and Physics: From Air Pollution to Climate Change*. Wiley: New York, 1998.
16. Orzechowska, G. E.; Nguyen, H. T.; Paulson, S. E., *J. Phys. Chem. A* **2005,** *109*, 5366-5375.
17. Pandis, S. N.; Wexler, A. S.; Seinfeld, J. H., *J. Phys. Chem.* **1995,** *99*, 9646-9659.
18. McFiggans, G.; Artaxo, P.; Baltensperger, U.; Coe, H.; Facchini, M. C.; Feingold, G.; Fuzzi, S.; Gysel, M.; Laaksonen, A.; Lohmann, U.; Mentel, T. F.; Murphy, D. M.; O'Dowd, C. D.; Snider, J. R.; Weingartner, E., *Atmos. Chem. Phys.* **2006,** *6*, 2593-2649.
19. Poschl, U., *Angew. Chem. Int. Ed.* **2005,** *44*, 7520-7540.
20. Kawamura, K., *Anal. Chem.* **1993,** *65*, 3505-3511.
21. Masson, P., *J. Chromatogr. A* **2000,** *881*, 387-394.
22. Park, Y. J.; Kim, K. R.; Kim, J. H., *J. Agri. Food Chem.* **1999,** *47*, 2322-2326.
23. Ray, J.; McDow, S. R., *Atmos. Environ.* **2005,** *39*, 7906-7919.
24. Simon, P. K.; Dasgupta, P. K., *Anal. Chem.* **1995,** *67*, 71-78.
25. Ullah, S. M. R.; Takeuchi, M.; Dasgupta, P. K., *Environ. Sci. Technol.* **2006,** *40*, 962-968.
26. Adler, H.; Siren, H.; Kulmala, M.; Riekkola, M. L., *J. Chromatogr. A* **2003,** *990*, 133-141.
27. Dabek-Zlotorzynska, E.; Piechowski, M.; McGrath, M.; Lai, E. P. C., *J. Chromatogr. A* **2001,** *910*, 331-345.
28. Gao, S. D.; Rudolph, J., *J. Chromatogr. Sci.* **2004,** *42*, 323-328.

29. Tam, W. F. C.; Tanner, P. A.; Law, P. T. R.; Bachmann, K.; Potzsch, S., *Anal. Chim. Acta* **2001,** *427*, 259-269.
30. Dabek-Zlotorzynska, E.; Dlouhy, J. F., *J. Chromatogr. A* **1995,** *706*, 527-534.
31. Krivacsy, Z.; Molnar, A.; Tarjanyi, E.; Gelencser, A.; Kiss, G.; Hlavay, J., *J. Chromatogr. A* **1997,** *781*, 223-231.
32. Dabek-Zlotorzynska, E.; Aranda-Rodriguez, R.; Buykx, S. E. J., *Anal. Bioanal. Chem.* **2002,** *372*, 467-472.
33. Dabek-Zlotorzynska, E.; Kelly, M.; Chen, H.; Chakrabarti, C. L., *Anal. Chim. Acta* **2003,** *498*, 175-187.
34. Dabek-Zlotorzynska, E.; Kelly, M.; Chen, H. D.; Chakrabarti, C. L., *Chemosphere* **2005,** *58*, 1365-1376.
35. Iinuma, Y.; Herrmann, H., *J. Chromatogr. A* **2003,** *1018*, 105-115.
36. Garcia, C. D.; Engling, G.; Herckes, P.; Collett, J. L.; Henry, C. S., *Environ. Sci. Technol.* **2005,** *39*, 618-623.
37. Liu, Y.; MacDonald, D. A.; Yu, X. Y.; Hering, S. V.; Collett, J. L.; Henry, C. S., *Analyst* **2006,** *131*, 1226-1231.
38. Dabek-Zlotorzynska, E.; Dlouhy, J. F., *J. Chromatogr. A* **1994,** *671*, 389-395.
39. Dabek-Zlotorzynska, E.; Dlouhy, J. F., *J. Chromatogr. A* **1994,** *685*, 145-153.
40. Souza, S. R.; Tavares, M. F. M.; de Carvalho, L. R. F., *J. Chromatogr. A* **1998,** *796*, 335-346.
41. Souza, S. R.; Vasconcellos, P. C.; Carvalho, L. R. F., *Atmos. Environ.* **1999,** *33*, 2563-2574.
42. Dabek-Zlotorzynska, E.; Piechowski, M.; Keppel-Jones, K.; Aranda-Rodriguez, R., *J. Sep. Sci.* **2002,** *25*, 1123-1128.
43. Masar, M.; Bodor, R.; Kaniansky, D., *J. Chromatogr. A* **1999,** *834*, 179-188.
44. Virtanen, P.; Korpela, T.; Paavilainen, S., *J. Sep. Sci.* **2001,** *24*, 141-147.
45. Herckes, P.; Leenheer, J. A.; Collett, J. L., *Environ Sci Tech* **2006,** *ASAP*.
46. Doble, P.; Haddad, P. R., *J. Chromatogr. A* **1999,** *834*, 189-212.
47. Johns, C.; Macka, M.; Haddad, P. R., *Electrophoresis* **2003,** *24*, 2150-2167.
48. Wang, T.; Hartwick, R. A., *J. Chromatogr.* **1992,** *589*, 307-313.
49. Beckers, J. L., *J. Chromatogr. A* **1994,** *662*, 153-166.
50. Beckers, J. L., *J. Chromatogr. A* **1996,** *741*, 265-277.
51. Beckers, J. L., *J. Chromatogr. A* **1997,** *764*, 111-126.
52. Doble, P.; Haddad, P. R., *Anal. Chem.* **1999,** *71*, 15-22.
53. Motellier, S.; Gurdale, K.; Pitsch, H., *J. Chromatogr. A* **1997,** *770*, 311-319.
54. Doble, P.; Macka, M.; Haddad, P. R., *J. Chromatogr. A* **1998,** *804*, 327-336.
55. Johns, C.; Macka, M.; Haddad, P. R., *Electrophoresis* **2000,** *21*, 1312-1319.
56. Johns, C.; Shaw, M. J.; Macke, M.; Haddad, P. R., *Electrophoresis* **2003,** *24*, 557-566.
57. Meszaros, R.; Thompson, L.; Bos, M.; Varga, I.; Gilanyi, T., *Langmuir* **2003,** *19*, 609-615.
58. Sidhu, J.; Bloor, D. M.; Couderc-Azouani, S.; Penfold, J.; Holzwarth, J. F.; Wyn-Jones, E., *Langmuir* **2004,** *20*, 9320-9328.
59. Shamsi, S. A.; Danielson, N. D., *Anal. Chem.* **1994,** *66*, 3757-3764.
60. Bruin, G. J. M.; Vanasten, A. C.; Xu, X. M.; Poppe, H., *J. Chromatogr.* **1992,** *608*, 97-107.

61. Poppe, H., *Anal. Chem.* **1992,** *64*, 1908-1919.
62. Horvath, J.; Dolnik, V., *Electrophoresis* **2001,** *22*, 644-655.
63. Kaneta, T.; Tanaka, S.; Taga, M., *J. Chromatogr. A* **1993,** *653*, 313-319.
64. Lucy, C. A.; Underhill, R. S., *Anal. Chem.* **1996,** *68*, 300-305.
65. Tavares, M. F. M.; Colombara, R.; Massaro, S., *J. Chromatogr. A* **1997,** *772*, 171-178.
66. Fung, Y. S.; Lau, K. M., *Electrophoresis* **2003,** *24*, 3224-3232.
67. Quirino, J. P.; Terabe, S., *J. Chromatogr. A* **2000,** *902*, 119-135.

CHAPTER 3. INTEGRATED MEMBRANE FILTERS FOR MINIMIZING HYDRODYNAMIC FLOW AND FILTERING IN MICROFLUIDIC DEVICES

CHAPTER FOREWORD

Early in the development of a microchip electrophoresis system for online aerosol analysis, there was concern that insoluble particles in the sample would clog the microfluidic channels. To remedy this, I developed a process to include polycarbonate filter membranes between the sample reservoir and the microfluidic channel. Membranes also served to dampen hydrodynamic flow, improving performance when connected to samplers that utilize a pressure drop for sampling. The work was published in the journal *Analytical Chemistry*,[1] and the text and figures from that publication are used here. Though successful, the membrane approach was ultimately abandoned during the development of the aerosol-monitoring instrument. There were two primary reasons for this. First, the need for filtering was precluded by operating the microchip in counter-EOF mode, which excluded all but highly charged species from entering the capillary. Second, the hydrodynamic flow reduction was superseded by an isobaric air duct network (see chapter 6) that eliminated all pressure-driven flow in the microchip. Nevertheless, the work is included here because it was important in the development of the aerosol monitoring system and will be useful in other areas of research.

ABSTRACT

Microfluidic devices have gained significant scientific interest due to the potential to develop portable, inexpensive analytical tools capable of quick analyses with low sample consumption. These qualities make microfluidic devices attractive for point-of-use measurements where traditional techniques have limited functionality. Many samples of interest in biological and environmental analysis, however, contain insoluble particles that can block microchannels, and manual filtration prior to analysis is not desirable for point-of-use applications. Similarly, some situations involve limited control of the sample volume, potentially causing unwanted hydrodynamic flow due to differential fluid heads. Here, we present the successful inclusion of track-etched polycarbonate membrane filters into the reservoirs of poly(dimethylsiloxane) (PDMS) capillary electrophoresis microchips. The membranes were shown to filter insoluble particles with selectivity based on the membrane pore diameter. Electrophoretic separations with membrane-containing microchips were performed on cations, anions, and amino acids and monitored using conductivity and fluorescence detection. The dependence of peak areas on head pressure in gated injection was shown to be reduced by up to 92%. Results indicate that separation performance is not hindered by the addition of membranes. Incorporating membranes into the reservoirs of microfluidic devices will allow for improved analysis of complex solutions and samples with poorly controlled volume.

INTRODUCTION

The field of microfluidics has grown rapidly in diversity during the past decade. Modern microfluidic chips are capable of capillary electrophoresis (CE), liquid chromatography, derivatization, immunoassays, enzymatic digestions, polymerase chain reaction (PCR), coupling to mass spectrometry, microdialysis, valving and pumping, and liquid-liquid extractions and have been reviewed extensively.[2] Combining several of these techniques onto a single, concerted microchip is done with the goal of developing miniaturized total analysis systems (μTAS). Such integrated systems exhibit increased functionality and should have a comparable increase in performance.[2]

One area requiring improvement in the μTAS field is the ability to directly analyze complex liquid samples without concern over sample volume or suspended particulate matter. One approach to managing unknown sample size and particulate matter is to incorporate nanoporous membranes in the microfluidic chip to retard hydrodynamic flow and filter the sample. Several groups have already incorporated membranes into microchips. Applications include microdialysis,[3-10] filtering of cells or blood,[10-14] protein digestion,[15,16] membrane chromatography,[16,17] pumping,[18] desalting of proteins prior to MS analysis,[19,20] gated injection and construction of multilayer microchips,[21-29] gas sensing,[30] creating an electrospray ionization (ESI) interface,[31] establishing pH gradients,[28] liquid-liquid extraction,[32] and electrophoretic stacking.[33] Sweedler, Bohn, and coworkers have characterized flow properties through nanoporous membranes incorporated in microfluidic channels.[34,35] They found that fluid flow through nanofluidic membranes was dependent on ionic strength, pore diameter, pH, and relative

hydrophilicity of the membrane material. Membrane materials commonly used in microchips include polycarbonate (PC)[8,11-14,21-29] and poly(vinylidene fluoride) (PVDF),[15-17,19,20] although other materials can be used as well.[13] A wide variety of microchip substrate materials have been used for incorporating membranes including PC,[4,31] poly(methyl methacrylate) (PMMA),[28,29,36] poly(dimethylsiloxane) (PDMS),[7,12-17,21-28,37,38] glass,[8,31,32] and polyimide.[37] Two reviews cover the developments of membranes in microfluidic devices in more detail.[39,40]

In the current literature, most membranes are placed between microfluidic channels at junctions, although Thorslund et al. placed a membrane between the sample reservoir and a network of microchannels.[13] There are several advantages to placing the membrane at the reservoir. For instance, filtering the sample prior to entrance into any microfluidic channels prevents clogging due to particulates. During electrophoresis, the membrane does not contact the separation channel, avoiding band broadening due to differences in surface composition and charge. One important aspect of membranes in microfluidics that has been mostly ignored is the ability of membranes to reduce hydrodynamic flow because of the small pore size. In microchip CE, reservoir heights must be optimized to prevent unwanted hydrodynamic flow.[41] Pressure heads from solution reservoirs can change injection volume, affect migration times, and decrease separation efficiency.

In this paper we present the successful incorporation of track-etched polycarbonate membrane filters between the reservoirs and microchannels in PDMS microchips. These chips are shown to successfully remove insoluble particles before they can enter the

channel. Separations of cations, anions, and fluorescently-labeled amino acids show the compatibility of the membrane method with different analyte types, background electrolytes, electroosmotic flows, detection methods, and injection methods. The separation performance with a range of reservoir heights is characterized for microchips without membranes, with a membrane on only the sample reservoir, and membrane inclusion on all four reservoirs. The results show the potential of the membrane filters to improve analyses for a variety of applications where suspended particles and unequal reservoir heights can be problematic.

MATERIALS AND METHODS

Materials

Potassium chloride, magnesium sulfate heptahydrate, sodium nitrate, sodium bicarbonate, sodium tetraborate, sodium dodecyl sulfate (SDS), boric acid, glutamic acid, L-histidine (HIS), dimethyl sulfoxide (DMSO) toluene, ethyl acetate, and acetone were purchased from Fisher Scientific. Oxalic acid, 1,2-diaminocyclohexane (DACH, mixture of *cis*- and *trans*-), and propylene glycol methyl ether acetate were obtained from Aldrich. N-dodecyl-N,N-dimethyl-3-ammonio-1-propanesulfonate (DDAPS), 3-morpholino-2-hydroxypropanesulfonic acid (MOPSO), and L-arginine were purchased from Sigma. Fluorescein-5-isothiocyanate (FITC Isomer I) was purchased from Invitrogen. Piperazine was obtained from Acros Organics. Amino acids used for fluorescent labeling were obtained from Fluka. All chemicals were used without further purification. Solutions were prepared in 18.2 MΩ*cm water from a Milli-Q purification system. Gold microwires (25-μm diameter) were obtained from GoodFellow Corp. Track-etched

polycarbonate membranes with pore sizes of 200 nm and 800 nm were purchased from Whatman. Fluorescent particles were obtained from Duke Scientific.

Microchip Construction

Construction of PDMS microchips,[42] inclusion of microwires for electrochemical detection,[43] and the extraction of PDMS oligomers from the bulk polymer[44] were performed as described previously and are summarized below. 100-mm silicon wafers (Silicon Inc.) were cleaned with acetone and then spin coated with SU-8 (Microchem) photoresist at 2100 rpm. A negative mask was placed on the wafer, exposed to ultraviolet light, and developed in propylene glycol methyl ether acetate to give a positive relief of the microchannels on the wafer surface. Sylgard 184 (Dow Corning) elastomer was mixed with crosslinking agent (10:1 ratio), degassed under vacuum, poured onto the wafer, and cured at 60 °C for at least 2 hours. Reservoirs were cut with 3- or 4-mm biopsy punches (Robbins Instruments). Irreversible sealing of the PDMS was accomplished with a 45-s air plasma exposure at 18 W (Harrick Scientific PDC-32G) followed by conformal contact of the oxidized pieces. For extracted chips, oligomers were removed by submerging cured PDMS chips in toluene, ethyl acetate, and acetone, respectively, for at least 2 hours each. Extracted chips were sealed with a 2-min plasma exposure according to previously published work.[44]

For microchips utilizing conductivity detection, gated injection was used.[45] Channel widths were 76 μm, injection arms were 7 mm in length, separation channel length was 4 cm, and detection-to-waste spacing was 3 mm. Microwire spacing was 150 μm center-

to-center. For microchips using fluorescence detection, a double-T intersection was used for pinched injection. Channel widths were 50 μm, while injection arms were 7 mm long with a 250-μm offset. Fluorescence detection was performed 1.5 cm down channel from the double-T intersection.

Inclusion of a membrane in a microfluidic device requires formation of a good seal to prevent leakage and dead volume. PDMS prepolymer has been shown to be effective in aiding sealing when used as a glue.[21,29] Figure 3.1 schematically shows the inclusion of a membrane into a microfluidic device. Uncured PDMS was spin-coated (1500 rpm) onto a blank piece of cured PDMS. Reservoir holes were cut in the desired locations using biopsy punches (3 or 4 mm, depending on experiment). The membrane was cut to the desired size (slightly larger than the reservoir) and shape with scissors then placed over the reservoir. The uncured PDMS soaked into the pores of the membrane, helping to flatten the membrane to the chip. No significant lateral diffusion of the polymer into the reservoir area of the membrane was observed.

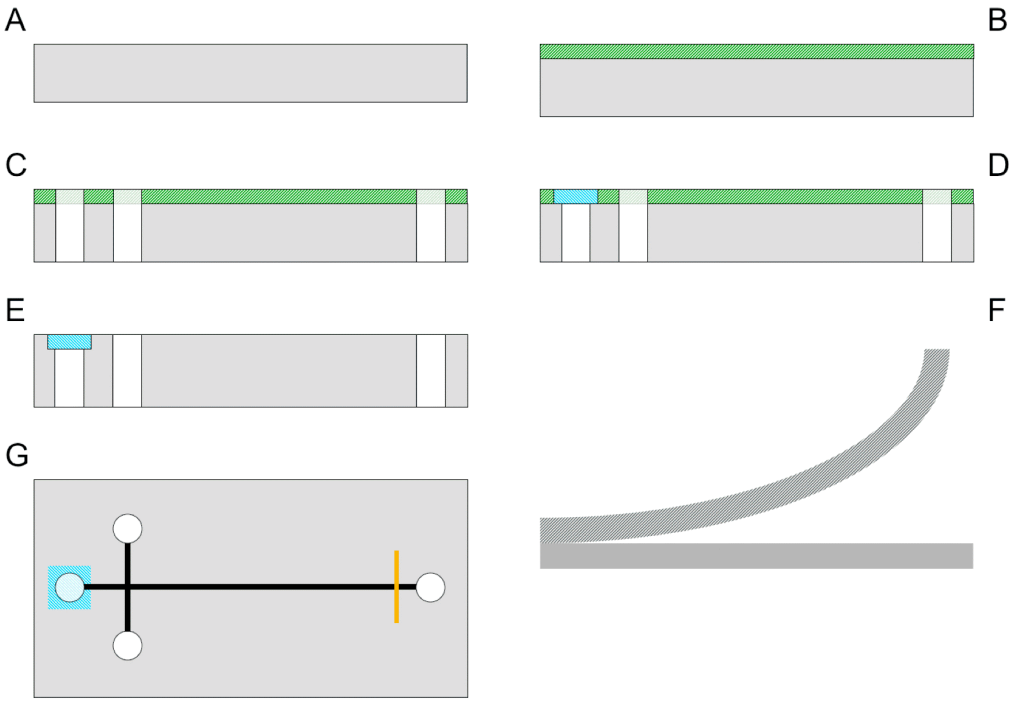

Figure 3.1. Construction steps for membrane inclusion: (a) start with a PDMS blank, (b) spin-coat a layer of uncured PDMS on the blank substrate, (c) punch reservoir holes, (d) place membrane over reservoir, (e) cure PDMS in oven at 60 °C, (f) use a rolling motion to help ensure air bubbles avoid microchannels during sealing, (g) top-down view of constructed microchip with membrane on sample reservoir.

This half of the microchip was cured at 60°C for at least 40 min. After curing, the membrane side of the chip was plasma sealed to the channel side to form an irreversible seal. Poor sealing of the membrane could result in leakage zones at the membrane edge where bubbles of unsealed PDMS could be present (Figure 3.2). Occurrences of this poor seal were reduced by using a relatively thin (< 2 mm) blank piece of PDMS for the membrane side of the chip and applying additional pressure in the membrane region of chip during the sealing process. Problems could also be avoided by rolling (Figure 3.1f) the PDMS during sealing to ensure any air bubbles avoided the microchannel, similar to the approach of Hediger et al. with paraffin foil and glue.[11]

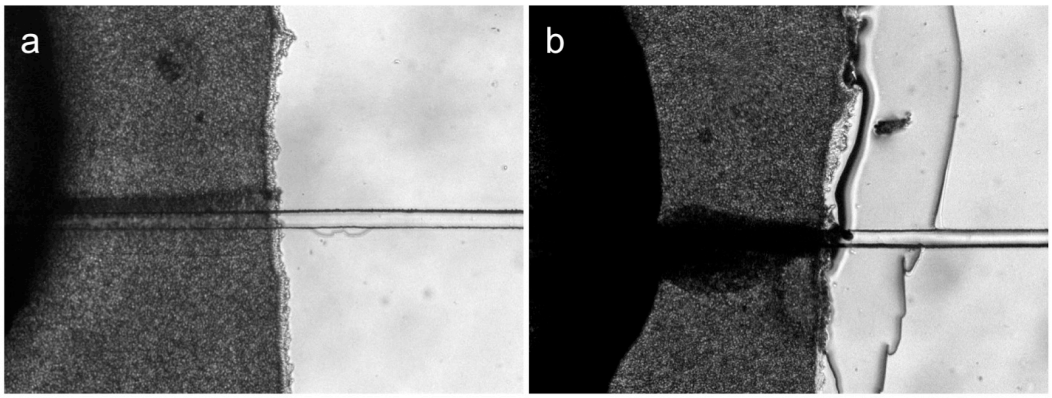

Figure 3.2. Bright field images showing (a) a well-sealed membrane with no air pocket formation; (b) air pocket formation at the membrane edge due to poor PDMS sealing.

For membrane incorporation into extracted PDMS, the above procedure was modified since the spin coated PDMS is unextracted. A sacrificial piece of PDMS was spin-coated with un-cured PDMS followed by punching reservoirs using the biopsy punch. The membrane was applied to the sacrificial piece and prepolymer allowed to soak into the pores. The membrane was then transferred to an extracted PDMS piece, placed over the desired reservoir, and cured. The remainder of the sealing process remained the same, and no difference in sealing success rate was observed between the two methods.

FITC Labeling of Amino Acids

Stock solutions of amino acids (10 mM) were prepared in 10-mM sodium bicarbonate, pH 9.0. Solutions of 1-mM FITC I isomer were prepared fresh daily in DMSO. Each amino acid was labeled with FITC individually by combining 90 μL of 10-mM amino acid solution and 10 μL of 1-mM FITC then reacted in the dark for 2 hours with gentle

mixing. Mixtures of derivatized amino acids were prepared in the BGE (10-mM borate, 1-mM SDS, pH 9.0) and diluted to 5 μM prior to injection.

Instrumentation

The high voltage power supplies used for capillary electrophoresis were described previously.[46] Fluorescence data was acquired with a Nikon Eclipse TE2000-U microscope and Photometrics Cool Snap HQ^2 camera at 20 Hz. Electropherograms were generated using Metamorph software and filtered with a 3-point median filter. Conductivity detection was accomplished by connecting the leads of a Dionex CD20 to the detection microwires. The CD20 was set to monitor the 0-200-μS range and output 0-1 V. Output from the CD20 was monitored with a National Instruments USB-6210 DAQ and LabView 8.0 software. Data was collected at 20 kHz and every 2000 points boxcar averaged to give an effective collection rate of 10 Hz. This data was smoothed with a rectangular half-width of two points.

RESULTS AND DISCUSSION

Filtering of Particulate Matter

Membrane performance was first measured by testing the ability of the membranes to pass small molecules while retaining larger objects. Microchips were constructed with one straight channel connecting a membrane-containing reservoir to a reservoir without a membrane. The fluorescence of the solution in the channel at the membrane edge could then be monitored to see if fluorescent components passed through the membrane and down the channel. This measurement was performed both before and after voltage

application. When a solution of fluorescein was tested, fluorescence was observed to travel down the channel just as it would without a membrane, confirming the membranes permit small molecules to migrate into the channel. To test membrane performance for larger components, 500-nm rhodamine-containing polystyrene particles were used. The results are shown in Figure 3.3. Prior to applying a voltage to the reservoir, no particles were observed in the channel. When a voltage was applied to the channel, particles were observed to pass through a 800-nm pore membrane and down the microchannel. The same experiment with a 200-nm pore membrane showed no particles entering the channel. The results confirm that the membranes can selectively dictate what components enter the microfluidic channel based on size. One benefit of filtering at the reservoir appears in applications involving particulate-containing samples. With on-chip filtering, channel clogging is prevented.

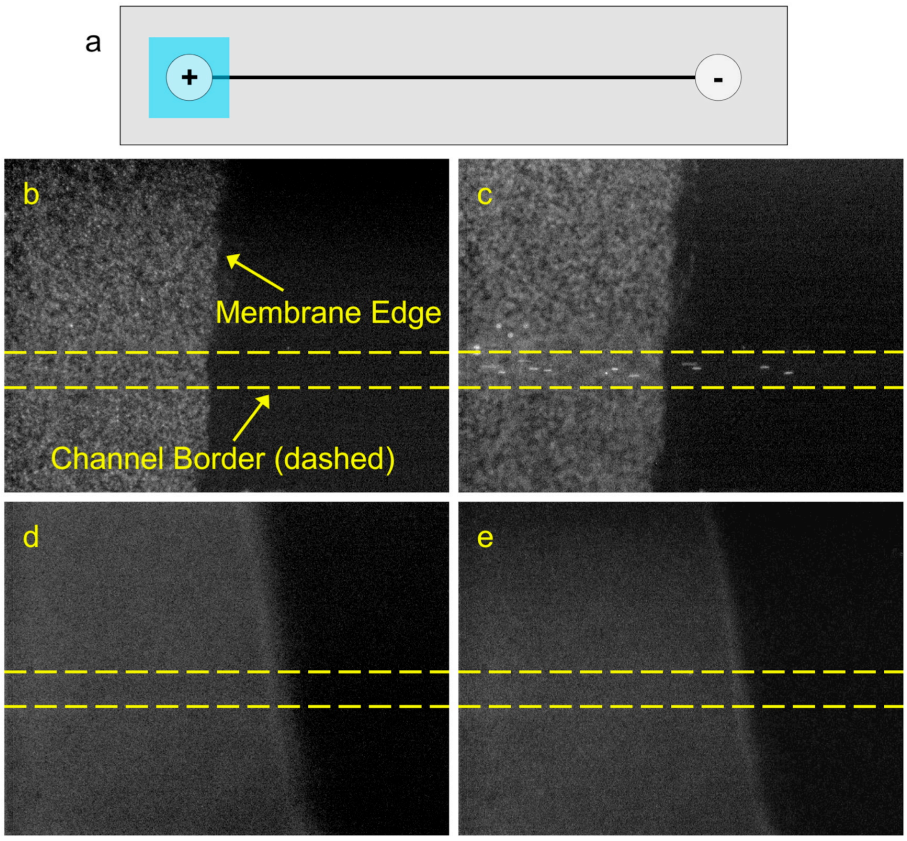

Figure 3.3. (a) Membrane chip and voltage configuration (b) 800-nm pore membrane edge prior to voltage application shows no particles. (c) 800-nm pore membrane edge after applying voltage shows 500-nm particles have passed through membrane and into channel. (d) 200-nm pore membrane edge prior to voltage application shows no particles. (e) 200-nm pore membrane edge after applying voltage shows no particles, indicating successful filtration.

Electrophoretic Separations

The compatibility of membrane incorporation with capillary electrophoresis was confirmed next. A separation of the anions chloride, nitrate, sulfate, and oxalate is shown in Figure 3.4a, while an example cation separation of potassium, sodium, piperazine, and arginine is shown in Figure 3.4b.

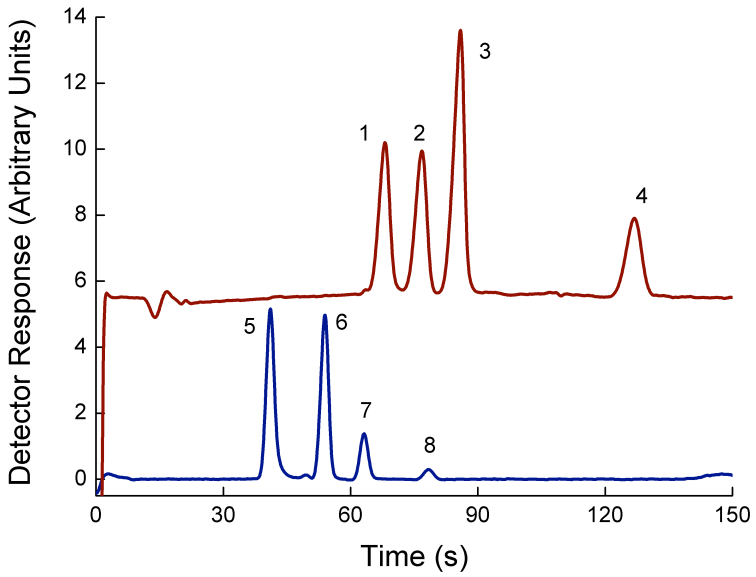

Figure 3.4. Separation of anions (top) and cations (bottom) using gated injection and conductivity detection; peak identities are (1) chloride, (2) nitrate, (3) sulfate, (4) oxalate, (5) potassium, (6) sodium, (7) piperazine, (8) L-arginine. Separation electric fields of –110 V cm^{-1} used for anions and +110 V cm^{-1} for cations. Anion BGE: pH 3.9; 10-mM glutamic acid; 1.2-mM DACH; 10-mM DDAPS; 0.2-mM EDTA. Cation BGE: pH 6.4; 15-mM MOPSO; 15-mM HIS; 5-mM DDAPS.

These two separations exhibit the compatibility of the membranes with hydrophilic compounds and gated injection. No change in migration order, relative peak height, or band broadening was observed between membrane chips and nonmembrane chips, showing the advantage of placing the membrane away from the separation channel. For instance, chips without membranes gave a sulfate (50 μM) peak area of 241 ± 31 (arbitrary units), whereas chips with membranes on all four reservoirs showed a peak area of 255 ± 37, which is not statistically different (Figure 3.5).

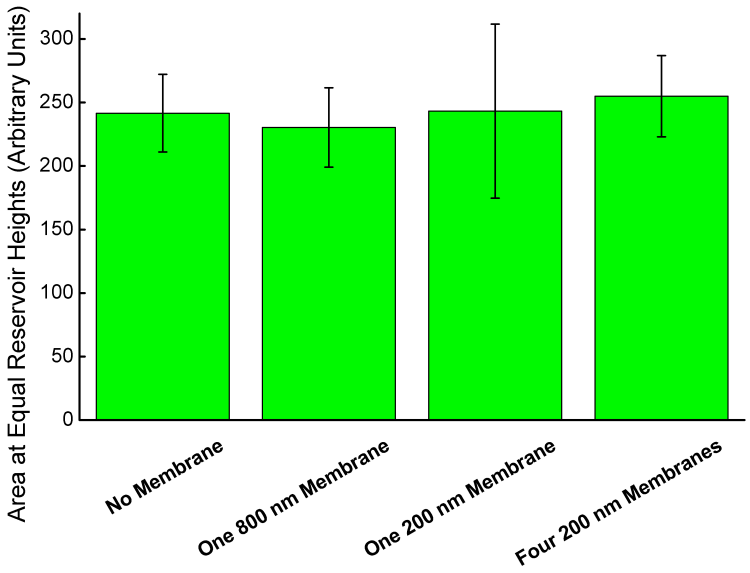

Figure 3.5. Comparison of non-membrane and membrane chips when all reservoir heights are equal. Y-axis is the peak area of 50-μM sulfate using the conditions in Figure 3.4. Error bars are standard deviations of peak areas for three microchips. No significant differences between membrane and non-membrane chips are observed.

No significant effect was observed on the electrophoretic separation, so membranes can be added to many existing analyses without modifying separation protocols. To test membranes with relatively hydrophobic compounds, pinched injection, and extracted PDMS, fluorescently labeled amino acids were separated. Figure 3.6 shows separations of FITC-labeled histidine, glycine, and valine with both native PDMS and extracted PDMS surfaces. Extracted PDMS exhibits a faster EOF, as expected. Again, the presence of the membrane has no significant effect on the separation chemistry, showing that the membrane does not inhibit the migration of the analytes of interest. It should be noted that although each example separation utilized background electrolytes containing surfactants, surfactants are not required to permit analyte flow through the membranes, and successful separations were performed without surfactants (data not shown).

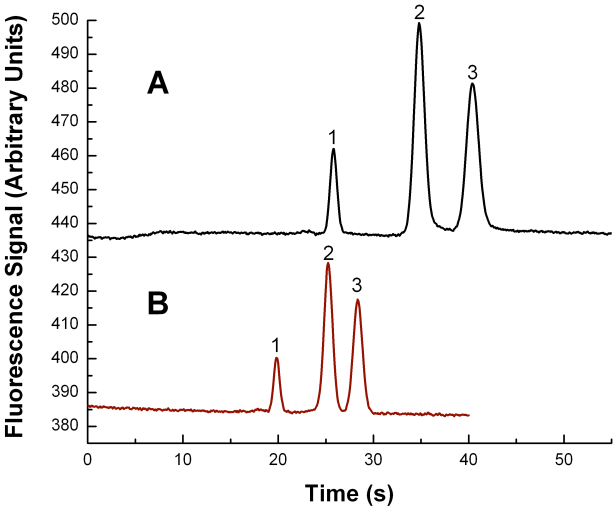

Figure 3.6. Separation of FITC-labeled amino acids with pinched injection and fluorescent detection on native PDMS (A) and extracted PDMS (B). Mixtures of 5-μM histidine (1), valine (2), and glycine (3) were injected for 30 s at 292 V cm^{-1} and separated at 267 V cm^{-1}. Fluorescence was detected 1.5 cm from injection. BGE was 10-mM Borate, 1-mM SDS, pH 9.0.

Dampening Hydrodynamic Flow

Hydrodynamic flow in microchannels caused by differences in fluid pressure heads can be detrimental to separations. The ability of membranes to retard hydrodynamic flow in the microchannels was characterized in gated injection mode by monitoring the peak area of sulfate (50 μM) while varying reservoir heights (Figure 3.7). The three reservoirs containing buffer had equal heights, and their heights were varied with respect to the sample reservoir. For systems without hydrodynamic flow restriction, peak area should scale proportionally to the height difference of the sample and buffer reservoirs due to the effect of hydrodynamic flow on the injected sample size.

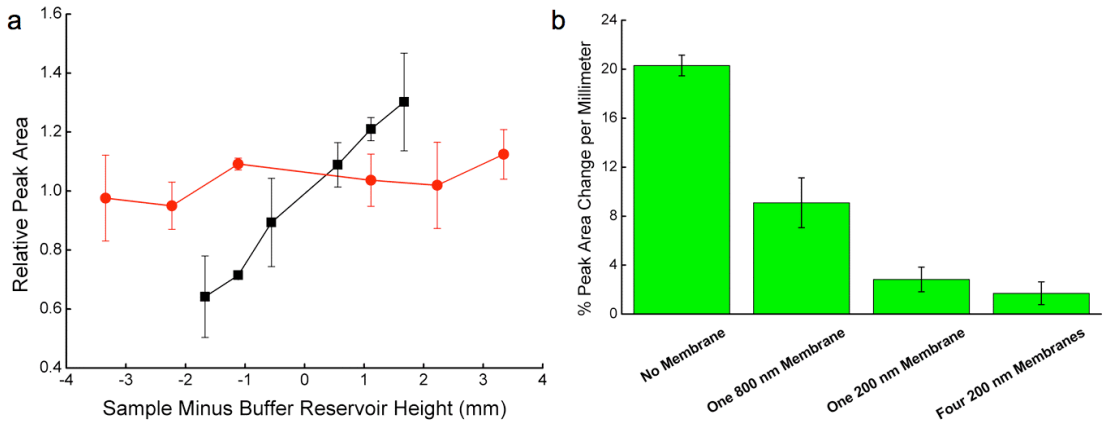

Figure 3.7. (a) Relative peak area of sulfate with changing sample-buffer reservoir heights for a microchip without a membrane and one with membranes on all four reservoirs. Conditions are the same as those used for the anions in Figure 3.4. Error bars are standard deviations of three chips. (b) Slopes of the plot shown in 'a' for several membrane configurations. Error bars are 95% confidence intervals.

Microchips without membranes are sensitive to this trend, showing peak area changes of 20% per millimeter of reservoir height. For instance, when the sample height was 1.1 mm above that of the buffers, peak area increased by 21%. This height difference would require only a 7.8-μL discrepancy between reservoirs when using 3-mm diameter reservoirs. However, peak areas for chips containing membranes show significantly less change with respect to reservoir height differences, even at larger height discrepancies. As expected, smaller pore membranes perform better than those with larger pores. 800-nm membranes reduced hydrodynamic dependence of peak area by 55%, while 200-nm membranes reduced peak area dependence by 86%. Placing 200-nm membranes on every reservoir dampened hydrodynamic flow even more effectively than using only a single membrane, reducing the peak area dependence by 92%. At the same 1.1-mm height difference mentioned earlier for nonmembrane chips, a peak area increase of only 2% was observed, approximately ten times less than the effect seen in chips without

membranes. Similar trials with pinched injection and fluorescent compounds also showed benefit from the membranes. When the sample was 1 mm below the buffer, the injection arm would not fill with analyte on microchips lacking membranes, so no separations could be performed. When a membrane was included on the sample reservoir, this problem was not encountered. Additionally, analyte peak areas were less sensitive to reservoir height when a membrane was included on the sample reservoir than when no membrane was used. Sensitivity to the pressure head from the reservoirs was decreased by ~60% when a 200-nm pore membrane was placed on the sample reservoir in pinched injection (Figure 3.8).

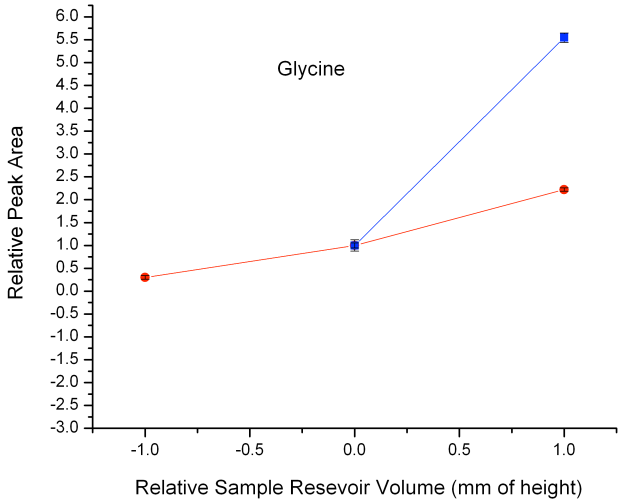

Figure 3.8. Hydrodynamic effects for double-T microchips utilizing pinched injection. 5-µM glycine analyte with the same conditions as Figure 3.6. Membrane chip (circles) shows much less sensitivity to reservoir head than non-membrane chip (squares).

The ability of membranes to reduce hydrodynamic flow allows the use of different solution volumes in different reservoirs without losing quantitative accuracy. Some potential applications include the analysis of small samples where buffer reservoirs have

fluid heights above the sample, situations where sample volume cannot be strictly controlled, three-dimensional microfluidic chips with reservoirs located on different chip levels, and adaptation to automatic sampling interfaces that may operate at pressures slightly above or below atmospheric pressure.

Reproducibility and Durability

Although the construction of membrane-containing microchips does require some degree of technique, the inclusion of the membranes onto the reservoir is fairly robust. We found that following the construction scheme shown in Figure 3.1 yielded 40 successful chips in 41 attempts (98%), where success was considered a membrane that had a good seal with the channel and no leakage of solution at the membrane interface. For best dampening of hydrodynamic flow, we observed that the membrane area under the reservoir must be free of dead volume and therefore the membrane should have no creases or wrinkles. With this stipulation, 34 successful chips were prepared in 41 attempts (83%). Additionally, after construction of the device, the membrane could be creased by either flexing the PDMS at the membrane location or by applying considerable pressure (no exact value measured, but at least several PSI) to the microfluidic system.

CONCLUSIONS

The successful incorporation of polycarbonate track-etched membranes between the reservoirs and microchannels of PDMS microfluidic devices was demonstrated. Membranes were shown to filter polystyrene microparticles, preventing them from

entering the microchannel underneath the reservoir. Filtering was shown to be size selective and dependent on membrane pore diameter. Separations of cations, anions, and fluorescently labeled amino acids demonstrated the compatibility of the membranes with both gated and pinched injections and fluorescence and conductivity detection. The monitoring of analyte peak area at various sample reservoir volumes showed the ability of membranes to dampen hydrodynamic flow in microfluidic chips. Results indicate that including membranes into the reservoirs of microfluidic chips will protect the microchannels from particulate matter and help to increase the ruggedness and applicability of microchip capillary electrophoresis analyses in situations applications of limited or uncontrolled sample volume and high sample complexity.

CLOSING COMMENTS

Although originally intended as way to avoid interference from insoluble particles and unwanted hydrodynamic flow when connected to an aerosol collector during online monitoring, these functionalities were instead respectively gained through counter-EOF operation and an isobaric air duct network, so the membrane approach was abandoned. However, membrane inclusion using the described method may still be useful in other areas of research. Because this work was my first experience in developing microfluidic technology, several of my protocols were inferior to what I later used. For instance, measurement of the reduction in hydrodynamic flow was accomplished by monitoring the peak area of 50-μM sulfate, which was injected from a sample matrix of water. Sample matrixes composed of buffer yield more reproducible results. Results could have been further improved by monitoring multiple species at the same time, and the actual

linear velocity changes of the bulk solution in the separation channel could have been monitored via the analyte migration times. Also, at the time of this work, my microchips were not yet designed from the standpoint of electric field modeling. Electric field modeling is described in Appendix 1 and was included in this project during the time between the development described in chapters 2 and 3. After implementing this approach, the functionality and reproducibility of the microchip performance increased. Detection performance has also improved since this work. Specifically, the implementation of a bubble cell detection zone (see chapter 4) improved the signal-to-noise ratio and allowed higher fields to be utilized. Detection reproducibility has increased through modifications in the microchip construction protocol. Therefore, I suggest that if the methods developed in this chapter are utilized in the future, all of the aforementioned improvements should be employed. Despite the fact that the membrane method is no longer used, several other parts of this chapter are still important. Specifically, the original publication of this work was the first report of using the Dionex CD20 detector for conductivity detection in microchip electrophoresis. Another novelty is the anion separation shown in Figure 3.4. It used diaminocyclohexane to complex sulfate and separates it from nitrate, thus supporting the hypothesis presented in chapter 2 that the protonated 1,2-diamine moiety can bind sulfate.

REFERENCES

1. Noblitt, S. D.; Kraly, J. R.; VanBuren, J. M.; Hering, S. V.; Collett, J. L.; Henry, C. S., *Anal. Chem.* **2007,** *79*, 6249-6254.
2. Dittrich, P. S.; Tachikawa, K.; Manz, A., *Anal. Chem.* **2006,** *78*, 3887-3907.
3. Xu, N. X.; Lin, Y. H.; Hofstadler, S. A.; Matson, D.; Call, C. J.; Smith, R. D., *Anal. Chem.* **1998,** *70*, 3553-3556.
4. Lamoree, M. H.; van der Hoeven, R. A. M.; Tjaden, U. R.; van der Greef, J., *J. Mass Spectrom.* **1998,** *33*, 453-460.
5. Xiang, F.; Lin, Y. H.; Wen, J.; Matson, D. W.; Smith, R. D., *Anal. Chem.* **1999,** *71*, 1485-1490.
6. Martin, P. M.; Matson, D. W.; Bennett, W. D.; Lin, Y.; Hammerstrom, D. J., *J. Vac. Sci. Technol., A* **1999,** *17*, 2264-2269.
7. Jiang, Y.; Wang, P. C.; Locascio, L. E.; Lee, C. S., *Anal. Chem.* **2001,** *73*, 2048-2053.
8. Hsieh, Y. C.; Zahn, J. D., *Sensor. Actuat. B-Chem.* **2005,** *107*, 649-656.
9. Song, S.; Singh, A. K.; Shepodd, T. J.; Kirby, B. J., *Anal. Chem.* **2004,** *76*, 2367-2373.
10. Kurita, R.; Yabumoto, N.; Niwa, O., *Biosens. Bioelectron.* **2006,** *21*, 1649-1653.
11. Hediger, S.; Fontannaz, J.; Sayah, A.; Hunziker, W.; Gijs, M. A. M., *Sensor. Actuat. B-Chem.* **2000,** *63*, 63-73.
12. Hediger, S.; Sayah, A.; Horisberger, J. D.; Gijs, M. A. M., *Biosens. Bioelectron.* **2001,** *16*, 689-694.
13. Thorslund, S.; Klett, O.; Nikolajeff, F.; Markides, K.; Bergquist, J., *Biomed. Microdevices* **2006,** *8*, 73-79.
14. Long, Z. C.; Liu, D. Y.; Ye, N. N.; Qin, J. H.; Lin, B. C., *Electrophoresis* **2006,** *27*, 4927-4934.
15. Gao, J.; Xu, J. D.; Locascio, L. E.; Lee, C. S., *Anal. Chem.* **2001,** *73*, 2648-2655.
16. Jiang, Y.; Lee, C. S., *J. Chromatogr. A* **2001,** *924*, 315-322.
17. Wang, P. C.; Gao, J.; Lee, C. S., *J. Chromatogr. A* **2002,** *942*, 115-122.
18. Effenhauser, C. S.; Harttig, H.; Kramer, P., *Biomed. Microdevices* **2002,** *4*, 27-32.
19. Lion, N.; Gobry, V.; Jensen, H.; Rossier, J. S.; Girault, H., *Electrophoresis* **2002,** *23*, 3583-3588.
20. Lion, N.; Gellon, J. O.; Jensen, H.; Girault, H. H., *J. Chromatogr. A* **2003,** *1003*, 11-19.
21. Ismagilov, R. F.; Ng, J. M. K.; Kenis, P. J. A.; Whitesides, G. M., *Anal. Chem.* **2001,** *73*, 5207-5213.
22. Cannon, D. M.; Kuo, T. C.; Bohn, P. W.; Sweedler, J. V., *Anal. Chem.* **2003,** *75*, 2224-2230.
23. Kuo, T. C.; Cannon, D. M.; Chen, Y. N.; Tulock, J. J.; Shannon, M. A.; Sweedler, J. V.; Bohn, P. W., *Anal. Chem.* **2003,** *75*, 1861-1867.
24. Kuo, T. C.; Cannon, D. M.; Shannon, M. A.; Bohn, P. W.; Sweedler, J. V., *Sensor. Actuat. B-Phys.* **2003,** *102*, 223-233.
25. Tulock, J. J.; Shannon, M. A.; Bohn, P. W.; Sweedler, J. V., *Anal. Chem.* **2004,** *76*, 6419-6425.

26. Iannacone, J. M.; Jakubowski, J. A.; Bohn, P. W.; Sweedler, J. V., *Electrophoresis* **2005,** *26*, 4684-4690.
27. Chang, I. H.; Tulock, J. J.; Liu, J. W.; Kim, W. S.; Cannon, D. M.; Lu, Y.; Bohn, P. W.; Sweedler, J. V.; Cropek, D. M., *Environ. Sci. Technol.* **2005,** *39*, 3756-3761.
28. Fa, K.; Tulock, J. J.; Sweedler, J. V.; Bohn, P. W., *J. Am. Chem. Soc.* **2005,** *127*, 13928-13933.
29. Flachsbart, B. R.; Wong, K.; Iannacone, J. M.; Abante, E. N.; Vlach, R. L.; Rauchfuss, P. A.; Bohn, P. W.; Sweedler, J. V.; Shannon, M. A., *Lab Chip* **2006,** *6*, 667-674.
30. Timmer, B. H.; van Delft, K. M.; Otjes, R. P.; Olthuis, W.; van den Berg, A., *Anal. Chim. Acta* **2004,** *507*, 137-143.
31. Wang, Y. X.; Cooper, J. W.; Lee, C. S.; DeVoe, D. L., *Lab Chip* **2004,** *4*, 363-367.
32. Cai, Z. X.; Fang, Q.; Chen, H. W.; Fang, Z. L., *Anal. Chim. Acta* **2006,** *556*, 151-156.
33. Zhang, Y.; Timperman, A. T., *Analyst* **2003,** *128*, 537-542.
34. Kuo, T. C.; Sloan, L. A.; Sweedler, J. V.; Bohn, P. W., *Langmuir* **2001,** *17*, 6298-6303.
35. Chatterjee, A. N.; Cannon, D. M.; Gatimu, E. N.; Sweedler, J. V.; Aluru, N. R.; Bohn, P. W., *J. Nanopart. Res.* **2005,** *7*, 507-516.
36. Kim, J. E.; Cho, J. H.; Paek, S. H., *Anal. Chem.* **2005,** *77*, 7901-7907.
37. Metz, S.; Trautmann, C.; Bertsch, A.; Renaud, P., *J. Micromech. Microeng.* **2004,** *14*, 324-331.
38. Chueh, B. H.; Huh, D.; Kyrtsos, C. R.; Houssin, T.; Futai, N.; Takayama, S., *Anal. Chem.* **2007,** *79*, 3504-3508.
39. Wang, P. C.; DeVoe, D. L.; Lee, C. S., *Electrophoresis* **2001,** *22*, 3857-3867.
40. de Jong, J.; Lammertink, R. G. H.; Wessling, M., *Lab Chip* **2006,** *6*, 1125-1139.
41. Backofen, U.; Matysik, F. M.; Lunte, C. E., *Anal. Chem.* **2002,** *74*, 4054-4059.
42. McDonald, J. C.; Duffy, D. C.; Anderson, J. R.; Chiu, D. T.; Wu, H. K.; Schueller, O. J. A.; Whitesides, G. M., *Electrophoresis* **2000,** *21*, 27-40.
43. Liu, Y.; Vickers, J. A.; Henry, C. S., *Anal. Chem.* **2004,** *76*, 1513-1517.
44. Vickers, J. A.; Caulum, M. M.; Henry, C. S., *Anal. Chem.* **2006,** *78*, 7446-7452.
45. Jacobson, S. C.; Koutny, L. B.; Hergenroder, R.; Moore, A. W.; Ramsey, J. M., *Anal. Chem.* **1994,** *66*, 3472-3476.
46. Garcia, C. D.; Liu, Y.; Anderson, P.; Henry, C. S., *Lab Chip* **2003,** *3*, 324-328.

CHAPTER 4. IMPROVING THE COMPATIBILITY OF CONTACT CONDUCTIVITY DETECTION WITH MICROCHIP ELECTROPHORESIS USING A BUBBLE CELL

CHAPTER OVERVIEW

Although the work in chapter 3 utilized contact conductivity detection in microchip electrophoresis, those devices exhibited relatively high noise and were limited to low separation field strengths (< 140 V cm^{-1}). At higher fields, bubbles formed at the detection electrodes. For aerosol monitoring, fast analyses with low detection limits are needed, which was not possible with the original conductivity detection. At first, the cause of the bubble formation was unknown. However, modeling the microfluidics as an electrical circuit with Ohm's and Kirchoff's current laws permitted proper electric field calculation, making the problem apparent. The separation field induces a voltage drop across the detection electrodes, facilitating electrochemical reactions, specifically the electrolysis of water. Analysis of the literature on the subject showed that other contact conductivity detection systems for microchip electrophoresis suffered from this problem, even if the authors did not realize it. This chapter, originally published as an article in *Analytical Chemistry*,[1] shows the development of an approach to reduce the voltage drop across the detection electrodes in microchip electrophoresis, improving detection limits and analysis time.

ABSTRACT

A new approach for improving the compatibility between contact conductivity detection and microchip electrophoresis was developed. Contact conductivity has traditionally been limited by the interaction of the separation voltage with the detection electrodes because the applied field creates a voltage difference between the electrodes, leading to unwanted electrochemical reactions. To minimize the voltage drop between the conductivity electrodes and therefore improve compatibility, a novel bubble cell detection zone was designed. The bubble cell permitted higher separation field strengths (600 V cm^{-1}) and reduced background noise by minimizing unwanted electrochemical reactions. The impact of the bubble cell on separation efficiency was measured by imaging fluorescein during electrophoresis. A bubble cell four times as wide as the separation channel led to a decrease of only 3% in separation efficiency at the point of detection. Increasing the bubble cell width caused larger decreases in separation efficiency, and a four-fold expansion provided the best compromise between loss of separation efficiency and maintaining higher field strengths. A commercial chromatography conductivity detector (Dionex CD20) was used to evaluate the performance of contact conductivity detection with the bubble cell. Mass detection limits (S/N = 3) were as low as 89 ± 9 amol, providing concentration detection limits as low as 71 ± 7 nM with gated injection. The linear range was measured to be greater than two orders of magnitude, from 1.3 μM to 600 μM for sulfamate. The bubble cell improves the compatibility and applicability of contact conductivity detection in microchip electrophoresis, and similar designs may have broader application in electrochemical

detection as the expanded detection zone provides increased electrode surface area and reduced analyte velocity in addition to the reduction of separation field effects.

INTRODUCTION

Microfluidic chip function and performance have improved considerably since the inception of microfluidics in the early 1990s.[2-6] Modern microchips can perform a variety of tasks, including capillary electrophoresis (CE), liquid chromatography, immunoassays, polymerase chain reaction, derivatization, coupling to mass spectrometry, and liquid-liquid extractions.[6] The combination of multiple techniques on a single microchip with the ambition of developing miniaturized total analysis systems (μTAS) for rapid and portable analyses is a pressing goal in analytical chemistry and has been reviewed extensively.[2-6] Due to low cost, short analysis times, portability, and low sample consumption, microchip CE devices are desirable for performing quantitative measurements at the point of use. However, the small injection volume, typically less than 1 nL, and low concentrations of analytes in samples place high demands on the detection equipment to attain adequate limits of detection (LOD).

Much of the early work with microchip CE utilized fluorescence detection to overcome poor sensitivity because fluorescence has intrinsically high sensitivity and detection limits near the single molecule level.[7] However, fluorescence systems are traditionally expensive and bulky, and thus in direct opposition to the development of portable systems. Some success has been met in reducing the footprint of fluorescence systems.[8,9] However, smaller detectors do not combat other limitations of fluorescence detection –

analytes must be fluorescent and relatively few compounds are natively fluorescent. Derivatization is required to measure non-fluorescent compounds but is time and reagent intensive, can lead to measurement artifacts, and cannot be performed on many small molecules.

To allow for less expensive, more compact, and more widely applicable detection in microchip CE, electrochemical and conductometric detection techniques have been explored.[10-13] Electrochemical methods such as amperometry, potentiometry, and voltammetry require an electroactive analyte or an electrochemical system that can be perturbed by the analyte.[14] Consequently, these methods offer some selectivity and may be tuned for specific compounds depending on the electrochemical approach and/or oxidation potential used. In contrast, conductivity is a physicochemical property, and conductometric measurements respond to any change in the conductivity of the solution, regardless of the specific identity of the compound.[15] This method has the advantage of being universal but also has the disadvantages of detecting any system peaks and changes in background signal due to evaporation or ion depletion. Despite these disadvantages, conductivity detection remains one of the only direct methods for sensing small inorganic and organic ions that lack native fluorescence, electrochemical activity, strong chromaphores, or functional groups for derivatization.

Conductivity detection in microchip CE can be performed in two modes – contact and contactless. Contactless conductivity detection, also referred to as oscillometric detection[16] and capacitively coupled contactless detection (C^4D),[17] relies on high

excitation frequencies and capacitive coupling between the electrodes and solution to make measurements.[18] This method has the advantage of placing the electrodes outside of the solution, minimizing interference from the separation field and preventing electrode fouling. Contactless detection has been employed in electrophoresis in both microchip and capillary formats and has been reviewed extensively.[15,18-23] Typical concentration detection limits for contactless detection in the chip format are 1-10 μM, although the Hauser group has reported sub-micromolar detection limits by increasing the excitation voltage.[15,24]

In contrast to contactless conductivity detection, contact conductivity detection utilizes electrode-solution contact to make either DC or AC measurements of the solution conductivity.[15,22] The drawback to this approach is the potential for unwanted interaction between the electrodes and the separation field, resulting in electrochemical side reactions and fouling of the sensing electrodes. Despite these issues, contact detection has been shown by several groups to be successful in traditional capillary electrophoresis, yielding detection limits similar or superior to contactless detection.[15,25-28] Contact detection has proven less successful in the microchip format, often due to interactions between the separation field and detection electronics.[15] Specifically, higher fields give increased voltage drops between the conductivity electrodes, leading to unwanted electrochemical reactions, electrolysis of water, and consequently bubble formation and increased noise. Several approaches have been used to avoid high voltage drops and bubble formation with contact conductivity detection. Li and coworkers designed a microchip using a side channel at the end of the separation channel and measured

conductivity by monitoring the potential in this side channel.[29] Detection limits were ~1 μM. The same group later developed a floating resistivity detector utilizing a double-T detection design and avoiding direct analyte-electrode contact to prevent fouling.[30] Detection limits were in the 10-80-μM range. The Girault group developed a detection cell that utilized the separation field for detection by monitoring the potential difference between two electrodes with a high-impedance voltmeter.[31] This design provided detection limits around 20 μM. The Soper group developed a conductivity detector utilizing a 5-kHz bipolar pulse waveform and connected it to an electrode system composed of two opposed 127-μm wires.[32] Reported detection limits were 8 nM for amino acids using indirect conductivity detection. This detector was later utilized with a different electrode configuration in an array format and detection limits of 7 μM were reported.[33] Despite the success obtained with this detector, the approach still suffers from the same voltage drop problem as all in-channel contact conductivity measurements and is limited to low field strengths.

In order to achieve improved performance from contact conductivity detection in microchip CE, the separation field-induced voltage drop between the detection electrodes must be minimized. Traditionally this has been done in electrochemical detection using current decouplers consisting of palladium wires placed upstream of the detection electrodes, limiting analyses to normal polarity and co-EOF operation.[34,35] In this work, we present the implementation of a capillary expansion at the detection zone, termed a bubble cell, to lower the effective separation field in the conductivity cell and consequently reduce the voltage drop between the detection electrodes. The reduced

voltage drop allows for higher field strengths to be used without bubble formation. Separation efficiency as a function of bubble cell position was monitored via fluorescent imaging and found to decrease by only 3% at the conductivity cell with a detection zone four times larger than the separation channel. A variety of bubble sizes were subsequently tested with conductivity detection, and wider cells were observed to degrade separation efficiency more substantially than smaller ones. The bubble cell was shown to have the benefits of reducing system noise and allowing for higher separation fields (up to 600 V cm^{-1}), shortening analysis times four-fold. In addition to the bubble cell, we present the use of a commercial liquid chromatography conductivity detector for microchip CE. Relative signal response was compared to theory for molecular conductivity and found to agree favorably. Mass detection limits ranged from 89-210 amol for a series of inorganic anions, corresponding to concentration detection limits of 71-500 nM. Field amplified sample stacking with gated injection allowed for concentration detection limits of 9-44 nM. The benefits of the bubble cell should have widespread applicability for contact conductivity detection in microchip CE applications and may also provide significant gains in performance for other electrochemical detection techniques in microchip CE.

THEORY

Conductivity detection measures the physical conductivity of the solution passing through the detection zone, which is related to the individual chemical components as given in eq 4.1, where Λ is the conductivity (S), k_{cell} is the cell constant (cm^{-1}), $C_{i,det}$ is the

concentration of compound i in the detection zone (mol L^{-1}), and λ_i is the molar conductivity of compound i (mS m^2 mol^{-1}).

$$\Lambda = \frac{\sum_i C_{i,\mathrm{det}} \lambda_i}{100 k_{cell}} \tag{4.1}$$

The molar conductivity is related to the electrophoretic mobility for a given species, μ (cm^2 V^{-1} s^{-1}), as given in eq 4.2, where z is the formal charge of the ion and F is the Faraday constant (96485 C mol^{-1}).

$$\lambda = \frac{z \mu F}{10} \tag{4.2}$$

As discussed in some of the earliest work with conductivity detection in CE and reviews on the subject, the relationships in eqs 4.1 and 4.2 imply that response is predictable based on the chemical properties of the analyte.[20,22,26] Ideally, measuring an internal standard's peak area would allow calculation of the concentrations of all analytes because signal differences are proportional to the analyte concentration and charge. The appearance of a peak in conductivity detection in CE is thus dependent on the change in the molar conductivity of the analyte migrating through the detection zone, the amount of sample injected, and the amount of band broadening occurring during separation. Eq 4.1 gives the physical conductivity of the solution measured by the instrument. Evaluation of the numerator of this equation is not straightforward. However, the *change* in the numerator can be calculated assuming a charge-balanced electrophoretic zone with a BGE consisting of one co-ion and one counter-ion, giving eq 4.3.

$$\Delta \sum_i C_{i,\mathrm{det}} \lambda_i = C_{A,\mathrm{det}} \left(\lambda_A - \eta \lambda_B + \frac{(\eta z_B - z_A)}{z_C} \lambda_C \right) \tag{4.3}$$

Here, the analyte (subscript A) concentration in the detection zone (C_{det}, mol L^{-1}) affects the concentration of every compound in the sample plug since the concentration of the co-ion (subscript B) displaced is, by definition, equal to $C_{A,det}$ multiplied by the transfer ratio, η. The concentration of the counter-ion (subscript C) is then dictated by maintaining charge balance, where the charge of species i is given by the symbol z_i. Using the results of eq 4.3 as the numerator of eq 4.1 and substituting eq 4.2 for the molar conductivities gives eq 4.4 for the *change* in conductivity.

$$\Delta\Lambda = \frac{FC_{A,\mathrm{det}}}{1000k_{cell}}\left(z_A\mu_A - \eta z_B\mu_B + \left(\eta z_B - z_A\right)\mu_C\right) \tag{4.4}$$

The analyte concentration at the detection zone is not equal to the concentration initially injected but can be determined by accounting for injection and band broadening effects. The plug injected can be considered to have a uniform concentration of analyte ($C_{A,inj}$, mol L^{-1}) with a volume that is the channel cross-sectional area at the injection point (A_{inj}, m^2) multiplied by the length of the plug. For electrokinetic injection, sample biasing occurs based on the electrophoretic velocity. Therefore, the injected amount (mol) is given by eq 4.5, where E_{inj} (V cm^{-1}) is the electric field during injection, μ_A and μ_{EOF} (cm^2 V^{-1} s^{-1}) are the electrophoretic and electroosmotic mobilities, respectively, and t_{inj} (s) is the injection time.

$$10C_{A,inj}A_{inj}\left(\mu_A + \mu_{EOF}\right)t_{inj}E_{inj} \tag{4.5}$$

$C_{A,det}$ (mol L^{-1}), the peak concentration of the analyte in the detection zone, differs from $C_{A,inj}$ due to band broadening during separation. However, the moles of analyte in the detection peak is equivalent to the moles injected (assuming no losses to chemical reactions or adsorption processes). Assuming a Gaussian peak, the amount of analyte

passing through the detection zone (mol) can be determined using the expression for area of a Gaussian peak and is represented by eq 4.6.

$$\frac{10\sqrt{\pi}C_{\mathrm{det},A}w_{1/2,p}A_{\mathrm{det}}}{2\sqrt{\ln(2)}} \tag{4.6}$$

Here, $w_{1/2,p}$ (cm) is the physical half-width of the peak and A_{det} (m^2) is the cross-sectional area of the channel in the detection zone. In electrophoresis, each analyte moves through the detection zone at a different velocity and therefore time-domain half-width ($w_{1/2,t}$, s) measurements made from electropherograms must be adjusted for this difference by multiplying by the analyte velocity. Becuase analyte velocity equals the separation field (E_{sep}, V cm^{-1}) multiplied by the sum of μ_A and μ_{EOF}, eq 4.6 is rewritten as eq 4.7.

$$\frac{10\sqrt{\pi}C_{\mathrm{det},A}w_{1/2,t}A_{\mathrm{det}}E_{sep}\left(\mu_A+\mu_{EOF}\right)}{2\sqrt{\ln(2)}} \tag{4.7}$$

Equating eqs 4.5 and 4.7 and solving for the detected concentration gives eq 4.8.

$$C_{\mathrm{det},A}=\frac{2\sqrt{\ln(2)}C_{A,inj}A_{inj}t_{inj}E_{inj}}{\sqrt{\pi}w_{1/2,t}A_{\mathrm{det}}E_{sep}} \tag{4.8}$$

The results of eq 4.8 can then be substituted into eq 4.4 to give the full equation for change in conductivity for an injection of an analyte at a given concentration, eq 4.9.

$$\Delta\Lambda=\frac{\sqrt{\ln(2)}A_{inj}t_{inj}E_{inj}F}{500\sqrt{\pi}k_{cell}A_{\mathrm{det}}E_{sep}}\frac{C_{A,inj}}{w_{1/2,t}}\left(z_A\mu_A-\eta z_B\mu_B+\left(\eta z_B-z_A\right)\mu_C\right) \tag{4.9}$$

The first fraction in this equation possesses a large number of constants that are not always known. However, for any given analysis, these values are equal for all analytes and can be lumped into a single constant of proportionality (K_{prop}, C cm s mol^{-1}). By assuming the co-ion is displaced completely ($\eta = z_A/z_B$), the counter-ion term falls out and eq 4.10 results.

$$\Delta\Lambda = K_{prop} \frac{C_{A,inj} z_a (\mu_A - \mu_B)}{w_{1/2,t}} \tag{4.10}$$

Eq 4.10 indicates that relative peaks heights in a single electropherogram can be estimated from the width of the peak, co-ion mobility, and analyte concentration, charge, and migration time. In practice, analytes displace some background electrolyte co-ions, and the transfer ratio is not always predictable.[36]

The effects of bubble cells on separation field strength and peak width have previously been considered.[37,38] For a rectangular capillary, the electric field strength (E) in the bubble cell region (BC) is inversely proportional to the width (w) ratio between the bubble cell and separation capillary (SC), as given by eq 4.11

$$E_{BC} = E_{SC} \frac{w_{SC}}{w_{BC}} \tag{4.11}$$

Eq 4.11 indicates that the analyte velocity decreases in the bubble cell. However, peak width in the time domain should remain constant because continuity dictates that the analyte band must compress axially in inverse proportion to the field strengths. Previous consideration has shown that band broadening from changes in channel cross section should not occur as long as the intrinsic electroosmotic flow (EOF) in the channel remains constant.[37]

MATERIALS AND METHODS

Materials

Sodium dodecylsulfate, sulfamic acid, potassium iodate, potassium hexafluorophosphate, ammonium perrhenate, lithium trifluoromethanesulfonate (triflate), sodium

methanesulfonate, sodium ethanesulfonate, sodium benzenesulfonate, tribromoacetic acid, oxalic acid, glutaric acid, adipic acid, monopotassium acetylenedicarboxylic acid, propylene glycol methyl ether acetate, and N-(2-hydroxyethyl)piperazine-N'-(4-butanesulfonic acid) (HEPBS) were obtained from Sigma-Aldrich (St. Louis, MO, USA). Sodium tetraborate, sodium nitrate, sodium chlorate, and Triton X-100 were purchased from Fisher Scientific (Fair Lawn, NJ, USA). Malonic, succinic, and pimelic acids were acquired from Acros Organics (Geel, Belgium). Potassium perchlorate was obtained from J.T. Baker (Phillipsburg, NJ, USA). Fluorescein was purchased from Eastman (Rochester, NY, USA). 2,2-Bis(hydroxymethyl)-2,2',2''-nitrilotriethanol (BIS-TRIS) and nicotinic acid were acquired from Fluka (Buchs, Switzerland). SU-8 2035 photoresist was obtained from Microchem (Newton, MA, USA). Sylgard 184 elastomer base and curing agent were provided by Dow Corning (Midland, MI, USA). All chemicals were used without further purification. Solutions were prepared in 18.2 MΩ cm water from a Millipore Milli-Q purification system (Billerica, MA, USA). All microwires were obtained from GoodFellow Corp. (Huntingdon, UK).

Microchip Construction

Construction of PDMS microchips and inclusion of microwires for detection were performed as described previously.[39-41] Briefly, 100-mm silicon oxide wafers (University Wafer, South Boston, MA, USA) were cleaned with acetone and then spin coated with SU-8 2035 photoresist at 2500 or 4000 rpm, resulting in feature heights of 39.6 ± 0.9 μm and 23.7 ± 1.2 μm, respectively. A negative mask was placed on the wafer, exposed to ultraviolet light, and developed in propylene glycol methyl ether acetate to give a positive

relief of the microchannels on the wafer surface. Sylgard 184 elastomer was mixed with curing agent in a 10:1 ratio, degassed via vacuum, poured onto the wafer, and cured at 60 °C for at least 2 hours. Cylindrical reservoirs were added with 5-mm biopsy punches (Robbins Instruments, Chatham, NJ, USA). Irreversible sealing of the PDMS was accomplished with a 30-s air plasma exposure at 18 W (Harrick Scientific PDC-32G, Pleasantville, NY, USA) followed by conformal contact of the oxidized pieces. A schematic of the microchip design is shown in Figure 4.1. Effective separation capillary length was 5 cm.

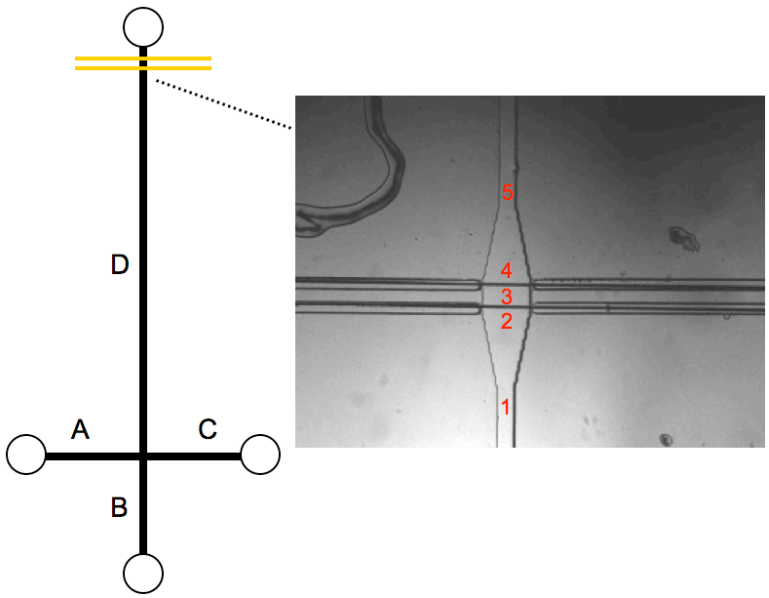

Figure 4.1. Microchip design used in this work. Gated injected was used for all analyses, and the channel were designated as follows: A = sample waste, B = sample, C = buffer, D = separation. The numbers designate locations monitored with fluorescent imaging.

Channels were 50-μm wide with the exception of the systems without a bubble cell, where 70-μm channels were used. For the fluorescent and material noise studies, microwires of various sizes and composition were placed with center-to-center spacing of 120 μm, channels were 39.6 ± 0.9-μm deep as measured by profilometry, the separation

reservoir was 2 mm after the detection zone, sample channels were 1.5 cm, and sample waste and buffer channels were 1.0 cm. For all other studies, 15-μm gold-plated tungsten wires were spaced at 100 μm, channels were 23.7 ± 1.2-μm deep, the separation reservoir was 1 mm after the detection zone, sample and buffer channels were 2 cm, and sample waste was 1.5 cm. For bubble cells, the channel was expanded linearly until the detection zone was reached, width remained constant in the detection cell, and the channel was contracted linearly after the downstream detection wire. The bubble cell ramp length was defined as the length of separation channel between the start of channel expansion and the detection zone. The ramp angle was defined as the angle between the ramping wall and the separation channel vector, so channels with no expansion had an angle of 0.

Instrumentation and Data Acquisition

Conductivity detection was performed by modifying a Dionex CD20 conductivity detector to allow the detection leads to connect to microwires used in the microchip detection zone. The 0-1 V output from the CD20 was monitored with a National Instruments USB-6210 DAQ and LabView 8.0 software. Data was collected at 20 kHz and each set of 2000 samples averaged to give an effective collection rate of 10 Hz. No additional software data filtration was performed. Baseline drift due to electrolyte evaporation was corrected by subtracting a polynomial baseline fit from the raw data. EOF estimates were made by adjusting literature electrophoretic mobilities for ionic strength effects using PeakMaster software and setting the EOF value to best correlate expected and experimental migration times.[42,43] Limits of detection (LOD) are given as

the concentration giving a signal-to-noise ratio (S/N) of 3, and reported uncertainties are the standard deviation of the signal at the LOD.

To prevent electronic coupling of the CD20 detection system to the electrophoresis high voltage power supply (HVPS), a custom-built, floating HVPS was utilized. DC-DC converters were obtained from Ultravolt and controlled by a Measurement Computing USB-3103 DAQ. DAQ communication was accomplished using LabView software, and the HVPS was electronically isolated from computer control through an Opticis M2-100 optical USB cable. Power for the HVPS was provided by a series of AA batteries.

Fluorescence data was acquired with a Nikon Eclipse TE2000-U microscope, Exfo X-Cite 120 lamp, and Photometrics Cool Snap HQ^2 camera. Electropherograms were generated using Metamorph 7.1.7 software.

RESULTS AND DISCUSSION

Separation Efficiency in the Bubble Cell

Fluorescent imaging was used to monitor changes in separation efficiency as fluorescein passed through a bubble cell with a width four times that of the separation channel (4x). As depicted in Figure 4.1, five positions were monitored: the separation channel before the bubble cell expansion (1), immediately before the upstream detection electrode (2), between the detection wires (3), immediately after the downstream electrode (4), and the channel after the bubble cell (5). Measuring separation efficiency prior to the bubble cell allowed for relative changes to be monitored, reducing the impact of any chip-to-chip

differences in injection or EOF. This analysis was performed with and without detection wires to determine what effects, if any, the wires had on separation efficiency. Three different wire sizes were tested, 15, 25, and 40 μm, and measurements were made both with and without the wires connected to the detection electronics. Results are shown in Figure 4.2. For the design without microwires, the decrease in separation efficiency at the detection point (3) is only 3%, equivalent to a peak width increase of only 1.5%. This decrease in separation efficiency is acceptable for most applications. It should be noted that separation degradation in the bubble cell might be condition dependent. For instance, a similar experiment performed in borate/SDS BGE showed no decrease in separation efficiency through the entire bubble cell (Figure 4.3). One reason for the lack of degradation in the borate BGE may be that Joule heating was occurring in the separation channel but not the bubble cell, as separation efficiencies at position 1 were on average 73% lower (13700 vs. 3700 plates) in the borate BGE than the BGE used with the experiments shown in Figure 4.2. Inclusion of 15- or 25-μm wires was observed to have a negligible effect on separation efficiency, but the larger 40-μm wires decreased separation efficiency further, agreeing with previous work using amperometry where a 50-μm wire showed a separation efficiency 30% lower than a 25-μm one.[40] The difference may be due to the larger electrode having a diameter nearly matching that of the channel height, severely perturbing fluid flow from the large, abrupt change in channel cross section. Connecting the detection wires to the CD20 detector yielded insignificant changes in measured separation efficiency.

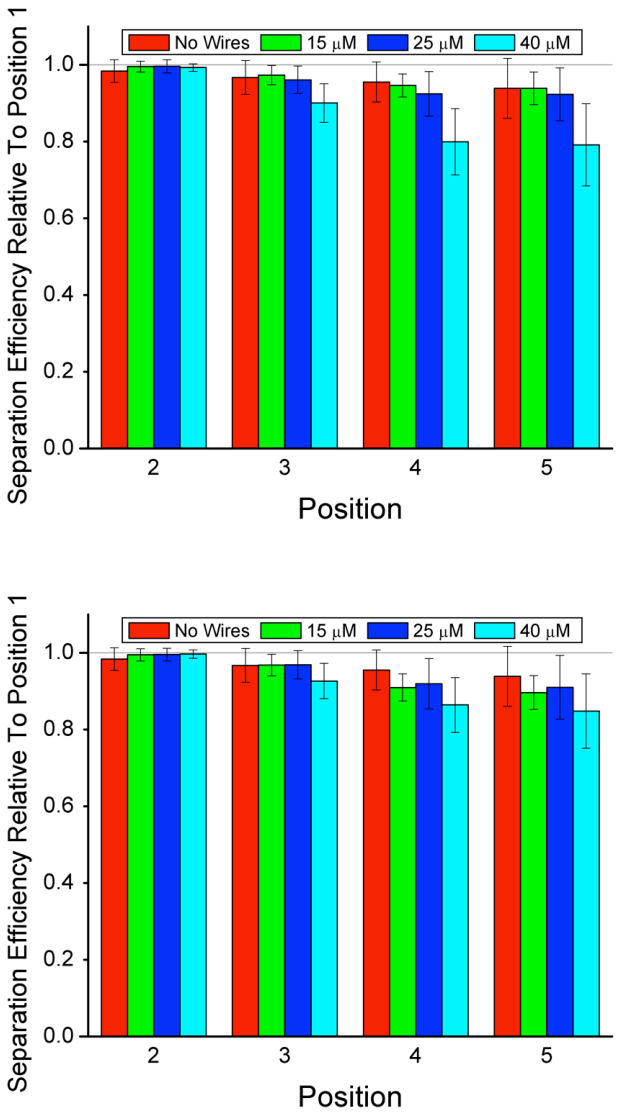

Figure 4.2. Separation efficiency of 20-μM fluorescein through a 4x bubble cell. (Top) Results obtained with detection wires disconnected. (Bottom) Results obtained with the wires connected to the detection electronics. All values are normalized to the separation efficiency at position 1. Error bars represent standard deviation from three microchips. Conditions: 200 V cm^{-1}-separation field; 0.75-s gated injection; BGE = 25-mM BIS-TRIS/10-mM HEPBS/1-mM SDS (pH 7.6).

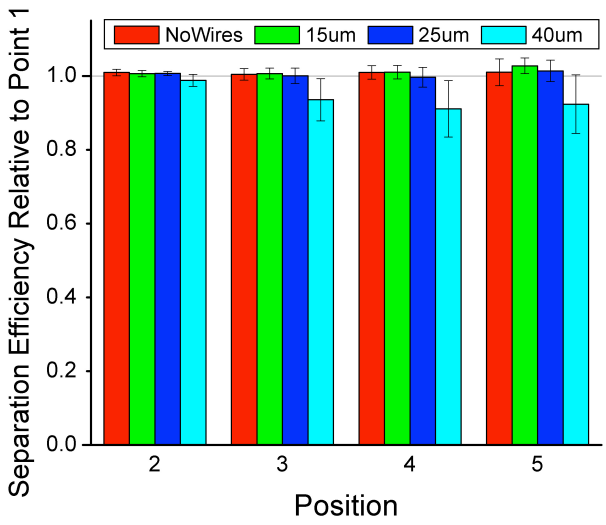

Figure 4.3. Separation efficiency of 25-μM fluorescein through a 4x bubble cell with detection wires disconnected. All values are normalized to the separation efficiency at position 1. Error bars represent standard deviation from three microchips. Conditions: 200-V cm^{-1} separation field; 0.50-s gated injection; BGE = 5-mM sodium tetraborate/1-mM SDS (pH 9.3). Except for the microchips with 40-μm wires, no decrease in separation efficiency was observed, which is in contrast to the results in Figure 4.2.

The combination of the bubble cell and microwire inclusion leading to a decrease of only 3% in separation efficiency indicates that most separations will not be significantly degraded by the addition of these components into the microfluidic network. To confirm that the bubble cell has minimal effect on the quality of separations, analyses of inorganic anions were performed with and without a bubble cell and are shown in Figure 4.4. Without a bubble cell, resolution between peaks was measured at 1.50, 1.68, 1.25, and 2.50, respectively. With a 3x bubble cell, values of 1.46, 1.70, 1.27, and 2.56, respectively, were obtained. These statistically insignificant differences show that the separation degradation is minor in practical separations, encouraging the use of bubble cells to improve detection compatibility.

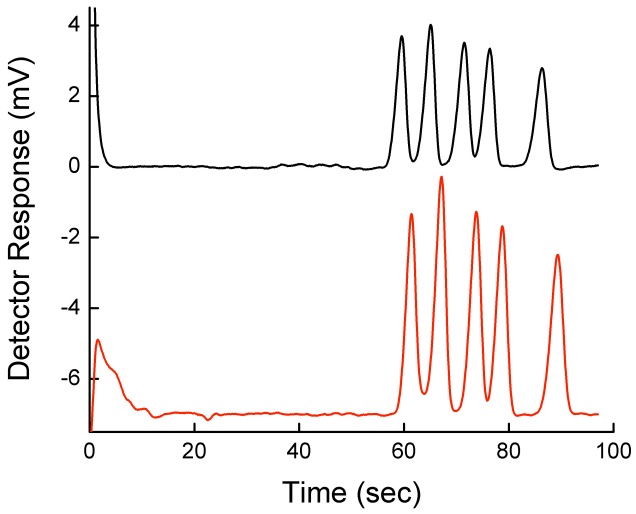

Figure 4.4. Comparison of separations obtained without a bubble cell (top) and with a 3x bubble cell and 17.7° ramp angle (bottom). Conditions: –150 V cm^{-1} and 1.40-s injection. BGE = 10-mM nicotinic acid/0.05-wt% Triton X-100 (pH 3.6). Detector range = 100 mS. Analytes are 25 μM. Peak order is chloride, nitrate, perchlorate, chlorate, hexafluorophosphate. The slight discrepancy in migration times is due to differences in the EOF between microchips.

Effect of Bubble Cell Size

To test the effect of the bubble cell size on the separation performance, separation efficiency was monitored using conductivity detection for several bubble cell sizes and a range of separation fields. Width ratios of 3x, 5x, 8x, and 12x were compared with results obtained with no bubble cell (1x). The effect of the bubble cell length was tested by comparing results from a constant ramp length of 333 μm to a constant ramp angle of 17.7°. Microchips without bubble cells were limited to 125 V cm^{-1} and the 3x bubble cell was used at a maximum of 425 V cm^{-1}. All other designs were tested up to 575 V cm^{-1}. Results using sulfamate as a model analyte are shown in Figure 4.5.

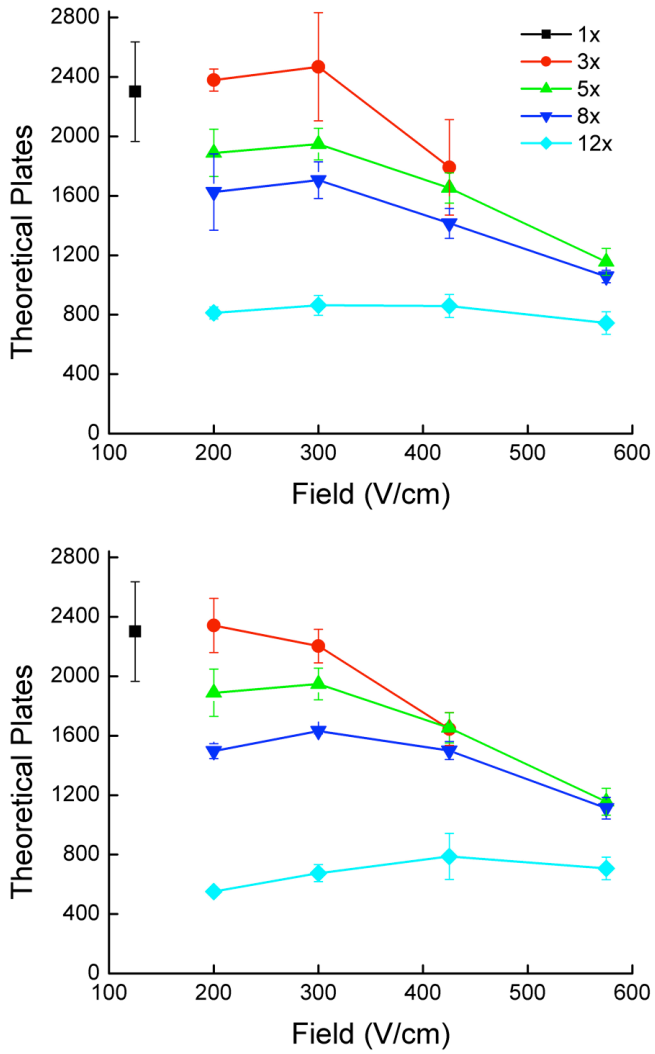

Figure 4.5. Separation efficiency of 50 μM sulfamate for several field strengths and a variety of bubble cell sizes. (Top) Bubble cells with a constant ramp length of 333 μm. (Bottom) Bubble cells with a constant ramp angle of 17.7°. BGE = 10-mM nicotinic acid/0.1-wt% Triton X-100 (pH 3.6). Injection times were as follows: 125 V cm^{-1} = 1.25 s, 200 V cm^{-1} = 1.0 s, 300 V cm^{-1} = 0.9 s, 425 V cm^{-1} = 0.6 s, 575 V cm^{-1} = 0.5 s. Reverse polarity used. Direct voltage comparisons cannot be made due to potential Joule heating effects and differing injection volumes.

Sulfamate was selected as the model analyte due to its intermediate electrophoretic mobility ($5.01*10^{-4}$ cm^2 V^{-1} s^{-1}) relative to other inorganic anions.[42] The trends observed for sulfamate were compared with perchlorate and iodate, and similar results were

obtained (data not shown). The 3x bubble cell was found to give similar separation efficiencies as the straight channel design (5750 plates for 1x at 125 V cm^{-1} vs. 5950 (constant length) and 5860 (constant angle) plates for 3x at 200 V cm^{-1}), agreeing with the fluorescence data using a 4x bubble cell and the resolution measurements from Figure 4.4. However, a systematic decrease in separation efficiency with increasing bubble cell ratio indicates that band broadening becomes increasingly significant as the expansion ratio increases. Effects are moderate at 5x and 8x ratios, where separation efficiencies are 12-31% lower than observed with the 3x ratio at 300 Vcm^{-1} (4080-4870 plates for the 5x and 8x configurations, and 6170 and 5510 plates for 3x configurations). However, with a 12x expansion, separation efficiency drops by 65-69% relative to the 3x bubble cell at 300 V cm^{-1} (2150 and 1970 plates for constant length and angle, respectively). These results agree with those of Xue and Yeung, where a dramatic increase in peak broadening was observed when switching from an 8x to a 15x radial bubble cell in a traditional capillary using absorbance detection.[38] At 425 V cm^{-1}, the advantage in separation efficiency of a 3x cell over a 5x is gone. We suspect this is due to the increased voltage drop between the electrodes in the 3x cell at this voltage. If electrochemical reactions are becoming significant, changes in current in the detection zone may also increase band broadening. These results indicate that the optimal bubble cell expansion depends on the conditions used. A balance must be achieved between minimizing voltage drop by increasing the cell width while minimizing band broadening by reducing the width.

Evaluation of Conductivity Detection Performance

Several instrument configurations were tested to measure the performance and limitations of the detection system. 25-μm gold, platinum, and tungsten electrodes spaced center-to-center by 120 μm were tested in a 4x bubble cell with field strengths of 200-600 V cm^{-1} (Figure 4.6).

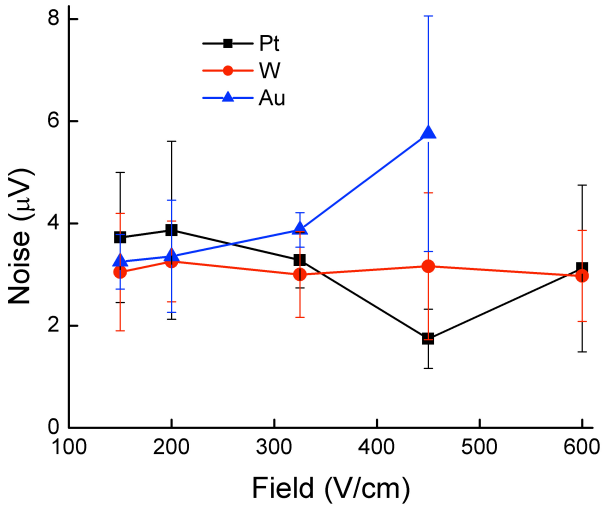

Figure 4.6. RMS noise as a function of field strength for platinum, tungsten, and gold microwires. Voltages were reverse polarity. All wires had 25-μm diameters and were spaced 120-μm center-to-center. The observed noise is lower than the limit of the 16-bit output used (15-μV step), so limits of detection were considered to be concentrations yielding 3 signal step changes. The gold wires could not be tested at 600 V cm^{-1} due to bubble formation. BGE conditions are the same as in Figure 4.5.

No significant changes in performance were observed between materials at low voltages, but the gold wires generated bubbles by 600 V cm^{-1}. The reason for this discrepancy is unknown, but it may be that the gold surface nucleates bubbles more readily due to differing surface roughness or impurities. The presence of the electric field across the detection cell does not hinder performance when the HVPS ground is located in the separation waste reservoir. Specifically, baseline RMS noise was low enough (less than

4 μV) that individual 15-μV steps were observed in the baseline, corresponding to the limit of the 16-bit output of the commercial detector. Consequently, the limit of detection was determined as the analyte concentration yielding three of these steps and would be improved if a detector with higher resolution output or an adjustable baseline were utilized. It was also noted that placing the high voltage electrode (instead of the ground electrode) at the channel end resulted in transient bubble formation upon HVPS activation, limiting applied electric fields to using a ground at the end of the separation channel.

Limits of detection were measured using a 3x bubble cell, 17.7° ramp angle, 200 V cm^{-1} separation field, 1.2-s gated injection, and a BGE of 10-mM nicotinic acid/0.05% Triton X-100. Model analytes dithionate, perchlorate, sulfamate, and iodate gave concentration detection limits of 71 ± 7, 200 ± 40, 310 ± 30, and 500 ± 120 nM, corresponding to mass detection limits of 89 ± 9, 210 ± 40, 170 ± 20, and 200 ± 50 amol, respectively. These values compare well with previous conductivity detection in microchip electrophoresis, with only one report giving lower detection limits.[32] Preparing the sample in dilute BGE (0.25-mM nicotinic acid/0.05% Triton X-100) established a solution conductivity difference, enabling moderate field amplified sample stacking. In dilute BGE with 2.0-s gated injection, respective concentration detection limits were 9 ± 1, 22 ± 5, 41 ± 7, and 44 ± 10 nM. Calibration curves for sulfamate without stacking showed excellent linearity from 1.3 μM to 150 μM (R^2 = 0.9999) and only moderate deviation from linearity up to 600 mM (R^2 = 0.9986). Utilizing an internal standard to account for injection discrepancies allowed high linearity to be maintained up to 400 μM (R^2 = 0.99995). Both

detection limit and linear range are highly dependent on the analytes and BGEs, and results for other chemical systems will differ. As mentioned earlier, detection limits with the bubble cell should be improved further by utilizing a detector with higher resolution output or adjustable offset because the baseline noise is currently dictated by the 16-bit output of the CD20 detector.

As shown in eq 4.10, conductivity detection offers predictable relative peak heights. Analysis of 12 monoanions in equimolar concentrations was performed to confirm that the observed behavior followed eq 4.10. The electropherogram and predicted peak heights, as indicated by the red dots, are shown in Figure 4.7. The EOF was estimated at $2.0*10^{-4}$ $cm^2\ V^{-1}\ s^{-1}$, and the co-ion mobility was calculated with PeakMaster software to be $-0.0913*10^{-4}$ $cm^2\ V^{-1}\ s^{-1}$, leaving the proportionality constant as the only variable.[42,43] A proportionality constant of $3.36*10^7\ V^2\ s^2$ m gave the best fit (note that this is not equal to the K_{prop} shown in eq 4.10 due to transduction in the CD20 converting conductivity to a voltage). The median discrepancy between the experimental and predicted values was 2.8%, and only tribromoacetate had a predicted value differing more than 10% from the experimental value. The main source of error is likely ignoring the transfer ratio, which varies for each analyte.

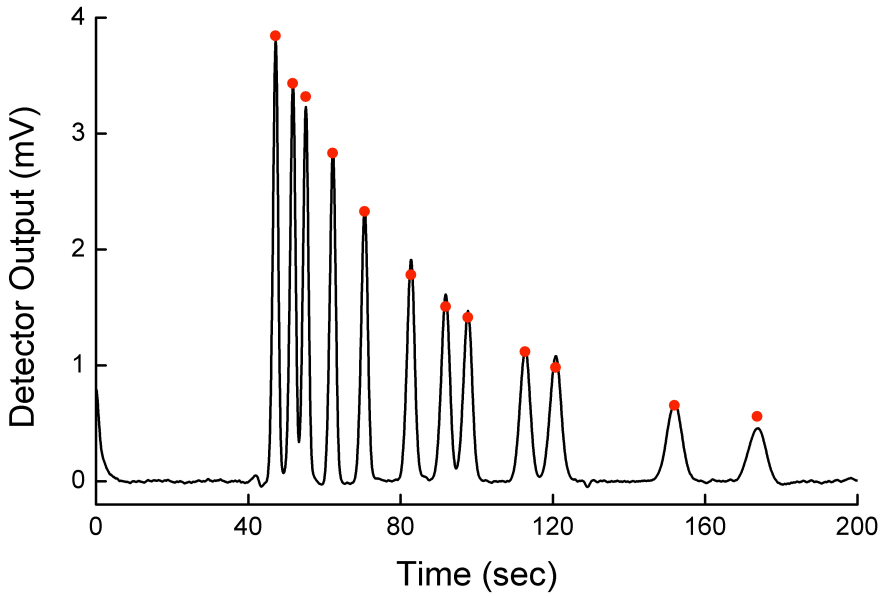

Figure 4.7. Electropherogram (line) of 12 monoanions at 25 μM and predicted peak heights (points) using eq 4.10. Conditions: –200 V cm^{-1}; 1.0-s injection, and 3x bubble cell with 17.7° ramp angle. BGE is the same as Figure 4.5. Detector range = 100 μS. Peak order is nitrate, perchlorate, chlorate, hexafluorophosphate, perrhenate, sulfamate, methanesulfonate, triflate, iodate, ethanesulfonate, benzenesulfonate, tribromoacetate.

Advantages of the Bubble Cell Design

The primary benefit offered by the bubble cell is the reduced electric field in the detection zone which leads to a decreased voltage drop between conductivity electrodes. Consequently, experimental advantages include decreased noise due to the reduction of unwanted electrochemical reactions and the ability to decrease analysis time by operating at higher separation field strengths. To quantify both effects, a separation of chloride and a series of dicarboxylates was performed in a BGE containing 12-mM histidine at pH 6.4. Histidine exhibits electrochemical activity, and its oxidized product is known to adsorb to electrodes.[44] Without a bubble cell, the electroactivity of the BGE caused a high RMS

noise level of 0.19 mV at 125 V cm^{-1}. A microchip with a 5x bubble cell was then operated at several fields between 125 and 450 V cm^{-1} for comparison (Figure 4.8).

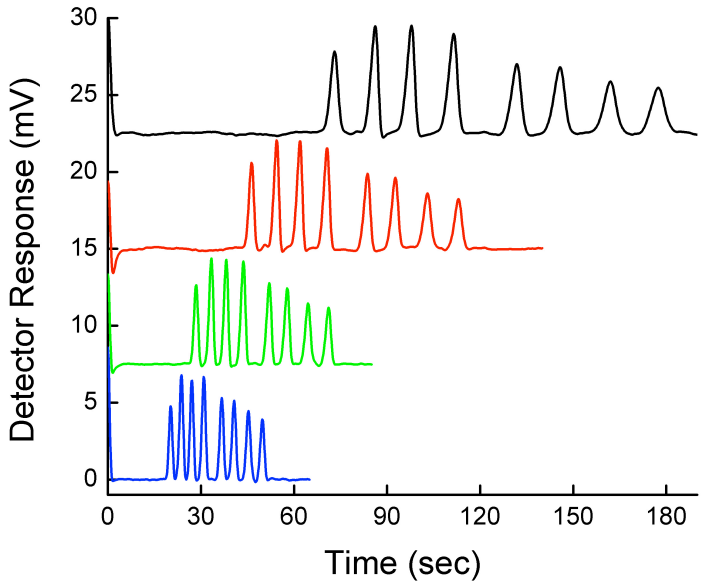

Figure 4.8. Separation of 50-μM anions at the following separation fields and injection times (top to bottom): –125 V cm^{-1} with 2.2-s inj., –200 V cm^{-1} with 1.7-s inj., –325 V cm^{-1} with 1.5-s inj., and –450 V cm^{-1} with 1.2-s inj. Bubble cell = 5x with 333-μm ramp. Detector range = 300 μS. BGE = 12-mM histidine/6-mM MES/0.05-wt% Triton X-100 (pH 6.4). Peak order is chloride, oxalate, acetylenedicarboxylate, malonate, succinate, glutarate, adipate, pimelate.

At 450 V cm^{-1}, noise was measured at 17 μV, 11 times lower than at 125 V cm^{-1} without a bubble cell. This is especially significant given the electrode area is approximately five times higher with the bubble cell. Additionally, the higher field strength allowed the analysis to be performed in under 1 min as compared to ~3 min with the 1x system. In this case, application of the bubble cell reduced noise by over an order of magnitude while simultaneously shortening the analysis time by over three-fold, from 184 s to 52 s. This evaluation shows that use of the bubble cell has the potential to dramatically shorten

analysis times while also improving sensitivity due to the decrease in noise when using electroactive components in the BGE.

In addition to the reduced electrical field in the bubble cell, the larger cross-sectional area yields an increased signal because the electrode area is inversely proportional to the conductivity cell constant.[31] Therefore, improved limits of detection might be expected. For non-electroactive BGEs, this improvement was not realized with the current system. The cause stems from the electronics of the detector used – the higher signal from the bubble cell requires a proportional decrease in instrument sensitivity to prevent an off-scale signal. Consequently, peak heights for the CD20 do not change with a bubble cell, and because the noise was dictated by the 16-bit output of the instrument, signal-to-noise ratio also remained constant. For detectors with higher resolution output and/or an adjustable baseline offset, significant improvements in signal-to-noise are anticipated for larger bubble cells, particularly if the noise is dominated by fluctuations in the separation current, which should not change in magnitude with inclusion of the bubble cell. This mechanism of improvement would be analogous to optical methods employing bubble cells which increase signal due to the larger detection pathlength.[37,38] However, the fabrication of the conductivity bubble cell, which is in the plane of the microchip, is far simpler than that of optical bubble cells, which are orthogonal to the plane of the microchip.[45,46] Similar in-plane bubble cells should also improve electrochemical modes of detection due to the lower field strength and an increased collection efficiency that stems from the slower analyte velocity and increased electrode surface area.

CONCLUSIONS

A novel bubble cell zone demonstrated improved compatibility of contact conductivity detection with microchip electrophoresis. The mechanism of improvement results from the decreased separation field in the detection zone instead of the increased pathlength that benefits optical detection utilizing bubble cells. The lower localized separation field yields a smaller voltage drop between the detection electrodes, reducing electrochemical reactions and baseline noise. The result is a system that can operate at higher field strengths than straight channel designs. A bubble cell to channel width ratio of 4 allowed operation at 600 V cm^{-1} but resulted in only a 3% drop in separation efficiency. Larger bubble cells gave lower separation efficiencies, making the optimum bubble cell width dependent on the separation requirements. Conductivity detection in the bubble cell was evaluated using a commercial chromatography conductivity detector. Detection limits for inorganic anions were 71-500 nM without stacking and 9-44 nM with stacking in gated injection. These detection limits are adequate for a variety of biological and environmental analyses. The linear range for the sulfamate ion extended as high as 600 μM, indicating this system could be used for simultaneous monitoring of compounds with concentrations differing by two orders of magnitude. The bubble cell should also benefit electrochemical detection methods because collection efficiency will increase due to the increased electrode surface area and decreased analyte velocity.

CLOSING COMMENTS

The research discussed here was pivotal towards development of an online aerosol monitoring system using microchip electrophoresis because it permitted fast

electrophoresis using conductivity detection while achieving low limits of detection. Since this original work, detection limits have improved by nearly an order of magnitude through the use of the analog output offset functionality (circumvents the 16-bit output limit), electronic shielding, changes to detection settings, and improvements in separation chemistry. Currently, this detection approach gives the best detection limits of any conductivity detection method in microchip electrophoresis. The detection limits are 10-500 times better than those obtainable with contactless conductivity detection (10-20 nM for sulfate versus 0.2-5 μM for contactless detection). Separation efficiencies with the bubble cell system are better than with contactless systems because of the narrower detection zone. Additionally, the contact system should show greater improvements in the future because it is a younger technology.

REFERENCES

1. Noblitt, S. D.; Henry, C. S., *Anal. Chem.* **2008,** *80*, 7624-7630.
2. Reyes, D. R.; Iossifidis, D.; Auroux, P. A.; Manz, A., *Anal. Chem.* **2002,** *74*, 2623-2636.
3. Auroux, P. A.; Iossifidis, D.; Reyes, D. R.; Manz, A., *Anal. Chem.* **2002,** *74*, 2637-2652.
4. Vilkner, T.; Janasek, D.; Manz, A., *Anal. Chem.* **2004,** *76*, 3373-3385.
5. Dittrich, P. S.; Tachikawa, K.; Manz, A., *Anal. Chem.* **2006,** *78*, 3887-3907.
6. West, J.; Becker, M.; Tombrink, S.; Manz, A., *Anal. Chem.* **2008,** *80*, 4403-4419.
7. Effenhauser, C. S.; Bruin, G. J. M.; Paulus, A.; Ehrat, M., *Anal. Chem.* **1997,** *69*, 3451-3457.
8. Burns, M. A.; Johnson, B. N.; Brahmasandra, S. N.; Handique, K.; Webster, J. R.; Krishnan, M.; Sammarco, T. S.; Man, P. M.; Jones, D.; Heldsinger, D.; Mastrangelo, C. H.; Burke, D. T., *Science* **1998,** *282*, 484-487.
9. Webster, J. R.; Burns, M. A.; Burke, D. T.; Mastrangelo, C. H., *Anal. Chem.* **2001,** *73*, 1622-1626.
10. Schlautmann, S.; Wensink, H.; Schasfoort, R.; Elwenspoek, M.; van den Berg, A., *J. Micromech. Microeng.* **2001,** *11*, 386-389.
11. Guijt, R. M.; Baltussen, E.; van der Steen, G.; Schasfoort, R. B. M.; Schlautmann, S.; Billiet, H. A. H.; Frank, J.; van Dedem, G. W. K.; van den Berg, A., *Electrophoresis* **2001,** *22*, 235-241.
12. Prest, J. E.; Baldock, S. J.; Fielden, P. R.; Brown, B. J. T., *Analyst* **2001,** *126*, 433-437.
13. Woolley, A. T.; Lao, K. Q.; Glazer, A. N.; Mathies, R. A., *Anal. Chem.* **1998,** *70*, 684-688.
14. Polesello, S.; Valsecchi, S. M., *J. Chromatogr. A* **1999,** *834*, 103-116.
15. Guijt, R. M.; Evenhuis, C. J.; Macka, M.; Haddad, P. R., *Electrophoresis* **2004,** *25*, 4032-4057.
16. da Silva, J. A. F.; do Lago, C. L., *Anal. Chem.* **1998,** *70*, 4339-4343.
17. Zemann, A. J.; Schnell, E.; Volgger, D.; Bonn, G. K., *Anal. Chem.* **1998,** *70*, 563-567.
18. Brito-Neto, J. G. A.; da Silva, J. A. F.; Blanes, L.; do Lago, C. L., *Electroanalysis* **2005,** *17*, 1198-1206.
19. Brito-Neto, J. G. A.; da Silva, J. A. F.; Blanes, L.; do Lago, C. L., *Electroanalysis* **2005,** *17*, 1207-1214.
20. Zemann, A. J., *Electrophoresis* **2003,** *24*, 2125-2137.
21. Kuban, P.; Hauser, P. C., *Electroanalysis* **2004,** *16*, 2009-2021.
22. Solinova, V.; Kasicka, V., *J. Sep. Sci.* **2006,** *29*, 1743-1762.
23. Kuban, P.; Hauser, P. C., *Anal. Chim. Acta* **2008,** *607*, 15-29.
24. Tanyanyiwa, J.; Hauser, P. C., *Electrophoresis* **2002,** *23*, 3781-3786.
25. Huang, X. H.; Pang, T. K. J.; Gordon, M. J.; Zare, R. N., *Anal. Chem.* **1987,** *59*, 2747-2749.
26. Huang, X. H.; Luckey, J. A.; Gordon, M. J.; Zare, R. N., *Anal. Chem.* **1989,** *61*, 766-770.

27. Avdalovic, N.; Pohl, C. A.; Rocklin, R. D.; Stillian, J. R., *Anal. Chem.* **1993,** *65*, 1470-1475.
28. Dasgupta, P. K.; Bao, L. Y., *Anal. Chem.* **1993,** *65*, 1003-1011.
29. Feng, H. T.; Wei, H. P.; Li, S. F. Y., *Electrophoresis* **2004,** *25*, 909-913.
30. Tay, E. T. T.; Law, W. S.; Sim, S. P. C.; Feng, H.; Zhao, J. H.; Li, S. F. Y., *Electrophoresis* **2007,** *28*, 4620-4628.
31. Bai, X. X.; Wu, Z. Y.; Josserand, J.; Jensen, H.; Schafer, H.; Girault, H. H., *Anal. Chem.* **2004,** *76*, 3126-3131.
32. Galloway, M.; Stryjewski, W.; Henry, A.; Ford, S. M.; Llopis, S.; McCarley, R. L.; Soper, S. A., *Anal. Chem.* **2002,** *74*, 2407-2415.
33. Shadpour, H.; Hupert, M. L.; Patterson, D.; Liu, C. G.; Galloway, M.; Stryjewski, W.; Goettert, J.; Soper, S. A., *Anal. Chem.* **2007,** *79*, 870-878.
34. Kok, W. T.; Sahin, Y., *Anal. Chem.* **1993,** *65*, 2497-2501.
35. Chen, D. C.; Hsu, F. L.; Zhan, D. Z.; Chen, C. H., *Anal. Chem.* **2001,** *73*, 758-762.
36. Doble, P.; Andersson, P.; Haddad, P. R., *J. Chromatogr. A* **1997,** *770*, 291-300.
37. Liu, S. R.; Dasgupta, P. K., *Anal. Chim. Acta* **1993,** *283*, 747-753.
38. Xue, Y. J.; Yeung, E. S., *Anal. Chem.* **1994,** *66*, 3575-3580.
39. Duffy, D. C.; McDonald, J. C.; Schueller, O. J. A.; Whitesides, G. M., *Anal. Chem.* **1998,** *70*, 4974-4984.
40. Liu, Y.; Vickers, J. A.; Henry, C. S., *Anal. Chem.* **2004,** *76*, 1513-1517.
41. Noblitt, S. D.; Kraly, J. R.; VanBuren, J. M.; Hering, S. V.; Collett, J. L.; Henry, C. S., *Anal. Chem.* **2007,** *79*, 6249-6254.
42. Lucy, C. A., *J. Chromatogr. A* **1999,** *850*, 319-337.
43. Jaros, M.; Vcelakova, K.; Zuskova, I.; Gas, B., *Electrophoresis* **2002,** *23*, 2667-2677.
44. Chen, L. C.; Chang, C. C.; Chang, H. C., *Electrochim. Acta* **2008,** *53*, 2883-2889.
45. Tseng, W. L.; Lin, Y. W.; Chen, K. C.; Chang, H. T., *Electrophoresis* **2002,** *23*, 2477-2484.
46. Lu, Q.; Copper, C. L.; Collins, G. E., *Anal. Chim. Acta* **2006,** *572*, 205-211.

CHAPTER 5. HIGH SENSITIVITY MICROCHIP ELECTROPHORESIS DETERMINATION OF INORGANIC ANIONS AND OXALATE IN ATMOSPHERIC AEROSOLS WITH ADJUSTABLE SELECTIVITY AND CONDUCTIVITY DETECTION

CHAPTER OVERVIEW

In chapter 4, a novel bubble cell detection scheme was demonstrated for microchip electrophoresis with conductivity detection. The detection limits achieved with this detection approach are low enough to measure aerosol composition for many inorganic ions, even during online operation. However, the separation chemistry demonstrated in chapter 4 was generic and didn't offer the selectivity and resolution between important analytes needed for aerosol monitoring. The primary inorganic anions in atmospheric aerosols are sulfate and nitrate, and chloride and nitrite can be present in some samples also. Although a large number of organic acids can contribute to the anionic fraction, oxalate is by far the dominant organic anion, is more acidic than most of the other organics, and has an electrophoretic more closely resembling the inorganic species than the organic ones. Therefore, the separation chemistry targeted oxalate and the dominant inorganic anions while purposefully avoiding the other organics. The work was published in *The Journal of Chromatography A*,[1] and the text and figures in this chapter are taken from that article.

ABSTRACT

A sensitive and selective separation of common anionic constituents of atmospheric aerosols, sulfate, nitrate, chloride, and oxalate, is presented using microchip electrophoresis. The optimized separation is achieved in less than 1 min and at low background electrolyte ionic strength (2.9 mM) by combining a metal-binding electrolyte anion (17-mM picolinic acid), a sulfate-binding electrolyte cation (19-mM HEPBS), a zwitterionic surfactant with affinity towards weakly-solvated anions (19-mM TDAPS), and operation in counter-EOF mode. The separation is performed at pH 4.7, permitting pH manipulation of oxalate's mobility. The majority of low-concentration organic acids are not observed at these conditions, allowing for rapid subsequent injections without the presence of interfering peaks. Because the mobilities of sulfate, nitrate, and oxalate are independently controlled, other minor constituents of aerosols can be analyzed, including nitrite, fluoride, and formate if desired using similar separation conditions. Contact conductivity detection is utilized, and the limit of detection (LOD) for oxalate (S/N = 3) is 180 nM without stacking. Sensitivity can be increased with field-amplified sample stacking by injecting from dilute electrolyte with a detection limit of 19 nM achieved. The high sensitivity, counter-EOF operation, and short analysis time make this separation well suited to continuous on-line monitoring of aerosol composition.

INTRODUCTION

Atmospheric aerosols have gained attention due to their considerable impact on both weather and human health.[2-5] Aerosols originate from a diverse range of biogenic, anthropogenic, and geogenic sources and can undergo a variety of oxidation and aging

reactions.[3,6-10] As a result, aerosol compositions exhibit high temporal and spatial variability.[3,7-9,11,12] Because of their ubiquity, high variability, and effects on health, visibility and climate, rapid and routine characterization of the chemical composition of atmospheric aerosols is in increasing demand for environmental monitoring.[3,13] The water-soluble anionic fraction of aerosols is one major constituent of interest. This fraction is typically dominated by nitrate and sulfate, while chloride is present in coastal regions and numerous organic acids are also present at lower concentrations.[3,8,11,12] Of the organic acids, oxalate is often the most prevalent, with typical concentrations ranging from ng m^{-3} to nearly 1 μg m^{-3}.[9,10,14]

Water-soluble anions in aerosols are currently measured by a variety of methods. Filter collection followed by offline analysis with ion chromatography or capillary electrophoresis is common.[15-24] However, because offline analyses cannot provide real-time concentration information, considerable effort has focused on developing semi-continuous analysis methods, and several new instruments have been demonstrated. Stolzenburg and Hering developed a nitrate aerosol analyzer that flash vaporizes particles into the gas phase, converts nitrate to NO, and detects via a chemiluminescent reaction with ozone. Time resolution was 10 min and the detection limit (LOD) was 400 ng m^{-3}.[25] Simon and Dasgupta developed an aerosol monitoring system that mixed steam with a 10-L min^{-1} air stream. Analysis was performed with a concentrator column and ion chromatography (IC), providing a sulfate LOD of 2.2 ng m^{-3} and 8-min sampling time.[26] Weber and co-workers developed a particle-into-liquid-sampler and coupled it to ion chromatography (PILS-IC). Both cations and anions could be analyzed when using

separate chromatographs, and a temporal resolution of 7 min and LOD of 100 ng m^{-3} were achieved.[27] Modifications to the PILS-IC have since improved both the temporal resolution and the LOD for major inorganic ions to 2.45 min and 1-288 ng m^{-3}, respectively.[28,29] Longer analysis times are required to monitor oxalate, formate, and acetate. Several variations and alternative designs related to the aforementioned steam collection devices have also been developed.[30-35] However, the temporal resolution of these instruments is limited by the inherent slowness of the chromatographic step. This limitation can be avoided by performing continuous aerosol monitoring via single particle mass spectrometry. This approach has recently gained interest due to the wealth of qualitative and quantitative information attainable.[36,37] However, high cost and limited ability to decipher individual organic species limit its use in many applications.[36,37]

Capillary electrophoresis (CE) is a promising alternative technique for performing rapid separations of aerosol components due to CE's inherent ability to quickly separate many components with low sample and reagent consumption. Separations of aerosol components have been presented using traditional CE instrumentation.[15,18-23,38-49] The majority of these protocols utilize indirect UV detection due to the low molar absorptivities of these analytes. Using contactless conductivity detection can improve detection limits over indirect absorbance detection, although this detection method has seen little use in aerosol-specific analyses.[15,50] To date, traditional CE methods have mostly targeted offline analysis of organic acids, focusing on CE's high peak capacity and not taking advantage of its short separation times for inorganic anions.

Consequently, typical CE analysis times for the most abundant aerosol anions are not considerably better than optimized IC analyses (2.5-4 min).[28,29]

Although modification of current CE aerosol protocols could readily achieve analysis times below 2 min for potential online analyses, better results may be possible by switching from traditional CE to microchip capillary electrophoresis (MCE). The field of microfluidics, including MCE, has shown that miniaturization allows analyses to be performed in shorter time scales with less sample and reagent consumption.[51] Separations of common inorganic anions with contactless conductivity detection have already been presented, and some of the best results show analysis times in the 30-60-s range and LODs of 1.5-5 μM.[52-54] Until recently, contact conductivity detection in MCE was limited by high background noise and low separation voltages due to the presence of a significant voltage drop between electrodes.[55] Consequently, detection limits were typically 5-1000 μM.[55] We recently introduced a bubble cell detection design which improves the compatibility of contact conductivity detection with microchip electrophoresis.[56] Higher separation voltages and lower noise were achieved, allowing for detection limits of 500 nM or better for inorganic ions without stacking. Although these detection limits are 1-2 orders of magnitude higher than IC on a concentration basis, much of the deficit can be overcome with longer injections and field-amplified sample stacking.[28,57] For instance, increasing the injection time from 1.2 to 2.0 s and injecting from dilute background electrolyte (BGE) improved the LOD for perchlorate from 200 nM to 22 nM with contact conductivity detection in a bubble cell.[56] Furthermore, mass detection limits are much lower for the MCE method than the IC

methods. Despite the potential of using MCE for the rapid analysis of water-soluble components in atmospheric aerosols, only two reports have applied this approach. The first report demonstrated the analysis of levoglucosan and other carbohydrates in aerosols from biomass combustion.[58] Pulsed amperometric detection was used, and the reported detection limit was 16.7 μM for levoglucosan. The only reported MCE analysis of inorganic anions in aerosols focused solely on nitrate and sulfate.[59] LODs were reported at 1 μM, and the ions were separated in under 2 min. No consideration was made for the potentially interfering ions chloride and nitrite. Additionally, analysis times of real samples were longer than 2 min because the electroosmotic flow (EOF) and any low-mobility ions migrate well after sulfate and nitrate, preventing this method from being used for rapid online monitoring.

In this report, we present the development of a selective MCE separation of common anionic constituents of aerosols using a poly(dimethylsiloxane) (PDMS) microchip. The separation approach utilizes a piperazine moiety-containing buffer cation for selective interaction with sulfate, uses a zwitterionic surfactant for selective interaction towards weakly-solvated ions (i.e. nitrate), and operates below pH 5 to allow modification of the electrophoretic mobility of oxalate. Because the separation approach allows for independent adjustment of individual electrophoretic mobilities, a variety of separation protocols can be used and additional analytes (nitrite, fluoride, and formate) detected. Additional resolution between analytes is achieved by operating in counter-EOF mode. Because the separation is low-pH, counter-EOF, and uses electrokinetic injection, little interference is observed from low concentration organic acids. Consequently, subsequent

injections can be performed immediately after the final analyte is detected. Analysis time for a separation of chloride, sulfate, nitrate, oxalate, and an internal standard is less than 25 s at –575 V cm^{-1}. The oxalate LOD without sample stacking was 180 nM, about three times lower than the best MCE measurement previously reported.[60] Injection from dilute buffer lowered the oxalate detection limit to 19 nM. The adjustable selectivity, short analysis time, freedom from interfering compounds, and high sensitivity make this separation an ideal fit for coupling to an aerosol collection system for semi-continuous online analysis.

EXPERIMENTAL

Materials

Sodium fluoride, oxalic acid, potassium 1,3-propanedisulfonate (PDS), sulfamic acid, picolinic acid, monopotassium acetylenedicarboxylic acid (ACD), N-(2-hydroxyethyl)piperazine-N'-(4-butanesulfonic acid) (HEPBS), and phosphorous acid were purchased from Sigma-Aldrich (St. Louis, MO, USA). Potassium chloride, ammonium sulfate, sodium nitrate, formic acid, sodium chlorate, sodium nitrite, sodium carbonate, sodium bicarbonate, and methanol were obtained from Fisher Scientific (Fair Lawn, NJ, USA). 2,2-Bis(hydroxymethyl)-2,2',2''-nitriloethanol (BIS-TRIS), N-tetradecyl,N,N-dimethyl-3-ammonio-1-propansulfonate (TDAPS), and methanesulfonic acid were procured from Fluka (Buchs, Switzerland). SU-8 2035 photoresist was purchased from Microchem (Newton, MA, USA). Sylgard 184 elastomer base and curing agent were purchased from Dow Corning (Midland, MI, USA). All chemicals

were used as obtained. Aqueous solutions were prepared in 18.2 MΩ cm water from a Millipore Milli-Q purifier (Billerica, MA, USA).

Microchip Construction

Construction of PDMS microchips and inclusion of microwire electrodes for conductivity detection have been described previously.[56,61-63] Specific dimensions are summarized here. The sample channel was 1.5 cm, buffer and sample waste channels were 1.0-cm long, and the separation channel was 5.2 cm (5.0-cm effective length). Channels were 39.6 ± 0.9-μm deep (n=4) and 50-μm wide as measured by profilometry. Sample and buffer reservoirs were 5 mm in diameter and were cut with 5-mm biopsy punches (Robbins Instruments, Chatham, NJ, USA). The detection zone was 200-μm wide and had an expansion distance of 375 μm (yielding an expansion angle of 11.3°) on both upstream and downstream sides.[56] 15-μm gold-plated tungsten wires (GoodFellow Corp., Huntingdon, UK) were spaced at a center-to-center distance of 120 μm perpendicularly to the separation channel, defining the conductivity cell.

Instrumentation and Data Analysis

Conductivity detection for MCE was performed by connecting the leads of a Dionex CD20 conductivity detector to the microchip detection wires. A Faraday cage was not placed around the microchip to reduce environmental noise. A home-built, floating high voltage power supply (HVPS) was used to apply separation potentials and maintain compatibility with the CD20. The HVPS was used to switch the buffer reservoir potential to the potential of the channel intersection during injection mode, performing

gated injection, which is electrokinetically biased.[64] Analog output (0-1 V) from the detector was monitored with a National Instruments USB-6210 DAQ and LabView 8.0 software running a homemade virtual instrument. Data were collected at 20 kHz and averaged in sets of 2000 to give an effective collection rate of 10 Hz. No additional data filtration was used. Baseline drift caused by background electrolyte evaporation and ion depletion was corrected by subtracting 6th order polynomial baseline fits from raw data. Because baseline noise is less than the 16-bit analog output resolution of the CD20, the LODs for the separation were considered to be the analyte concentrations that resulted in three of these 16-bit baseline steps (45.8 μV). All LODs are reported for concentrations giving this signal, and presented LOD uncertainties are the standard deviations of the peak height at LOD. All ionic strength calculations and electrophoresis simulations were performed using PeakMaster 5.2 software (available on the internet at http://www.natur.cuni.cz/~gas/).[65] OriginPro 7.0 was used for Gaussian peak fits to determine migration times and peak areas with MCE. IC peak identification and integration were performed using PeakNet software (Dionex Corp., Sunnyvale, CA, USA).

Filter Extract Analysis

Natural air samples for method comparison were collected in the Rocky Mountains intermountain area in September 2008 using an automated annular denuder/filter pack systems (URG-3000C, University Research Glassware, Inc., Chapel Hill, NC, USA). Air was passed through a 10-L min^{-1} PM2.5 cyclone inlet, followed by two coated denuders (URG, Inc., P/N URG-2000-30X242-3CSS) in series (sodium chloride and phosphorous

acid coating) to remove gaseous HNO_3, SO_2, and NH_3. A filter pack containing a nylon filter was used to collect fine particles (Nylasorb, pore size 1.0 μm, Pall Corp., East Hills, NY, USA), followed by another phosphorous acid-coated annular denuder to capture any ammonia volatilized from collected particles. Filters were extracted in water using an ultrasonic bath, and extracts were refrigerated between extraction and analysis. Anions were separated by IC with an AS14A column followed by an ASRS ULTRA II suppressor and detected using a CD20 conductivity detector (all devices by Dionex Corp.). MCE analyses used the above collection protocol with an additional 20% dilution for the addition of background electrolyte and internal standard to the sample. The later was done to ensure consistency of the sample conductivity and allow accurate quantitation of the unknown samples.

RESULTS AND DISCUSSION

General Separation Approach

The separation approach chosen in electrophoresis can have a large impact on the sensitivity, peak resolution, and analysis time. With conductivity detection, highest sensitivity is achieved by minimizing the conductivity of the displaced co-ion in the background electrolyte. Thus, for anion analyses, a large (thus low conductivity) weak acid is preferred in the background electrolyte (BGE) instead of smaller, more mobile anions. For the BGE counter-ion, theoretical considerations indicate that highest analyte signal comes from more mobile counter-ions (which enter the analyte zone to ensure charge balance when incomplete displacement of the co-ion occurs).[66] However, higher conductivity of the counter-ion causes higher background signal, often negating benefits

from a more-mobile counter-ion. Consequently, both the acid and base should be large, low-conductivity compounds. For lowest background signal, the pK_a of the acid should be higher than the pK_a of the base's conjugate acid, and the operating pH should be between these two pK_a values. Thus, required buffering capacity is maintained while keeping the buffer components primarily in their uncharged, nonconductive states.

Peak resolution between analytes is affected by a variety of separation conditions. Surfactant micelles are commonly used to alter separations, and this approach is termed micellar electrokinetic chromatography (MEKC).[67] MEKC of inorganic anions has been performed using sulfobetaine zwitterionic surfactants, which show affinity towards weakly-solvated anions.[68,69] Complexation using small molecule additives is also popular for improving separations. For example, 18-crown-6 is often used to bind potassium, barium, and strontium in inorganic cation separations.[70] However, this approach is rare for inorganic anions because strong, selective binding agents are uncommon, and known complexing agents are often highly-charged (i.e. metal ions).[71] Instead, inorganic anion selectivity is often obtained by modifying the ionic strength of the BGE, reducing the mobilities of dianions relative to monoanions.[71] However, an ionic strength increase yields a background signal increase in conductivity detection, so low-conductivity complexing molecules were sought for this separation. For modification of the mobilities of weak acids, operating at a pH near the pK_a values is typical.

Although surfactants, complexing agents, and pH selection can all affect the mobilities (therefore resolution) of individual analytes, selection of the bulk flow (EOF) can

universally affect resolution between peaks and has been discussed previously.[72-74] Improved resolution is observed with an EOF moving in the opposite direction of the analytes (counter-EOF), albeit at the expense of a longer analysis time. However, the separation channels in MCE are shorter than in traditional CE, so rapid separations are still readily achieved. Because the surface of PDMS is negatively charged in solution, counter-EOF operation was obtained without addition of cationic surfactants or other modifications to the PDMS surface. EOF measurements made with PDMS devices used in this work using solutions containing zwitterionic micelles below pH 5 showed typical EOF values of ~2 x 10^{-4} cm^2 V^{-1} s^{-1}.

From the discussion above, the separation approach chosen was to use a zwitterionic surfactant to modify the mobility of nitrate via MEKC, a BGE pH in the 4.5-5.0 range to control the migration of weak acids, and a weak counter-EOF to accentuate differences in ionic mobilities. The low pH of the separation has the side benefit of protonating most of the weak acids commonly observed in atmospheric aerosols other than oxalate and formate, lowering their mobilities and conductivities. Combined with the counter-EOF approach and electrokinetic biasing of gated injection,[64] these potential interferences should not be observed at typical concentrations. Consequently, late-migrating baseline fluctuations from these compounds or system peaks will not be anticipated, and subsequent injections can often be performed immediately after the last analyte (typically formate) is detected, making this separation approach attractive for rapid continuous-monitoring applications.

Background Electrolyte Cation

One shortcoming of the separation approach discussed so far is the lack of anticipated chloride/sulfate resolution. As already discussed, the preferred BGE counter-ion for this separation was a low-mobility base with a conjugate acid pK_a below 4.5. Additionally, complexation with either chloride or sulfate is desirable to resolve these two analytes without using high ionic strength. Small molecule complexation of anions is uncommon, and, to the authors' knowledge, no molecules meeting the aforementioned requirements have been identified for electrophoretic separations. However, previous work from our laboratory identified an interaction between protonated piperazine and sulfate, and this complexation was attributed to the protonated diamine moiety.[49] Unfortunately, piperazine is highly mobile at the desired pH, leading to rapid ion depletion since it electrokinetically exits the buffer reservoirs at a high rate. Ion depletion is undesirable because it causes shifts in the separation BGE composition, ionic strength, and pH.[75] Therefore, consideration was given to large, zwitterionic buffers containing the piperazine moiety. HEPBS was a promising option, and titration by sulfamic acid found the pK_a of the conjugate acid of the second amine to be 3.90 ± 0.02 ($n = 6$). The large size, low charge, and moderate pK_a value of HEPBS all met the aforementioned requirements. To determine if HEPBS complexes sulfate, comparisons were made between HEPBS and predicted behavior using PeakMaster (see Experimental section) and experimental results using other bases that were not anticipated to significantly interact with sulfate. Figure 5.1 shows these comparisons and indicates that both sulfate and oxalate interact with HEPBS, but no significant deviations from prediction were observed for these ions with other bases. Assuming no chlorate-BGE interactions, the

chlorate peak was used to calculate the EOF and, subsequently, mobilities of the other ions. At pH 4.7 and 3.0-mM ionic strength, the predicted mobility of sulfate was –7.51 x 10^{-4} cm^2 V^{-1} s^{-1}, but the measured mobility was measured at –7.01 x 10^{-4} cm^2 V^{-1} s^{-1} in HEPBS (6.7% slower). Similarly, oxalate was predicted at –6.28 x 10^{-4} cm^2 V^{-1} s^{-1} but measured at –6.03 x 10^{-4} cm^2 V^{-1} s^{-1} (3.9% slower). Comparisons between electrolytes were also made for two possible dianionic internal standards, acetylenedicarboxylate (ACD) and 1,3-propanedisulfonate (PDS). ACD was found to migrate at –6.19 x 10^{-4} cm^2 V^{-1} s^{-1} in HEPBS and –6.39 x 10^{-4} cm^2 V^{-1} s^{-1} in BIS-TRIS, a difference of 3.1%. PDS was observed at –5.70 x 10^{-4} cm^2 V^{-1} s^{-1} in HEPBS but at –5.78 x 10^{-4} cm^2 V^{-1} s^{-1} in BIS-TRIS (1.5% discrepancy). The differences in relative mobility shifts for the dianions show that the magnitude of HEPBS binding differs with chemical structure and is not due to only the analyte charge. The amount of binding is expected to change with HEPBS concentration. Therefore, concentration was varied and mobilities measured (Figure 5.1). The dianions, especially sulfate, all show larger mobility drops with concentration than predicted, further indicating complexation. The results from this study allow for the desired chloride/sulfate resolution to be achieved by choosing the appropriate ionic strength.

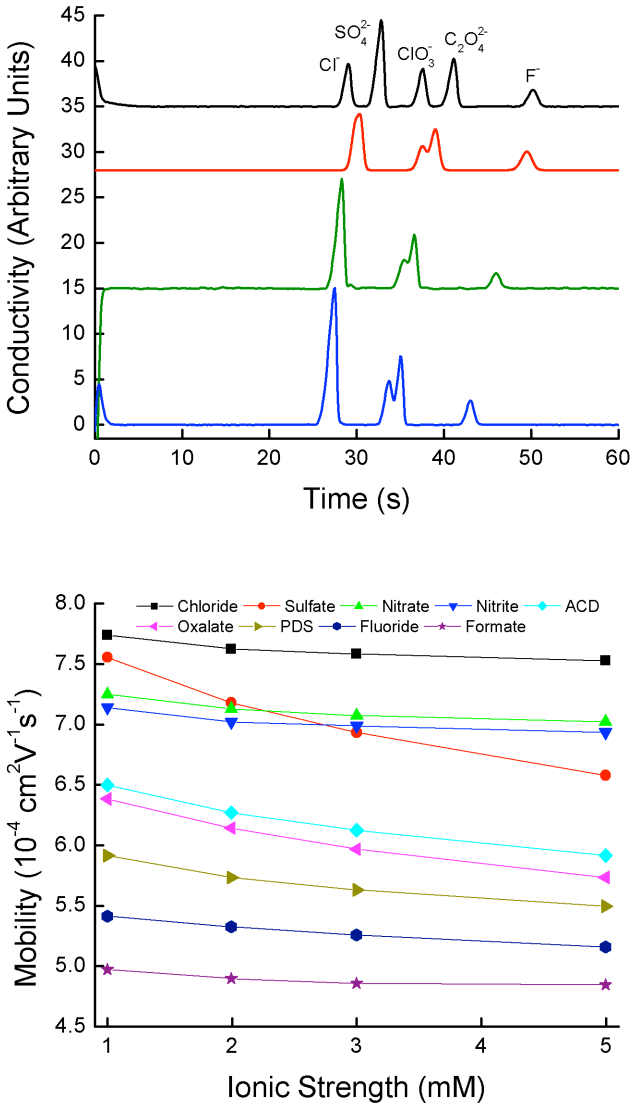

Figure 5.1. (Top) Simulation and experimental evaluation of buffer bases. All results obtained with picolinic acid at pH 4.7 and 3.0-mM ionic strength. Traces (top to bottom) are HEPBS, PeakMaster simulation, BIS-TRIS, and nicotinamide. Separations were performed at –300 V cm^{-1} with 25-µM analytes. Simulation conditions: –17340 V; 17-cm separation channel; EOF = 1.96 x 10^{-4} cm^2 V^{-1} s^{-1}. (Bottom) Effect of picolinic acid/HEPBS (pH 4.7) BGE concentration on the ionic mobilities of analyte anions and possible internal standards. Both sulfate and oxalate are observed to decrease in mobility more than predicted with higher ionic strengths due to interactions with the HEPBS cation. Sulfamate was used as an internal standard to account for changes in EOF, and its mobility was assumed equivalent to predicted values from PeakMaster. The calculated EOF was subtracted from the effective mobilities to give the presented ionic mobilities.

Background Electrolyte Surfactant

Zwitterionic surfactant micelles selectively interact with weakly-hydrated anions without increasing BGE conductivity.[68] Two sulfobetaine zwitterionic surfactants have been explored for use in capillary electrophoresis, N-dodecyl,N,N-dimethyl-3-ammonio-1-propansulfonate (DDAPS), and its tetradecyl- counterpart, TDAPS. For this separation, TDAPS was chosen due to its lower critical micelle concentration (CMC) coupled with the desire to avoid possible interactions with surfactant monomer. The effect of TDAPS concentration on the mobilities of the analytes and possible internal standards is shown in Figure 5.2.

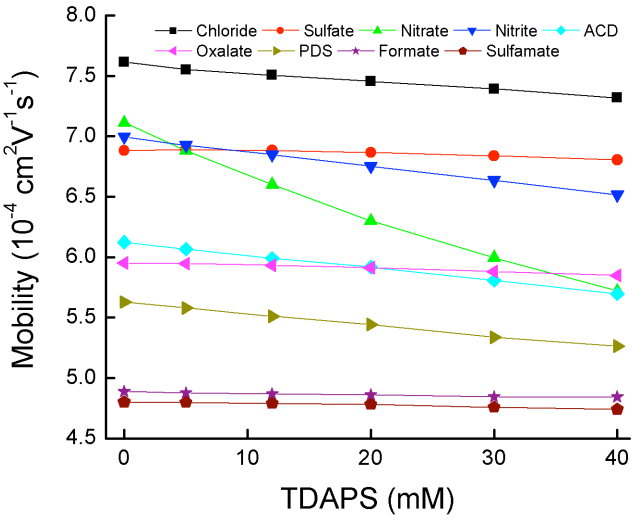

Figure 5.2. Effect of TDAPS concentration on ionic mobility. Experimental conditions: –300 V cm^{-1}; BGE = 16.9-mM picolinic acid/20.6-mM HEPBS (pH 4.7 at 3.0-mM ionic strength). Fluoride was assumed to not interact with the surfactant (mobility = –5.26 x 10^{-4} cm^2 V^{-1} s^{-1}) and was used to adjust for EOF variability. The calculated EOF was subtracted from the effective mobilities to give the presented ionic mobilities.

As expected from solvation considerations, nitrate shows the largest interactions with TDAPS. Nitrite also shows significant interactions with the surfactant, agreeing with

literature.[68,69] ACD and PDS both show some interaction with TDAPS, which is unexpected given their dianionic charge but may be due to the larger sizes of these molecules. The heavily-solvated sulfate and oxalate show almost no interactions with the surfactant, as expected, but chloride shows some low-level interactions with TDAPS, agreeing with previous observations.[68] The effect of TDAPS on chloride could potentially allow for a low ionic strength separation to be devised where sulfate migrates before chloride, but this approach was not explored in this work.

Background Electrolyte Anion and pH Optimization

The criteria for the BGE acid were discussed earlier. A variety of options were available, but picolinic acid was chosen due to its pK_a (5.4) being above the operating pH and also because it is a known metal chelator that could complex heavy metals, magnesium, and calcium in the sample or on the PDMS surface. Figure 5.3 compares separations using picolinic acid and its structural isomer nicotinic acid. The relative peak height for oxalate is lower in the nicotinic acid BGE, possibly due to oxalate interacting with cationic surface impurities.[49] Although channel preconditioning could be added to remove these impurities and allow for a non-chelating acid to be used, metals may still be present in real sample solutions, potentially binding oxalate and leading to incorrect quantitation. Quinaldic acid was also considered in addition to picolinic acid given its larger size (and thus lower background/higher conductivity sensitivity). However, quinaldic acid was observed to increase the EOF in the presence of the TDAPS surfactant, indicating that quinaldic acid is partitioning into the micelles and increasing the magnitude of the surface charge.

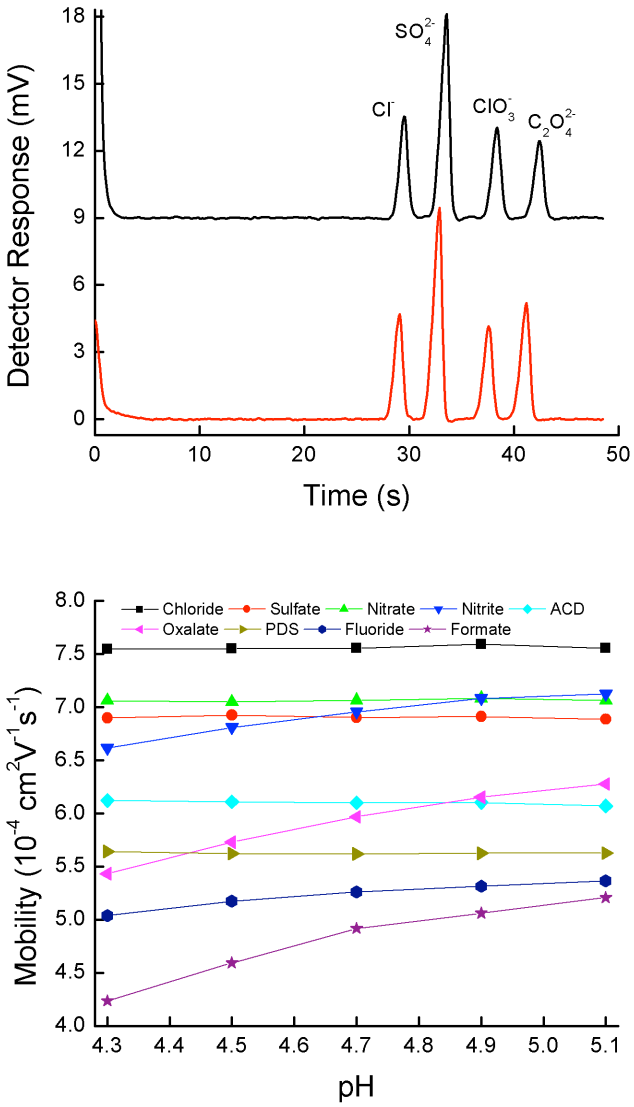

Figure 5.3. (Top) Comparison of nicotinic (top) and picolinic (bottom) acids in the BGE. Conditions: pH 4.7; 3.0-mM ionic strength; –300 V/cm field strength; 1.4-s injection; HEPBS base. Analytes are 25 µM. (Bottom) Effect of pH on ionic mobility. Experimental condition: –300 V cm^{-1} and 3.0-mM ionic strength. Background electrolyte consisted of picolinic acid and HEPBS. Sulfamate was assumed to be unaffected by pH changes in this range (mobility = –4.80 x 10^{-4} cm^2 V^{-1} s^{-1}), and was used to account for EOF changes. The calculated EOF was subtracted from the effective mobilities to give the presented ionic mobilities.

Using a picolinic acid/HEPBS buffer, the effect of pH on the analyte mobilities was tested (Figure 5.4). As expected, the mobilities of the weak acids oxalate, formate, nitrite, and fluoride all show pH dependencies, and the magnitude of this change depends on the proximity of the pH to the pK_a. Surprisingly, ACD shows no pH dependence, indicating that both of its pK_a values are below 3.0. As expected, no pH effect was observed in this range for chloride, nitrate, sulfate, and PDS. Although the effect of pH on electrophoretic separations is typically considered predictable, these empirical results allow for easy selection of operating pH.

Separation Performance

The studies on the effects on BGE cation, surfactant, and pH were used to generate a variety of potential separations, shown in Figure 5.4. These electropherograms show that several different migration orders and internal standards can be used, and operating conditions depend on the application. When nitrite levels are low and quantitation of nitrite is not desired, the first separation in Figure 5.4 will likely provide the best overall performance. Addition of an equimolar level of nitrite to this separation gave a sulfate/nitrite resolution of 0.82 ± 0.02 ($n = 11$). When increased nitrite resolution is needed, a lower pH and higher surfactant concentration result in nitrite migrating between sulfate and nitrate (Figure 5.4, second separation). This improved resolution comes at the cost of reduced sensitivity for both nitrate and oxalate and is due to the combined effects of an electrokinetically biased injection and a decrease in the molar conductivities (from complexation and protonation). The third separation in Figure 5.4 shows a separation that should provide increased oxalate sensitivity.

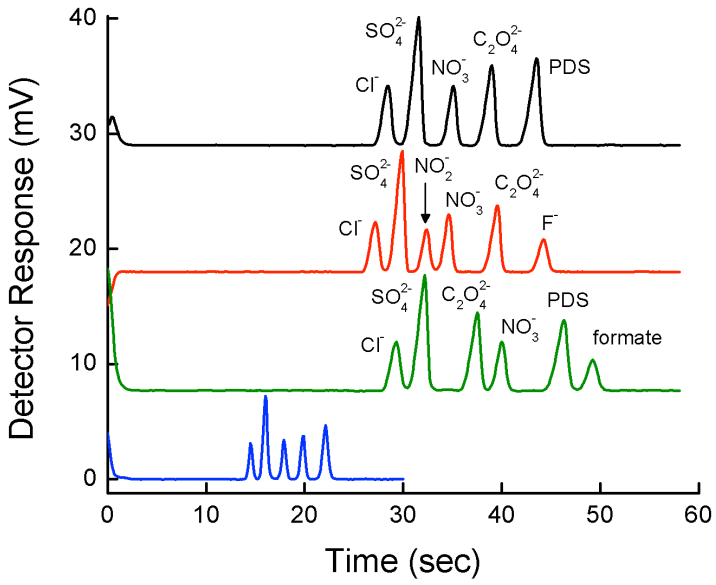

Figure 5.4. Possible separations using the described electrolyte system. Top separation: BGE = 17-mM picolinic acid/19-mM HEPBS/19-mM TDAPS (pH 4.68). 2nd separation: 26-mM picolinic acid/12-mM HEPBS/26-mM TDAPS (pH 4.45). 3rd separation: 9-mM picolinic acid/35-mM HEPBS/35-mM TDAPS (pH 5.0). The first three separations used –300 V cm^{-1} with 1.4-s injections. The 4th separation is identical to the first, but used –575 V cm^{-1} and a 0.7-s injection.

Here, the BGE is at pH 5.0 and the surfactant concentration has been increased in order to place oxalate between sulfate and nitrate in the separation. However, at these conditions the PDS internal standard comigrates with fluoride, so another internal standard would be required in samples where fluoride is present, which is typically only in heavily-polluted environments.[76] This separation also suffers from poor sulfate/nitrite resolution (0.86 ± 0.03, n = 12), and would require an increase in TDAPS to gain full resolution for these two analytes. The first three separations in Figure 5.4 were performed at –300 V cm^{-1} and analyses were completed in less than 55 s. The last separation in Figure 5.4 was performed at –575 V cm^{-1}, and gave a total analysis time for chloride, sulfate, nitrate, oxalate, and the internal standard of less than 25 s. If coupled to a semi-continuous

aerosol collector, subsequent injections could be performed at this rate and would lead to unprecedented temporal resolution for non-mass spectrometric monitoring of multiple aerosol species.

The BGE conditions used for the first electropherogram in Figure 5.4 were chosen for determining the LODs and linear ranges for the analytes because this separation is the one most likely to be used for general aerosol monitoring. Measurements were made with analytes dissolved in BGE to ensure pH control and non-stacking operation. With a 1.7-s gated injection and –300 V cm^{-1} separation, the measured LODs were 190 ± 30 nM for chloride, 260 ± 50 nM for nitrate, 180 ± 30 nM for oxalate, and 160 ± 30 nM for the PDS internal standard. To the authors' knowledge, these are the best LODs reported for these analytes using MCE and conductivity detection without stacking. The improved performance was attributed to the optimized separation chemistry and the bubble cell design. The sulfate LOD could not be accurately measured due to low-level contamination. The source of this contamination was unknown, but the ubiquity of sulfate is known to cause measurement problems at submicromolar concentrations, and potential sources are trace levels in the water, impurities in the buffer, leaching from storage containers, and dust contamination.[77] The obtained LODs without stacking are superior to traditional CE analyses utilizing indirect UV absorbance detection (optimized LODs = 0.5-5 μM),[18,19,41,43] but they are 3-5 times higher than CE with conductivity detection.[15] The MCE LODs are 5-100 times higher than values obtainable by IC.[18,28] Preparing the sample in dilute BGE allowed for field-amplified stacking, increasing concentration sensitivity and proportionally lowering detection limits. Utilizing a sample

dissolved in dilute BGE (dilution factor of 10) lowered the LODs to 19 ± 2 nM for oxalate and 20 ± 5 nM for PDS. At these lower concentrations, contamination problems from chloride and nitrate were also encountered, preventing measurement of their detection limits. The low detection limits with stacking indicate that, given a typical sample size of 20 μL, as little as 34 pg of oxalic acid need to be collected to reach the detection limit. Assuming a typical oxalate concentration of 50 ng m^{-3} and 1-L min^{-1} collection rate, a sampling time of only 41 s would be required for detection of oxalate in a 20-μL sample. Use of smaller sample volumes is possible and would proportionally decrease the required mass and sampling time. An additional benefit of MCE over most other methods is that only a small fraction of the sample is injected, allowing multiple injections to be performed and improved measurement precision to be achieved. As noted earlier, analyte sensitivity varies with separation protocol. Therefore, a higher pH should provide a lower detection limit for oxalate.

Linear range measurements were made at the same conditions as the LOD measurements. Because changes in bulk solution conductivity (and thus, amount injected) occur with high analyte concentrations, peak area measurements were made relative to a 25-μM PDS internal standard. Calibrations were measured from 500 nM and found linear to 300 μM (R^2 for chloride = 0.9996, sulfate = 0.9997, nitrate = 0.9998, and oxalate = 0.9997). The linear range is nearly three orders of magnitude, in line with other MCE separations with conductivity detection.[56] For stacking operation, calibrations were made relative to 3 μM PDS and measured from 40 nM to 90 μM. Linearity was maintained to 90 μM for chloride, sulfate and nitrate (R^2 = 0.9997, 0.9995, 0.9997, respectively), but oxalate could

only be monitored to 30 μM (R^2 = 0.9998) due to poor resolution between oxalate and the internal standard at higher concentrations. Deviations from linearity at high concentrations are due to overloading, which depends on the injected mass in addition to BGE and analyte conductivities. At higher concentrations of analyte, the sample conductivity is increased, thereby lowering the injected mass. For instance, 90-μM ammonium sulfate in the dilute BGE had an estimated conductivity (4.9 mS m^{-1}) more than twice that of the dilute BGE alone (2.2 mS m^{-1}). Consequently, linearity is maintained for a larger relative range but at the expense of an increased detection limit for analytes at low concentrations in the sample, such as oxalate.

Analysis of Real Samples

Eight aerosol sample extracts were analyzed to test the applicability of the MCE separation with real sample matrices, and quantitative accuracy of the MCE method with these samples was tested by comparing with IC measurements of chloride, sulfate, and nitrate (Figure 5.5). Both chloride and sulfate lacked systematic deviations, but showed random deviations on both sides of the 1:1 line, which is expected for fluctuations in the IC injection volumes and addition of the MCE internal standard. In contrast, nitrate was measured to be systematically high with the MCE method. The reason for this deviation was not determined. Despite this deviation, the correlation coefficient between the two methods for the three analytes tested was 0.981. To test the reproducibility of the MCE measurements, the conditions used for the second trace in Figure 5.4 ("separation 2") were compared with the above MCE results (top trace in Figure 5.4, "separation 1"), and

the same sample solutions were used to avoid any deviations in the internal standard amount. Results are shown in Figure 5.5.

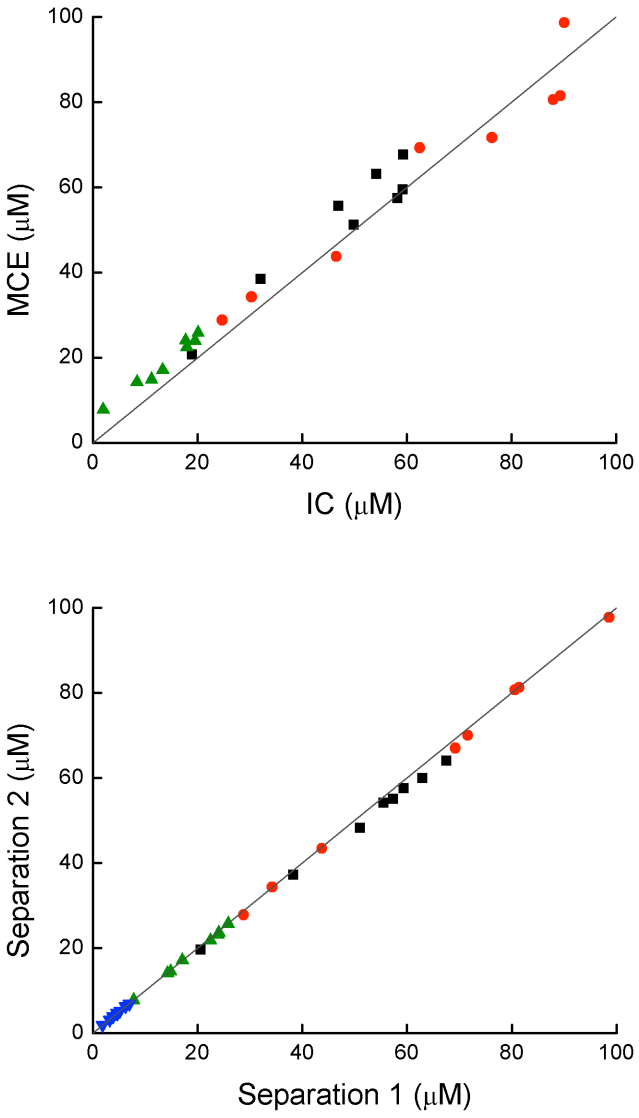

Figure 5.5. (Top) Comparison of concentrations for 8 sample extracts as determined by MCE and IC. Separation conditions were the same as the top trace in Figure 5.4. (Bottom) Comparison of MCE analyses of samples using two microchips and two separation protocols. X-axis used the conditions from the top trace of Figure 5.4, and the y-axis used the conditions from the second trace in Figure 5.4. Squares = chloride, circles = sulfate, triangles = nitrate, inverted triangles = oxalate. The 1:1 correlation is represented by the solid line. All MCE values are an average of four replicate injections.

Excellent agreement is observed between the two methods, and the only systematic deviation observed was for chloride, which was systematically lower with separation 2. For the four analytes compared, a correlation coefficient of 0.999 was observed between the methods. These results indicate that the uncertainty of the MCE method may be dominated by fluctuations in the quantity of internal standard added to the sample.

For automated, extended aerosol monitoring applications, the MCE separation should show long-term stability and not be compromised by small changes in buffer composition due to ion depletion.[75] Because the BGE consists of low-mobility compounds and operates at low EOF, the BGE lifetime was expected to be relatively long. To test the longevity of the BGE, a separation field of –300 V cm^{-1} was applied, injections were performed at 60-s intervals, and analyte migration times monitored. Figure 5.6 shows migration times over a 110-min analysis period. A slight decrease in migration time is observed with time and is attributed to EOF equilibration, but otherwise fluctuations are minor. The long lifetime of the BGE for this separation makes it acceptable for use in semi-continuous applications where extended analysis times without manual BGE replenishment may be needed. Ultimately for continuous use a buffer replacement system will be developed that permits replacement of the buffer at multiple hour intervals.

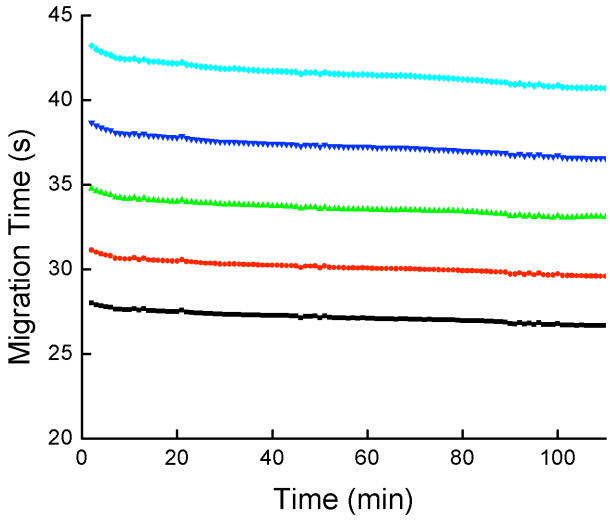

Figure 5.6. Migration times for the analytes and internal standard during extended monitoring. Separation conditions are the same as the top trace in Figure 5.4. A slight decrease observed over time is attributed to EOF equilibration. Analytes (from shortest to longest migration times) are chloride, sulfate, nitrate, oxalate, and PDS.

CONCLUSIONS

A new microchip electrophoresis separation protocol for the common aerosol constituents chloride, sulfate, nitrate, and oxalate is presented. The buffer cation was chosen for selective complexation of sulfate, allowing for baseline resolution at relatively low ionic strength. The nature of the background electrolyte allows for independent control of the electrophoretic mobilities of most of the analytes, providing for a variety of separation condition options as well as monitoring of the less-prominent aerosol components nitrite, fluoride, and formate. Detection limits for oxalate were 180 nM without stacking and 19 nM when injection from dilute background electrolyte enabled field-amplified sample stacking. These LODs are superior to other microchip electrophoresis protocols for oxalate and other inorganic anions. Analyses were less than 25 s when operating at –575

V cm^{-1}. The combination of a low-pH electrolyte, counter-EOF operation, and electrokinetic biasing with gated injection permits subsequent injections to be performed immediately after the final analyte (typically formate) is detected, making this an ideal candidate for rapid analyses with online aerosol monitoring systems.

CLOSING COMMENTS

The chemistry discussed in this chapter was another step towards the online monitoring of aerosol anions. As such, it was explicitly used during the development of the first online monitoring system for aerosol composition using MCE, discussed in Chapter 6. Also, due to limitations to the length of the text during its publication, specific details on some of the unique requirements on the separation were not given here. Instead, they can be found in chapter 7. Since collecting the data discussed above, the figures of merit for this technique have improved dramatically via changes in detector settings, employment of the detector offset functionality, changes in detection electrode composition, and improved electronic shielding. Detection limits are now 6-8 times lower and separation efficiencies have improved. Details are given in chapter 8. The reproducibility and expected results of calibrations using the described chemistry can be found in Appendix 2.

REFERENCES

1. Noblitt, S. D.; Schwandner, F. M.; Hering, S. V.; Collett, J. L.; Henry, C. S., *J. Chromatogr. A* **2009,** *1216*, 1503-1510.
2. Bernstein, J. A.; Alexis, N.; Barnes, C.; Bernstein, I. L.; Bernstein, J. A.; Nel, A.; Peden, D.; Diaz-Sanchez, D.; Tarlo, S. M.; Williams, P. B., *J. Allergy Clin. Immunol.* **2004,** *114*, 1116-1123.
3. Poschl, U., *Angew. Chem. Int. Ed.* **2005,** *44*, 7520-7540.
4. Kanakidou, M.; Seinfeld, J. H.; Pandis, S. N.; Barnes, I.; Dentener, F. J.; Facchini, M. C.; Van Dingenen, R.; Ervens, B.; Nenes, A.; Nielsen, C. J.; Swietlicki, E.; Putaud, J. P.; Balkanski, Y.; Fuzzi, S.; Horth, J.; Moortgat, G. K.; Winterhalter, R.; Myhre, C. E. L.; Tsigaridis, K.; Vignati, E.; Stephanou, E. G.; Wilson, J., *Atmos. Chem. Phys.* **2005,** *5*, 1053-1123.
5. Lohmann, U.; Feichter, J., *Atmos. Chem. Phys.* **2005,** *5*, 715-737.
6. FinlaysonPitts, B. J.; Pitts, J. N., *Science* **1997,** *276*, 1045-1052.
7. Raes, F.; Van Dingenen, R.; Vignati, E.; Wilson, J.; Putaud, J. P.; Seinfeld, J. H.; Adams, P., *Atmos. Environ.* **2000,** *34*, 4215-4240.
8. Pandis, S. N.; Wexler, A. S.; Seinfeld, J. H., *J. Phys. Chem.* **1995,** *99*, 9646-9659.
9. Chebbi, A.; Carlier, P., *Atmos. Environ.* **1996,** *30*, 4233-4249.
10. Kawamura, K.; Kasukabe, H.; Barrie, L. A., *Atmos. Environ.* **1996,** *30*, 1709-1722.
11. Putaud, J. P.; Raes, F.; Van Dingenen, R.; Bruggemann, E.; Facchini, M. C.; Decesari, S.; Fuzzi, S.; Gehrig, R.; Huglin, C.; Laj, P.; Lorbeer, G.; Maenhaut, W.; Mihalopoulos, N.; Mulller, K.; Querol, X.; Rodriguez, S.; Schneider, J.; Spindler, G.; ten Brink, H.; Torseth, K.; Wiedensohler, A., *Atmos. Environ.* **2004,** *38*, 2579-2595.
12. Saxena, P.; Hildemann, L. M., *J. Atmos. Chem.* **1996,** *24*, 57-109.
13. Sipin, M. F.; Guazzotti, S. A.; Prather, K. A., *Anal. Chem.* **2003,** *75*, 2929-2940.
14. Kawamura, K.; Ikushima, K., *Environ. Sci. Technol.* **1993,** *27*, 2227-2235.
15. Valsecchi, S.; Tartari, G.; Polesello, S., *J. Chromatogr. A* **1997,** *760*, 326-332.
16. Fukushi, K.; Takeda, S.; Chayama, K.; Wakida, S., *J. Chromatogr. A* **1999,** *834*, 349-362.
17. Timerbaev, A. R.; Dabek-Zlotorzynska, E.; van den Hoop, M. A. G. T., *Analyst* **1999,** *124*, 811-826.
18. Dabekzlotorzynska, E.; Dlouhy, J. F., *J. Chromatogr. A* **1994,** *671*, 389-395.
19. Dabekzlotorzynska, E.; Dlouhy, J. F.; Houle, N.; Piechowski, M.; Ritchie, S., *J. Chromatogr. A* **1995,** *706*, 469-478.
20. Dabekzlotorzynska, E.; Dlouhy, J. F., *J. Chromatogr. A* **1995,** *706*, 527-534.
21. Dabek-Zlotorzynska, E.; Aranda-Rodriguez, R.; Buykx, S. E. J., *Anal. Bioanal. Chem.* **2002,** *372*, 467-472.
22. Blanco-Heras, G. A.; Turnes-Carou, M. I.; Lopez-Mahia, P.; Muniategui-Lorenzo, S.; Prada-Rodriguez, D.; Fernandez-Fernandez, E., *Electrophoresis* **2008,** *29*, 1347-1354.
23. Souza, S. R.; Tavares, M. F. M.; de Carvalho, L. R. F., *J. Chromatogr. A* **1998,** *796*, 335-346.
24. Ammann, A. A.; Ruttimann, T. B., *J. Chromatogr. A* **1995,** *706*, 259-269.
25. Stolzenburg, M. R.; Hering, S. V., *Environ. Sci. Technol.* **2000,** *34*, 907-914.

26. Simon, P. K.; Dasgupta, P. K., *Anal. Chem.* **1995,** *67*, 71-78.
27. Weber, R. J.; Orsini, D.; Daun, Y.; Lee, Y. N.; Klotz, P. J.; Brechtel, F., *Aerosol Sci. Technol.* **2001,** *35*, 718-727.
28. Orsini, D. A.; Ma, Y. L.; Sullivan, A.; Sierau, B.; Baumann, K.; Weber, R. J., *Atmos. Environ.* **2003,** *37*, 1243-1259.
29. Peltier, R. E.; Sullivan, A. P.; Weber, R. J.; Brock, C. A.; Wollny, A. G.; Holloway, J. S.; de Gouw, J. A.; Warneke, C., *Atmospheric Chemistry and Physics* **2007,** *7*, 3231-3247.
30. Slanina, J.; ten Brink, H. M.; Otjes, R. P.; Even, A.; Jongejan, P.; Khlystov, A.; Waijers-Ijpelaan, A.; Hu, M., *Atmos. Environ.* **2001,** *35*, 2319-2330.
31. Zellweger, C.; Ammann, M.; Hofer, P.; Baltensperger, U., *Atmos. Environ.* **1999,** *33*, 1131-1140.
32. Khlystov, A.; Wyers, G. P.; Slanina, J., *Atmos. Environ.* **1995,** *29*, 2229-2234.
33. Loflund, M.; Kasper-Giebl, A.; Tscherwenka, W.; Schmid, M.; Giebl, H.; Hitzenberger, R.; Reischl, G.; Puxbaum, H., *Atmos. Environ.* **2001,** *35*, 2861-2869.
34. Al-Horr, R.; Samanta, G.; Dasgupta, P. K., *Environ. Sci. Technol.* **2003,** *37*, 5711-5720.
35. Ullah, S. M. R.; Takeuchi, M.; Dasgupta, P. K., *Environ. Sci. Technol.* **2006,** *40*, 962-968.
36. Jayne, J. T.; Leard, D. C.; Zhang, X. F.; Davidovits, P.; Smith, K. A.; Kolb, C. E.; Worsnop, D. R., *Aerosol Sci. Technol.* **2000,** *33*, 49-70.
37. Canagaratna, M. R.; Jayne, J. T.; Jimenez, J. L.; Allan, J. D.; Alfarra, M. R.; Zhang, Q.; Onasch, T. B.; Drewnick, F.; Coe, H.; Middlebrook, A.; Delia, A.; Williams, L. R.; Trimborn, A. M.; Northway, M. J.; DeCarlo, P. F.; Kolb, C. E.; Davidovits, P.; Worsnop, D. R., *Mass Spectrom. Rev.* **2007,** *26*, 185-222.
38. Dabek-Zlotorzynska, E.; Piechowski, M.; Keppel-Jones, K.; Aranda-Rodriguez, R., *J. Sep. Sci.* **2002,** *25*, 1123-1128.
39. Dabek-Zlotorzynska, E.; Kelly, M.; Chen, H.; Chakrabarti, C. L., *Anal. Chim. Acta* **2003,** *498*, 175-187.
40. Dabek-Zlotorzynska, E.; Kelly, M.; Chen, H. D.; Chakrabarti, C. L., *Chemosphere* **2005,** *58*, 1365-1376.
41. Krivacsy, Z.; Molnar, A.; Tarjanyi, E.; Gelencser, A.; Kiss, G.; Hlavay, J., *J. Chromatogr. A* **1997,** *781*, 223-231.
42. Garcia, S. T.; Valenzuela, M. I. A.; Gil, E. P., *Talanta* **2008,** *75*, 748-752.
43. DabekZlotorzynska, E.; Piechowski, M.; Liu, F.; Kennedy, S.; Dlouhy, J. F., *J. Chromatogr. A* **1997,** *770*, 349-359.
44. Dabek-Zlotorzynska, E.; Piechowski, M.; McGrath, M.; Lai, E. P. C., *J. Chromatogr. A* **2001,** *910*, 331-345.
45. Tam, W. F. C.; Tanner, P. A.; Law, P. T. R.; Bachmann, K.; Potzsch, S., *Anal. Chim. Acta* **2001,** *427*, 259-269.
46. Adler, H.; Siren, H.; Kulmala, M.; Riekkola, M. L., *J. Chromatogr. A* **2003,** *990*, 133-141.
47. Gao, S. D.; Rudolph, J., *J. Chromatogr. Sci.* **2004,** *42*, 323-328.
48. Sierau, B.; Stratmann, F.; Pelzing, M.; Neususs, C.; Hofmann, D.; Wilck, M., *J. Aerosol Sci.* **2003,** *34*, 225-242.

49. Noblitt, S. D.; Mazzoleni, L. R.; Hering, S. V.; Collett, J. L.; Henry, C. S., *J. Chromatogr. A* **2007,** *1154*, 400-406.
50. Kuban, P.; Kuban, P.; Kuban, V., *Electrophoresis* **2002,** *23*, 3725-3734.
51. West, J.; Becker, M.; Tombrink, S.; Manz, A., *Anal. Chem.* **2008,** *80*, 4403-4419.
52. Kuban, P.; Hauser, P. C., *Electrophoresis* **2005,** *26*, 3169-3178.
53. Tanyanyiwa, J.; Abad-Villar, E. M.; Hauser, P. C., *Electrophoresis* **2004,** *25*, 903-908.
54. Tanyanyiwa, J.; Hauser, P. C., *Electrophoresis* **2002,** *23*, 3781-3786.
55. Guijt, R. M.; Evenhuis, C. J.; Macka, M.; Haddad, P. R., *Electrophoresis* **2004,** *25*, 4032-4057.
56. Noblitt, S. D.; Henry, C. S., *Anal. Chem.* **2008,** *80*, 7624-7630.
57. Simpson, S. L.; Quirino, J. P.; Terabe, S., *J. Chromatogr. A* **2008,** *1184*, 504-541.
58. Garcia, C. D.; Engling, G.; Herckes, P.; Collett, J. L.; Henry, C. S., *Environ. Sci. Technol.* **2005,** *39*, 618-623.
59. Liu, Y.; MacDonald, D. A.; Yu, X. Y.; Hering, S. V.; Collett, J. L.; Henry, C. S., *Analyst* **2006,** *131*, 1226-1231.
60. Masar, M.; Zuborova, M.; Kaniansky, D.; Stanislawski, B., *J. Sep. Sci.* **2003,** *26*, 647-652.
61. Duffy, D. C.; McDonald, J. C.; Schueller, O. J. A.; Whitesides, G. M., *Anal. Chem.* **1998,** *70*, 4974-4984.
62. Liu, Y.; Vickers, J. A.; Henry, C. S., *Anal. Chem.* **2004,** *76*, 1513-1517.
63. Noblitt, S. D.; Kraly, J. R.; VanBuren, J. M.; Hering, S. V.; Collett, J. L.; Henry, C. S., *Anal. Chem.* **2007,** *79*, 6249-6254.
64. Jacobson, S. C.; Koutny, L. B.; Hergenroder, R.; Moore, A. W.; Ramsey, J. M., *Anal. Chem.* **1994,** *66*, 3472-3476.
65. Jaros, M.; Vcelakova, K.; Zuskova, I.; Gas, B., *Electrophoresis* **2002,** *23*, 2667-2677.
66. Nielen, M. W. F., *J. Chromatogr.* **1991,** *588*, 321-326.
67. Terabe, S.; Otsuka, K.; Ando, T., *Anal. Chem.* **1985,** *57*, 834-841.
68. Woodland, M. A.; Lucy, C. A., *Analyst* **2001,** *126*, 28-32.
69. Yokoyama, T.; Macka, M.; Haddad, P. R., *Anal. Chim. Acta* **2001,** *442*, 221-230.
70. Okada, T., *J. Chromatogr. A* **1999,** *834*, 73-87.
71. Lucy, C. A., *J. Chromatogr. A* **1999,** *850*, 319-337.
72. Kar, S.; Dasgupta, P. K., *Microchem. J.* **1999,** *62*, 128-137.
73. Jorgenson, J. W.; Lukacs, K. D., *Anal. Chem.* **1981,** *53*, 1298-1302.
74. Jorgenson, J. W.; Lukacs, K. D., *Science* **1983,** *222*, 266-272.
75. Bello, M. S., *J. Chromatogr. A* **1996,** *744*, 81-91.
76. Feng, Y. W.; Ogura, N.; Feng, Z. W.; Zhang, F. Z.; Shimizu, H., *Water Air Soil Poll.* **2003,** *145*, 95-107.
77. Haber, C.; VanSaun, R. J.; Jones, W. R., *Anal. Chem.* **1998,** *70*, 2261-2267.

CHAPTER 6. INTERFACING MICROCHIP ELECTROPHORESIS TO A GROWTH TUBE PARTICLE COLLECTOR FOR SEMI-CONTINUOUS MONITORING OF ATMOSPHERIC AEROSOL COMPOSITION

CHAPTER FOREWORD

This chapter discusses the development and testing of the prototype Aerosol Chip Electrophoresis (ACE) instrument, which was the first online system employing microfluidics for the analysis of aerosol chemical composition. The separation chemistry described in chapter 5 was developed specifically for the purpose of online monitoring, and the methods from that chapter were used as a platform here. This work was published in the journal *Analytical Chemistry*,[1] and most of the text and figures come from that article.

ABSTRACT

Semi-continuous monitoring of aerosol chemical composition has continually increased in demand because of the high spatial and temporal variability of atmospheric particles and the effects these aerosols have on human health and the environment. To address this demand, we describe the preliminary development of a semi-continuous aerosol composition analyzer consisting of a growth tube particle collector coupled to a microfluidic device for chemical analysis. The growth tube enlarges particles through water condensation in a laminar flow, permitting inertial collection into the microchip sample reservoir. Analysis is done by electrophoresis with conductivity detection. To avoid hydrodynamic interference from the sampling pressure, the microchip was operated isobarically by sealing the buffer reservoirs from the atmosphere and interconnecting all the reservoirs with air ducts. The collector samples at 1 L min^{-1} and deposits particles into 30 μL of solution. Sample accumulates with time, and sequential injections are performed as aerosol concentration increases. For extended analyses, a sample rinsing system flushes the sample collection reservoir periodically. For inorganic anions, temporal resolution of 1 min and estimated detection limits of 70-140 ng m^{-3} min were obtained. The system was used to measure sulfate and nitrate, and results were compared to a Particle-Into-Liquid-Sampler running in parallel. Results indicate that the prototype growth tube-microchip system (termed Aerosol Chip Electrophoresis, ACE) could provide a useful compliment to existing aerosol monitoring technologies, especially when less-expensive and/or rapid analyses are desired.

INTRODUCTION

Particles suspended in the atmosphere, commonly known as aerosols, originate from a wide variety of biogenic, anthropogenic, geogenic, and secondary sources and can react in the atmosphere via numerous mechanisms to produce a highly variable distribution of particles.[2-7] The variability of the size, shape, and composition of the particles and the low mass concentration (typically μg m^{-3}) make characterizing the particle chemistry challenging.[2,8,9] The difficulty in making these measurements coupled with aerosols' ubiquity, large size range, wide compositional spectrum, and high temporal and spatial variability make aerosols one of the most significant unknowns in both human health and climate.[10-12]

In terms of aerosol composition, measurement of the water-soluble fraction is an area of particular interest. The most common water-soluble species in ambient aerosols can be categorized as inorganic cations (ammonium, potassium, calcium, sodium, and magnesium), inorganic anions (sulfate, nitrate, nitrite, chloride, and oxalate), and organic carbon (termed WSOC).[2,13,14] Other species, including heavy metals and organic amines, are also measured.[15,16] Various methods have been developed to measure water-soluble species, including both offline analyses and online instrumentation (for semi-continuous monitoring in near real-time). Offline measurements involve filter or inertial impactor collection, extraction, and analysis using conventional techniques such as ion chromatography (IC), gas chromatography (GC), and capillary electrophoresis (CE). These analyses have the advantage of requiring less-integrated instrumentation and permit improved results through preconcentration techniques and replicate analyses.

However, because analyses are not real-time, these methods can suffer from low sampling frequency and sampling artifacts.[8,17,18]

To overcome some of the artifacts from offline sampling and to permit easier on-site data evaluation, several online monitoring systems have been developed.[19,20] One instrument is the aerosol mass spectrometer (AMS), which provides both qualitative and quantitative information with particle size data with a high time resolution.[21-24] High cost, however, prohibits its routine use. An alternative is a steam collection approach where sampled air is mixed with steam and then impacted into a stream of flowing water for analysis, typically by IC. Dasgupta and coworkers pioneered this approach, and a variety of different designs have been presented.[25-35] One of the most widespread is the Particle-Into-Liquid-Sampler (PILS).[27] Several PILS-IC iterations have been developed, and sampling intervals as fast as 2.5 min and limits of detection (LODs) in the 1-300 ng m^{-3} range have been reported for inorganic species, while longer times are needed for organic acid analyses.[28,29]

The temporal resolution of aerosol collectors coupled to separation instrumentation is typically limited by the separation step. One promising speciation technique for faster analyses is CE. A variety of offline aerosol analyses have been developed for CE.[36-39] However, conventional CE instruments are roughly the same size as IC equipment, and increased portability is desirable. Also, many CE analyses have not been optimized for short sampling intervals. A smaller, quicker, and less expensive alternative to traditional CE is microchip capillary electrophoresis (MCE).[40] MCE can provide rapid, sensitive

analyses using small samples and has been exploited in bioanalytical chemistry.[40] However, until recently, this technology had not been explored for aerosol composition analysis. Our group recently developed a MCE protocol for the separation of inorganic anions in aerosol extracts.[41] The method provided LODs below 300 nM and sub-minute time resolution. Additionally, the separation scheme allowed for immediate subsequent injections and therefore was ideal for online analyses. However, until now no interface permitted coupling of MCE to aerosol collectors to utilize this functionality.

Here, we report the interfacing of MCE to a water-based condensation growth tube collector for online monitoring of aerosol composition. The prototype integrated system, called Aerosol Chip Electrophoresis (ACE), uses the laminar-flow water condensation principle of the water–based condensation particle counter (WCPC).[42] Air is sampled downward through the growth tube, particles are enlarged into the supermicrometer size range, and the resulting droplets are impacted into the buffer-filled microchip sample reservoir. In its current, proof of principal design, the instrument continuously accumulates aerosol mass and analyte concentrations are determined differentially from electrophoresis measurements. The sample reservoir was augmented with a flushing system to periodically remove the sample and replenish with fresh solution. To extend microchip operation, relatively large (125-μL) background electrolyte (BGE) volumes were employed to minimize buffer depletion effects. Additionally, the effects of sample ion depletion were considered theoretically, and results were used to optimize the sample regeneration interval. ACE was tested with inorganic anions in ambient aerosols, showing the potential for 1-min resolution with estimated detection limits of 70-140 ng

m^{-3} min when sampling at 1 L min^{-1}. In the future, better time resolution may be achieved with higher separation voltages, and lower detection limits may be reached using smaller liquid volumes or stacking. Currently, the system has only limited applicability in field analyses due to its particle count upper limit of ~20 000 cm^{-1} and relatively short unattended operation limit of ~3 h. These issues are currently being addressed, and in the future we expect ACE to provide the possibility of routine aerosol compositional monitoring with high temporal resolution, increased portability, and reduced cost.

GROWTH TUBE COLLECTOR APPROACH

Except for hygroscopic materials, particles do not readily grow through vapor condensation unless exposed to vapor supersaturation. Due to surface tension, the equilibrium water vapor pressure over the surface of small particles is higher than that over a similarly composed flat surface. Smaller particles have higher equilibrium vapor pressures and hence require higher supersaturation to activate growth.

The approach used here to create the supersaturation necessary to activate condensational growth is the same as that in the laminar-flow WCPC.[42] The growth tube utilizes the differing rates of heat and water vapor diffusion in a laminar flow. In its simplest form, the growth tube consists of a wet-walled tube, through which aerosols flow laminarly. The first half of the growth tube is cooled; the second half is heated. A thermal break between the two sections gives a sharp (near step function) increase in the wall temperature at this juncture. Likewise, the vapor pressure of water at the surface of the

wetted walls increases. As air flows from the cooled region into the warm section of the growth tube, both the air temperature and water vapor concentration increase. The increase is not discontinuous, but lags behind the change at the walls. This lag is most pronounced along the centerline. Because the mass diffusivity of water vapor (0.265 cm^2 s^{-1}) is larger than the thermal diffusivity of air (0.215 cm^2 s^{-1}), the rate of water vapor transport is faster than the rate of heat transfer. Consequently, water vapor reaches the flow centerline more quickly than the flow warms. A region of water vapor supersaturation results, with its maximum along the centerline. As is typical of condensation devices, once initiated, the condensational growth is rapid, and all particles tend to reach a uniform size. For water, this characteristic size is in the supermicrometer range, and the droplets are readily deposited by impaction.

MICROCHIP THEORY

Quantitative aerosol composition analysis requires that measured solution concentrations be converted to ambient air concentrations. ACE continuously accumulates aerosols for periodic analysis, so a differential method is employed. For analyte 'i', molar accumulation rate (dn_{acc}/dt, μmol s^{-1}) from the growth tube is equal to ambient aerosol concentration (C_{aer}, μg m^{-3}) multiplied by sampling rate (Q_{samp}, L min^{-1}) and divided by the molecular weight (M, g mol^{-1}), resulting in eq 6.1, where t (s) is collection time.

$$\frac{dn_{acc,i}}{dt} = \frac{C_{i,aer}Q_{samp}}{60000M_i} \tag{6.1}$$

For non-destructive techniques when no analyte is leaving the system, the aqueous concentration (C_{aq}, μmol L^{-1}) can be obtained by dividing by the sample volume (V_{liq}, μL), yielding eq 6.2.

$$\frac{dC_{i,aq}}{dt} = \frac{50C_{i,aer}Q_{samp}}{3M_iV_{liq}} \tag{6.2}$$

In MCE, the assumption of no analyte consumption is not the case because a small portion of the sample exits to microfluidic network for analysis, termed ion depletion.[43] The rate of depletion from the reservoir is equal to the analyte's volumetric flow rate multiplied by the solution concentration, C_{aq} (μmol L^{-1}). The volumetric flow rate is defined by the exiting velocity (v, cm s^{-1}) multiplied by the channel cross-sectional area (A, m^2). In the absence of hydrodynamic flow, the velocity is the product of the electric field (E, V cm^{-1}) and the sum of the ionic and electroosmotic mobilities (μ and μ_{EOF}, cm^2 V^{-1} s^{-1}), eq 6.3.

$$v = E\left(\mu_i + \mu_{EOF}\right) \tag{6.3}$$

Eq 6.3 allows the molar rate of depletion (dn_{dep}/dt, μmol s^{-1}) to be written as eq 6.4.

$$\frac{dn_{dep}}{dt} = 10C_{i,aq}E\left(\mu_i + \mu_{EOF}\right)A \tag{6.4}$$

The net change in moles of an analyte in the sample reservoir (dn/dt, μmol s^{-1}) is the accumulation rate minus the depletion rate, yielding eq 6.5.

$$\frac{dn}{dt} = \frac{C_{i,aer}Q_{samp}}{60000M_i} - 10C_{i,aq}E\left(\mu_i + \mu_{EOF}\right)A \tag{6.5}$$

The change in moles can be converted to change in concentration by dividing by the sample solution volume (V_{liq}, μL). Appropriate unit conversions then give eq 6.6.

$$\frac{dC_{i,aq}}{dt} = \frac{50C_{i,aer}Q_{samp}}{3M_iV_{liq}} - \frac{10^7C_{i,aq}E\left(\mu_i + \mu_{EOF}\right)A}{V_{liq}} \tag{6.6}$$

This equation is difficult to evaluate in sampling situations because C_{aer}, C_{aq}, and V_{liq} all change with time, and μ_{EOF} may fluctuate. Assuming constant μ_{EOF} and the absence of any hydrodynamic flow, evaporation, or condensation, the only significant change in reservoir volume is due to electroosmotic pumping. V_{liq} is thus given by eq 6.7, where V_o (μL) is the initial reservoir volume.

$$V_{liq} = V_o - 10^7 E\mu_{EOF} At \tag{6.7}$$

Determining C_{aer} in sampled air is further complicated because electrokinetic injections are sensitive to the sample conductivity and an internal standard must be used to account for both conductivity and volume changes.[44] A linear response is expected for the ratio of analyte to internal standard, typically using peak areas (P_i and P_{IS}, respectively).[44] Eq 6.8 describes this behavior, where F is the relative response (calibration slope) and C_{IS} (μM) is the internal standard concentration.

$$C_{i,aq} = \frac{C_{IS}}{F}\frac{P_i}{P_{IS}} \tag{6.8}$$

In most applications, the internal standard and analyte concentrations are assumed constant at initial values. For this system, eq 6.6 shows that each ion depletes at a different rate, including the internal standard, so calculated concentrations (aqueous and aerosol) increasingly deviate from actual concentrations with time. In practice, eqs 6.2 and 6.8 are used to calculate C_{aer}, requiring experiments to be designed so the depletion term in eq 6.6 is small to ensure an acceptable level of systematic error.

MATERIALS AND METHODS

Chemicals

KCl, $(NH_4)_2SO_4$, and $NaNO_3$ were obtained from Fisher Scientific (Fair Lawn, NJ). Picolinic acid, N-(2-hydroxyethyl)piperazine-N'-(4-butanesulfonic acid) (HEPBS), oxalic acid, and potassium 1,3-propanedisulfonate (PDS) were purchased from Sigma-Aldrich (St. Louis, MO). N-tetradecyl-N,N-dimethyl-3-ammonio-1-propanesulfonate (TDAPS) was procured from Fluka (Buchs, Switzerland). Sylgard 184 elastomer base and curing agent were purchased from Dow Corning (Midland, MI). All chemicals were used without further purification, and aqueous solutions were prepared with water (18.2 MΩ cm) from a Millipore Milli-Q purifier (Billerica, MA).

Growth Tube Collector

The growth tube collector was constructed from the condensation growth tube used in the first WCPC (TSI Model 3785). It consists of a single tube, 250 mm in length, lined with a wetted wick with an inner diameter of 9.2 mm. The first half of the tube is cooled by a thermoelectric device, while the second half is warmed by means of an electric heater. Air is drawn downward through the growth tube and a single 1.6-mm diameter Delrin plastic nozzle. From there it impinges onto the surface of 30 μL of analysis solution in the microchip sample reservoir. The airflow then exits through the flat-bottomed exhaust chamber surrounding the nozzle. A device schematic is shown in Figure 6.1.

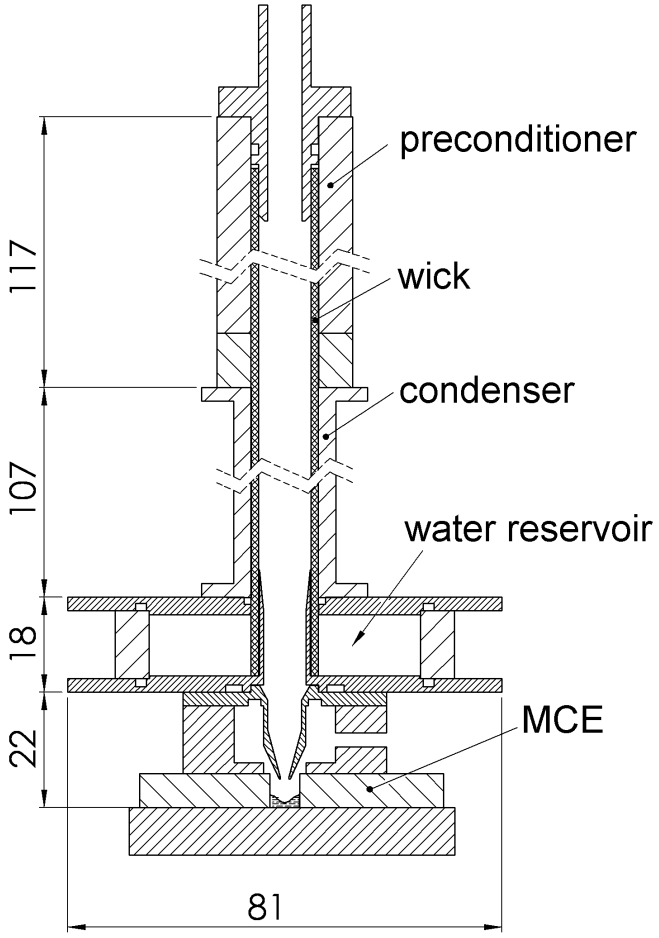

Figure 6.1. Schematic of the Aerosol Chip Electrophoresis (ACE) system, showing growth tube collector, water reservoir for passive wetting of the wick, and the microchip into which the aerosols are deposited. All dimensions are shown in millimeters.

In contrast to its use in the WCPC, the growth tube is wetted passively with a water reservoir at the bottom. A standpipe in the bottom of the wick prevents water from flowing through the wick, while a pressure equalization line allows the system to be operated at varying inlet pressures. Growth tube temperatures are controlled by a custom controller based on a USB-6008 DAQ (National Instruments, Austin, TX), and interfaced

to a computer by means of an in-house program. User-selectable inputs include both preconditioner and condensing region temperatures.

The microchip was interfaced directly to the exhaust chamber, with the seal provided by contact between the PDMS chip and the chamber bottom. This configuration had advantages of ease of access and visual inspection, but did not allow for temperature control of the chip. As a result, to avoid condensation on the chip and nozzle, the condenser region operating temperature could not be set above room temperature.

Size-dependent particle collection efficiencies were measured using monodisperse aerosols of ammonium fluorescein, a non-hygroscopic material. These were generated by nebulization and size-selected using a differential mobility analyzer. Size-dependent efficiencies were determined by comparison of upstream and downstream particle concentration measurements. Overall efficiency was determined by fluorescence analysis of collection into the microwell as compared to a parallel filter.

Microchip Construction and Operation

Construction of PDMS devices and the use of a bubble cell for improved contact conductivity detection were performed as previously described.[45-47] Briefly, PDMS for microchip construction was prepared by thoroughly mixing Sylgard 184 silicone elastomer base in a 10:1 (wt:wt) ratio with the Sylgard 184 silicone elastomer curing agent. After mixing, the uncured PDMS was degassed prior to pouring onto silicon wafer molds. The wafers/PDMS were then placed on a level hot plate (95 °C) for > 10 min for

at least partial curing to ensure nearly uniform thickness. Curing was completed in an oven at 65 °C or higher for at least 1 hr. Chip layers were sealed together by conformal sealing after 20 s of plasma oxidation (18 W with a Harrick Scientific PDC-32G). For the detection zone, 30-μm channels (tapered to 15 μm near the separation channel) were placed perpendicularly to the separation channel. These channels terminated 40 μm before reaching the separation channel, forming a PDMS "bridge" that improved the stability of the wire location and decreased solution leakage from the separation channel. The detection zone bubble cell was four times the width of the separation channel (thus, 200 μm), and it had a ramp-up length (separation channel length from start of the bubble cell expansion to the maximum expansion width) of 375 μm. Center-to-center wire spacing was 100 μm, yielding an estimated DC potential drop of 0.75 V between electrodes at the –300 V cm^{-1} separation field present in the standard operating conditions used in this work. Several modifications were made to the microchip to permit coupling to the growth tube, and the design is illustrated in Figure 6.2. Four PDMS layers were combined to assemble the microchip.

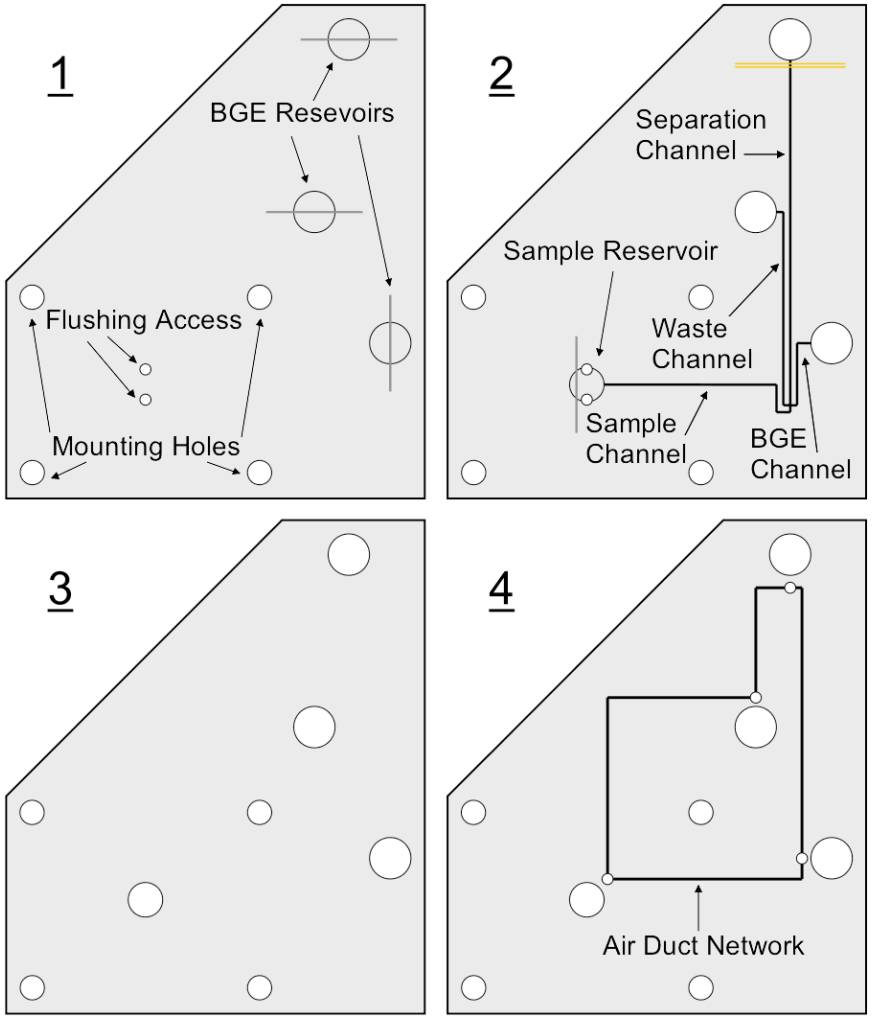

Figure 6.2. Exploded view of microchip design. Specific dimensions are given in the text. Gray lines are platinum electrophoresis electrodes, gold lines are gold-plated tungsten detection electrodes, black lines are microchannels, white circles are holes in the PDMS, and gray circles show the location of where the holes in the adjacent layer are aligned. The chip is assembled bottom-to-top, layers 1-4.

The bottom layer (~2.3-mm thick; 41-μm feature height) formed BGE reservoir bottoms (6-mm diameter), and each reservoir included a 25-μm platinum electrode (all electrodes from Goodfellow Corp., Huntingdon, UK) for electrophoresis. The second layer (~2.5-mm thick; 28-μm features) contained the microfluidic channels (50-μm wide), detection electrodes, bottom of the sample reservoir (5-mm diameter), and a 25-μm electrode in the reservoir for electrophoresis. For sample flushing, the reservoir contained two 1.5-mm

diameter holes, and 200-μm ID/1.59-mm OD Teflon tubing (Upchurch Scientific, Oak Harbor, WA) was inserted into these holes and connected to 3-mL syringes in syringe pumps (Model NE-1000; New Era Pump Systems, Farmingdale, NY). Channel lengths (mm) were as follows: buffer = 12, sample = 30, waste = 30, and separation = 51 (50 effective). Detection electrodes (15-μm diameter) were composed of gold-plated tungsten. The third layer (~2.3-mm thick) was a "blank" used to increase reservoir volumes and separate the second and fourth layers. The final layer (~0.9-mm thick; 57-μm features) contained 0.75-mm wide air ducts that connected the four reservoirs. The air ducts routed to outside of the chip adjacent to each reservoir. The pressure at the sample reservoir was defined by the sampling conditions, so placing airtight lids over the three background electrolyte (BGE) reservoirs allowed isobaric operation and minimized interference from pressure-induced flow. Capping the reservoirs also minimized evaporation, reducing compositional changes in the BGE. A photograph of the integrated growth tube-microchip ACE system is shown in Figure 6.3. A close-up of the microchip end of the ACE system is shown in Figure 6.4. MCE separations of aerosol anions were performed using previously-published conditions.[41] This work used 30 μL of BGE and internal standard (15-μM PDS) as the sample and 125 μL of BGE in the other reservoirs. The small sample volume was chosen to increase sensitivity during sampling, and the large BGE volumes were used to combat buffer depletion during long analyses.[43]

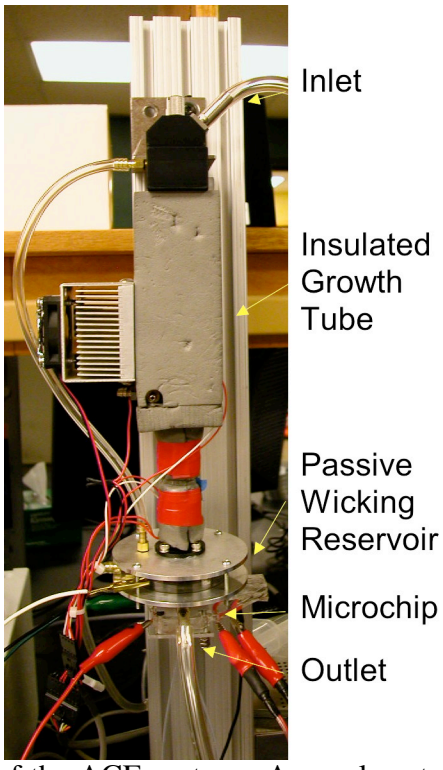

Figure 6.3. Photograph of the ACE system. Aerosols enter the growth tube from the top, are chilled at the top of the growth tube, and warmed/enlarged in the bottom half, and inertially impact into the microchip at the bottom before air exits from the outlet. The white wire is grounded and connects to the exit of the growth tube. The other wires connect to the electrophoresis and detection electrodes.

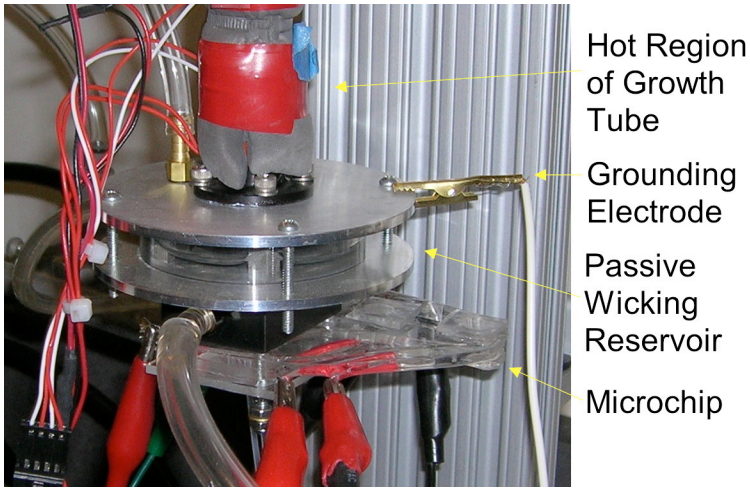

Figure 6.4. Close-up of the outlet end of the growth tube.

Although some flow was induced from fluid height and Laplace pressures,[48] effects from

these were negligible because the fluid height differences were small, the Laplace pressures in each reservoir were similar because of the comparable and large reservoir radii, and hydrodynamic flow should affect the calibration and sampling analyses similarly. –2227 V were applied to the sample and buffer reservoirs grounding the waste and separation reservoirs, providing a –300 V cm^{-1} separation field. Gated injections (1.5 s) were performed by matching the buffer reservoir voltage to that calculated for the channel intersection (–859 V).[49]

Instrumentation and Data Analysis

A CD20 (Dionex, Sunnyvale, CA) detector was attached to the detection electrodes for conductivity detection. A range of 50 μS, rise time of 0.2 s, and baseline offset of 15% were used. 0-1 V output from the CD20 was monitored with a USB-6210 DAQ and LabView 8.0 software (National Instruments, Austin, TX). A LabView virtual instrument was used for data analysis; 10-kHz collection was used with boxcar averaging set to 1000 for a 10-Hz effective rate. No additional data filtration was used. The virtual instrument used manual peak location input and subtracted a polynomial fit from the remaining baseline to adjust for drift from ion depletion, temperature changes, and evaporation. The program fit peaks to normal distributions, providing peak height, area, and migration time. Simulations of eqs 6.2 and 6.4 were evaluated with the following parameters: C_{aer} = 1 μg m^{-3}; Q = 1 L min^{-1}; V_0 = 31 μL; E = –300 V cm^{-1}; A = 1.41*10^{-9} m^2; μ_{EOF} = 2.0 (10^{-4} cm^2 V^{-1} s^{-1} for all mobilities); $\mu_{chloride}$ = –7.598; $\mu_{sulfate}$ = –7.042; $\mu_{nitrate}$ = –6.487; $\mu_{oxalate}$ = –6.002; μ_{PDS} = –5.558. Results were calculated using an initial slope

iterative approximation (Euler's Method). All statistical uncertainties provided in this work represent experimental standard deviations.

Ambient Sampling Comparison

Ambient monitoring tests were conducted in Fort Collins, CO. The growth tube was operated at 1.0 L min^{-1}, initially with the preconditioner at 2 °C and the conditioner at 26 °C. During collection at night, room temperature decreased and operation was switched to 1 °C and 24 °C to prevent condensational dripping into the microchip sample reservoir. Incoming air for the growth tube was passed through a 3 L min^{-1}, $PM_{2.5}$ cyclone (URG-2000-30EQ, URG Corp., Chapel Hill, NC), and two annular denuders (URG-2000-30x242-3CSS), one coated with citric acid (removes NH_3) and the other with sodium carbonate (removes HNO_3 and SO_2) to prevent interference with target $PM_{2.5}$ analytes. The MCE system injected every 1 min with a sample-flushing interval of ~60 min and manual BGE replenishment every ~180 min. During BGE changes, injections were not performed for ~19 min. During sample flushing, two flushing cycles were done and injections were not performed for ~4 min. One cycle consisted of solution removal followed by a 35-s wait and then a solution input of 30 μL, followed by a 15-s wait. Prior to the first injection after flushing, an additional 1.5 min was waited. All flushing pumping was performed at 0.9 mL min^{-1}. The larger volume of the solution removal and the delay times were used to avoid hysteresis effects from operating in non-steady state format with plastic syringes.

The PILS-IC was operated with a 17 L min^{-1} sampling rate. Incoming air was passed through a $PM_{2.5}$ cyclone (URG-2000-30EH) and two denuders (URG-2000-30x242-3CSS), one coated with phosphorous acid and the other with sodium carbonate. The PILS liquid flow rate to the IC was set to 12 μL min^{-1}, and the IC injected every 15 min, used a Dionex AS14A separation column (8/1-mM sodium carbonate/bicarbonate eluent), and utilized a Dionex ASRS-ULTRA II suppressor.

RESULTS AND DISCUSSION

To evaluate the ACE system, each component was first characterized individually. Specifically, the growth tube collection efficiency was measured because it operated with a smaller temperature gradient than typically used. In MCE, operation typically proceeds for minutes, whereas aerosol monitoring ensues for hours between buffer replenishments, so testing on a longer time scale was performed. Also, the sample-flushing interface was tested for precision and accuracy. The complete, integrated system was then tested in terms of electrophoresis baseline noise because the microchip-growth tube coupling yielded a unique MCE operating environment and the conductivity detection is coupled to the high voltages used for separation.

Particle Collection Efficiency

Figure 6.5 shows size-dependent collection efficiencies into the buffer-filled microchip sample reservoir for the growth tube using a 1.6-mm diameter impaction orifice.

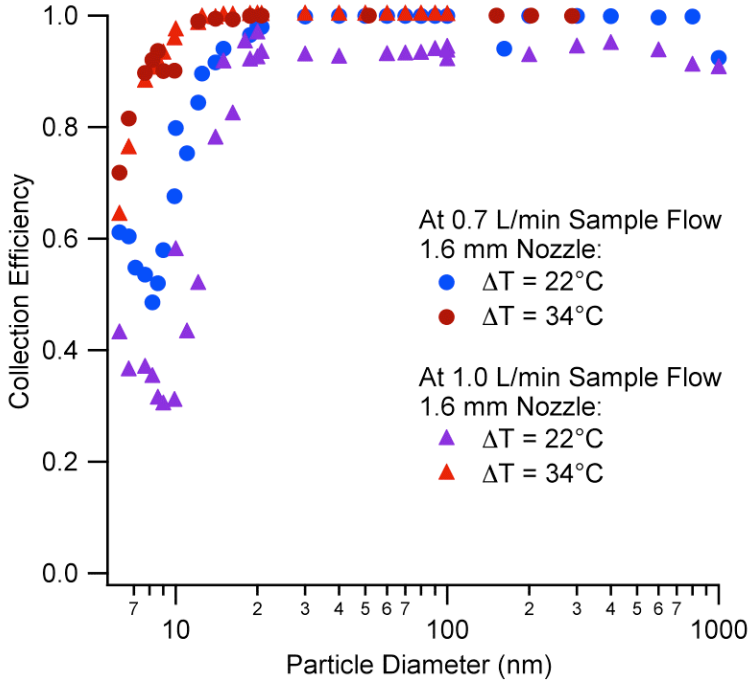

Figure 6.5. Size-dependent collection efficiencies for the growth tube interfaced to the microchip.

Data are for air sampling rates of 0.7 and 1 L min^{-1}, preconditioner temperature of 2 °C, and condenser temperature of 24 °C and 36 °C. At the 34 °C temperature differential, the lower cutpoint, defined as the size collected with 50% efficiency, is below 7 nm for both flow rates. For the smaller differential of 22 °C, the lower cutpoint varies from 9 to 12 nm, depending on sampling rate. The lower flow rate provides more time for droplet growth, creating larger droplets that are more readily collected. For the specific design utilized in these experiments, the collection efficiencies decline at particle concentrations above 20 000 cm^{-3}, irrespective of particle size. This is due to condensational heating which limits the extent of droplet growth. The system has been redesigned and is currently undergoing testing to eliminate this effect for concentrations as high as 200 000 cm^{-3}.

Extended Microchip Analysis Times

The majority of MCE analyses extend for only a period of a few minutes, so sample composition is not expected to change significantly. For this application, however, the sample is monitored for hours, making the depletion term in eq 6.6 significant. Because eqs 6.2 and 6.8 are used to calculate the aerosol concentrations, the amount of depletion indicated by eq 6.6 was calculated and evaluated with respect to quantitation with eq 6.8, and the acceptable amount of systematic error was decided in order to determine the proper sample regeneration interval. First, the validity of the equations was tested experimentally by analyzing an aqueous sample for ~3 h. Experimental measurements were compared to theoretical values considering depletion of both analyte and standard (Figure 6.6a). Although agreement is not quantitative, qualitative conformity of the magnitude of depletion during operation was good enough to allow the theory to be extended to predicting the effects of depletion for aerosol monitoring. For this calculation, constant aerosol concentrations of 1 $\mu g\ m^{-3}$ for all analytes were assumed, and simulation results for a differential analysis are shown in Figure 6.6b. The prediction is surprising, as the largest deviations are observed for analytes that most closely match the mobility of the internal standard, which is opposite of the behavior seen in Figure 6.6a. This effect is rationalized by realizing that the depletion of the internal standard will affect apparent analyte concentrations uniformly, but this effect is offset by depletion of the analytes, and early-migrating ions deplete more rapidly. Consequently, any analytes migrating after the internal standard would show higher positive deviations, and if an ion with a higher mobility than chloride was analyzed, it would show increased negative deviations.

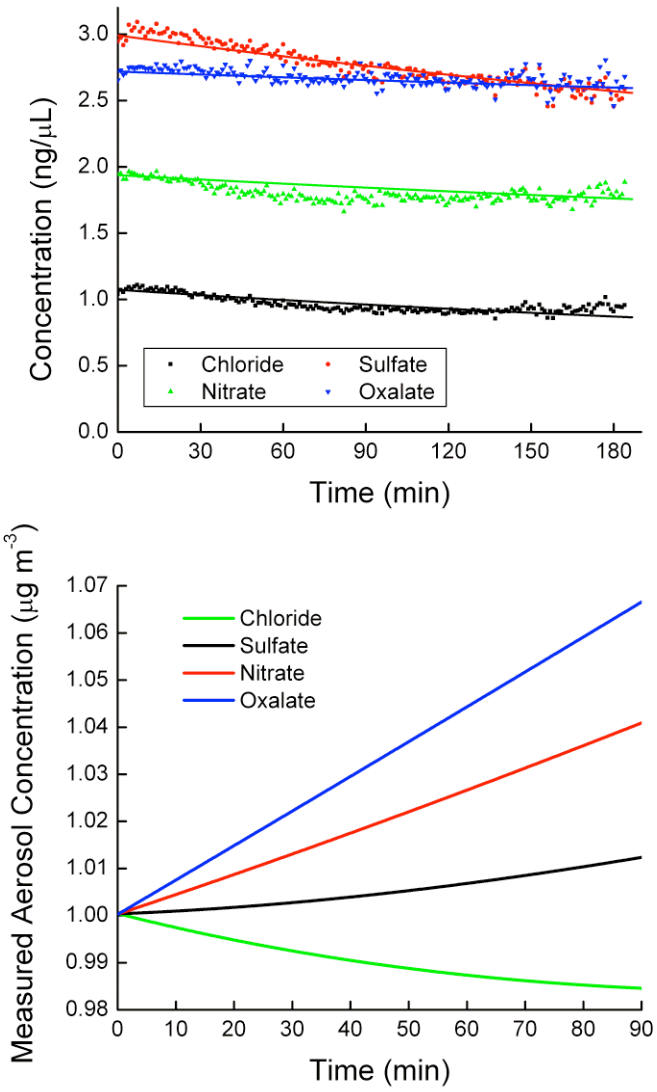

Figure 6.6. (a) Top: Experimental measurements (points) of an aqueous sample analyzed for over 3 h and predicted measured concentrations using depletion theory (lines). Experimental conditions: 31-μL sample; –233 V cm^{-1} sample field. (b) Calculated aerosol concentration simulation using differential measurements when sampling a 1 μg m^{-3} constant concentration. Depletion causes systematic offsets in measured values at finite measuring times. Internal standard depletion induces positive systematic errors in the aqueous measurements, but depletion of the analytes themselves partially (or with chloride, completely) offsets this.

Figure 6.6b shows that systematic deviations are about +4.4% for oxalate, +2.7% for nitrate, +0.7% for sulfate, and –1.3% for chloride for 1-h sampling, and this error is acceptable for most applications. In addition to the simulation for differential analysis

shown in Figure 6.6b, the case of using only the first and last measurements in an accumulation was simulated (these might be required when measuring very low concentrations and is the opposite extreme of using every point generated to calculate concentrations differentially), and the results are shown in Figure 6.7. The systematic error is roughly one-half of that for the differential method, thus allowing analyses of 2 h or longer to achieve lower LODs.

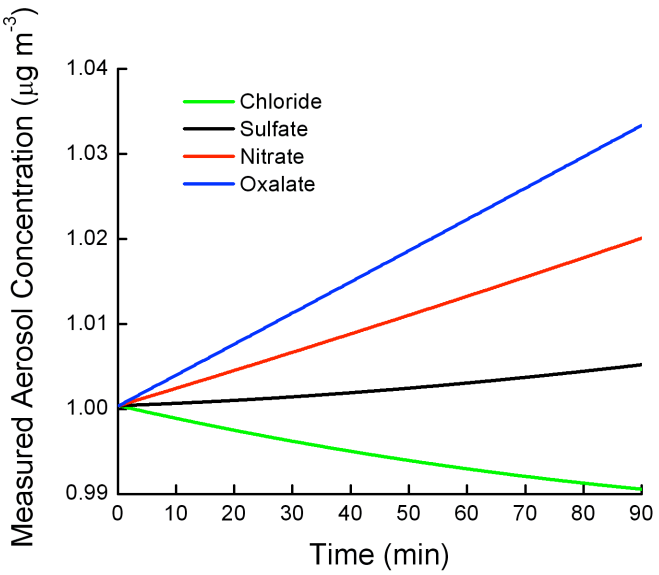

Figure 6.7. Simulation of the calculated aerosol concentration using the last-point method when sampling a constant concentration of 1 µg m^{-3}. Ion depletion causes a systematic deviation in the measurement which increases with sampling time. This method exhibits roughly half of the deviation inherent in the point-to-point method shown in Figure 6.6b.

Microchip Sample Reservoir Flushing

With required sample rinsing interval characterized, the efficiency and precision of the flushing system were evaluated. To test flushing efficiency, a sample of ~50-µM analytes was analyzed after 0-3 flushes (each performed with fresh solution to avoid depletion effects). Results are shown in Figure 6.8. Calculated single-flush efficiencies

were 95.3 ± 0.4% for chloride, 93.9 ± 0.7% for sulfate, 95.1 ± 0.6% for nitrate, and 94.6 ± 0.8% for oxalate (n=6 for all).

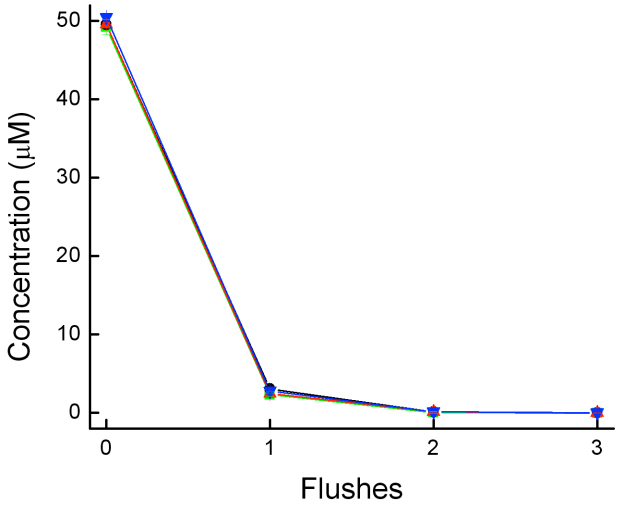

Figure 6.8. Characterization of the sample flushing system. An aqueous sample underwent 0, 1, 2, or 3 sample flushing cycles, followed by quantitative analysis. Each point shown is the average of 6 independent trials (3 replicate injections per trial). Chloride (black), sulfate (red), nitrate (green), and oxalate (blue) show similar removal efficiency for each analyte (~95% per flush).

Although low concentrations after two flushes make analyses less certain, respective two-flush efficiencies were 100.0 ± 0.2%, 99.8 ± 0.2%, 99.8 ± 0.2%, and 99.7 ± 0.2% (corresponding to 98.3 ± 7.0%, 95.3 ± 2.0%, 95.6 ± 1.9%, and 94.8 ± 1.8% single-flush efficiencies). Three consecutive flushes yielded concentrations below the LODs. For ambient analyses, a two-flush cycle was chosen because this minimizes instrument downtime (~3 min) while still achieving nearly quantitative flushing. Increased handling of materials contacting the sample when assembling the flushing interface led to significant non-zero blank concentrations for chloride and sulfate, and trace nitrate was also observed. However, the differential approach employed allowed this contamination to be subtracted as a blank after sample regeneration. Low-level fluoride was sometimes

observed when using the flushing system and was believed to originate from the tubing. This may hinder analysis of fluoride in aerosols or the use of fluoride as an internal standard.

Flushed volume precision is of critical importance because this volume defines the quantity of internal standard present in the sample. The precision of the dispensed volume was found to be 30.05 ± 0.48 μL (n=100), a relative standard deviation (RSD) of 1.6%. This value is acceptable for online aerosol measurements where collection uncertainties are similar in magnitude. Dispensed precision is specific to pump-syringe combinations and will vary with both pump model and syringe diameter.

Integrated System Performance

Coupling the microchip to the growth tube provided a unique MCE operating environment, so online and offline performance was compared before attempting ambient sampling. Baseline noise measurements were made both offline and online at a variety of growth tube flow rates (using filtered air), and the results are shown in Figure 6.9. The collector flow rate (in the tested range) was not found to have an effect, but online operation (aggregate of five flow rates, 0-1.3 L min^{-1}) had 65% higher baseline noise than offline (36 ± 11 μV, n=92, compared to 22.1 ± 3.8 μV, n=30). However, grounding the metal portions of the collector near the exiting stream lowered the online noise to 21.1 ± 3.5 μV (0-1.3 L min^{-1}, n=92), comparable to the offline figure.

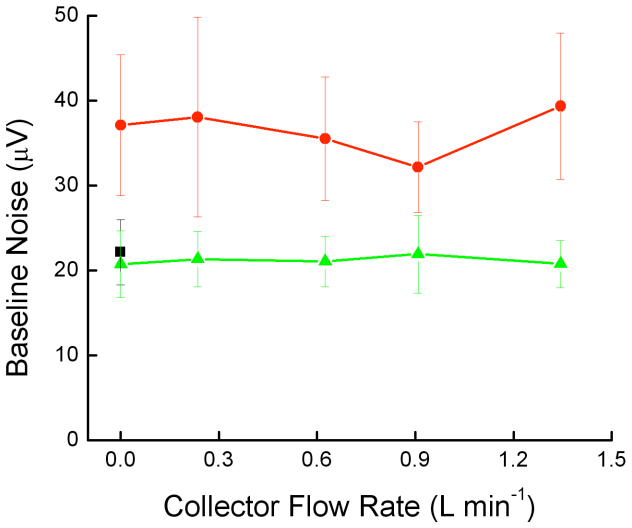

Figure 6.9. RMS noise measured as a function of growth tube flow rate for the following operating configurations: offline (black), online without collector grounding (red), and online with grounding (green). Although flow rate does not significantly affect baseline noise, online performance does suffer from higher noise unless the growth tube outlet metal is grounded. After grounding, online noise levels are equal to or lower than offline values. Noise measurements were acquired from the standard deviation of the baseline in 10-s windows. n=30 for offline mode and n=17-21 for each online measurement.

Ambient analyses will often be done while sampling low aerosol concentrations that are near the instrument's LOD, so detection limits for ACE were estimated from calibration data. Sensitivities of 1.00, 2.11, 0.84, and 1.28 mV μM^{-1} were obtained for chloride, sulfate, nitrate, and oxalate, respectively, corresponding to aqueous LODs of 63, 30, 75, and 50 nM in grounded online mode. These detection limits are 3-4 times lower than previously-published results for this separation.[41] The improvement is attributed to the CD20 analog output offset functionality and improved electronic shielding. These LODs are the best reported to date with these analytes using MCE without stacking and are roughly twenty times better than reported for contactless conductivity detection.[50] With a

1-L min^{-1} collection rate and 30-μL sample volume, aerosol detection limits are estimated at 67, 86, 140, and 131 ng m^{-3} min, respectively. For a 15-min sampling time, respective detection limits are predicted to be 4, 6, 9, and 9 ng m^{-3}, which are about 3-4 times higher than the lowest reported detection limits for PILS-IC.[28] LODs can be lowered by increasing sampling times, lowering sample volume, or using a low-conductivity sample matrix to enable electrophoretic stacking. For instance, in the development of the separation chemistry, LODs were lowered by a factor of nine by using a sample matrix of 10% BGE.[41] This approach may not be as effective as desired if the collected aerosols significantly increase the matrix conductivity.

Functionality of the air duct network for pressure equilibration was confirmed by analyzing an aqueous mixture of 15-μM analytes in three modes of operation: offline, online with airtight reservoir lids, and online without lids. Electropherograms are shown in Figure 6.10. No discernible differences were seen for the offline and online measurements with reservoir lids. Without application of the lids, migration times increase and peak areas decrease, especially for later-migrating species. Online percent recovery measurements (defined by the measured online/offline concentration ratios) for chloride, sulfate, nitrate, and oxalate were determined using a single offline calibration curve. Values of 98.7 ± 5.0%, 100.0 ± 0.7%, 100.2 ± 2.3%, and 99.8 ± 0.6% (n=5) were obtained, respectively, confirming isobaric operation and the equivalence of offline and online modes when using reservoir lids. In contrast, respective recoveries without lids were 118.7%, 118.2%, 112.9%, and 104.7% due to altered injection biasing from unwanted hydrodynamic flow.

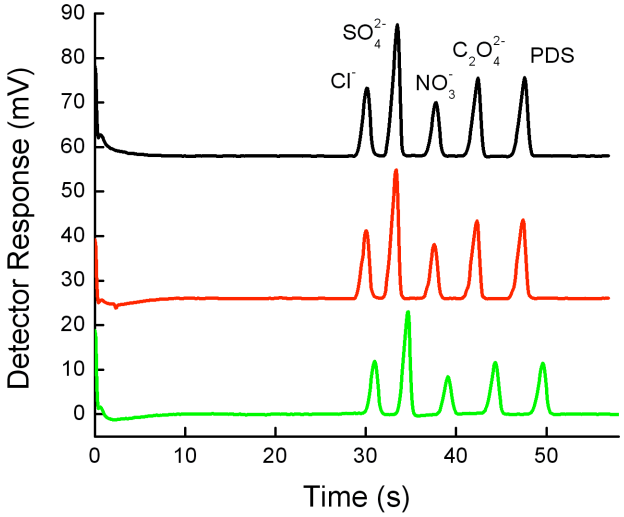

Figure 6.10. Electropherograms obtained from different operational configurations: offline (black), online using airtight reservoir lids (red), and online without lids (green). The use of airtight lids makes offline and online operation indistinguishable, but without the lids migration times increase and peak areas decrease due to the induced hydrodynamic flow. Collector flow rate was set to 0.9 L min^{-1}. PDS is the internal standard.

Ambient Air Analysis

With the laboratory performance characterized, ACE was used to monitor ambient air in Fort Collins, CO over a period of ~28 h on June 30-July 1, 2009, and results were compared to those from a PILS-IC operated concurrently. ACE provided 1371 injections, compared to 109 PILS-IC injections. Each of the target analytes, chloride, sulfate, nitrate, and oxalate, were observed, although chloride was typically seen only as blank contamination and nitrate and oxalate were only detected several injections into accumulations. Qualitatively, the instrument performed similarly to the laboratory testing with filtered air. However, baseline noise in ambient testing varied between that

measured with filtered air to values several times higher. This fluctuation is believed to be due to particle impaction inducing disturbances to the solution surface, leading to small pressure pulses in the MCE that cause an unstable baseline with conductivity detection. In the future, increasing the hydrodynamic resistance in the microchip or modifying growth tube operation will minimize this effect.

To test device stability in ambient analyses, migration time consistency during the analysis was evaluated. A plot of migration times throughout the analysis is given in Figure 6.11. RSDs for migration times were 0.94% for chloride (n=1179), 1.04% for sulfate (1370), 1.01% for nitrate (1249), 0.88% for oxalate (854), and 1.09% for PDS (1371), which are excellent for MCE. These figures may be improved in the future with improved temperature control.

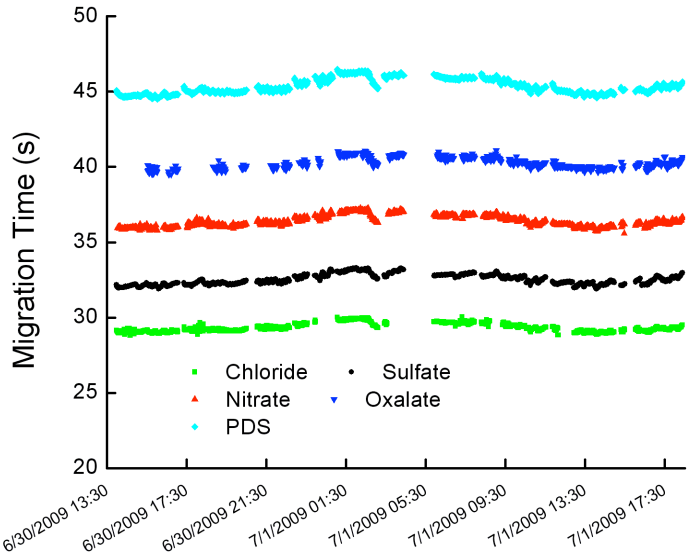

Figure 6.11. Analyte migration times during ambient testing. No large shifts in migration times for any of the analytes were detected during operation, confirming the stability of the buffer for extended analysis times.

Scatter in the ambient ACE data made it clear that, at the concentrations measured, the precision of the aqueous measurements was too low to provide precise results in a point-by-point (minute-by-minute) differential analysis. Reduced data scatter was obtained by averaging adjacent aqueous concentration points and using the average values with eqs 6.2 and 6.8. Although time resolution is lost using the averaging technique, scatter in the data is reduced by a factor of $n^{3/2}$. The derivation of this improvement factor is given in the following discussion. As shown in eq 6.2, the change in aqueous concentration with time is the analytical parameter of interest. Finite time differences were used, and this value is calculated using eq 6.9, which comes from eq 6.8.

$$\frac{\Delta C_{i,aq}}{\Delta t} = \frac{C_{IS}}{F\Delta t}\left(\frac{P_{i,2}}{P_{IS,2}} - \frac{P_{i,1}}{P_{IS,1}}\right) \tag{6.9}$$

F is the relative response factor and P is the peak area. Uncertainty in the internal standard concentration, calibration slope, and time span do not increase scatter (these values are considered constant for all time points in the data analysis). Thus, uncertainty propagation and simplification provide eq 6.10, where s is the uncertainty and r is the analyte/standard ratio.

$$\sigma_{\Delta C_{aq}/\Delta t} = \frac{C_{IS}}{F\Delta t}\sqrt{\sigma_{r1}^2 + \sigma_{r2}^2} \tag{6.10}$$

The relative response, F, is dictated by the physicochemical properties of the analytes/separation and cannot be intentionally changed to improve scatter. Decreasing the internal standard concentration would appear to lower the uncertainty, but this would also increase the uncertainty of the area ratio (smaller internal standard peak), which counters any potential advantages. However, averaging adjacent points (by number=n) lowers the uncertainties of the area ratio by $n^{1/2}$ (boxcar averaging improvement) and also

increases the time span by n, giving eq 6.11 (Δt now represents the time between individual injections). Note that the uncertainty given in eq 6.11 is directly proportional to the uncertainty in the calculated aerosol concentration (see eq 6.2).

$$\sigma_{\Delta C_{aq}/\Delta t} = \frac{C_{IS}}{Fn^{3/2}\Delta t}\sqrt{\sigma_{r1}^2 + \sigma_{r2}^2} \tag{6.11}$$

The benefits of adjacent averaging are shown in Figure 6.12, where aerosol concentrations of nitrate and sulfate are shown for the original data set and for adjacent averaging with n = 2-6.

To evaluate the accuracy of ACE, results were compared to the PILS-IC data. To help alleviate data scatter due to noise, aqueous concentrations from sets of three adjacent injections were averaged for sulfate and five adjacent injections were averaged for nitrate (as described above, note that sulfate was present at higher concentration and is detected more sensitively by ACE, therefore requiring less averaging), and the results were used to provide data with one-third and one-fifth the time resolution of the original analysis, respectively. This averaging was applied to the entire ACE dataset, and the complete time series is shown in Figure 6.13 versus the PILS-IC. The ACE and PILS-IC sulfate measurements show a similar, consistent sulfate background. The PILS-IC results exhibit more temporal variability, perhaps because the measured values were near the LOD of the instrument. For nitrate, ACE measured concentrations below the PILS-IC detection limit for most of the analysis time, but an increase in nitrate concentration from 8:30 to 14:00 on the second day of analysis was measured by ACE and marked the only time that the PILS-IC consistently detected nitrate.

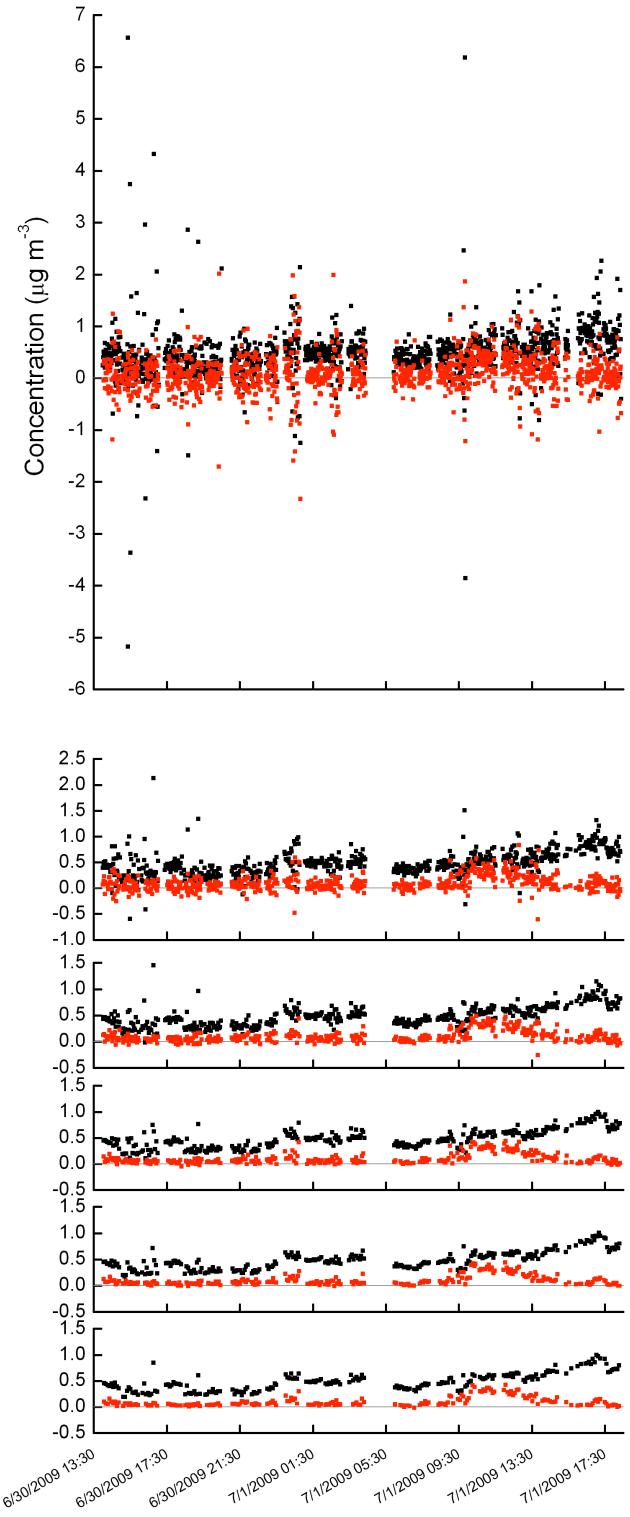

Figure 6.12. Comparison of averaging adjacent points on the ACE differential analysis for sulfate (black) and nitrate (red). Plots (top to bottom) represent every point, 2-, 3-, 4-, 5-, and 6-point adjacent averaging. Y-axes are adjusted to ensure consistent spacing.

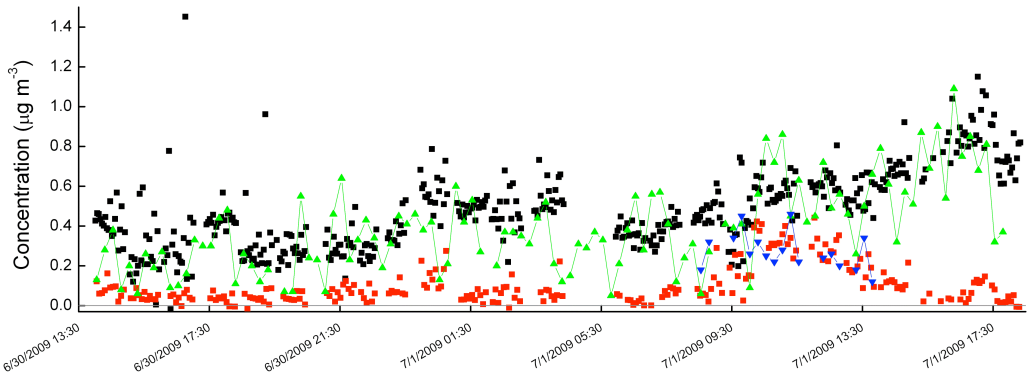

Figure 6.13. (Top) Time series for sulfate/nitrate for the 28 h of analysis for both PILS-IC and ACE. ACE sulfate is black, ACE nitrate is red, PILS-IC sulfate is green, and PILS-IC nitrate is blue. The ACE data for sulfate is shown with 3-min time resolution, and nitrate is shown at 5-min resolution. The low concentrations resulted in scatter for the PILS-IC data, and nitrate concentrations were too low to be detected by the IC except for the nitrate episode during 8:30-14:00 on the second day.

To illustrate the difference in what the operator observes in the low level data, series of electropherograms showing accumulation of aerosols are shown in Figure 6.14, and a low-nitrate episode is compared to a high-nitrate episode. The differences in nitrate behavior are obvious even without quantitation. To quantitatively compare the two instruments, average measured values for times when both instruments detected analytes were compared. ACE measured 0.48 μg m^{-3} for sulfate and 0.23 μg m^{-3} for nitrate, whereas the PILS-IC measured 0.39 μg m^{-3} and 0.27 μg m^{-3}, respectively. Thus, PILS-IC measurements were ~19% lower than the ACE observations for sulfate (n=98) and ~18% higher for nitrate (n=17). Deviations of this amount are not unexpected when measuring at these low concentration levels, near the detection limit of the PILS-IC used in this study. Some of the sulfate overestimation by ACE relative to PILS-IC may be due to the comigration of nitrite in MCE, although this would likely only account for part of the deviation as gas phase NO_2 levels, which could produce artifact nitrite in the collected sample, were likely low under the conditions sampled.

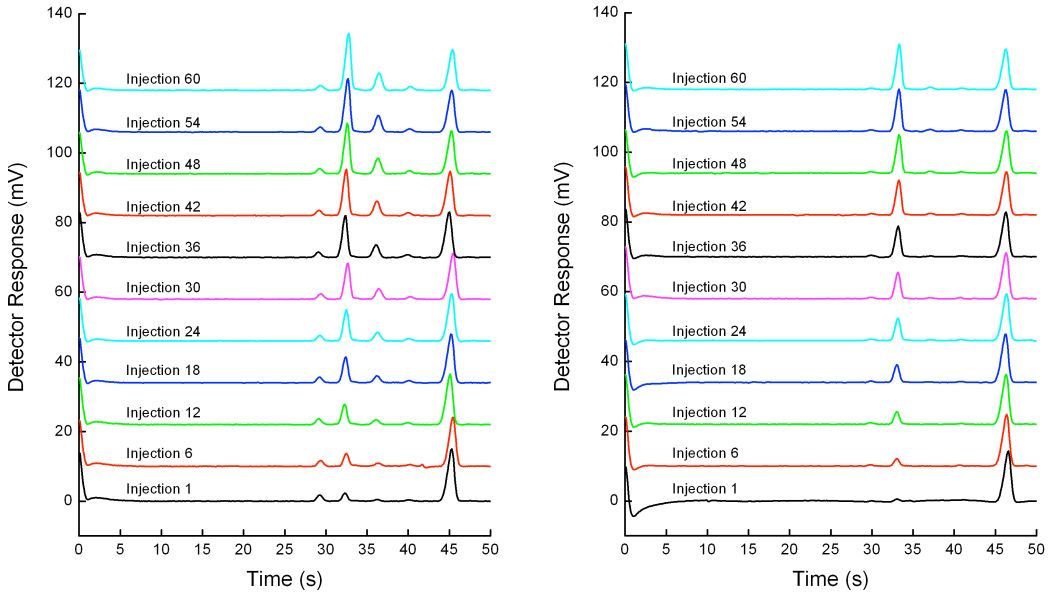

Figure 6.14. (a) Left: Electropherograms from the ambient analysis during one accumulation event with high nitrate. Accumulation of sulfate, nitrate, and oxalate are evident. The first injection was done at 10:33 on 07/01/09. (b) Right: Electropherograms from the ambient sampling analysis during one accumulation event with low nitrate. Accumulation of sulfate is evident, but only low levels of nitrate and trace amounts of oxalate were collected due to their low ambient concentrations. The first injection was done at 1:04 on 07/01/09. For both plots, small decreases in the chloride and internal standard peak heights are observed due to ion depletion and electrophoretic de-stacking. Peak order is the same as Figure 6.10.

Modifying the separation to include nitrite resolution was previously accomplished,[41] and this may be needed in the future to ensure accurate sulfate measurements in areas with elevated NO_2. Another possibility is that the PILS-IC measured sulfate systematically low, as previously reported.[51] A scatter plot of ACE versus the PILS-IC (Figure 6.15) showed ACE to have a significant intercept for sulfate relative to the PILS-IC. Because the differential approach automatically corrects for blank sulfate values, it is suspected that this intercept is an artifact of working near the LOD of the PILS-IC and not an inherent problem with ACE. Future testing at higher sulfate levels is needed to evaluate this issue.

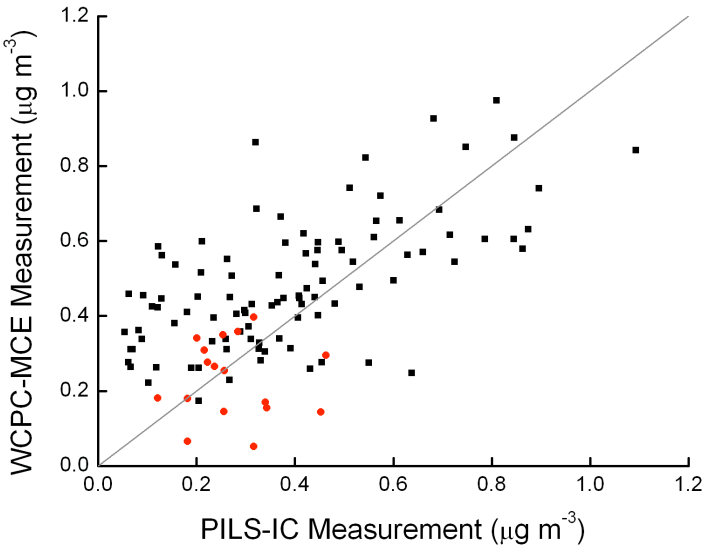

Figure 6.15. Scatter plot generated from the data shown in Figure 6.13.

Although significant amounts of chloride and oxalate were not measured by the PILS-IC during the ambient study, oxalate was detected with the ACE system after considerable accumulation, and chloride was present in most of the blanks and also showed a slight concentration increase. Figure 6.16 shows the determined concentrations for these two ions during ambient testing using 10-point adjacent averaging. Of note is the oxalate episode that coincides temporally with the nitrate increase. Estimated detection limits based on instrument sensitivity and noise levels were mentioned earlier, but system blanks were collected during the ambient analysis to permit more practical LOD calculations. Neither nitrate nor oxalate peaks were observed in blanks, so the aforementioned estimates should be accurate. However, chloride and sulfate signals were detected in blanks, and estimated detection limits of 198 ng m^{-3} min and 270 ng m^{-3} min were calculated (results from three-injection averaging).

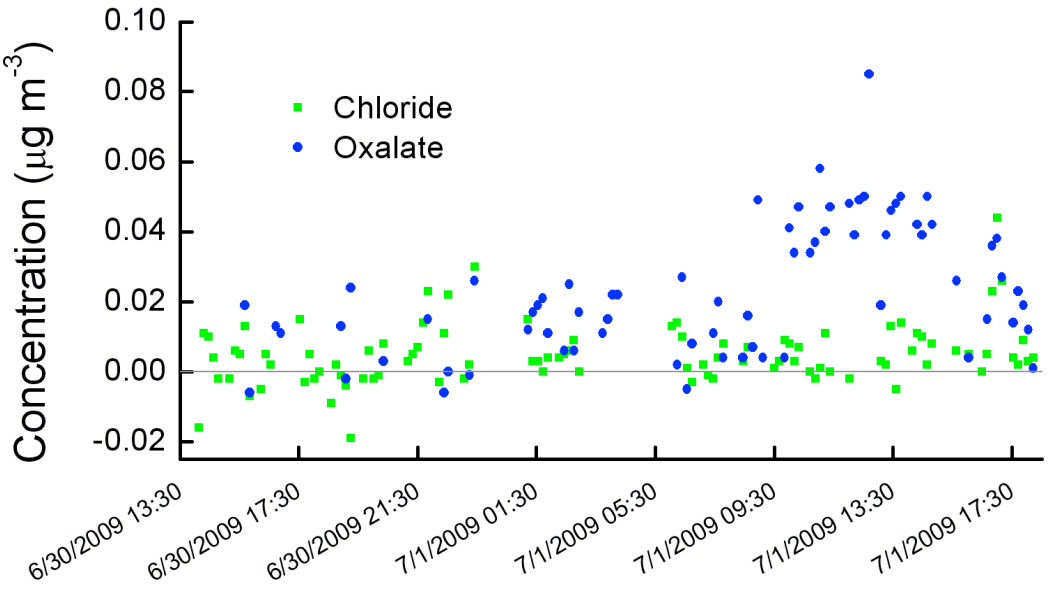

Figure 6.16. Aerosol concentrations of chloride and oxalate during the ambient study. The low concentration prevented detection by PILS-IC, but the ACE system was able to quantify the values.

In terms of overall instrument uncertainty, at 1 μg m^{-3} and assuming an air flow rate uncertainty of 3%, the 95% confidence interval for sulfate was estimated at ±8% and nitrate was estimated at ±6% (using three- and five-injection averaging, respectively). Currently, the majority of the uncertainty is due to injection-to-injection quantitation variability, thus uncertainty decreases with increasing analyte concentration and vice versa. For example, at 2.5 μg m^{-3}, uncertainty for both analytes was estimated at ±5%. We are currently working to improve peak quantitation precision to lower these uncertainty values.

Overall, the ambient measurements illustrate that ACE can provide an alternative for real-time, semi-continuous monitoring of aerosol composition, and the high sensitivity and short analysis times are encouraging. However, the described prototype currently has several issues that limit its use in field studies. For instance, the three-hour BGE replenishment requires considerable instrument downtime and manual operation. This will be addressed in the future by increasing buffer reservoir size and utilizing smaller electrophoresis channels. Injection-to-injection precision is currently too low to provide precise quantitation at low aerosol concentrations unless time resolution is sacrificed. Utilization of 3-mL syringes for the flushing system currently limits the system to ~2 days of operation, and application of larger syringes (or an alternate pumping system) without sacrificing dispensing accuracy will need to be solved. Perhaps most importantly, the 20 000 cm^{-3} particle upper limit restricts the instrument to environments of low particle concentrations. As mentioned earlier, growth tube modifications to increase this limit by an order of magnitude are already being tested. One additional benefit of ACE not mentioned previously is its low reagent consumption, which will be beneficial in extended field studies when the aforementioned issues limiting field deployment are corrected. During the ambient monitoring, ACE required about 0.2% of the solution volume that the IC analysis needed (3.75 mL versus 1.64 L). In addition to the aforementioned problems, further characterization of the instrument will be needed to determine its limitations, advantages, and potential for improvement.

CONCLUSIONS

Coupling of MCE to a growth tube particle collector was demonstrated, and the integrated system showed the potential for measuring aerosol composition with 1-min time resolution. The growth tube collection efficiency was shown to be adequate (for aerosol concentrations below ~20000 cm^{-3}) at the conditions necessary to remain compatible with deposition into the microchip. Despite using contact conductivity detection, which is coupled to the separation voltages, MCE baseline noise and quantitation did not significantly change when coupled to the collector, although noise levels did fluctuate during ambient analyses, and this issue is currently being evaluated. Estimated detection limits for the system are 70-140 ng m^{-3} min for inorganic anions when collecting into 30 μL of solution at 1 L min^{-1}. The integrated system was evaluated for over 24 h with ambient air, and results agreed reasonably well with those from a PILS-IC, especially given the low $PM_{2.5}$ concentrations measured. The prototype instrument is not yet ready for routine field deployments due to its upper particle limit of ~20 000 cm^{-3} and limited unattended operation time. Both the growth tube and microchip are currently being improved to address these issues, and we expect future field deployments to improve the versatility, robustness, and precision of the instrument. The ACE system represents a new approach to aerosol composition monitoring that is smaller, faster, and more portable than most current instrumentation. This technology may be extended beyond electrophoresis and a growth tube collector, and a variety of aerosol collectors and microfluidic analyses may be coupled to extend the range of aerosol composition measurements.

CLOSING COMMENTS

This chapter covered the development of the prototype ACE instrument and is the only published work on this topic. Recent improvements include replacing the isobaric air duct network with a temperature-controlled box that completely encloses the microchip, replacing the syringe pumps with solenoid-operated pumps, switching from gold-plated detection wires to platinum (or platinum alloy) wires, and increasing both the buffer and sample longevity. Details on these changes, difficulties encountered with the new system, and preliminary data obtained with it are discussed in chapter 8.

REFERENCES

1. Noblitt, S. D.; Lewis, G. S.; Liu, Y.; Hering, S. V.; Collett, J. L.; Henry, C. S., *Anal. Chem.* **2009,** *81*, 10029-10037.
2. Poschl, U., *Angew. Chem. Int. Ed.* **2005,** *44*, 7520-7540.
3. Raes, F.; Van Dingenen, R.; Vignati, E.; Wilson, J.; Putaud, J. P.; Seinfeld, J. H.; Adams, P., *Atmos. Environ.* **2000,** *34*, 4215-4240.
4. Pandis, S. N.; Wexler, A. S.; Seinfeld, J. H., *J. Phys. Chem.* **1995,** *99*, 9646-9659.
5. Chebbi, A.; Carlier, P., *Atmos. Environ.* **1996,** *30*, 4233-4249.
6. Kawamura, K.; Kasukabe, H.; Barrie, L. A., *Atmos. Environ.* **1996,** *30*, 1709-1722.
7. FinlaysonPitts, B. J.; Pitts, J. N., *Science* **1997,** *276*, 1045-1052.
8. Sipin, M. F.; Guazzotti, S. A.; Prather, K. A., *Anal. Chem.* **2003,** *75*, 2929-2940.
9. Sullivan, R. C.; Prather, K. A., *Anal. Chem.* **2005,** *77*, 3861-3885.
10. Bernstein, J. A.; Alexis, N.; Barnes, C.; Bernstein, I. L.; Bernstein, J. A.; Nel, A.; Peden, D.; Diaz-Sanchez, D.; Tarlo, S. M.; Williams, P. B., *J. Allergy Clin. Immunol.* **2004,** *114*, 1116-1123.
11. Kanakidou, M.; Seinfeld, J. H.; Pandis, S. N.; Barnes, I.; Dentener, F. J.; Facchini, M. C.; Van Dingenen, R.; Ervens, B.; Nenes, A.; Nielsen, C. J.; Swietlicki, E.; Putaud, J. P.; Balkanski, Y.; Fuzzi, S.; Horth, J.; Moortgat, G. K.; Winterhalter, R.; Myhre, C. E. L.; Tsigaridis, K.; Vignati, E.; Stephanou, E. G.; Wilson, J., *Atmos. Chem. Phys.* **2005,** *5*, 1053-1123.
12. Lohmann, U.; Feichter, J., *Atmos. Chem. Phys.* **2005,** *5*, 715-737.
13. Saxena, P.; Hildemann, L. M., *J. Atmos. Chem.* **1996,** *24*, 57-109.
14. Putaud, J. P.; Raes, F.; Van Dingenen, R.; Bruggemann, E.; Facchini, M. C.; Decesari, S.; Fuzzi, S.; Gehrig, R.; Huglin, C.; Laj, P.; Lorbeer, G.; Maenhaut, W.; Mihalopoulos, N.; Mulller, K.; Querol, X.; Rodriguez, S.; Schneider, J.; Spindler, G.; ten Brink, H.; Torseth, K.; Wiedensohler, A., *Atmos. Environ.* **2004,** *38*, 2579-2595.
15. Dias, G. M.; Edwards, G. C., *Hum. Ecol. Risk Assess.* **2003,** *9*, 699-721.
16. Sorooshian, A.; Murphy, S. N.; Hersey, S.; Gates, H.; Padro, L. T.; Nenes, A.; Brechtel, F. J.; Jonsson, H.; Flagan, R. C.; Seinfeld, J. H., *Atmos. Chem. Phys.* **2008,** *8*, 5489-5520.
17. Appel, B. R.; Tokiwa, Y.; Haik, M.; Kothny, E. L., *Atmos. Environ.* **1984,** *18*, 409-416.
18. Pathak, R. K.; Yao, X. H.; Chan, C. K., *Environ. Sci. Technol.* **2004,** *38*, 254-259.
19. Stolzenburg, M. R.; Hering, S. V., *Environ. Sci. Technol.* **2000,** *34*, 907-914.
20. Huntzicker, J. J.; Hoffman, R. S.; Ling, C. S., *Atmos. Environ.* **1978,** *12*, 83-88.
21. Jayne, J. T.; Leard, D. C.; Zhang, X. F.; Davidovits, P.; Smith, K. A.; Kolb, C. E.; Worsnop, D. R., *Aerosol Sci. Technol.* **2000,** *33*, 49-70.
22. Canagaratna, M. R.; Jayne, J. T.; Jimenez, J. L.; Allan, J. D.; Alfarra, M. R.; Zhang, Q.; Onasch, T. B.; Drewnick, F.; Coe, H.; Middlebrook, A.; Delia, A.; Williams, L. R.; Trimborn, A. M.; Northway, M. J.; DeCarlo, P. F.; Kolb, C. E.; Davidovits, P.; Worsnop, D. R., *Mass Spectrom. Rev.* **2007,** *26*, 185-222.
23. Suess, D. T.; Prather, K. A., *Chem. Rev.* **1999,** *99*, 3007-+.
24. Noble, C. A.; Prather, K. A., *Mass Spectrom. Rev.* **2000,** *19*, 248-274.
25. Simon, P. K.; Dasgupta, P. K., *Anal. Chem.* **1995,** *67*, 71-78.

26. Simon, P. K.; Dasgupta, P. K., *Environ. Sci. Technol.* **1995,** *29*, 1534-1541.
27. Weber, R. J.; Orsini, D.; Daun, Y.; Lee, Y. N.; Klotz, P. J.; Brechtel, F., *Aerosol Sci. Technol.* **2001,** *35*, 718-727.
28. Orsini, D. A.; Ma, Y. L.; Sullivan, A.; Sierau, B.; Baumann, K.; Weber, R. J., *Atmos. Environ.* **2003,** *37*, 1243-1259.
29. Peltier, R. E.; Sullivan, A. P.; Weber, R. J.; Brock, C. A.; Wollny, A. G.; Holloway, J. S.; de Gouw, J. A.; Warneke, C., *Atmos. Chem. Phys.* **2007,** *7*, 3231-3247.
30. Slanina, J.; ten Brink, H. M.; Otjes, R. P.; Even, A.; Jongejan, P.; Khlystov, A.; Waijers-Ijpelaan, A.; Hu, M., *Atmos. Environ.* **2001,** *35*, 2319-2330.
31. Khlystov, A.; Wyers, G. P.; Slanina, J., *Atmos. Environ.* **1995,** *29*, 2229-2234.
32. Zellweger, C.; Ammann, M.; Hofer, P.; Baltensperger, U., *Atmos. Environ.* **1999,** *33*, 1131-1140.
33. Loflund, M.; Kasper-Giebl, A.; Tscherwenka, W.; Schmid, M.; Giebl, H.; Hitzenberger, R.; Reischl, G.; Puxbaum, H., *Atmos. Environ.* **2001,** *35*, 2861-2869.
34. Ullah, S. M. R.; Takeuchi, M.; Dasgupta, P. K., *Environ. Sci. Technol.* **2006,** *40*, 962-968.
35. Al-Horr, R.; Samanta, G.; Dasgupta, P. K., *Environ. Sci. Technol.* **2003,** *37*, 5711-5720.
36. Fukushi, K.; Takeda, S.; Chayama, K.; Wakida, S., *J. Chromatogr. A* **1999,** *834*, 349-362.
37. Timerbaev, A. R.; Dabek-Zlotorzynska, E.; van den Hoop, M. A. G. T., *Analyst* **1999,** *124*, 811-826.
38. Valsecchi, S. M.; Polesello, S., *J. Chromatogr. A* **1999,** *834*, 363-385.
39. Dabek-Zlotorzynska, E.; Celo, V.; Yassine, M. M., *Electrophoresis* **2008,** *29*, 310-323.
40. Dolnik, V.; Liu, S. R., *J. Sep. Sci.* **2005,** *28*, 1994-2009.
41. Noblitt, S. D.; Schwandner, F. M.; Hering, S. V.; Collett, J. L.; Henry, C. S., *J. Chromatogr. A* **2009,** *1216*, 1503-1510.
42. Hering, S. V.; Stolzenburg, M. R.; Quant, F. R.; Oberreit, D. R.; Keady, P. B., *Aerosol Sci. Technol.* **2005,** *39*, 659-672.
43. Kelly, M. A.; Altria, K. D.; Clark, B. J., *J. Chromatogr. A* **1997,** *768*, 73-80.
44. Altria, K. D., *Lc Gc Europe* **2002,** *15*, 588-594.
45. Duffy, D. C.; McDonald, J. C.; Schueller, O. J. A.; Whitesides, G. M., *Anal. Chem.* **1998,** *70*, 4974-4984.
46. Noblitt, S. D.; Henry, C. S., *Anal. Chem.* **2008,** *80*, 7624-7630.
47. Noblitt, S. D.; Kraly, J. R.; VanBuren, J. M.; Hering, S. V.; Collett, J. L.; Henry, C. S., *Anal. Chem.* **2007,** *79*, 6249-6254.
48. Crabtree, H. J.; Cheong, E. C. S.; Tilroe, D. A.; Backhouse, C. J., *Anal. Chem.* **2001,** *73*, 4079-4086.
49. Jacobson, S. C.; Koutny, L. B.; Hergenroder, R.; Moore, A. W.; Ramsey, J. M., *Anal. Chem.* **1994,** *66*, 3472-3476.
50. Kuban, P.; Hauser, P. C., *Electrophoresis* **2009,** *30*, 176-188.
51. Yao, X. H.; Shairsingh, K.; Lam, P. H.; Evans, G. J., *J. Environ. Monitor.* **2009,** *11*, 1292-1297.

CHAPTER 7. OVERCOMING CHALLENGES IN USING MICROCHIP ELECTROPHORESIS FOR EXTENDED MONITORING APPLICATIONS

CHAPTER FOREWORD

This chapter was written and submitted for peer review as a book chapter for the upcoming book Fundamental Concepts, Practical Applications, and Limitations of Capillary Electrophoresis and Microchip Capillary Electrophoresis. This book will be edited by Drs. Carlos D. Garcia and Emanuel Carrilho and published by John Wiley & Sons, Inc. The focus of the chapter includes my own novel ideas and experiments, a review of the relevant literature, and a practical tutorial for researchers pursuing an increase in the longevity of their microchip electrophoresis analyses. Many of the ideas presented here were critical to the success of the work shown in chapters 5 and 6 but were only briefly discussed there. This chapter brings together several existing lines of research and additional new thoughts to provide a summary of many of the challenges faced when attempting extended monitoring applications with microchip electrophoresis and potential ways to circumvent or overcome these issues.

INTRODUCTION

Analytical instrumentation for routine online monitoring of the chemical composition of dynamic systems has exhibited a continual increase in demand for a variety of applications. One specific area of particular importance is clinical biology, where studies of transient biological processes are desired. Another area of interest is in environmental monitoring, where both atmospheric and water quality monitoring are in high demand. Online measurement systems are needed in these areas because these applications often exhibit rapid compositional changes as well as short-term analyte stability. Traditional offline measurement techniques may not be sufficient because their poor temporal resolution and inherent delay between sample collection and compositional analysis can result in measurement artifacts and/or the loss of information on important, short-lived events. This loss or distortion of chemical information can affect the evaluation of reaction mechanisms or potential impact on human and environmental health. Often, higher frequency offline sampling can only partly address these issues. Thus, replacing offline measurements with online sampling systems can increase both data quality and quantity. Because online instruments operate at nearly steady-state conditions, they are less subject to systematic errors originating from transient operation. Additionally, online instrumentation, once installed, often requires less manual operation and intervention than offline analyses and is consequently less prone to human error.

Spectroscopic instrumentation is commonly employed for online monitoring systems because these instruments have few, if any, moving parts and offline instruments can often be easily adapted to online operation. However, for many applications involving

complex matrices, the matrix complexity forbids spectroscopic analysis because multiple component signals overlap. Consequently, a separation step is required in order to measure relevant analytes. Commonly used separation techniques for online monitoring include gas chromatography (GC) and liquid chromatography (LC). These technologies are mature and inherently use pressure-driven flow as a driving force. Thus, they can be integrated into online instrumentation using existing methods. However, both of these separation methods suffer from limitations that prevent their use in some online applications. GC requires volatile analytes or analytes that can be derivatized to be made volatile, and most derivatization reactions are difficult or impossible to perform online. Additionally, GC requires compressed gas and heat sources for operation and thus typically possesses a large footprint that is inconvenient for field applications. LC (and its subset, ion chromatography, IC) requires a sample size that can be too large for some applications. Many LC methods also require significant quantities of mobile phase. As an example, a mobile phase flow rate of 1 mL min^{-1} requires 10 L of eluent for one week of operation. For operation in the field, this amount of liquid waste is at the least inconvenient. Additionally, many LC and GC methods are unable to perform at the desired sampling rate or must undergo periodic stationary phase regeneration that interferes with continuous analyses. An alternative, faster separation technique with no stationary phase would therefore prove advantageous for some online monitoring applications.

Capillary electrophoresis (CE) presents a promising instrumental technique for online monitoring because of its simple instrumentation, lack of a solid stationary phase, small

energy footprint, small sample and reagent consumption, and short separation times.[3-5] However, CE presents some challenges to interfacing to online analyses. First, traditional LC injection methods are either incompatible with or have to be modified to work with CE because of the small sample injections (0.1-10 nL) involved. Even after an injection interface is devised, these small volumes can lead to relatively low reproducibilities. Second, online integration requires decoupling of the high separation potential from the sampling interface. Furthermore, hydrodynamic flow in CE typically degrades the separation and is unwanted. If the online system utilizes a continuously flowing sample, either the CE method has to be engineered to compensate for this flow or the flow has to be isolated from the separation capillary. Additionally, even though CE possesses no solid stationary phase, some components in the sample can adsorb to the capillary surface and interfere with the reproducibility of the separation. Finally, CE analyses alter the composition of the background electrolyte (BGE) over time through ion depletion and electrolytic reactions. If ignored, these effects can lower the reproducibility of the separation and quantitation. Several research groups have worked to interface CE instrumentation to online monitoring systems. Much of their work is discussed in review articles on the subject, and we direct interested readers to those reviews.[6-11] It should be noted that none of this work has focused on increasing the longevity of the BGE. One reason for this is that traditional CE does not suffer from BGE degradation as severely as microchip electrophoresis because of the larger buffer volumes. Another explanation for this lack of discussion is that many of these methods do not operated unattended for several days and instead were only tested for a few hours. Also, some methods avoid the issue of BGE degradation by employing a continuous flow

that constantly replenishes the BGE solution. However, several independent reports did focus specifically on instrumental modifications to increase separation longevity. Macka et al. demonstrated the importance of positioning the electrophoresis electrode an adequate distance from the capillary entrance.[12] This distance is important because it allows sufficient diffusional distance for the buffer to consume compositional changes generated at the electrodes, thereby increasing the usefulness of using large BGE reservoir volumes. The authors monitored changes in the buffer pH using indicator dyes and concluded that a capillary tip to electrode distance of 1 mm was sufficient to avoid deleterious effects. The necessary distance likely depends on a variety of factors, including the EOF magnitude and direction, total separation current, buffering capacity of the BGE, and diffusion constants of the BGE constituents. Independent reports by Desiderio et al. and de Jesus et al. illustrated the utility of employing BGE reservoirs with two compartments.[13,14] The separation capillary is positioned in one reservoir compartment, while the electrode is present in the other. The two reservoirs are connected, but via a medium that inhibits mass transport of electrolysis products from the electrodes. Desiderio utilized a cotton plug to inhibit mass transport, while de Jesus employed a salt bridge. Unfortunately, to the authors' knowledge, no comprehensive reviews on the subject of method longevity have been written. The closest publication to this type of review was an editorial by Mayer.[15] Even though a plethora of application-oriented CE reviews have been authored, they neglect to include discussion on long-term monitoring. However, one review, also by Mayer, does discuss some of the aspects of method longevity as subtopics.[16]

Microchip electrophoresis (MCE) provides an enticing alternative to traditional CE for interfacing to online monitoring systems. MCE has several advantages in addition to those of CE, including small size and portability, shorter analysis times, lower sample and energy consumption, ease of multiplexing several functions into a single device, facile incorporation of electrochemical detection, and potentially simpler interfacing to online flows due to MCE's native ability to interconnect multiple microfluidic channels into a single network.[17-24] MCE does possess several drawbacks that hinder online monitoring however, including lower BGE volumes (less than 100 μL in MCE versus several mL for traditional CE) that yield shorter operational times between BGE replacement, difficulty or inability to automate hydrodynamic rinsing of the separation channel between injections, less ideal capillary surface chemistry, and difficulty in reproducible quantitation due to sample ion depletion, small injection volumes, and changes in the surface or BGE during extended operation.[25] As with traditional CE, multiple groups have developed interfaces between flowing sample streams and MCE, permitting online operation.[26-35] Most of these instruments were not characterized with respect to long-term operation, although Büttgenbach and Wilke found that their instrument was limited to about 20 injections (about 24 minutes), which they attributed to analyte adsorption to the capillary surface.[27] Fang et al. also tested their system for a longer time interval and observed a migration time relative standard deviation (RSD%) of 4.9% for 166 injections performed during a 4-h run.[29] Independent of the development of these online systems, several research groups have made progress in overcoming one or more of the obstacles to extended monitoring. One highlight is the work by Oki et al. where the authors nearly eliminated pH changes in the BGE reservoirs through the use of

salt bridges or active neutralization via EOF pumping.[36] Several papers by Kennedy's group document and illustrate the importance of long-term operation. The group focused on analyzing insulin production from individual islets of Langerhans using MCE. Initial efforts yielded a method that could operate for 30 min,[37] and a later system improved this value to 2 h.[38] Continued development eventually led to an instrumental method capable of 24-h continuous operation via the continuous perfusion of all reagents,[39] which is a major breakthrough in the field of microfluidics and has relevance in this application because the insulin production exhibits cycles of various lengths. Unfortunately, the overall approach taken by Kennedy's group is the exception rather than the typical development path. Instead, the majority of reported MCE methods do not discuss operational longevity, and no follow-up efforts are made to increase the operation time. The review by Revermann and coworkers thoroughly covers many of the limitations of MCE and some solutions to these issues.[25] The review has the additional benefit of discussing some of the early traditional CE literature that investigates the fundamental phenomena behind these limitations.

In this chapter, we discuss the challenges in designing MCE instrumentation and zone electrophoresis separations for extended monitoring applications. Particular focus is given to ensuring the ability to perform rapid sequential injections in real samples where the analytes of interest are high-mobility ions (absolute infinite dilution ionic mobilities greater than 4×10^{-4} cm^2 V^{-1} s^{-1}). Specific topics covered include the following:

1. Choosing a buffer system and microchip design that allow long-term operation

2. Achieving rapid sequential injection performance by selecting appropriate injection procedures and avoiding system peaks from the BGE
3. Ensuring robust quantitation by protecting the surface of the capillary from contamination, accounting for and avoiding sample ion depletion effects, and choosing an appropriate internal standard to help compensate for fluctuations in conditions

The discussion will focus on operation with sample solutions that are spatially static, but much of this subject matter can be directly applied to systems that monitor flowing sample streams.

BACKGROUND ELECTROLYTE (BGE) LONGEVITY

The composition of the BGE is perhaps the most crucial component in electrophoretic separations. Several review articles discuss the important role of the BGE and rules of thumb in their preparation for CE.[40-42] The basics of buffering covered in these reviews should be understood before attempting BGE design for electrophoresis. However, the long-term stability of the BGE is a critical issue in online MCE that is often ignored in discussions on buffering. Although depleted BGE can be replaced with fresh solution via either manual replacement or an automated drain/fill procedure, this process temporarily terminates the near-steady-state separation process, resulting in data gaps and an increase in the potential for instrumental and systematic errors during each BGE replacement. Even in instruments employing automated refilling procedures, higher longevity BGEs will allow these instruments to operate for longer periods between the replenishment processes, reducing the number of data gaps. For systems using a continuous refilling

procedure, replacing a normal BGE with a long lasting one will lower the required perfusion rate, decreasing sample consumption and the amount of hydrodynamic interference. Consequently, increased buffer longevity is desirable for all online MCE systems. This section will discuss why certain BGEs exhibit poor longevity and reproducibility as well as ways to lengthen the useful BGE operational time by proper manipulation of buffer composition and microchip physical parameters.

To understand the importance of BGE stability in electrophoresis, the relationship of BGE composition with analyte migration time must be considered. Normally, capillary zone electrophoresis (CZE) assumes a uniform composition throughout the capillary. During an electrophoretic run, however, electric current passing through the capillary changes the BGE composition, a process termed "buffer depletion".[43] When this occurs, intra- or inter-run migration times are affected. In addition to complicating qualitative identification in MCE, migration time shifts also affect peak areas. This phenomenon is due to the fact that peak areas are proportional to migration time for many CE detection methods (methods where this is not true are those where analyte is consumed during detection, including mass spectrometry and amperometry).[16] Another complication arises from irreproducible migration times when quantifying analytes from electrokinetically biased injections. This is due to the injected volume of analyte being proportional to the migration velocity of the analyte, thus the injected sample quantity exhibits similar variance as the migration time. Thus, this mechanism uniformly affects all separations regardless of the detector type.

Potentially the most important factor in buffer depletion is pH, which is the primary reason that BGEs must be well buffered. During CE, electrolysis occurs at the separation electrodes, resulting in the anodic reservoir solution increasing in acidity and the cathodic solution increasing in basicity. These electrolytic reactions can cause an overall change in the pH of the system as well as the establishment of a pH gradient across the separation capillary. The change in pH directly affects the ionic mobility (μ, $m^2\ V^{-1}\ s^{-1}$) of weak acids and bases. For a particular ionizable group, the average ionic charge of an acid (z_A) is given by eq 7.1.

$$z_A = \frac{10^{pH-pK_a}}{1+10^{pH-pK_a}} \tag{7.1}$$

Similarly, the average ionic charge of a basis moiety (z_B) is given by eq 7.2 (note: in this discussion, all references to the pK_a of a base actually refer to the acid dissociation constant for the protonated conjugate acid of that base).

$$z_B = \frac{1}{1+10^{pH-pK_a}} \tag{7.2}$$

Because the ionic mobility is proportional to the charge of the ion, some separations, particularly those operating near the pK_a of an analyte(s), are very sensitive to BGE pH changes. As an example, a cation with one ionizable group will exhibit an ionic mobility that is 4.7% faster at 0.02 pH units below its pK_a than at 0.02 units above it (assuming no change in hydrodynamic radius with protonation percentage). pH changes can also affect migration times for strong electrolytes by altering the electroosmotic flow (EOF). EOF is proportional to the zeta potential of the capillary surface, which in turn is related to the surface charge. Therefore, changes in the charge state of ionizable surface groups will affect all components of the separation. Strong electrolytes can also be affected by pH

changes when they are complexed by a BGE component that is pH sensitive because the fraction of the analyte undergoing complexation changes with pH.

In addition to pH changes, individual buffer species concentrations in the BGE can also change during operation. Just as with pH, this can alter separations where complexation reactions are utilized. More importantly, nearly all separations will be affected by concentration and pH changes via ionic strength effects. This is particularly important when simultaneously analyzing both monovalent and polyvalent species. More highly charged species are more highly affected by ionic strength than less highly charged ones, and unintended ionic strength changes can cause previously resolved species of different valence to comigrate. The mobility dependence on ionic strength is classically estimated by assuming a reduction in mobility that is directly proportional to the magnitude of the analyte charge and proportional to the square root of the BGE ionic strength. This approximation is not strictly valid due to the finite size of real ions. Li and coworkers performed a thorough investigation of this phenomenon and found that infinite-dilution mobilities can be more accurately adjusted for finite ionic strengths using eq 7.3.[44] Here, μ_0 is the infinite dilution mobility, 'i' is the ionic strength, and 'j' is a constant that should be determined empirically but can be estimated using the Pitts equation.[45]

$$\mu \approx \mu_0 - \frac{jz\sqrt{i}}{1+2.4\sqrt{i}} \tag{7.3}$$

The important points of this equation are that changes in mobility are more pronounced for polyvalent species and that ionic strength changes have a larger relative effect on BGEs with a lower nominal ionic strength.

With some of the mechanisms of BGE failure under extended electrophoresis elucidated above, discussion can focus on engineering BGEs to minimize these effects. Several articles have been written on the empirical consequences of buffer depletion, as well as the theory behind it.[43,46-48] The important factors affecting the percentage of BGE compositional change with time are total BGE volume, separation current, and buffer capacity. Of these, volume of the BGE is the easiest to discuss and understand. Put simply, BGE volume impacts none of the depletion processes on a mass or molar basis. Therefore, all fractional or percentile changes to the BGE, the relevant measure when observing empirical phenomena, are inversely proportional to volume. Consequently, the acceptable BGE longevity should be exactly proportional to volume. This has a dramatic importance in microfluidic devices. For instance, an MCE system with a 2 mm diameter, 1 mm tall fluid reservoir can only hold about 3.1 μL of BGE. Changing the reservoir size to a 10-mm diameter and the fluid height to 2 mm increases the volume to 157 μL, a 50-fold increase. If the small reservoir could support a 5-min analysis, the larger one would last over 4 hours, even without any other changes to the system. Additional benefits of larger microchip reservoirs included reduced Laplace (meniscus) pressures and a lower surface area-to-volume ratio in the reservoir.[49] Both of these factors decrease the reproducibility of the separation as they increase in magnitude, thus reducing them improves the integrity of the separation.

The electrical current induced by the separation potential(s) is a primary driver of buffer depletion and should be minimized. This is due to the electrical current being directly proportional to the electrolysis occurring at the electrodes, and thus proportional to the

hydronium and hydroxide being produced at the anode and cathode, respectively. The separation current, I (A), is given by eq 7.4, where R_e is the electrical resistance of the channel (Ω), U is the applied potential (V), ρ is the resistivity of the BGE (Ω*m), A is the capillary cross-sectional area (m^2), L is the total capillary length (m), E is the applied electric field ($V\ m^{-1}$), and κ is the solution conductivity ($S\ m^{-1}$).

$$I = \frac{U}{R_e} = \frac{UA}{\rho L} = \kappa EA \tag{7.4}$$

While this equation is based on electrical current and the resulting electrolysis, similar results can be achieved by starting from the ionic mobility of the buffer constituents and modeling the system from a charge balance perspective (with hydronium and hydroxide production needed to maintain charge balance from the exiting ions). Due to the intrinsic dependence of electrical current on the mobility of the electrolyte components, these are actually equivalent models that are just mathematically derived from different approaches. Consequently, depletion effects from individual components electrophoretically migrating out of the reservoir should correlate well with current as long as all the ionic BGE components are similar in both mobility and concentration. Thus, all further discussion will use separation current as a proxy for all buffer depletion effects. It is important to note that eq 7.4 contains both voltage and capillary length, and thus it is not the absolute magnitude of the applied voltage that decides the depletion rate, but instead it is the applied electric field. Consequently, post-detection column length does not change the depletion rate despite increasing the required separation potential. However, it should be realized that for a given required maximum separation time, shorter capillaries yield reduced depletion effects because they utilize lower field strengths (and also have the cost of decreased resolving power). Another important

factor is that most MCE systems employ multiple BGE reservoirs and electrophoretic channels, so proper design of the microfluidic network is needed to ensure that none of the other channels have a considerably higher applied field than does the separation channel, as that high-field channel and reservoir may then become the limiting factor in operational longevity. This is especially true when utilizing gated injection, as this method employs continuous flows in all four capillary segments.[50] Discussion of proper gated injection design has been provided in several publications,[51-53] and these approaches can be applied to designing microchips for long-term analysis. One effective way to decrease separation current and therefore increase operation time is to employ narrower capillaries, a change that is easily accomplished with many MCE fabrication protocols. Decreasing cross-sectional area has the additional benefits of decreasing any Joule heating effects, increasing hydrodynamic resistance, and decreasing volumetric EOF pumping that can lead to hydrodynamic artifacts over time (and will be discussed later). Smaller channel cross sections do have several potential drawbacks, including reduced detection sensitivity, increased analyte adsorption to the capillary surface, and an increase in relative channel dimension uncertainty. The choice of a final channel size is therefore dependent on an appropriate compromise of the aforementioned effects.

The final term in eq 7.4 is the only chemistry specific term in the equation—solution conductivity. The conductivity of the BGE is inherently tied to its buffer capacity and so the two will be discussed together. Intuitively, it is easy to assume that higher buffer capacity will lead to increased resistance to buffer depletion, which has been previously reported.[43] However, this is not always effective, as was shown in Bello's work for a

buffer operating at its pK_a.[46] Intuitively, this is rationalized by noting that depletion effects are proportional to the solution conductivity, and conductivity is roughly proportional to the concentration of the BGE (with some deviations—as ionic strength increases, the molar conductivity decreases, resulting in small longevity benefits). Therefore, the ratio of buffer capacity to solution conductivity is the relevant figure of merit, as was discussed by Reijenga et al.[54] This is shown graphically in Figure 7.1, where PeakMaster 5.2 simulation results are shown for the conductivity, buffer capacity, and buffer capacity-to-conductivity ratio as a function of the concentration of a BGE composed of an equimolar mixture of 2-(N-morpholino)ethanesulfonate (MES) and histidine (HIS).[1]

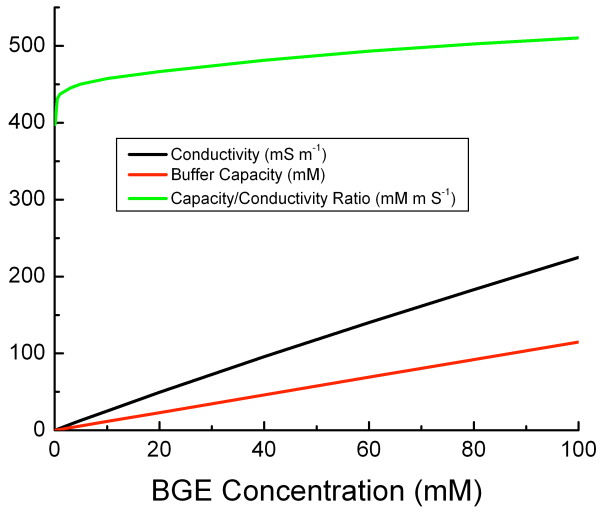

Figure 7.1. PeakMaster 5.2 simulation results for an equimolar mixture of MES and HIS (x-axis is concentration of each component, not total concentration).[1] Buffer capacity increases proportionally with concentration, whereas solution conductivity increases with a nearly linear response and only a slight decrease in molar conductivity with increasing concentration. The ratio of buffer capacity to conductivity is effectively proportional to BGE longevity (with respect to pH change) and shows only weak dependence on BGE concentration. The y-axis units for each trace are given in the legend.

The ratio of conductivity and buffer capacity is representative of buffer longevity, and this plot shows it to only be weakly dependent on buffer concentration, agreeing with the results of Bello.[46] It should be stated, however, that this result is only valid when all the components added to the BGE are buffering in nature (either a buffering ion or a titrating species). When non-buffering salts (i.e. NaCl) are added to the BGE to alter ionic strength or perform complexation chemistry, then an improved buffer capacity-to-conductivity ratio will be achieved when increasing the concentration of the buffer as long as the non-buffering ion concentration does not increase. Therefore, if a predetermined ionic strength is required for desired selectivity or EOF, then it is best to achieve the higher ionic strength by increasing the concentration of the buffering ions instead of through the addition of non-buffering salts. Although the weak dependence of buffering capacity-to-conductivity ratio on the concentration of the BGE indicates that an arbitrary concentration can be selected, the effects of sample matrix on the BGE are not concentration independent and therefore the BGE concentrations need to be decided with the sample composition in mind.

As stated above, buffer concentration and conductivity are inherently related. Therefore, the conductivity of the BGE must be decreased via a method other than total concentration in order to increase buffer longevity. The solution to this is intentional and well-planned buffer choices. First and most importantly, the buffer should be composed of both a weak acid and a weak base at a pH in both buffering regions. This permits every ion in solution to contribute to buffer capacity instead of only half of the ions, essentially doubling buffer capacity. The next step in preparing a low conductivity BGE

is to choose buffering compounds that have low molar conductivities. Foremost in this approach is to ensure that each component has a net charge of 1 or less. Additional charge typically does not increase buffering capacity (because multiple acidity constants typically do not have overlapping buffering regions), but it often greatly increases solution conductivity because molar conductivity is nearly proportional to the square of the ionic charge (due to the molar conductivity being proportional to both the charge and the mobility, with the mobility itself also being proportional to charge). Polyvalent ions are also known to lead to other problems in the BGE, particularly the formation of additional system zones.[55,56] The next step in lowering molar conductivity is to utilize large buffering molecules. Ionic mobility is inversely proportional to the hydrodynamic radius, so larger molecules are less conductive. A good rule of thumb is to target compounds with mobilities below $3*10^{-8}$ m^2 V^{-1} s^{-1}, as significant further improvements are difficult to achieve because very few common buffers have mobilities below $2*10^{-8}$ m^2 V^{-1} s^{-1}. It is common to find claims that zwitterionic buffers should be employed because their net charge is nearly zero. This is misleading, as the real reason that zwitterions often exhibit low molar conductivities is that charged moieties require more solvating molecules than neutral structures, thus they considerably increase the hydrodynamic volume in zwitterionic species. However, this low net charge claim is related to the final step in lowering conductivity, which is rarely discussed, and that is to employ a buffering acid with a pK_a above the BGE pH and a base with a pK_a below the operating pH.[2] Intuitively, the benefit to this approach is apparent by realizing that when the acid is below its pK_a, it is mostly uncharged and vice versa for bases. To show this graphically, PeakMaster 5.2 was used to simulate hypothetical buffers composed of

equimolar acid and base components, each having mobilities of $2.5*10^{-8}$ m^2 V^{-1} and pK_a values averaging 6.0.[1] Buffer capacity was kept constant at 15 mM, and the buffer concentration to attain this capacity and the resulting conductivity are plotted as a function of buffer pK_a in Figure 7.2.

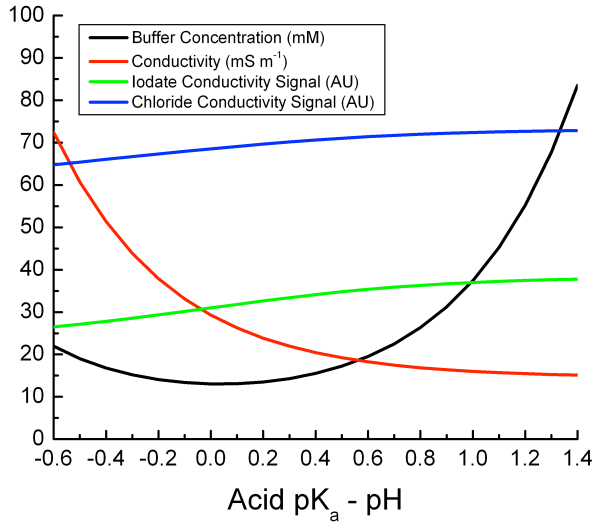

Figure 7.2. PeakMaster 5.2 simulation results for hypothetical pH 6.0 BGEs consisting of equimolar acid and base having pK_a values at equal but opposite values from 6.0 and electrophoretic mobilities of $2.5*10^{-4}$ cm^2 V^{-1} s^{-1}.[1] The x-axis in this plot is $pK_{a,acid}$ minus pH, or equivalently, pH minus base $pK_{a,base}$. Buffering capacity was kept constant and the necessary buffer concentration to achieve these conditions and the resulting conductivity are shown. The calculated conductivity detection signals for chloride and iodate are also shown.

The x-axis in this plot is the acid pK_a minus pH, or equivalently, pH minus the base pK_a. It is clear that the aforementioned rule of thumb of keeping the acid pK_a above the pH and the base pK_a below the pH is a powerful way to reduce buffer conductivity while maintaining constant buffer capacity. Figure 7.2 also shows that the common perception of operating at a buffer's pK_a to yield best results is not always true. For instance, utilizing an acid with a pK_a 1 unit above the BGE pH and a base with a pK_a 1 unit below the pH results in a conductivity that is 45% lower than when $pH=pK_a$, increasing buffer

longevity by 83%. Additionally, reported buffer capacity is derived from a differential computation (infinitesimally small addition of acid or base), and for larger, finite additions of perturbing acid or base, the lower conductivity BGE should actually undergo even less pH change than in the BGE where pK_a=pH. Figure 7.2 also illustrates that the buffering approach recommended here for long-term monitoring is also beneficial for most conductivity detection applications in electrophoresis, where a low background signal is desired. As stated above, the conductivity background drops by 45% when using a pH-pK_a differential of 1. The PeakMaster simulation shows that the same changes in conditions result in a 6% increase in signal for chloride due to changes in the mobility and displacement of the BGE co-anion.[1] Because the mobility of iodate is closer to the mobility of the BGE co-anion, iodate shows an even larger percent increase in signal, 19%. Assuming the background noise is proportional to the background signal, these improvements combine to yield a signal-to-noise ratio increase of 93% and 118% for chloride and iodate, respectively. The similarities in BGE conditions for conductivity detection and BGE longevity make conductivity detection an appealing option for extended monitoring applications.

The plot in Figure 7.2 indicates that indefinitely increasing the pK_a difference from the operating pH would result in the best performance. However, in practice, a variety of complications arise that limit this approach. One of these is solubility, which imparts a physical limitation on the BGE composition. Also, changes in solution viscosity or unexpected, significant complexation phenomena may present problems at high buffer concentrations. Another issue is ionic strength. Although not shown in Figure 7.2, the

ionic strength follows the same behavior as the conductivity, dropping from 17.97 mM at –0.6 pH units to a value of 3.40 mM at +1.4 pH units. This drop in ionic strength will need to be accounted for when designing separation conditions because polyvalent species will migrate faster relative to monovalent ions at the lower ionic strength. The reduced ionic strength can also cause an increased EOF magnitude. The lower ionic strength and conductivity also lead to increased peak broadening during sample overloading, limiting resolution and/or useful linear range. Perhaps the most problematic issue with increasing buffer concentration is trace buffer contamination. As an example, if a HEPES buffer (MW=238.3) has 200-ppm sulfate impurity, this equates to 50-μM sulfate in a BGE containing 100-mM HEPES. While not enough to significantly increase the background conductivity of the solution, this concentration is high enough to interfere with sensitive conductivity or indirect UV detection (particularly at low ionic strength) through competitive displacement, high blank values, or the introduction of unwanted system zones. Consequently, we recommend employing buffers that have pK_a values displaced 0.5-1.0 units from the pH. Relative to the case where $pH=pK_a$, this increases buffer longevity by 52-83% and only requires a buffer concentration increase of 32-102%.

Although the above discussion on buffer depletion does not appear to be affected by EOF, investigations have shown long-term electrophoresis stability to be affected by the EOF.[43] Confounding this issue is that not all the studies tied the concentration dependence of the BGE stability to the EOF even though that was a core factor. For instance, earlier we mentioned that some research found the BGE longevity significantly

depended on buffer concentration even though Bello's work indicated this to be untrue.[46] The reported concentration dependence is in fact an EOF effect, as increasing BGE concentration (and thus ionic strength) decreases the EOF magnitude. Several mechanisms contribute to the reproducibility and longevity being dependent upon EOF magnitude. First, the EOF pumps solution from one reservoir to another, lowering the volume in one reservoir while increasing the volume in the other. The change in volume affects both head height and Laplace pressures, inducing unwanted hydrodynamic flow.[49,57] This pressure-driven flow changes migration times and peak areas, and it can also increase band broadening. Because these changes lower reproducibility and induce systematic changes with time, they give the appearance of buffer depletion even if buffer composition remains constant. A second mechanism to the reduction in reproducibility with an increased EOF is that migration time uncertainty is inherently tied to the EOF uncertainty. This becomes clear from examining the equation for migration time in electrophoresis, eq 7.5, where L_{eff} (m) is the effective separation distance, t_{mig} (s) is the migration time, and μ is mobility ($m^2\ V^{-1}\ s^{-1}$) for both the ion and EOF.

$$t_{mig} = \frac{L_{eff}}{E\left(\mu + \mu_{EOF}\right)} \tag{7.5}$$

Typically, EOF is the primary factor in migration time uncertainty because other factors, including ionic mobility (dependent on temperature and viscosity), electric field (dependent on total length, applied potential, and a uniform BGE conductivity through the capillary), and effective separation length, are nominally constant. Therefore, with otherwise ideal conditions, the uncertainty (σ) in the migration time is given by eq 7.6.

$$\sigma_{t_{mig}} = \frac{\sigma_{\mu_{EOF}} L_{eff}}{E\left(\mu + \mu_{EOF}\right)^2} \tag{7.6}$$

Relative standard deviation (RSD) is often a better indicator of separation reproducibility than absolute uncertainties, and combining eqs 7.5 and 7.6 and rewriting them in terms of RSD values yields eq 7.7.

$$RSD_{t_{mig}} = \frac{RSD_{EOF}\left|\mu_{EOF}\right|}{\left|\mu + \mu_{EOF}\right|} \tag{7.7}$$

The results of this equation are graphically illustrated in Figure 7.3 where each trace shows the RSD of the migration time induced by a 3% RSD in the electroosmotic mobility for a range of typical ionic mobility values.

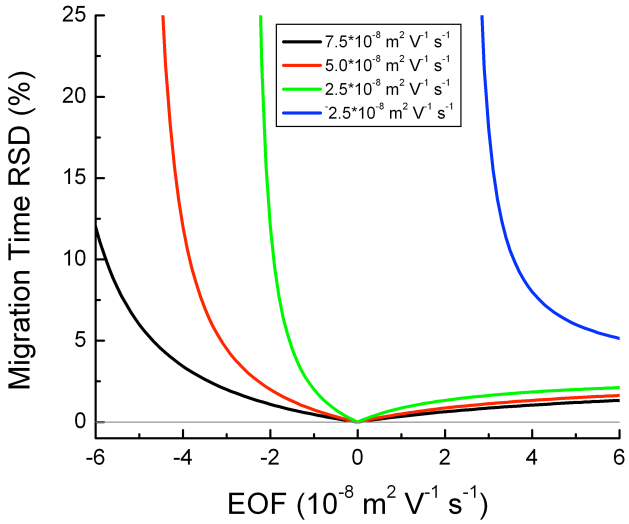

Figure 7.3. Expected migration time uncertainty (RSD) as a function of EOF using eq 7.7 and assuming RSD_{EOF} = 3%. Note that equivalent plots are obtained with oppositely charged ions and a mirrored x-axis.

Separations with analytes in regions with large EOF values will show higher sensitivity to BGE degradation because small changes in BGE composition induce changes in the EOF, and these separations are more sensitive to EOF fluctuations. The traces in Figure 7.3 indicate that the most reproducible results will come from separations where the EOF is near zero. Additionally, the large differences in the behavior of the low-mobility

cations from the low-mobility anions makes it apparent that low-mobility anions would be better analyzed by reversing the polarity and analyzing with a slow co- or counter-EOF than by using a high EOF to "drag" anions to the cathode. Note that equivalent results are obtained when plotting oppositely charged ions using a mirrored x-axis. A third and final mechanism for EOF effects to reduce the BGE longevity and/or reproducibility is one where the EOF actually changes the rate of BGE compositional change. This occurs when the volume reduction in one reservoir due to EOF pumping is large enough that it significantly increases the rate of compositional change in the BGE caused by electrolysis. The volumetric flow from EOF (Q_{EOF}, $m^3\ s^{-1}$) is easily calculated using eq 7.8.

$$Q_{EOF} = E\mu_{EOF}A \tag{7.8}$$

Typically, these values are small, but extended monitoring can make these values significant in extreme cases, such as a combination of high EOF magnitude, small BGE reservoirs, and large capillary cross-sectional areas. For instance, at 300 V cm^{-1} and an EOF of $6*10^{-8}$ $m^2\ V^{-1}\ s^{-1}$ in a 50-μm x 50-μm channel, 1 hour of operation will transfer about 16 μL of solution. That volume is significant in most MCE applications, and the volume loss may result in depletion rates up to 50% higher than expected neglecting EOF when the BGE volume in one reservoir is 30-40 μL, as is common in MCE. Overall, the easiest way to minimize EOF contributions to separation degradation is to suppress the EOF using surfactants, polymers, and/or covalent modification. In addition to reducing the volumetric transfer rate from one reservoir to another (inducing hydrodynamic flow through the channel and increased depletion in the reservoir the EOF exits from),

lowering EOF should also improve reproducibility when small fluctuations in EOF occur, as was shown in Figure 7.3.

Although BGE longevity and reproducibility in MCE are typically evaluated with respect to operation time, any other factors that affect composition, pH, or ionic strength can also limit BGE lifetime even if electrophoresis is not occurring at all times. Some of these include temperature, carbonate dissolution, and component volatility, reactivity, and stability. Temperature not only directly affects ionic mobility and EOF, but it also changes the pK_a of buffers and therefore the pH. Typically, higher temperatures lower the pK_a of a molecule, and amine moieties tend to exhibit higher temperature dependencies than carboxylates.[41,58] Additionally, higher temperatures yield higher electrophoretic currents, so any change in temperature should be taken into consideration when determining BGE operational times. One often overlooked factor concerns changes in the ambient temperature throughout the day. Obviously, operation outdoors is highly susceptible to this phenomenon. In some outdoor environments, normal day-night changes can be 20 K or larger. This is particularly troublesome when ambient temperatures go below the freezing point of water. Therefore, rigorous outdoor MCE monitoring must utilize a container with temperature control. Such a container is often needed indoors also, as indoor temperatures can also show large variance (5 K is not unreasonable). Changes indoors can be due to external forcing effects, energy-saving thermostating systems, changes in the quantity of personnel in the building throughout the day, and seasonal differences. Because of all the unknown factors contributing to the

ambient temperature, temperature monitoring alongside the MCE system during operation may be needed for rigorous performance evaluation and troubleshooting.

Carbonate dissolution from atmospheric carbon dioxide is a well-understood process, though it is often ignored, and it causes serious reproducibility problems in MCE at high pH. An excellent discussion on atmospheric carbonate contamination in CE is given in a buffering review by Persat,[41] so only the most pertinent points will be summarized here. Below pH 5.5, contamination from carbon dioxide is negligible except for the most rigorous applications. Above this, bicarbonate concentration becomes significant, and by pH 8 the divalent carbonate concentration reaches significant levels. In addition to pH and ionic strength changes, carbonate can complex with both buffer and sample cations and even form insoluble precipitates. Carbonate contamination also makes sensitive conductivity detection of anions above pH 8.5 nearly impossible due to carbonate's high molar conductivity that increases background signal and induces relatively high mobility system zones. To overcome carbonate dissolution effects, three options are readily available. The first and easiest is operation at low pH. This solution works well for strong inorganic acids as well as most inorganic cations (where the low pH will also help avoid interference from hydroxide). Clearly, this solution will not work as well when pH selectivity requirements demand operation near the pK_a of protonated amines (8-12) or when detection modes require high pH (pulsed amperometric detection, for instance). A second option is to engineer and operate the BGE for use in fully equilibrated carbon dioxide environments. This approach requires additional calculations in the BGE design as well as an additional wait time after the BGE solution is prepared to ensure

equilibration with the atmosphere. This method is only recommended for intermediate pH values where the BGE will not be dominated by carbonate and will not work in cases where insoluble carbonates will form. A third possibility to preventing carbonate interference is to prepare and operate the BGE in a carbon dioxide-free environment such as a glovebox or glovebag. Note that the source water will need to be properly degassed prior to use with this method. Although a variety of difficulties may be introduced from this approach, if the continuous operation already requires rigorous environmental control, then the additional requirement of a carbon dioxide-free environment may not be too severe.

In addition to carbonate and temperature effects, the chosen BGE constituents themselves can also lead to unintended compositional changes over time. Component volatility is a leading culprit here. Even if none of the specific BGE components are volatile, all aqueous solutions will still undergo evaporation of water with time, leading to concentration and ionic strength increases as well as possible changes in surfactant behavior. Operating in an environment with nearly 100% relative humidity can minimize water evaporation, although care must be taken to avoid arcing between the high voltage connections used for electrophoresis when applying potentials in a high humidity environment. Another option is to employ BGE reservoir covers that minimize the mass transfer cross-sectional area, reducing evaporation effects approximately proportionally to this reduction in cross section (or even reduce them beyond the proportional size if turbulent mixing effects are eliminated with this step). Noblitt and coworkers successfully utilized this approach in an online monitoring instrument employing MCE

for aerosol analysis.[59] In that instrument, the covering lids were airtight and interconnected to permit isobaric operation. However, in the majority of cases, airtight seals are not desired because they can hydrodynamically close the system, leading to unwanted pressure buildup. In addition to water evaporation, other volatile components can be problematic. This is especially true when organic co-solvents are utilized. Traditional organic modifiers like acetonitrile, methanol, ethanol, and acetone should not be used in extended online monitoring applications unless their volatilization can be limited or, preferably, eliminated. Less volatile organics such as dimethylsulfoxide (DMSO) can likely still be used. Though typically less prone to volatilization problems, even buffering ions and complexation additives can suffer from volatilization over extended times. Acetic acid and 15-crown-5, respectively, are examples of commonly used constituents that are volatile. In addition to volatilization effects, BGEs can also succumb to component degradation or reactions. Clearly, components that react with oxygen and carbon dioxide should be avoided. Compounds that hydrolyze on the timescales of interest should not be employed. Primary amines (unless completely protonated) and reduced sulfur species are often relatively reactive and should be avoided in BGEs. Large macromolecules can behave unpredictably and irreproducibly, especially with regards to channel surface chemistry. Heavy metal ions should be avoided because they can change surface chemistries with time, and some heavy metals undergo slow ligand exchange, changing the BGE composition over hours or days. Perhaps the most pernicious, least reproducible, and hardest to address problem in extended monitoring comes from microbial action on BGE solutions. This issue is ubiquitous, and although BGE filtering protocols and the inclusion of biocides in the BGE can limit microbial

action, in some cases the problem is unavoidable and can only be worked around by empirically determining operation time. This measurement should be performed in an environment as closely resembling the working environment as possible, and systems that exhibit stability in clean indoor air may be quickly consumed in unfiltered outdoor air. In summary, great care must go into design of the BGE for extended online monitoring with MCE even beyond buffer depletion considerations. If the separation functions properly initially but fails after longer operation, each component needs to be evaluated with regards to the above issues and problematic components replaced with acceptable alternatives.

Overall, the above paragraphs discuss the pertinent points in assembling a BGE that is robust with respect to both electrophoretic and non-electrophoretic degradation. The theoretical approach developed by Bello provides a way to calculate buffer longevity by determining the time needed to change the BGE pH by a predetermined amount.[46] However, we recommend measuring buffer longevity empirically because properly estimating the acceptable amount of pH change can be difficult and other effects like EOF alterations, ionic strength variance, and changes in the amount of complexation can also result from BGE degradation. To test BGE longevity, sequential analysis of a standard solution while monitoring migration times and peak areas works well (note that sample depletion can also affect peak areas and relative peak areas, so take measures to ensure this is not occurring during the longevity measurement through a sample replacement scheme). Because the final MCE device and BGE may be targeting several days of operation, it may be better to utilize a modified MCE device operating under less-

ideal longevity conditions to perform the test. The maximum operational time for the final device (O_2) can then be calculated using the proportionality in eq 7.9 and the maximum operational time for the testing device (O_1). In this equation, V (m^3) represents volume of the BGE reservoirs.

$$O_2 = O_1 \frac{V_2 E_1 A_1}{V_1 E_2 A_2} \tag{9}$$

Utilizing this approach comes with some limitations because performance may unexpectedly change with the different conditions. For example, changing the buffer volume may cause differences in Laplace pressures or evaporation rates. Operating at higher electric fields can alter behavior through Joule heating. Changing the channel cross-sectional area is particularly risky, as this may affect both the EOF and the surface adsorption effects. Other factors simply cannot be accounted for except with a true extended run, including BGE component degradation or reactions, capillary surface fouling, and evaporation effects. Consequently, eq 7.9 should only be considered approximate. Only a true extended analysis at the exact operating conditions can ensure long-term performance integrity. As a final example of the impact that the methods discussed in this section can accomplish, the combined benefits from the above discussion will be applied for a typical MCE system. The starting system in this case is a BGE of potassium phosphate at pH 7.0, a separation channel of 50 μm x 50 μm, and a 3-mm diameter buffer reservoir 2 mm in height. Changing the buffer system to a HEPES/Bis-Tris system reduces the background conductivity by 95.3% (calculation done with PeakMaster 5.2 for buffers of equal 15 mM buffering capacity).[1] Decreasing the channel size to 25 μm x 25 μm lowers the buffer consumption by 75%. Increasing the BGE reservoir size to 12-mm diameter by 3-mm tall changes the volume from 14 μL to

339 μL. The cumulative effect of these three changes results in an expected BGE longevity increase of over 2000-fold. If the original method was acceptable for 5 min, the adjusted method will operate for about 7 days. Additional changes such as suppressing the EOF, minimizing evaporation, and lowering the separation field strength will only further improve the system.

ACHIEVING RAPID SEQUENTIAL INJECTIONS

For many online monitoring instruments, short sampling intervals are required. Even when it is not required, high frequency collection is often still beneficial because it permits increased data averaging and/or improved confidence intervals. In separations, the frequency of data collection is inversely proportional to the minimum acceptable time between sequential injections *with a real sample*. Knowledge of the sample matrix is important in this endeavor because the appearance of peaks late in the separation, even if they are not important in the analysis, can interfere with analytes of interest if another injection has already been performed. In chromatography, frequently the only solution is to increase the interval between injections and allow the late-eluting peak to exit the column. Traditional CE, however, can avoid this limitation by hydrodynamically rinsing the capillary between analyses to remove any late-migrating ions or system zones. Often, several capillary volumes of solution can be flushed in less than one minute. Initially, one might expect MCE, due to its fast separation times, to be an ideal technique for performing rapid sequential injections during online monitoring. However, many MCE systems are incapable of automated hydrodynamic flushing. Consequently, they suffer from the same problems as chromatography systems with respect to late-migrating peaks.

Arguably, MCE systems may be even more limited in this aspect than chromatography because many electrophoresis separations exhibit late-migrating system zones. This section discusses approaches to minimizing or even eliminating unwanted, late-migrating ion peaks and system zones. Specifically, discussion will focus on design of the BGE, choice of the EOF direction, injection mode, and optimizing injection timing for maximum sampling frequency. Because the detection technique has ramifications on the sensitivity to system peaks and unwanted sample peaks, this will also be covered.

The first step in achieving rapid subsequent injections is to reduce the number of system zones (also known as system peaks, eigenzones, or eigenpeaks) due to BGE composition. The occurrence and prediction of system zones in CE have been covered by a variety of authors and publications.[40,60-69] Therefore, only the pertinent conclusions and rules-of-thumb will be discussed here. System zones are created by the interruption of the otherwise continuous BGE during sample introduction. This BGE perturbation then propagates through the capillary in the same manner as a true ion peak. The detector can then record the resulting system zones as peaks and/or dips, thus interfering with quantitation of analytes of interest. System zones can also induce peak broadening in nearby analyte peaks. Consequently, even separations employing detectors that do not directly detect the system zones (fluorescence, amperometry, and direct UV absorbance, for instance) can still be negatively impacted by their presence. When performing rapid sequential injections without hydrodynamically rinsing the system between injections, any system zones migrating significantly slower than the analytes of interest that were injected with a previous injection can interfere with the behavior of the faster analytes

injected in later runs. The best way to minimize system zones is to construct the BGE using only one base (cation) and one acid (anion). As long as both species are monovalent, this approach should yield two system zones that effectively migrate with or near the EOF, termed the injection zone. It should be noted that operation in either highly basic or highly acidic conditions could shift these two system zones away from the injection zone due to the interactions with hydroxide and hydronium, respectively. If the required selectivity is such that a BGE with only one acid and base cannot be utilized, then the next best choice is to utilize a BGE with one co-ion and two (or more) counter-ions. Employing this BGE will result in no interfering system zones in the separation near the ions with the polarity of interest, and n-1 system zones (apart for the injection zone) of the opposite polarity will be present, where n is the number of counter-ions. The opposite-polarity system zones can then be avoided by proper selection of the EOF direction and magnitude (discussed later). As a last resort, BGEs containing two or more co-ions can be used. These BGEs will exhibit system zones (following the n-1 rule) with the same migration direction as the polarity of interest. Note that if the low-conductivity BGE suggestions from the last section are followed, the resulting system zones should also be of a low mobility because system zones will appear between the mobilities of the two BGE co-ions. We recommend employing simulation software such as PeakMaster to predict the appearance of system zones when designing the BGE.[1,70] Software simulators will predict the location of the system zones with relative accuracy, and they will also quantitatively indicate when the operating pH is extreme enough to generate substantial system zones from either hydronium or hydroxide ions. Note that simulation software may fail to predict system zones correctly if the BGE components are sufficiently impure

so as to have a significant quantity of additional ions present. Therefore, only highly pure BGE components should be used. Choosing only the purest BGE components also helps increase lab-to-lab reproducibility. As a final recommendation, if BGE additives or modifiers are being used, we suggest choosing non-ionic compounds if possible, as these species will not add additional system zones to the separation.

Truly eliminating all system zones is an impossible task, as even the simplest BGE will always exhibit one effective system zone, the injection zone (or "water peak") that migrates with the EOF. As mentioned above, system peaks can affect separations even when they are invisible to the detector, and operating in a sequential injection mode complicates the issue further. Even if all the system zones could be eliminated, early injections might still interfere with later injections if unimportant, late-migrating ions are present in the sample. However, an easy way to eliminate both issues is through proper selection of EOF direction and magnitude. For instance, even a very slow counter-EOF flow will remove the injection zone, ions of opposite polarity, and any system zones resulting from multiple counter-ions. If there are slow, interfering ions with the same polarity as the analytes or system zones from multiple co-ions, then the EOF magnitude will need to be sufficiently high to remove these as well. Control of the EOF direction and magnitude is possible through dynamic modification with small molecules, surfactant micelles, and/or polymer additives. It can also be performed with static surface changes, including covalent modification, neutral polymers, and polyelectrolyte multilayers. These surface modification procedures are covered thoroughly in the literature and therefore will not be discussed here.[71-77] Despite its ability to eliminate system peaks,

counter-EOF approaches are not commonly used. Possibly the main reasoning behind this is the increase in analysis time caused by a counter-EOF flow. This argument, however, is a bit misleading because resolution increases with increasing counter-EOF magnitude, and the improved resolving power indicates that shorter capillaries can be employed that will somewhat offset the slower net analyte mobility.[3,4,78,79] Consequently, a quantitative understanding of the impact of EOF on resolution is needed to design highly optimized separation systems. Because selection and control of EOF magnitude is so important in long-term monitoring applications and also directly affects resolution, below we show how to calculate the theoretical resolution in MCE as a function of EOF. As an example, the resolution of three closely-migrating ion pairs (cesium/potassium, barium/1,5-diaminopentane, and sodium/trimethylamine) is calculated for a range of EOF values and a 5-cm MCE channel with an effective potential of 1500 V, 0.5-mm injection length (1% of the capillary length), and 0.5-mm detection zone (also 1% of the capillary length). To perform this calculation, the following derivation and assumptions were made. Separation efficiency, N, is given by eq 7.10, where $w_{0.5}$ (s) is the peak width at half height, w (s) is the baseline width of the peak, and the square of σ_{total} is the total variance of the peak in the separation.

$$N = 5.54\left(\frac{t_{mig}}{w_{0.5}}\right)^2 = 16\left(\frac{t_{mig}}{w}\right)^2 = \frac{L_{eff}^2}{\sigma_{total}^2} \tag{7.10}$$

Resolution between peaks 1 and 2, R_{sep}, is given by eq 7.11.

$$R_{sep} = \frac{2\left(t_{mig,2} - t_{mig,1}\right)}{w_1 + w_2} \tag{7.11}$$

Combining eqs 7.9 and 7.10 results in eq 7.12.

$$R_{sep} = \frac{t_{mig,2} - t_{mig,1}}{2}\left(\frac{\sqrt{N_1 N_2}}{t_{mig,1}\sqrt{N_2} + t_{mig,2}\sqrt{N_1}}\right) \tag{7.12}$$

Migration time can be written similarly to eq 7.5, but with the electric field separated into effective length and effective voltage (V_{eff}), resulting in eq 7.13.

$$t_{mig} = \frac{L_{eff}^2}{V_{eff}\left(\mu + \mu_{EOF}\right)} \tag{7.13}$$

Substituting eq 7.13 into eq 7.12 gives eq 7.14.

$$R = \frac{\left(\mu_1 - \mu_2\right)\sqrt{N_1 N_2}}{2\left(\sqrt{N_1}\left(\mu_1 + \mu_{EOF}\right) + \sqrt{N_2}\left(\mu_2 + \mu_{EOF}\right)\right)} \tag{7.14}$$

Substituting the right hand side of eq 7.10 into eq 7.14 results in eq 7.15.

$$R = \frac{L_{eff}\left(\mu_1 - \mu_2\right)}{2\left(\sigma_{total,2}\left(\mu_1 + \mu_{EOF}\right) + \sigma_{total,1}\left(\mu_2 + \mu_{EOF}\right)\right)} \tag{7.15}$$

Ideally, the only significant contributors to variance in an electrophoretic separation are the injection length, diffusional broadening, and the detection zone length. Thus, the total variance is given by eq 7.16 (note that other variance sources, including analyte-surface interactions and detection electronics, can also exist but are ignored here).

$$\sigma_{total}^2 = \sigma_{inj}^2 + \sigma_{diff}^2 + \sigma_{\det}^2 \tag{7.16}$$

The diffusional variance is given by the Einstein equation in eq 7.17. The injection and detection contributions are similar for rectangular profiles and are given in eqs 7.18 and 7.19. In these three equations, D is the diffusion constant, L_{inj} (m) is the physical length of the injected sample plug, and L_{det} (m) is the physical length of the detection window.[80]

$$\sigma_{diff}^2 = 2Dt_{mig} \tag{7.17}$$

$$\sigma_{inj}^2 = \frac{L_{inj}^2}{12} \tag{7.18}$$

$$\sigma_{\text{det}}^2 = \frac{L_{\text{det}}^2}{12} \tag{7.19}$$

The diffusion constant is related to the mobility through the Nernst-Einstein relationship, allowing eq 7.17 to be rewritten as eq 7.20, where F is the Faraday constant (98485 A s mol^{-1}), R_{gas} is the gas constant (8.314 J K^{-1} mol^{-1}), and T is temperature (K).

$$\sigma_{diff}^2 = \frac{2\mu R_{gas} T t_{mig}}{zF} \tag{7.20}$$

Inserting eqs 7.16, 7.18, 7.19, and 7.20 into eq 7.15 and simplifying gives eq 7.21.

$$R_{sep} = \frac{L_{eff}\left(\mu_1 - \mu_2\right)}{2\left(\sqrt{\frac{2\mu_2 R_{gas} T L_{eff}^2}{V_{eff} z_2 F\left(\mu_2 + \mu_{EOF}\right)} + \frac{L_{inj,2}^2}{12} + \frac{L_{\text{det}}^2}{12}}\left(\mu_1 + \mu_{EOF}\right) + \sqrt{\frac{2\mu_1 R_{gas} T L_{eff}^2}{V_{eff} z_1 F\left(\mu_1 + \mu_{EOF}\right)} + \frac{L_{inj,1}^2}{12} + \frac{L_{\text{det}}^2}{12}}\left(\mu_2 + \mu_{EOF}\right)\right)} \tag{7.21}$$

Eq 7.21 gives the expected resolution for two compounds using the easily measured terms effective length, effective voltage, ionic mobilities, electroosmotic mobility, injection length, detection length, and ionic charge. The equation is somewhat cumbersome; however, with some assumptions, it can be simplified. Assuming that the two separation efficiencies are similar (N_{avg}), the ionic mobility plus electroosmotic mobility quantities are similar ($\mu_{avg}+\mu_{EOF}$), and the injection lengths ($L_{inj,avg}$) are equal (not true for electrokinetically biased injections) results in eq 7.22, which is easier to compute than eq 7.21. Note that the assumption of average separation efficiency is usually accurate when the two species being compared have equivalent charges and similar mobilities. The assumption of equal ionic mobility plus electroosmotic mobility quantities is relatively accurate unless a counter-EOF approach with an EOF magnitude near that of the ionic mobilities is employed.

$$R_{sep} \approx L_{eff} \sqrt{\frac{12V_{eff}\left(\mu_{avg}+\mu_{EOF}\right)}{\frac{24\,\mu_{avg}R_{gas}TL_{eff}^{2}}{z_{avg}F}+V_{eff}\left(\mu_{avg}+\mu_{EOF}\right)\left(L_{inj,avg}^{2}+L_{\det}^{2}\right)}}\frac{\left(\mu_{1}-\mu_{2}\right)}{4\left(\mu_{avg}+\mu_{EOF}\right)} \qquad (7.22)$$

Eq 7.21 was used to calculate the expected resolution between the three pairs of closely migrating cations mentioned above for a range of EOF values. PeakMaster 5.2 was used to calculate the mobilities for these analytes for a chosen BGE of 250-mM acetic acid (commonly used for indirect detection of cations; pH 2.68, I=2.2 mM).[1,81] The resolution between each cation pair and the migration time of the slowest analyte (trimethylamine) are shown in Figure 7.4.

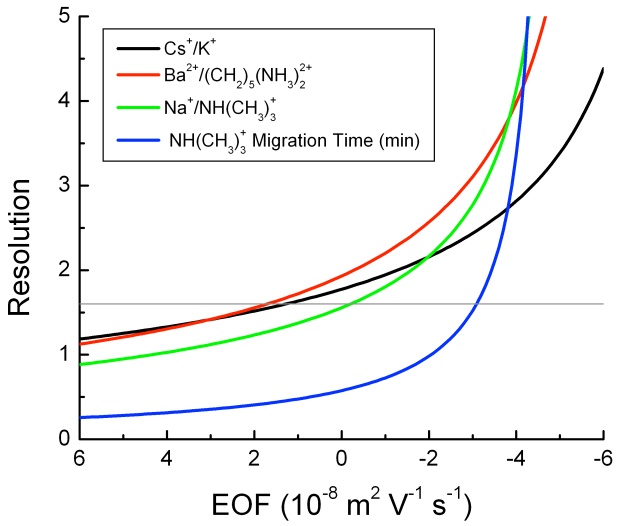

Figure 7.4. Calculated resolution between three closely migrating cation pairs as a function of EOF. The BGE was 250 mM acetic acid. Mobilities were calculated by PeakMaster 5.2 as cesium = 7.8524, potassium = 7.4645, barium = 6.2508, 1,5-diaminopentane = 5.9764, sodium = 5.0450, and trimethylamine = 4.8258 (all units 10^{-8} m^2 V^{-1} s^{-1}).[1] The migration time for the slowest analyte, trimethylamine, is also shown to illustrate the expected increase in analysis time. The gray horizontal line at a resolution of 1.6 represents complete baseline resolution. Calculations were performed using eq 7.21 for L_{eff} = 5 cm, V_{eff} = 1500 V, L_{inj} = 0.5 mm, L_{det} = 0.5 mm, and T = 25 ºC.

At an electroosmotic mobility of $6*10^{-8}$ m^2 V^{-1} s^{-1} (a common value for an unsuppressed EOF on many materials), none of the analyte pairs exhibit baseline resolution. By $2*10^{-8}$ m^2 V^{-1} s^{-1}, a common value for suppressed EOF, both cesium/potassium and barium/1,5-diaminopentane show a resolution above 1.5, nearly baseline resolution. At a slightly reversed EOF of $-3*10^{-9}$ m^2 V^{-1} s^{-1}, all of the species are baseline resolved and show a resolution improvement of 54% (cesium/potassium) to 83% (sodium/trimethylamine), relative to an EOF of $6*10^{-8}$ m^2 V^{-1} s^{-1}. The migration time of the slowest species, trimethylamine, also increases by 88%. However, the injection zone (the only system zone in this BGE) will not be observed, so subsequent injections can be performed immediately after the final analyte has migrated through the detection zone.

As mentioned above, in addition to system zones interfering with analyses, unwanted peaks from ions that are not of interest can also cause additional problems in sequential injection analyses. Prediction of the appearance of these interfering peaks can only be made when there is robust knowledge of the sample composition. In complex matrices like biological samples, this is not always possible. However, some general rules can be applied to minimize interfering peaks by reducing their mobilities so that they are removed by a counter-EOF approach. In effect, the goal is to make the separation as chemically selective possible. One type of analyte system where this is easily accomplished is in the analysis of strong electrolytes. In this case, the majority of interferences can be removed by operating at a pH that will reduce or eliminate the charge on most weak electrolytes of similar polarity. For instance, if inorganic anions are the target analytes, a low pH BGE should be selected because most inorganic anions have

pK_a values below 2. By operating at pH 4 or below, most organic acids will be nearly fully protonated. Using acetic acid as an example, at 10-mM ionic strength and pH 6.0, its mobility is $-3.68*10^{-8}$ m^2 V^{-1} s^{-1}. At pH 4.5, it has reduced in mobility to $-1.47*10^{-8}$ m^2 V^{-1} s^{-1}. At pH 4.0, it has dropped to $-0.63*10^{-8}$ m^2 V^{-1} s^{-1}, and by pH 3.5 its mobility is a very low $-0.22*10^{-8}$ m^2 V^{-1} s^{-1}, slow enough to not interfere in practically any counter-EOF separation (all calculations performed in PeakMaster for a BGE composed of benzoic acid and pyridine).[1] Note that the general approach of slowing down unwanted ions to reverse their net migration is not limited to pH methods. Complexation via small molecule binding or with high-affinity micelles can also be performed. However, whether by complexation or pH, this approach should be undertaken with the knowledge that an incomplete reduction in mobility of the unwanted ions might cause them to appear as very slow and broad peaks migrating at excessively long migration times, potentially interfering with subsequent injections.

Because selective separation chemistry often cannot eliminate all low-mobility interfering compounds, extra selectivity via the injection method is desirable. Additional consideration should be given to the injection method because some approaches require long injection times and/or can interfere with the pseudo steady-state MCE operation during extended monitoring. Three injection methods are common in MCE and will be discussed here. First, there are several variants of hydrodynamic sample introduction.[26-28,33,82,83] These injections ideally yield an unbiased sample plug (identical injection lengths/volumes for all species). This injection mode is excellent for separations with analytes having a wide range of mobilities. Hydrodynamic injections are typically

relatively short, which is a desirable quality for rapid sequential injection systems. However, hydrodynamic injections offer no selectivity gain and can often increase the complexity of the microfluidic instrument. Gated injection offers an alternative that is nominally the fastest of the injection methods (injection times shorter than 1% of the total separation time are common) and is operated with a simple, temporary change of applied potentials.[50] Theoretically, quantitation from separations using gated injection should suffer less from migration time drift (from EOF or pH changes) because while peak areas for most detection methods in CE are proportional to migration time, gated injection volumes are inversely proportional to migration time and the two effects should negate each other.[84] Because an analyte's injected volume is proportional to its apparent mobility, any unwanted, late-migrating peaks will only have a small fraction of the injected volume of early peaks. Thus, gated injection is likely the best option for performing rapid sequential injections in extended monitoring applications. However, the inherent electrokinetic biasing can also be undesirable when relevant analytes cover a large range of migration times. Additionally, gated injection has the drawback of continuously driving sample from the sample reservoir into a waste solution. For spatially static samples, this means that the sample is subjected to the same depletion phenomena that affect the BGE. To illustrate the differences between unbiased and biased injections, Figure 7.5 compares the relative signal when using electrokinetically biased injections and unbiased injections as a function of ionic mobility for monoanions in an example separation. The assumed conditions were a BGE of 30-mM Bis-Tris/15-mM mandelic acid with an EOF of $1.5*10^{-8}$ m^2 V^{-1} s^{-1}.

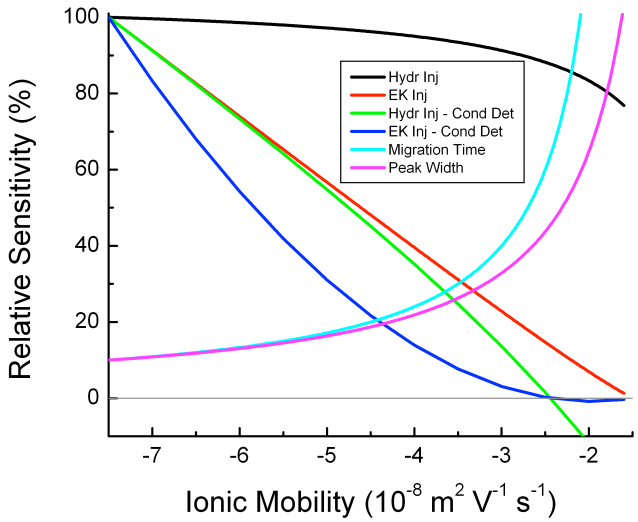

Figure 7.5. Relative sensitivity (peak heights) for two injection and detection modes and relative migration times and peak widths as a function of ionic mobility for a diffusion-limited separation. A BGE of 30-mM Bis-Tris and 15-mM mandelic acid is assumed. EOF for plot is $1.5*10^{-8}$ m^2 V^{-1} s^{-1}. The generic detector results assume constant molar detection sensitivity. Relative conductivity detection sensitivity was obtained from the "conductivity signal" calculated using simulation results from PeakMaster 5.2.[1] Signal was assumed to be proportional to the injection volume and inversely proportional to the physical peak width, which increases with time due to diffusional broadening.

Both the response from a generic detection method (equivalent sensitivity to all analytes) and the response with conductivity detection (which is inherently tied to the analyte mobility) are shown. Also shown are relative migration time and relative peak width. This figure illustrates why selectivity in the injection and/or detection steps is required. Without additional selectivity, an ion with a mobility of $-3*10^{-8}$ m^2 V^{-1} s^{-1} will give a peak that is 91.7% of the height of an equimolar ion with a mobility of $-7*10^{-8}$ m^2 V^{-1} s^{-1} while taking 3.67 times longer to reach the detection zone and exhibiting a peak that is wider by a factor of 3.03. With gated injection biasing, the relative injection volume for the slower ion is reduced by 72.7%, and when combined with conductivity detection biasing, the final peak height for an equimolar sample would be only 3.7% as large as

that for the higher mobility ion. The "background" signal from such a short, broad peak could be subtracted from the baseline if a faster ion from a subsequent peak comigrated with it. Other detection methods, particularly fluorescent and electrochemical detection, can offer increased selectivity over conductivity detection, although their selectivities are structure-dependent instead of mobility-dependent. Consequently, it can be surmised that the often unwanted biasing from gated injection, conductivity detection, or other detection methods can be advantageous if properly utilized when performing a rapid sequential injection analysis.

The third injection mode discussed here is pinched injection.[85] This approach to injection uses electric fields to drive the injection, but it attempts to remove electrokinetic biasing by defining an injection segment with a set length and then operating the injection for a long enough time to ensure that the injection volume is representative of actual sample concentrations. Consequently, under standard operation, the pinched injector is possibly the worst for rapid sequential injections because it has the longest injection process, interferes with the steady-state operation of the MCE separation, and does not provide any selectivity in the injection process. However, theoretically a pinched injection should be able to provide a relatively sharp mobility cutoff (thus, additional selectivity) if the injection time is set to permit only certain analytes to reach the injector, although the authors are unaware of this phenomenon previously being intentionally exploited. Essentially, this approach transforms the system into a pseudo two-dimensional separation system, with the first dimension being the injection process, which acts like a high-pass filter with respect to the velocity of the ions exiting the sample channel.

Assuming the sample matrix is similar to the separation BGE, the injection time can be estimated using eq 7.5, where L_{eff} represents the sample-to-injector distance and E is the electric field during the injection process for the channel connecting the sample reservoir and double-T injector. The potential gain in selectivity using this approach was evaluated theoretically for a microchip possessing a 1-cm injection channel, 0.5-mm injector length (typically defined by a double-T offset), injection field of –500 V cm^{-1}, EOF of $1.5*10^{-8}$ m^2 V^{-1} s^{-1}, and BGE of 15-mM MES and 15-mM histidine. Chloride ($–7.435*10^{-8}$ m^2 V^{-1} s^{-1}) reaches the start of the injector in 3.37 s and fills the injector at 3.54 s. Nitrate (mobility of $–6.995*10^{-8}$ m^2 V^{-1} s^{-1}), however, takes 3.67 s to reach the injector and fills it completely at 3.85 s. Because of diffusional broadening and experimental uncertainties, these two species likely could not be separated by selective injection. However, both analytes should be separable from acetate ($–3.737*10^{-8}$ m^2 V^{-1} s^{-1}), which takes 8.94 s to reach the injector and fills it completely at 9.39 s. Note that these calculations assume no diffusional broadening, which would need to be accounted for in real applications. Nevertheless, the predicted behavior illustrates that this method should be useful for some applications and needs to be further evaluated with real tests. The goal of such a test would be to exclude late-migrating peaks from the separation so that rapid sequential injections could be performed without interference. Presumably, longer injection channels and well-buffered sample solutions will need to be utilized to reproducibly succeed with this approach.

A final way to increase the sequential injection sampling frequency is to employ an injection interval that is shorter than the total separation time and utilizing a method

termed the peak overlap technique.[86] For some separations, the peak overlap technique is impossible because of sample complexity. However, when analyzing relatively simple sample matrices with only a few closely spaced peaks, or with several sets of closely spaced peaks separated with large areas of flat baseline, sampling frequency can be increased considerably by proper injection interval selection. Kuban and coworkers showcased this technique using a traditional CE system in continuous flow mode.[86] Specifically, they analyzed chloride, sulfate, nitrate, and carbonate in tap water using a thiosulfate internal standard. Carbonate migrated near 3.8 min, and the other ions appeared in closely spaced peaks totaling about 15-s wide and centered at a migration time of about 2.6 min. They demonstrated the ability to perform three rapid sequential injections spaced by 20 s that resulted in an electropherogram with three resolved groups of faster ions followed by three slow, broad carbonate peaks. Thus, they were able to obtain three separations in about 4.9 min, whereas a single injection would require about 4.2 min without the peak overlap approach. At steady state, this method allowed three injections to be performed every 2.5 min, for an average sampling rate of 72 h^{-1} even though sampling rate without peak overlap would be about 14 h^{-1}, an improvement of roughly a factor of 5. An illustrative example of the peak overlap technique can be seen in Figure 7.6. The top electropherogram in this figure shows the separation of four anions plus an internal standard compiled by Noblitt et al. specifically for use in online monitoring systems for aerosol composition.[2] The first peak in this separation begins around 26 s and the final peak terminates before 45 s.

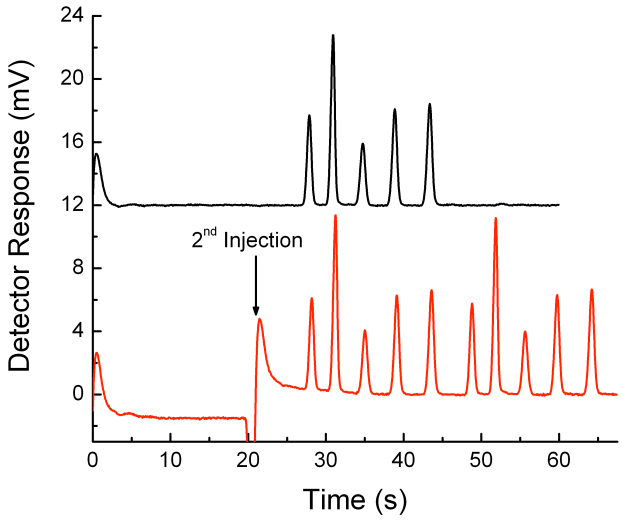

Figure 7.6. Electropherograms showing the advantage of optimizing injection interval timing to maximize sampling frequency where all analytes are detected after the second injection. The top trace shows a single injection. The bottom trace shows two injections with the second injection occurring at 21 s, prior to any of the peaks reaching the detection zone. Peak order is chloride, sulfate, nitrate, oxalate, and 1,3-propanedisulfonate (then repeated). BGE conditions and microchip design are those given by Noblitt et al. except for the following conditions: 5-μM analytes; 1.2-s gated injection; 20-μm platinum detection electrodes, and a 20-Hz effective collection rate.[2] Note that the baseline perturbation and step change occur from capacitive changes during injection when using contact conductivity detection.

Because the window from first peak to last peak is shorter than the window from injection to the first peak, a second injection can be started shortly before the first peak from the first injection reaches the detection zone. This approach is shown in the second electropherogram in Figure 7.6, where an injection scheme with alternating intervals of 21 s and 48 s is utilized. Without the peak overlap technique, a sampling rate of 75 h^{-1} is possible. Utilizing the peak overlap technique permits a throughput of 104 h^{-1}, a 39% improvement. Most sampling applications cannot utilize such ambitious use of the peak overlap technique, particularly when unwanted peaks are present in the separation. The top electropherogram in Figure 7.7 illustrates this by showing the previous separation

with the addition of an undesirable formate peak (which can appear as a gas phase impurity in aerosol sampling).

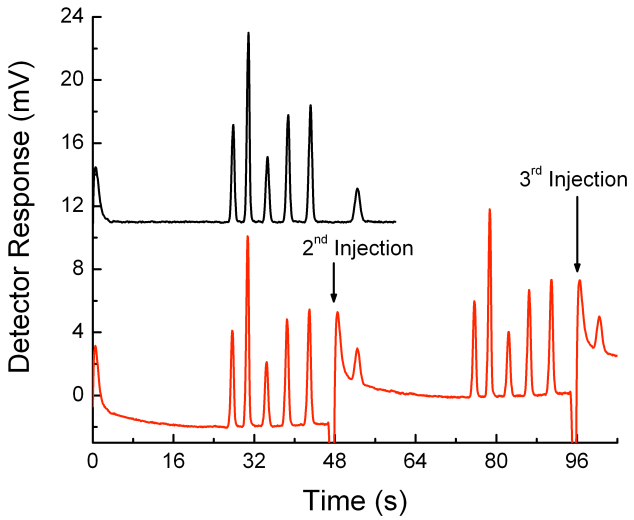

Figure 7.7. Electropherograms showing the advantage of optimizing injection interval timing to maximize sampling frequency where the final peak is detected after the subsequent injection. The top trace shows a single injection. The bottom trace shows three injections using a 48-s injection intervals. All conditions are the same as in Figure 7.6, with the additional sixth peak being formate.

The formate peak prevents the use of the sampling interval used in Figure 7.6, and waiting until the formate peak exits the capillary requires a sampling interval of at least 58 s. However, the original 48-s interval can still be applied here, a sampling frequency increase of 21% over the 58-s interval imposed by the addition of formate. Note that this approach can be used even if formate quantitation is desired, as the integrity of this peak is maintained. Strictly speaking, the examples given in Figures 7.6 and 7.7 are not utilizing the peak overlap technique because the faster ions in the second injection do not overtake the slower ions in the first injection (although such an example is easily possible with this separation, for instance if malate was present in the sample, it migrates at a time of ~85 s and would appear after the faster ions in a second injection). However, the

approach and results are the same as a true peak overlap method, and both Figures 7.6 and 7.7 illustrate the general concept. As a final cautionary note, when applying the peak overlap method one should confirm that quantitation is not significantly affected by either slow, broad peaks from the first injection or the injection procedure itself. Thus, shorter injection methods such as gated injection are preferred over the longer and more perturbing methods like pinched injection. To evaluate the effect of faster ions passing through zones of slower ions, only empirical testing can confirm quantitative accuracy. For proper evaluation, analyte concentrations during the test runs should be similar to those expected in real samples.

To conclude for this section, higher injection sampling frequencies result in higher quality data from either higher temporal resolution or increased precision via averaging. Achieving rapid sequential injections requires proper design of the BGE and robust knowledge of the sample matrix to avoid system zones and minimize undesirable, late-migrating ion peaks. Addition of specific complexing agents or strict pH selection can dramatically reduce the number of late-migrating species in some separations, making the separation highly selective. Proper selection of the EOF through either static or dynamic surface modification is needed to ensure that unwanted peaks migrate away from the detection zone. A weak counter-EOF separation is recommended and has the benefit of increasing resolution between peaks with only a modest increase in migration time. The available injection modes were discussed with respect to their advantages and disadvantages. Gated injection is recommended because of its short injection times and biasing that reduces the peak heights of unwanted, late migrating interferences.

However, gated injection has the drawbacks of continuously depleting the sample solution and also may not be acceptable when working with samples having a large range of migration times because the injection biasing may prevent acceptable sensitivity for slower species. Additional selectivity against slower species can be gained from certain detection methods. Conductivity detection was shown as an example, and its sensitivity towards ions is roughly proportional to the difference between the analyte's mobility and the BGE co-ion's mobility. Finally, the peak overlap technique was exhibited and showed how subsequent injections can be performed prior to all analytes being detected, increasing the injection rate. The combination of two or more of the aforementioned approaches to removing unwanted, late-migrating peaks will likely be needed to achieve desired results, and for more complex samples with a wide range of desired analytes, rapid sequential injections may not be possible and only a long sampling interval will be possible without a hydrodynamic flushing system.

ROBUST QUANTITATION

One of the most frequently cited limitations of CE and MCE is its poor reproducibility in quantitative analysis.[16] This is especially true during extended monitoring because accumulated changes to the BGE composition, alterations of the capillary surface conditions, depletion or matrix changes in the sample, and/or ambient temperature changes can lead to shifts in migration times. Because peak areas are proportional to the migration time for many detection methods in electrophoresis, variance in migration time will lower quantitative reproducibility. Additionally, injection volumes may drift in MCE due to changes in viscosity or fouling of the capillary surface. Several techniques

for improving the quantitative reproducibility of MCE, particularly in the case of extended online monitoring, will be discussed in this section. Much of the discussion will assume a static sample solution, but some of the topics also pertain to sampling from a continuous sample flow.

The most important step in attaining long-term quantitative reproducibility is to ensure that both the BGE and sample solutions are robustly buffered. The reasoning and methods for buffering the BGE were described earlier and will not be rehashed here. Buffering of the sample is critical because the sample composition affects injection quantities for many injection procedures. pH is a typical example of how sample matrix affects quantitation. Eqs 7.1 and 7.2 describe how pH changes an analytes protonation state, and ionic mobility is proportional to the charge of an ion. In electrokinetic injections, the injected volume is proportional to the effective mobility and is therefore very sensitive to pH when operating near the pK_a of an analyte. Thus, as concluded for the BGE pH, sample pH should be kept away from the analytes' pK_a values if possible. Additionally, many samples are not naturally buffered or at a consistent pH, so mixing of the sample with a buffering agent is often required. Another issue with sample composition is the bulk solution conductivity. Differences in the solution conductivity between the sample and BGE can induce stacking or destacking.[87] Although a low conductivity matrix may be tempting to use because of enhanced sensitivity through stacking, its use in extended monitoring applications is risky because any compositional changes induced by the sample will be relatively larger and the sample ions will also deplete more quickly because of the stacking. Instead, a sample matrix closely matching

the BGE or even one that is of a higher concentration than the BGE will yield more reproducible results. In general, the amount of sample buffering is application dependent, and only general knowledge of the sample composition and empirical testing will confirm the validity and reproducibility of a method.

Another important factor in quantitative reproducibility is the stability of the capillary surface chemistry. Clearly, this will affect the EOF, and the effects of EOF on quantitation were already shown in eq 7.7 and Figure 7.3. However, even aside from the EOF effects, surface changes can alter quantitation. The mechanism behind this is a change in the specific interactions occurring between particularly analytes and the capillary surface. One prime example is the adsorption of heavy metal ions onto negatively charged silanol groups on glass, fused silica, and poly(dimethylsiloxane) (PDMS) surfaces. If these interactions are reversible and occur on relatively fast timescales, then any surface changes may result in small shifts in migration times or a change in the amount of tailing present in the electropherogram. If the interactions are irreversible, then the apparent detection sensitivity likely will increase with time as the surface becomes saturated and the number of potential binding sites dwindles. Overall, the best way to avoid quantitation problems caused by slowly changing surface conditions is to try to eliminate all unintentional specific (and even non-specific) interactions between the sample and BGE species and the capillary surface. One easy way to minimize these interactions with small molecules is to modify the capillary surface so that its charge is of the same polarity as the analytes of interest. This approach has the additional benefit of inducing the counter-EOF flow that was recommended

earlier for eliminating extraneous, late-migrating peaks. To stabilize both the surface conditions and EOF, either surfactant dynamic coatings or polymeric static coatings are often sufficient. Effectively, these species out-compete other species for surface interactions and thus yield a more consistent surface status. However, care must be taken when using static coatings, as most static coatings slowing de-adsorb with time. Addition of small amounts of the static coating agent into the BGE can solve this issue. For separations of macromolecules, protecting the surface is more difficult and often requires special procedures or coatings. Much work has gone into protecting capillary surfaces from non-specific macromolecular adsorption, particularly by Lucy's group, and we direct interested readers to those publications.[71-73,77,88-99] One interesting surface-stability problem that has not been explored thoroughly is the contamination of the surface from trace impurities unintentionally present in the BGE. These impurities can bind to the surface and then interact with analyte species during the separation, thus causing nominally non-interacting ions to show wall adsorption behavior. For instance, Gassner et al. showed that trace amounts of iron (III) in the BGE adsorb to the capillary surface and subsequently bind some anions.[100] Potentially, microbial growth caused by not replacing the BGE can also generate BGE contamination that alters surface conditions, sometimes irreversibly. This issue can be difficult to diagnose and often does not appear in early laboratory tests. Problems from trace contaminants aren't limited to the BGE; trace species in the sample can also complex sample ions and interfere with proper injection of those ions. With metal ions, acidic rinses would likely maintain the integrity of the capillary surface with respect to contaminants in the BGE, but this approach will not solve the issue of unwanted complexation in the sample solution and also interferes

with steady-state operation during extended monitoring applications. An alternative to this approach that solves both the capillary surface and sample matrix issues is to utilize a BGE containing a species that competes with the analytes for binding to the contaminant species. The BGE binding species does not have to possess a higher binding constant to the contaminant than do the analytes (though this helps) as long as the BGE species is in sufficient excess to bind all significant amounts of the contaminant. Noblitt et al. utilized this approach for the analysis of anions in an MCE separation specifically designed for extended monitoring.[2] Picolinic acid, a common ligand for heavy metals, not only served as the buffering acid but was also used to bind any metal ions present in the sample or on the capillary surface. Results showed increased oxalate sensitivity when using picolinic acid compared to its non-complexing isomer nicotinic acid, indicating that the picolinic acid was protecting oxalate from slow or irreversible ligand exchanges with surface-bound metal contaminants.

Although the above considerations can help minimize irreproducibility in quantitative measurements, even very small, uncontrollable changes in sample composition, instrument temperature, or surface conditions will cause unacceptably large variance in response. To account for these changes, an internal standard is required. The concentration of an unknown can than be calculated from the peak area ratio relative to the internal standard, as given by eq 7.23 where C (μM) is the solution phase concentration of the analyte (i) and internal standard (IS), 'a' is the peak area, and m_i is the slope of the calibration curve (relative response of the analyte with respect to the internal standard).

$$C_i = \frac{C_{IS}}{m_i}\frac{a_i}{a_{IS}} \tag{7.23}$$

Several excellent studies have shown the importance of using internal standards,[101-104] so only the overall conclusions will be discussed here. The propagated uncertainty in the determined concentration from using eq 7.23 is given by eq 7.24. The impacts of the various parameters in this equation are not immediately apparent and are more easily comprehended when represented as RSD values, as shown in eq 7.25.

$$\sigma_{C_i} = \frac{\sqrt{\sigma_{C_{IS}}^2 a_i^2 + \sigma_{a_i}^2 C_{IS}^2 + \frac{\sigma_m^2 C_{IS}^2 a_i^2}{m_i^2} + \frac{\sigma_{a_{IS}}^2 C_{IS}^2 a_i^2}{a_{IS}^2}}}{m_i a_{IS}} \tag{7.24}$$

$$RSD_{C_i} = \sqrt{RSD_{C_{IS}}^2 + RSD_{a_i}^2 + RSD_{m_i}^2 + RSD_{a_{IS}}^2} \tag{7.25}$$

Note that rigorous sample preparation procedures can reduce the RSD of the internal standard concentration to nearly zero, and although evaporation effects will affect the internal standard concentration, they affect the analyte concentration equally, so this term can often be ignored. Sample depletion does affect the internal standard concentration and therefore the measured concentration of the analyte, but this behavior will be discussed in detail later. Eq 7.25 also shows that reducing the relative uncertainty of the peak integration (thus, reducing uncertainty in 'a') will improve results. The precision in this measurement is dependent upon the integration procedure and the signal-to-noise ratio of the peak. For the analyte peak, the signal-to-noise is dependent upon the concentration of the analyte, of which the user has limited control. However, the uncertainty in the measured sample concentration is also dependent on the reproducibility of the internal standard peak integration. The user does have control over this uncertainty contribution, as larger internal standard peaks give more reproducible integrations

because of the smaller role of the noise in the quantitation. Therefore, we recommend using the highest possible internal standard concentration before significant overloading effects, such as band broadening, fronting or tailing, occur. Often the largest source of irreproducibility is the uncertainty in the slope of the calibration curve, m_i. Although rigorous calibration procedures can give the appearance of high certainty in m_i, differences in the sample matrix or operating conditions between the calibration standards and actual samples can change the relative response. Without an internal standard, injection volume is commonly the largest contributor to measurement uncertainty (by effectively changing m_i), as it can vary with temperature, viscosity, solution conductivity, injection time, and in the presence of unwanted hydrodynamic flow. However, application of an internal standard compensates for nearly all injection volume variance (the primary exception being for biased injections where the biasing factor changes by different amounts for the analyte and standard). Changes in the applied potential or from bulk solution evaporation are also fully corrected with an internal standard. Fluctuations in EOF, matrix composition, capillary surface interactions, hydrodynamic flow, or BGE conditions may not be entirely resolved with internal standard correction. To best account for variance in these aspects of the method, an internal standard that is as similar as possible to the analytes is best. Consequently, one should target an internal standard that is similar to the analytes in pK_a, valence, and mobility. One successful approach for improving reproducibility is to normalize the peak area by dividing it by the migration time.[16,105-109] The theory behind this approach is the cancellation of the dependence of peak area on migration time, so it may be less successful for detection techniques that consume the sample, including mass

spectrometry and some electrochemical methods. Another study found that transforming the x-axis of the electropherogram into the mobility domain resulted in higher qualitative and quantitative precision.[110] Presumably, these improvements were realized because this transformation accounted for some of the changes in peak width that are induced by changes in EOF or hydrodynamic flow. This conclusion further supports the recommendation of a low magnitude EOF. With a decreased EOF, there is lower uncertainty in migration time and also a reduced chance for the intrusion of unwanted hydrodynamic flow induced by fluid head heights or Laplace pressures. Additionally, some studies have shown that utilizing multiple internal standards is necessary to achieve acceptable reproducibility levels, particularly when using electrokinetic injection protocols.[111,112] However, these studies were performed using traditional CE instrumentation, which incorporates the physical movement of either the capillary or the buffer vials, a process that decreases reproducibility. From the authors' experience, MCE gated and pinched injections do not suffer from this additional physical step and therefore acceptable reprodubilities can be obtained with one internal standard except for the most rigorous applications. Finally, it should be realized that changes in some specific molecular interactions such as adsorption to capillary surfaces and complexation reactions could occur to certain analytes and not affect the internal standard. Consequently, those changes will affect the value of m_i and thus analyte quantitation while not altering the observed peak from the standard. The end user should be cognizant of these possibilities and take proper precautions to protect the surface and ensure a stable concentration of complexation agent in both the sample and BGE.

As alluded to earlier, one quantitation issue that is mostly limited to extended monitoring studies from static solutions and therefore has been mostly ignored in the literature is the phenomenon of sample ion depletion. The general mechanisms behind sample depletion are the same as those of buffer depletion, described in detail earlier. However, sample depletion directly affects the concentrations of specific ions in the sample solution, and the resulting quantified peaks will be representative of the depleted concentrations instead of the original ones. Although an internal standard will also undergo depletion, each species depletes at a unique rate and therefore internal standard correction is only approximate. Consequently, the apparent relative response factor shown in eq 7.23 will systematically deviate with time, although the physical mechanism is unwanted changes in both internal standard and analyte concentrations and not a change in the actual detection. This phenomenon is unavoidable when using static solutions. For injection methods utilizing transient sample consumption, such as pinched injection, the effect is typically negligible. For injection techniques that continually deplete the sample, including gated injection and some types of hydrodynamic injection, sample depletion is a major issue. Therefore, the user should be aware of the effect, take measures to minimize it, and calculate the longest acceptable operating time from a single sample solution. This calculation was performed by Noblitt et al. for an extended online monitoring system exhibiting both sample depletion and accumulation,[59] and the derivation for depletion only is given here. The velocity of an ion leaving a static solution is calculated using eq 7.26.

$$v = E\left(\mu_i + \mu_{EOF}\right) \tag{7.26}$$

The change in moles of analyte 'i' in the sample reservoir with time (dn_i/dt) equals that exiting velocity multiplied by the channel cross sectional area and the analyte concentration (C, mol L^{-1}), as given in eq 7.27. Note that the value of C in this equation is the concentration actually exiting the reservoir and therefore in systems exhibiting stacking or destacking will not be equal to the bulk solution concentration.

$$\frac{dn_i}{dt} = -1000 v_i A C_i \tag{7.27}$$

The change in concentration is inversely proportional to sample volume, which also changes with time. The volume change depends on the EOF. Ignoring any changes due to evaporation, condensation, or density alteration, the volume only depends on the volumetric flow rate of the EOF, which is given by eq 7.8. Combining eqs 7.8, 7.26, and 7.27 results in eq 7.28, which is the change in concentration of a sample species due to depletion with respect to time, where V_o is the sample volume at t=0. It should be realized that the electric field in this eq 7.is that for the channel connected to the sample reservoir and is often not equal to the separation field.

$$\frac{dC_i}{dt} = \frac{-EAC_i\left(\mu_i + \mu_{EOF}\right)}{V_o - EA\mu_{EOF}t} \tag{7.28}$$

This equation is only approximate in real applications, as any changes to the BGE or sample composition will affect the stacking factor, electric field, and/or mobilities. However, in the absence of significant stacking effects and in the presence of a relatively simple sample matrix, eq 7.28 should be sufficient for quantitative depletion estimates. Note that the fractional change in concentration is directly proportional to the electric field, channel cross-section, and effective mobility. It is inversely proportional to sample volume. Because the sample ions and internal standard all possess different effective

mobilities, they will deplete at different rates. Consequently, eq 7.23 only yields the correct result at t=0 and after that will show systematic deviations for all ions having a mobility different from the internal standard. To illustrate this quantitatively, Figure 7.8 shows the determined concentration using eq 7.23 for a theoretical depletion scenario at a variety of ionic mobilities and an internal standard mobility of $5.0*10^{-8}$ m^2 V^{-1} s^{-1}.

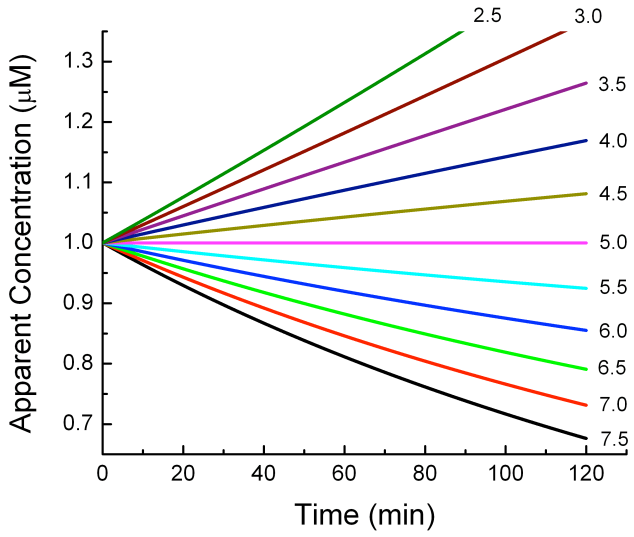

Figure 7.8. Effect of sample depletion on the quantitation of a static solution. The apparent concentration as calculated using eq 7.23 is shown assuming an internal standard mobility of $5.0*10^{-8}$ m^2 V^{-1} s^{-1}. Each trace represents an ion with the labeled mobility (in 10^{-8} m^2 V^{-1} s^{-1}). Simulation conditions: initial concentration = 1 μM, initial volume = 30 μL, channel cross-section = $2.5*10^{-9}$ m^2, separation field = 300 V cm^{-1}, EOF = $-1.75*10^{-8}$ m^2 V^{-1} s^{-1}. Equations were solved using a first-order iterative approximation (Euler's Method) with a step size of 2 s.

As expected, ions faster than the internal standard deplete more rapidly and show negative systematic deviations, whereas the slower ions show positive deviations. Specifically, after one hour an ion with a mobility of $7*10^{-8}$ m^2 V^{-1} s^{-1} would have depleted by 35.5% but be measured as 15.4% lower than the starting concentration using the internal standard. Conversely, an ion with a mobility of $3*10^{-8}$ m^2 V^{-1} s^{-1} would have decreased in concentration by 9.9%, but according to the internal standard the

concentration would have increased by 18.2%. For an ion with the same mobility as the internal standard, no deviations are observed, clearly illustrating one benefit of choosing a standard species that is similar to the analytes in mobility. While the simulation in Figure 7.8 is instructive, its practical applicability is low because no compositional changes are occurring other than those from electrophoretic depletion. In reality, static sample solutions can be used to monitor reaction rates or collected samples when the sample collection process has a negligible impact on the total solution volume. To achieve high time resolution in these applications, quantitation via a differential method (differences in point-to-point concentration measurements) is needed. The effect of sample depletion on differential quantitation is somewhat different than on a solution of otherwise constant sample concentrations, and simulation results for a differential method are shown in Figure 7.9. For this simulation, eq 7.28 was used but with the addition of an accumulation term equal to 100 fmol s^{-1} in the numerator. With this approach, deviations are systematically more positive than shown in Figure 7.8. This result is due to the analytes starting at a concentration of 0, whereas the standard began at a concentration of 1 μM (arbitrary and has no effect on the results unless internal standard accumulates also). Consequently, the standard begins with a high depletion rate, while the effect of the early depletion on the analyte concentrations is negligible. This is most apparent when considering an analyte with the same mobility as the internal standard ($5*10^{-8}$ m^2 V^{-1} s^{-1}). With finite starting concentrations and no accumulation, an ion with this mobility exhibits no systematic quantitative deviations. However, with zero initial concentration and constant accumulation, the differential measurement yields results that are 6.7%, 13.4%, and 19.4% high at analysis times of 30, 60, and 90 min, respectively.

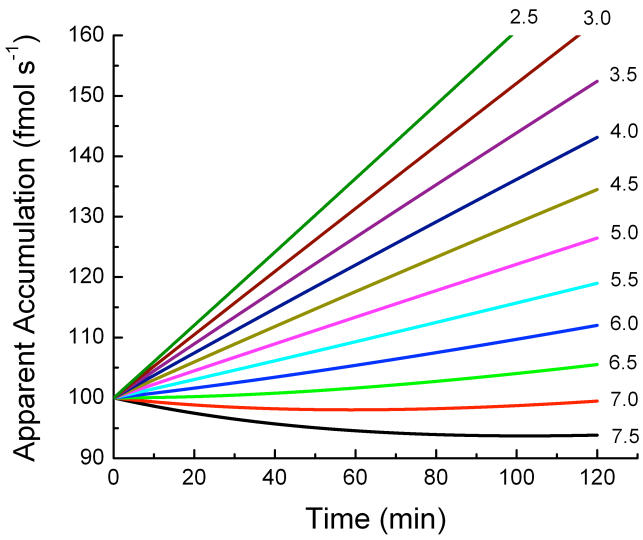

Figure 7.9. Effect of sample depletion on quantitation of a static solution accumulating sample ions when quantitation is performed using a differential method. Actual accumulation rate for sample ions = 100 fmol s^{-1}. Initial sample concentrations = 0. An internal standard mobility of $5.0*10^{-8}$ m^2 V^{-1} s^{-1} and initial concentration of 1 μM are used. Each trace represents the labeled mobility (in 10^{-8} m^2 V^{-1} s^{-1}). All simulation conditions are the same as in Figure 7.8.

The difference in this case is the initial concentration of the analytes versus the internal standard. The internal standard starts at a set concentration, depletes at its highest rate initially, and does not accumulate any new material during the analysis. Slower ions show even higher positive deviations than ions with the same mobility as the standard. Faster ions exhibit less positive deviations, and the fastest ions even exhibit negative deviations early in the analysis. With increasing analysis time, however, even the fastest ions will eventually begin to show positive deviations. This phenomenon is due to all sample ions approaching a steady state concentration where accumulation rate equals depletion rate. The internal standard, however, does not have an accumulation source and therefore all ions will eventually show an increasing concentration relative to the internal standard when undergoing constant accumulation. The most prominent

conclusion from Figure 7.9 is that the traditional rule-of-thumb of choosing a standard with a mobility as close as possible to the analytes is not necessarily valid when performing extended analyses with a differential quantitation method. Instead, an internal standard that is slower than the analytes is desirable, and calculating the actual depletion results similarly to what is done in Figure 7.9 is recommended. However, the best way to limit effects of sample depletion in injection methods that continually deplete the sample is to take the same measures used to limit buffer depletion. Larger sample volumes, smaller sample channels, and lower electric fields all reduce sample depletion. This approach requires a compromise, as MCE is often praised for its small sample volumes and short analysis times. However, for most systems that continuously deplete the sample during operation, the electric field in the sample channel can be decreased without sacrificing the electric field strength in the separation channel, and it is the separation field that determines the analysis time and separation efficiency.

Overall, achieving robust quantitation in MCE is difficult even without the additional complication of extended online operation. Stability of the BGE composition and surface chemistry are required to avoid analyte-specific effects that cannot be accounted for with an internal standard as well as changes to the injection volume or EOF that can only be partially accounted for using an internal standard. Employing an internal standard greatly increases the robustness of quantitation. For best results with an internal standard, the chosen standard should be similar to the analytes in pK_a, valence, and mobility. The internal standard concentration should be the highest concentration that does not result in a significantly overloaded (broad or triangular-shaped) peak because larger peaks give

more reproducible integration values. A problem that is specific to long term monitoring from a static sample solution is the issue of sample depletion. This phenomenon can be minimized using the same approach as that used to reduce buffer depletion. When accumulating sample ions into a static solution, a differential analysis method is often employed, and sample depletion results in some unique systematic deviations when using internal standards. The majority of ions show positive systematic deviations with increasing analysis time, and only ions considerably faster than the internal standard show negative deviations. Even these ions will eventually show positive deviations as the sample solution approaches a steady-state concentration of analyte while the internal standard concentration continues to diminish. When attempting a differential analysis, it is therefore recommended that the chosen internal standard be slower than the analytes.

CONCLUSIONS

Extended monitoring applications requiring high time resolution represent an enticing field that may be addressable by MCE because the instrumentation has short analysis times with a small physical footprint and high portability. However, MCE is notorious for its inability to maintain robust performance for extended monitoring times. This shortcoming is due to a variety of issues, particularly small BGE volumes, high electric fields, susceptibility to hydrodynamic flow interference, and unstable capillary surface conditions. Although most MCE analyses appear to be very rapid, many are often plagued by late-migrating system zones or unimportant sample ion peaks, limiting the method's ability to perform subsequent analyses at a high sampling frequency. This chapter discussed how to lengthen the longevity of the BGE integrity, improve the

robustness of the sample quantitation, and increase the sampling frequency by avoiding system zones and late-migrating interfering peaks. Each of these issues can be reduced or even eliminated with proper design of the MCE instrumentation and the separation BGE. To increase operation time, larger solution volumes, smaller capillary cross-sections, and a high buffer capacity to background conductivity ratio are important. The recommended BGE components are a low-mobility weak acid and base pair with the acid having its pK_a above the operating pH and the base having a pK_a below it. Other factors, including evaporation and component reactivity, also need to be minimized or eliminated. BGE longevity depends on a variety of factors, including the specific buffer and sample components and desired tolerance to fluctuations in migration time and quantitation. Therefore, we recommend empirically evaluating the final separation conditions and then scaling as appropriate using the proportionality given in eq 7.9. Additionally, the EOF should be suppressed to avoid any degrading effects caused by large discrepancies in reservoir head heights or meniscus pressures. These same BGE conditions naturally lead to separations with a minimal number of system zones, as the system zones will migrate with or near the injection zone. To remove this system zone entirely, a weak counter-EOF flow is suggested. Counter-EOF separations typically require longer migration times and result in broader peaks, but higher resolution between species is observed. Additionally, unwanted late-migrating sample ion peaks can be minimized by appropriate choice of operating pH, which will lead to many weak electrolytes migrating near the EOF, so they will also never be detected. Employing high-affinity surfactant micelles or selective small molecule binding agents to complex unwanted species is another method for removing unwanted peaks. To further increase selectivity against late-migrating

species, biased injection and detection methods can be utilized. Knowledge of the sample matrix is helpful, as it permits the development of these highly selective separations and allows determination of the applicability of the peak overlap technique. To achieve maximum quantitative reproducibility, it is essential to utilize an internal standard to account for changes in applied field, injection volume, and EOF. Typically, the chosen standard should be similar to the analytes in mobility, valence, and pK_a. When sampling static solutions in extended monitoring applications, sample ion depletion is an important issue. Sample depletion can be reduced using the same approaches used to minimize buffer depletion. However, sample depletion always occurs in finite amounts and results in systematic deviations in quantitation. An internal standard only partly accounts for this, and when a differential analysis method is used, the internal standard should be a slower ion than the analytes of interest. For a more complete prediction of the effects of depletion, we recommend solving eq 7.28 (including any necessary accumulation terms) and processing the results with eq 7.23 to evaluate the systematic deviations in quantitation induced by sample depletion.

It should be noted that every extended monitoring application is unique and the direction of the development depends heavily on the analytes of interest, the detection method, and the sample composition and conductivity. Thus, we recommend against employing traditional BGEs and microchip designs simply because they have been shown to work in short-term analyses. Typically, these systems will have little or no optimization for long-term monitoring. Often, only a few of the suggestions given in this chapter will be appropriate in a given system. In particular, complex sample matrices present severe

issues with capillary surface stability, achieving rapid sequential injections, and employing the peak overlap technique. For difficult matrices, reproducible, steady state operation with rapid sequential injections may be practically impossible. For these systems, it may be better to employ multiple microchips that alternate sampling duties while the other chips undergo hydrodynamic flushes and/or surface treatment. Overall, the area of extended monitoring with MCE is still in its infancy, and the authors expect the number of successful applications in this field to increase. As experience in this field increases, new solutions to some of the hurdles specific to MCE extended monitoring will likely not only be realized, but also addressed.

REFERENCES

1. Jaros, M.; Hruska, V.; Stedry, M.; Zuskova, I.; Gas, B., *Electrophoresis* **2004,** *25*, 3080-3085.
2. Noblitt, S. D.; Schwandner, F. M.; Hering, S. V.; Collett, J. L.; Henry, C. S., *J. Chromatogr. A* **2009,** *1216*, 1503-1510.
3. Jorgenson, J. W.; Lukacs, K. D., *Anal. Chem.* **1981,** *53*, 1298-1302.
4. Jorgenson, J. W.; Lukacs, K. D., *Science* **1983,** *222*, 266-272.
5. Mikkers, F. E. P.; Everaerts, F. M.; Verheggen, T., *J. Chromatogr.* **1979,** *169*, 11-20.
6. Chen, X. G.; Fan, L. Y.; Hu, Z., *Electrophoresis* **2004,** *25*, 3962-3969.
7. Fang, Z. L., *Anal. Chim. Acta* **1999,** *400*, 233-247.
8. Fang, Z. L.; Chen, H. W.; Fang, Q.; Pu, Q. S., *Analyt. Sci.* **2000,** *16*, 197-203.
9. Kuban, P.; Karlberg, B., *TrAC-Trend. Anal. Chem.* **1998,** *17*, 34-41.
10. Kuban, P.; Karlberg, B., *Anal. Chim. Acta* **2009,** *648*, 129-145.
11. Santos, B.; Simonet, B. M.; Rios, A.; Valcarcel, M., *TrAC-Trend. Anal. Chem.* **2006,** *25*, 968-976.
12. Macka, M.; Andersson, P.; Haddad, P. R., *Anal. Chem.* **1998,** *70*, 743-749.
13. Desiderio, C.; Fanali, S.; Bocek, P., *Electrophoresis* **1999,** *20*, 525-528.
14. de Jesus, D. P.; Brito-Neto, J. G. A.; Richter, E. M.; Angnes, L.; Gutz, I. G. R.; do Lago, C. L., *Anal. Chem.* **2005,** *77*, 607-614.
15. Mayer, B. X.; Muller, M., *LC GC N. Am.* **2000,** *18*, 694-+.
16. Mayer, B. X., *J. Chromatogr. A* **2001,** *907*, 21-37.
17. Willauer, H. D.; Collins, G. E., *Electrophoresis* **2003,** *24*, 2193-2207.
18. Dolnik, V.; Liu, S. R.; Jovanovich, S., *Electrophoresis* **2000,** *21*, 41-54.
19. Lacher, N. A.; Garrison, K. E.; Martin, R. S.; Lunte, S. M., *Electrophoresis* **2001,** *22*, 2526-2536.
20. Manz, A.; Graber, N.; Widmer, H. M., *Sensor. Actuat. B-Chem.* **1990,** *1*, 244-248.
21. Li, S. F. Y.; Kricka, L. J., *Clin. Chem.* **2006,** *52*, 37-45.
22. Dolnik, V.; Liu, S. R., *J. Sep. Sci.* **2005,** *28*, 1994-2009.
23. Felhofer, J. L.; Blanes, L.; Garcia, C. D., *Electrophoresis* **2010,** *31*, 2469-2486.
24. Faure, K.; Pravda, M.; Glennon, J. D., *Anal. Lett.* **2006,** *39*, 435-449.
25. Revermann, T.; Gotz, S.; Kunnemeyer, J.; Karst, U., *Analyst* **2008,** *133*, 167-174.
26. Attiya, S.; Jemere, A. B.; Tang, T.; Fitzpatrick, G.; Seiler, K.; Chiem, N.; Harrison, D. J., *Electrophoresis* **2001,** *22*, 318-327.
27. Buttgenbach, S.; Wilke, R., *Anal. Bioanal. Chem.* **2005,** *383*, 733-737.
28. Chen, S. H.; Lin, Y. H.; Wang, L. Y.; Lin, C. C.; Lee, G. B., *Anal. Chem.* **2002,** *74*, 5146-5153.
29. Fang, Q.; Xu, G. M.; Fang, Z. L., *Anal. Chem.* **2002,** *74*, 1223-1231.
30. Fang, Z. L.; Fang, Q., *Fresenius J. Anal. Chem.* **2001,** *370*, 978-983.
31. Li, M. W.; Huynh, B. H.; Hulvey, M. K.; Lunte, S. M.; Martin, R. S., *Anal. Chem.* **2006,** *78*, 1042-1051.
32. Lin, Y. H.; Lee, G. B.; Li, C. W.; Huang, G. R.; Chen, S. H., *J. Chromatogr. A* **2001,** *937*, 115-125.
33. Mecker, L. C.; Martin, R. S., *Anal. Chem.* **2008,** *80*, 9257-9264.
34. Reschke, B. R.; Schiffbauer, J.; Edwards, B. F.; Timperman, A. T., *Analyst* **2010,** *135*, 1351-1359.

35. Wang, M.; Roman, G. T.; Perry, M. L.; Kennedy, R. T., *Anal. Chem.* **2009,** *81*, 9072-9078.
36. Oki, A.; Takamura, Y.; Ito, Y.; Horiike, Y., *Electrophoresis* **2002,** *23*, 2860-2864.
37. Roper, M. G.; Shackman, J. G.; Dahlgren, G. M.; Kennedy, R. T., *Anal. Chem.* **2003,** *75*, 4711-4717.
38. Shackman, J. G.; Dahlgren, G. M.; Peters, J. L.; Kennedy, R. T., *Lab Chip* **2005,** *5*, 56-63.
39. Reid, K. R.; Kennedy, R. T., *Anal. Chem.* **2009,** *81*, 6837-6842.
40. Beckers, J. L.; Bocek, P., *Electrophoresis* **2003,** *24*, 518-535.
41. Persat, A.; Chambers, R. D.; Santiago, J. G., *Lab Chip* **2009,** *9*, 2437-2453.
42. Persat, A.; Suss, M. E.; Santiago, J. G., *Lab Chip* **2009,** *9*, 2454-2469.
43. Kelly, M. A.; Altria, K. D.; Clark, B. J., *J. Chromatogr. A* **1997,** *768*, 73-80.
44. Li, D. M.; Fu, S. L.; Lucy, C. A., *Anal. Chem.* **1999,** *71*, 687-699.
45. Pitts, E., *P. Roy. Soc. Lond. A Mat.* **1953,** *217*, 43-70.
46. Bello, M. S., *J. Chromatogr. A* **1996,** *744*, 81-91.
47. Hows, M. E. P.; Perrett, D., *Chromatographia* **1998,** *48*, 355-359.
48. Stoyanov, A. V.; Pawliszyn, J., *Analyst* **2004,** *129*, 979-982.
49. Crabtree, H. J.; Cheong, E. C. S.; Tilroe, D. A.; Backhouse, C. J., *Anal. Chem.* **2001,** *73*, 4079-4086.
50. Jacobson, S. C.; Koutny, L. B.; Hergenroder, R.; Moore, A. W.; Ramsey, J. M., *Anal. Chem.* **1994,** *66*, 3472-3476.
51. Ermakov, S. V.; Jacobson, S. C.; Ramsey, J. M., *Anal. Chem.* **2000,** *72*, 3512-3517.
52. Zhang, G. S.; Du, W.; Liu, B. F.; Hisamoto, H.; Terabe, S., *Anal. Chim. Acta* **2007,** *584*, 129-135.
53. Jacobson, S. C.; Ermakov, S. V.; Ramsey, J. M., *Anal. Chem.* **1999,** *71*, 3273-3276.
54. Reijenga, J. C.; Verheggen, T.; Martens, J.; Everaerts, F. M., *J. Chromatogr. A* **1996,** *744*, 147-153.
55. Beckers, J. L.; Gebauer, P.; Bocek, P., *J. Chromatogr. A* **2001,** *916*, 41-49.
56. Beckers, J. L.; Bocek, P., *Electrophoresis* **2002,** *23*, 1942-1946.
57. Yan, D. G.; Yang, C.; Huang, X. Y., *Microfluid. Nanofluid.* **2007,** *3*, 333-340.
58. Reijenga, J. C.; Gagliardi, L. G.; Kenndler, E., *J. Chromatogr. A* **2007,** *1155*, 142-145.
59. Noblitt, S. D.; Lewis, G. S.; Liu, Y.; Hering, S. V.; Collett, J. L.; Henry, C. S., *Anal. Chem.* **2009,** *81*, 10029-10037.
60. Gas, B.; Kenndler, E., *Electrophoresis* **2004,** *25*, 3901-3912.
61. Hruska, V.; Stedry, M.; Vcelakova, K.; Lokajova, J.; Tesarova, E.; Jaros, M.; Gas, B., *Electrophoresis* **2006,** *27*, 4610-4617.
62. Beckers, J. L., *J. Chromatogr. A* **1994,** *662*, 153-166.
63. Beckers, J. L.; Everaerts, F. M., *J. Chromatogr. A* **1997,** *787*, 235-242.
64. Beckers, J. L.; Bocek, P., *Electrophoresis* **2005,** *26*, 446-452.
65. Beckers, J. L.; Gebauer, P.; Bocek, P., *Electrophoresis* **2001,** *22*, 3648-3658.
66. Beckers, J. L.; Urbanek, M.; Bocek, P., *Electrophoresis* **2005,** *26*, 1869-1873.
67. Gebauer, P.; Beckers, J. L.; Bocek, P., *Electrophoresis* **2002,** *23*, 1779-1785.
68. Poppe, H., *J. Chromatogr. A* **1999,** *831*, 105-121.

69. Sellmeyer, H.; Poppe, H., *J. Chromatogr. A* **2002,** *960*, 175-185.
70. Hruska, V.; Jaros, M.; Gas, B., *Electrophoresis* **2006,** *27*, 984-991.
71. Dolnik, V., *Electrophoresis* **2004,** *25*, 3589-3601.
72. Horvath, J.; Dolnik, V., *Electrophoresis* **2001,** *22*, 644-655.
73. Lucy, C. A.; MacDonald, A. M.; Gulcev, M. D., *J. Chromatogr. A* **2008,** *1184*, 81-105.
74. Zhou, J. W.; Ellis, A. V.; Voelcker, N. H., *Electrophoresis* **2010,** *31*, 2-16.
75. Znaleziona, J.; Petr, J.; Knob, R.; Maier, V.; Sevcik, J., *Chromatographia* **2008,** *67*, S5-S12.
76. Melanson, J. E.; Baryla, N. E.; Lucy, C. A., *TrAC-Trend. Anal. Chem.* **2001,** *20*, 365-374.
77. Liu, J. K.; Lee, M. L., *Electrophoresis* **2006,** *27*, 3533-3546.
78. Lucy, C. A.; McDonald, T. L., *Anal. Chem.* **1995,** *67*, 1074-1078.
79. Lucy, C. A.; Yeung, K. K. C.; Fu, S. L.; Li, D. M.; Henselwood, T. L.; Underhill, R. S., *Can. J. Chem.* **1999,** *77*, 281-290.
80. Jones, H. K.; Nguyen, N. T.; Smith, R. D., *J. Chromatogr.* **1990,** *504*, 1-19.
81. Gong, X. Y.; Hauser, P. C., *Electrophoresis* **2006,** *27*, 468-473.
82. Backofen, U.; Matysik, F. M.; Lunte, C. E., *Anal. Chem.* **2002,** *74*, 4054-4059.
83. Price, A. K.; Culbertson, C. T., *Anal. Chem.* **2009,** *81*, 8942-8948.
84. vanderMoolen, J. N.; Boelens, H. F. M.; Poppe, H.; Smit, H. C., *J. Chromatogr. A* **1996,** *744*, 103-113.
85. Jacobson, S. C.; Hergenroder, R.; Koutny, L. B.; Warmack, R. J.; Ramsey, J. M., *Anal. Chem.* **1994,** *66*, 1107-1113.
86. Kuban, P.; Engstrom, A.; Olsson, J. C.; Thorsen, G.; Tryzell, R.; Karlberg, B., *Anal. Chim. Acta* **1997,** *337*, 117-124.
87. Beckers, J. L.; Bocek, P., *Electrophoresis* **2000,** *21*, 2747-2767.
88. Badal, M. Y.; Wong, M.; Chiem, N.; Salimi-Moosavi, H.; Harrison, D. J., *J. Chromatogr. A* **2002,** *947*, 277-286.
89. Baryla, N. E.; Lucy, C. A., *Anal. Chem.* **2000,** *72*, 2280-2284.
90. Cunliffe, J. M.; Baryla, N. E.; Lucy, C. A., *Anal. Chem.* **2002,** *74*, 776-783.
91. Huang, B.; Kim, S.; Wu, H.; Zare, R. N., *Anal. Chem.* **2007,** *79*, 9145-9149.
92. Kamande, M. W.; Fletcher, K. A.; Lowry, M.; Warner, I. M., *J. Sep. Sci.* **2005,** *28*, 710-718.
93. Liu, Q.; Li, Y. Q.; Tang, F.; Ding, L.; Yao, S. Z., *Electrophoresis* **2007,** *28*, 2275-2282.
94. Liu, Q.; Yang, Y. M.; Yao, S. Z., *J. Chromatogr. A* **2008,** *1187*, 260-266.
95. Luo, Y. Q.; Huang, B.; Wu, H.; Zare, R. N., *Anal. Chem.* **2006,** *78*, 4588-4592.
96. Melanson, J. E.; Baryla, N. E.; Lucy, C. A., *Anal. Chem.* **2000,** *72*, 4110-4114.
97. Wang, C. Z.; Lucy, C. A., *Electrophoresis* **2004,** *25*, 825-832.
98. Xiao, Y.; Yu, X. D.; Xu, J. J.; Chen, H. Y., *Electrophoresis* **2007,** *28*, 3302-3307.
99. Yeung, K. K. C.; Lucy, C. A., *Anal. Chem.* **1997,** *69*, 3435-3441.
100. Gassner, B.; Friedl, W.; Kenndler, E., *J. Chromatogr. A* **1994,** *680*, 25-31.
101. Altria, K. D., *Lc Gc Europe* **2002,** *15*, 588-594.
102. Haber, C.; VanSaun, R. J.; Jones, W. R., *Anal. Chem.* **1998,** *70*, 2261-2267.
103. Leube, J.; Roeckel, O., *Anal. Chem.* **1994,** *66*, 1090-1096.
104. Altria, K. D.; Fabre, H., *Chromatographia* **1995,** *40*, 313-320.

105. Nielen, M. W. F., *J. Chromatogr*. **1991,** *588*, 321-326.
106. Altria, K. D., *Chromatographia* **1993,** *35*, 177-182.
107. Hjerten, S.; Elenbring, K.; Kilar, F.; Liao, J. L.; Chen, A. J. C.; Siebert, C. J.; Zhu, M. D., *J. Chromatogr*. **1987,** *403*, 47-61.
108. Huang, X. H.; Coleman, W. F.; Zare, R. N., *J. Chromatogr*. **1989,** *480*, 95-110.
109. Watzig, H.; Dette, C., *J. Chromatogr*. **1993,** *636*, 31-38.
110. Schmitt-Kopplin, P.; Garmash, A. V.; Kudryavtsev, A. V.; Menzinger, F.; Perminova, I. V.; Hertkorn, N.; Freitag, D.; Petrosyan, V. S.; Kettrup, A., *Electrophoresis* **2001,** *22*, 77-87.
111. Dose, E. V.; Guiochon, G. A., *Anal. Chem*. **1991,** *63*, 1154-1158.
112. Dang, Q. X.; Yan, L. X.; Sun, Z. P.; Ling, D. K., *J. Chromatogr*. **1993,** *630*, 363-369.

CHAPTER 8. RECENT IMPROVEMENTS TO THE DEVELOPED MICROCHIP ELECTROPHORESIS (MCE) SYSTEM AND ITS EXTENSION INTO OTHER AREAS OF RESEARCH

CHAPTER FOREWORD

This section discusses some of the improvements to the instrumentation and methods discussed in chapters 2-7 since their publication and other work that was developed concurrently with the original research but was not published. The results shown here are preliminary and may ultimately be published in collaboration with other members of the Henry group. Much of the focus has centered on developing the Aersosol Chip Electrophoresis (ACE) system to improve the compatibility of the interface while also improving the growth tube collection efficiency. The new online collection interface has extended the range of possible aerosol collectors, and testing of a miniature cloud condensation nuclei collector (CCN) with the ACE interface has begun. Additional MCE improvements include the use of larger reservoirs and smaller capillaries to extend the operational lifetime of the device between background electrolyte (BGE) replacements. Several conductivity detection electrode materials have been tested with the goal of improved robustness of the MCE systems, and new conductivity detectors have also been evaluated. A new online aerosol interface that works by interfacing with a continuous liquid flow stream has been considered. Improvements to the separation chemistry and microchip design have increased the resolving power of the MCE devices.

AEROSOL COLLECTION SYSTEM IMPROVEMENTS

The prototype ACE system was described in chapter 7. One limitation of the ACE system was the requirement of maintaining the growth tube outlet at or below room temperature. This enforced a strict boundary on the growth tube temperature differential, limiting its collection efficiency and flow rate. With this configuration, the microchip was exposed to the surrounding environment, making it susceptible to changes in ambient temperature and also forcing the use of an isobaric air duct network, complicating the chip design. To remedy these issues, a new interface has been developed between the growth tube and the microchip. The new method encloses the entire microchip into a sealed, temperature controlled metal box. Advantages include operation at a higher outlet temperature to improve growth tube collection efficiency, temperature control of the microchip to improve migration time and quantitation reproducibilities, and the removal of the isobaric air duct network and airtight lids, which simplifies the microchip design. The box enclosure did introduce several new problems. The first of these is operation of the microchip in a high humidity environment. To prevent rapid evaporation of the sample solution, the box environment must be set to a temperature similar to the outlet of the growth tube (less than 1 °C higher). The moisture content in the box increases the likelihood of electrical shorting between high-voltage components. Additionally, condensation in the box is a possibility and can cause arcing with the high voltage, damaging the microchip and possibly the growth tube. To circumvent these issues, precise temperature control of the box at 0.5-1.0 °C above the growth tube outlet is utilized. To maximize the thermal conductivity of the box, the box was constructed from aluminum (anodized). However, the electrical conductivity of the box enclosure greatly

increased the baseline noise in MCE with conductivity detection unless the box was grounded. Grounding the box did not fix another major complication of the aluminum box, which was the large exposed area of a conductive material. To avoid arcing to the box, all electrical connections had to be adequately insulated from the box, and all wiring is now rated to at least 15 kV. Even after proper insulation, baseline noise on the microchip inside the box is still routinely several times higher than baseline noise in offline mode, and at least part of this problem is suspected to be due to the two additional sets of electrical connections (one to outside of the box and one on the inside of the box) needed for routing the electronics through the box. These issues are currently being addressed by replacing the existing connections (binding posts) with smaller and more heavily insulated ones. Preliminary ambient aerosol data with the initial box interface has been collected and is shown compared to PILS-IC data in Figure 8.1.

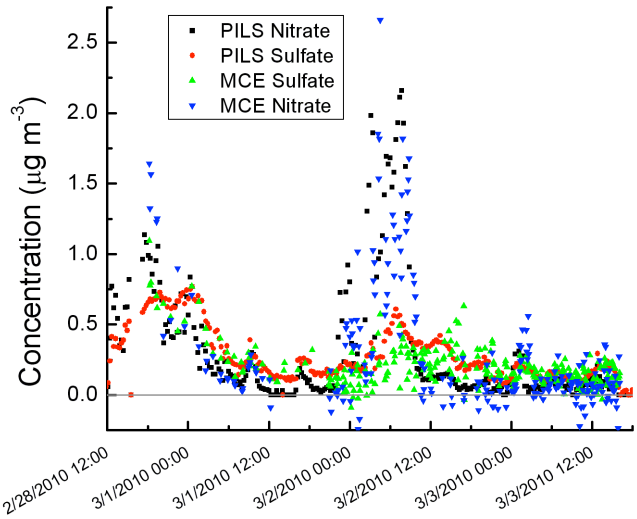

Figure 8.1. 3+ days of ambient aerosol data collected with the box enclosure interface and compared to PILS-IC. The increased noise using the metal box resulted in higher data scatter with the MCE monitoring. Data were collected in Mariposa, CA.

The increased noise with the box interface is apparent from the increased data scatter in the ACE time series. However, the ACE system still correlates well with the PILS-IC results, and a scatter plot of the data is shown in Figure 8.2.

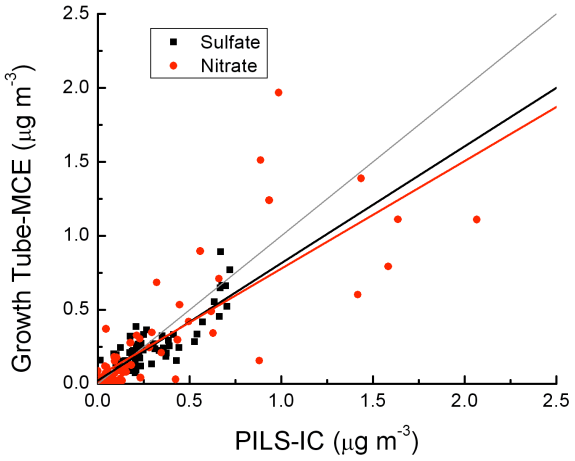

Figure 8.2. Scatter plot of the data shown in Figure 8.1 comparing the results of the ACE system to the PILS-IC. The gray line is the 1:1 line. The linear fits for sulfate and nitrate are shown in the black and red lines, respectively. Differences between the two instruments can be explained in part by the different size cut on the samplers. The growth tube sampled particles of 1-μm diameter and smaller, while the PILS sampled particles with diameters of 2.5 μm or less.

The scatter plot slope for sulfate was 0.79 (R^2 = 0.71), and nitrate exhibited a slope of 0.73 (R^2 = 0.62). The below unity slopes are not surprising because the ACE system was sampling PM_1 whereas the PILS-IC was monitoring $PM_{2.5}$, so the ACE system was excluding the larger particles. Comparing the time series of the two systems in Figure 8.1 shows that many of the changes in aerosol composition were observed with both systems. Additionally, both instruments showed increased data scatter at the higher concentrations of nitrate, and this is suspected to be due to the nitrate source being local and highly variable (as indicated by the relatively high frequency changes in its signal). Therefore, this may have also led to the increased discrepancy between instruments at

higher nitrate concentrations because the two instrument inlets were separated by approximately 10 m. Additional ACE data was collected at the same site in the absence of a PILS-IC. This data is shown in Figure 8.3 and shows less scatter than the data collected earlier due to lower electronic noise at the time.

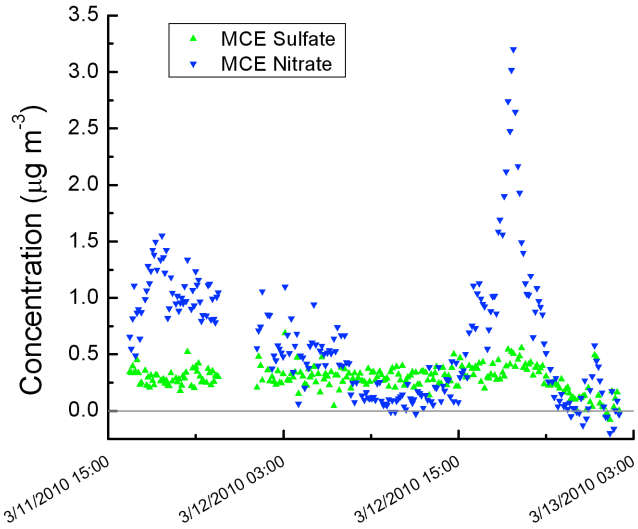

Figure 8.3. Online ambient aerosol measurements made in Maripsosa, CA with ACE using the box enclosure interface.

Since these data were collected in early 2010, an additional field study has been done in Rocky Mountain National Park where 5 days of nearly uninterrupted data were obtained with ACE,[1] which is currently the longest data set collected with the system.

Several microchip dimensions have been modified to allow improved performance of the ACE system. The main goal has been increased longevity between buffer replenishments. Because the separation chemistry was determined in chapter 5 and has not changed, only the microchip design and operational parameters govern the maximum operation time (O) between buffer replenishment is required. As discussed in chapter 7,

the operational time is directly proportional to the volume of the BGE (V) and inversely proportional to the electric field (E) and the channel cross-sectional area (A), as given by eq 8.1.

$$O \propto \frac{V}{EA} \tag{8.1}$$

The electric field governs the speed of the separation, and has remained at –300 V cm^{-1}. However, the channel cross section has been decreased and the BGE reservoir volumes increased since the original ACE prototype. For the data shown in Figures 8.1-3, the channel dimensions were changed from 50 μm x 28.1 μm (1400 μm^2) in the original prototype to 40 μm x 16.2 μm (650 μm^2). BGE reservoir diameters were increased from 6 mm in the ACE prototype to 12 mm with the new system. Respective BGE volumes changed from 125 μL to 550 μL. Thus, the first incremental improvement over the prototype increased the maximum operational time between buffer replacement from ~5 h to ~48 h. In more recent improvements, the BGE reservoirs sizes were increased to contain up to 1.5 mL of solution. Because the lowering of the channel cross-sectional area had decreased the instrument sensitivity, the channel dimensions have since been increased to 40 μm x 25 μm (1000 μm^2). Thus, the most recent design is capable of ~84 h (3.5 days) of operation between manual BGE replenishment. At this point, increased reservoir volumes are unlikely due to physical constraints of the microchip. Consequently, further increases in unattended operation time will require an automated BGE replenishment mechanism. The sample volume has also been changed. With the ACE system, sensitivity is inversely proportional to concentration, implying that maximum sensitivity can be obtained by minimizing the sample volume. However, the percentage of sample ion depletion is also inversely proportional to sample volume, so

reducing the sample volume will lower the operational time between sample flushes. To improve the system sensitivity, the sample volume was decreased from 30 μL in the prototype to 21 μL in the current system. Despite the smaller volume, the system used for Figures 8.1-3 was capable of 50% longer operation between sample flushes than the prototype instrument due to changes in channel size. However, the subsequent change to a channel cross section of 1000 μm^2 lowered the sampling interval to roughly equal of that in the prototype. To increase the sampling time between flushes, a new microchip design was implemented where the sample channel was half the width as the other channels. To my knowledge, this approach had never been used for gated injection. Tests showed the design to be successful (Figure 8.4) and predictable by simple modeling with Ohm's law and Kirchoff's current law. With the smaller sample channel, the maximum interval between flushes has now doubled relative to the prototype instrument.

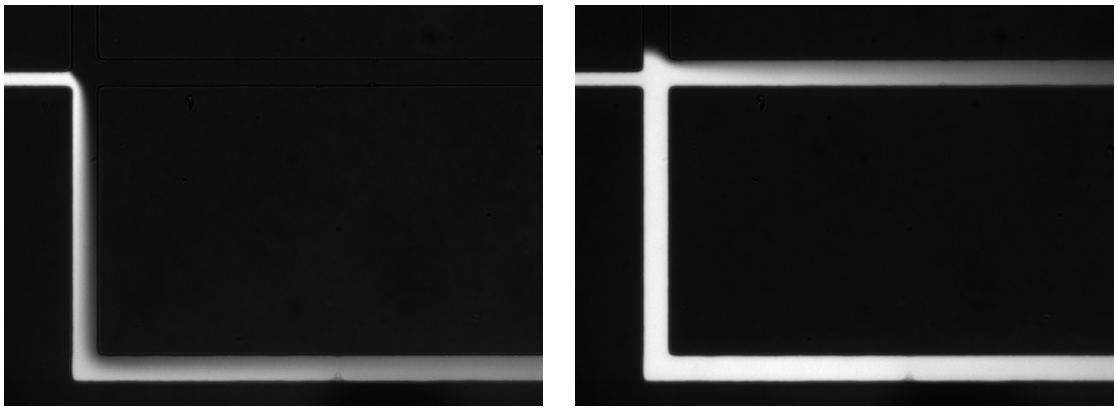

Figure 8.4. Fluorescent images of a gated injection using a microchip with the sample channel at half the width of the other channels. Sample comes in from the left and is normally routed to the sample waste channel in the bottom right (normal operation image on left). During injection (right), the sample also travels into the sample channel and exits right. There is also a fourth channel that holds only buffer exiting the top of the images.

The flushing system in the ACE instrument was also modified concurrently with the above improvements. Specifically, the syringe pumps were replaced with solenoid-actuated pumps that increase flushing speed. The main advantage to the solenoid pumps is that the outlet pump is unaffected by pulling air. Consequently, performance does not degrade with time due to the compressibility of air. The precision of the inlet volume from the solenoid pump is similar to that of the syringe pump. Currently, a 20-μL solenoid is employed, and the precision would increase if a smaller pump were used (requiring more pump actuations). Note that the 20-μL stated value is the ideal value under very little flow resistance. Actual dispensed volumes decrease with relatively high flow resistance, so the pumps must be calibrated using the expected flow resistance, which is a disadvantage of this pump design. The solenoid pumps do not have an inherent limitation in supply volume (unlike the syringe pumps), so the only limit on the unattended system longevity is the capacity of the solution vial employed.

Also in development is the coupling of MCE to a different aerosol collector using the same interface as that used in the ACE system. The aerosol collector being pursued is the miniature cloud condensation nuclei (CCN) collector developed by Roberts et al.[2] This instrument is similar to the growth tube in that it condenses water onto aerosol particles to enlarge them for inertial impaction. However, the growth tube attempts to activate all particles while the CCN collector only collects CCN-active particles via control of the supersaturation. Also, the CCN flow rate is, at maximum, only ~55 mL min^{-1}. Consequently, collected aerosol mass is 15-20 times lower than that with the growth tube. A coupled CCN-MCE system has been tested in offline mode with size-selected,

nebulized ammonium sulfate particles, and the results are shown in Figure 8.5. The generated aerosol was collected by both a growth tube and CCN, each instrument impacted the aerosol into a microchip sample solution, and the solutions were analyzed offline with MCE.

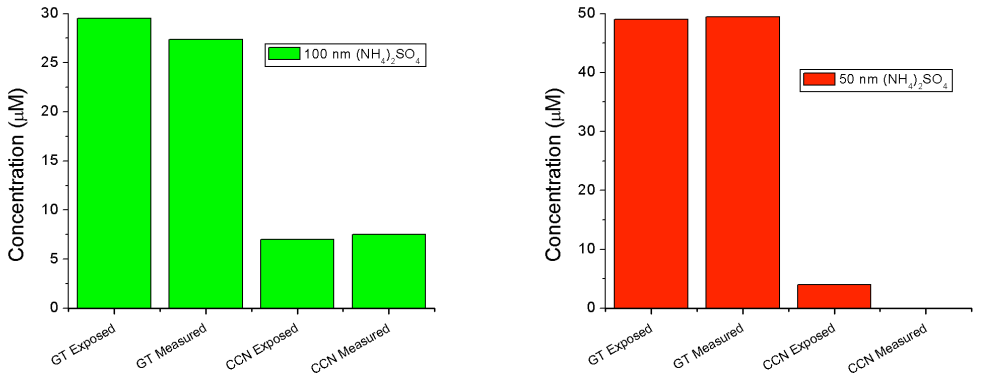

Figure 8.5. Offline testing of CCN-MCE compared to the growth tube (GT)-microchip using generated ammonium sulfate particles. The CCN supersaturation value was 0.2%, yielding a critical diameter of 80 nm for ammonium sulfate. The "exposed" values were the calculated masses generated from the nebulizer using a known particle diameter and count. The GT successfully collected the particles at both 50-nm and 100-nm diameters, but the CCN only collected particles larger than 80 nm, so it did not collect the 50-nm particles.

The measured concentration for the growth tube collection closely matched the predicted values for both 100-nm and 50-nm particles, indicating that the growth tube was collecting the particles with nearly 100% efficiency. The CCN was operated at a 0.2% supersaturation, a value that provides an activation cutoff of about 80 nm for ammonium sulfate. Successful collection/deposition by the CCN is indicated with the 100-nm results. However, with 50-nm particles, the amount of sulfate deposited into the microchip reservoir was below the detection limit of MCE. This observation is important because it confirms that the CCN is not activating the smaller particles and the amount of non-activated material being impacted into the sample reservoir is negligible. For online

analyses with a CCN-MCE instrument, the box enclosure interface will be required because the outlet of the CCN must have strict temperature control. Refinement of this interface is currently in progress. If the online instrument is successful, it will represent one of the first instruments capable of direct measurement of CCN chemistry, although a 2010 report demonstrated *in situ* CCN composition measurements using mass spectrometry.[3]

IMPROVEMENTS TO CONTACT CONDUCTIVITY DETECTION IN MCE

Despite the improvements to conductivity detection in MCE with the introduction of the bubble cell (chapter 4), one of the main limitations of MCE in the area of aerosol analysis is its poor concentration sensitivity. For ionic species, this means that improved conductivity detection is required. Since the report of the bubble cell, I improved detection limits further by utilizing the analog offset functionality of the Dionex CD20 detector to surpass the 16-bit analog output limit of the detector. This was apparent in chapter 6 with the ACE system where concentration detection limits were 3-4 times better than those presented in chapter 5 without the analog offset. Since then, detection limits have improved by a factor of 1.5-2. Part of this improvement is due to replacing the gold-plated tungsten wires with platinum wires (note that no significant difference in signal between wire types was observed in chapter 4, but this was before implementing the analog offset, which increased sensitivity). The tungsten wire was chosen because of its high tensile strength, which is roughly an order of magnitude higher than platinum's. To recoup some of this loss in strength, 20-μm platinum wires are used instead of 15 μm for the tungsten, and the size change may also contribute to the recent improvement in

performance via changes in the conductivity cell constant. Although tungsten is physically strong, the transition away from the tungsten wire was done because, under certain conditions, the tungsten wire can dissolve during operation. Even when gold plated, the wires can still dissolve if the plating contains a defect or is damaged during microchip construction or operation. Using platinum wires fixes this issue, but at the expense of physical robustness. To improve upon the platinum detection electrodes, I have performed a preliminary study on using platinum alloys for detection. Specifically, platinum/iridium alloys (90/10 and 80/20 ratios) have been tested (Figure 8.6).

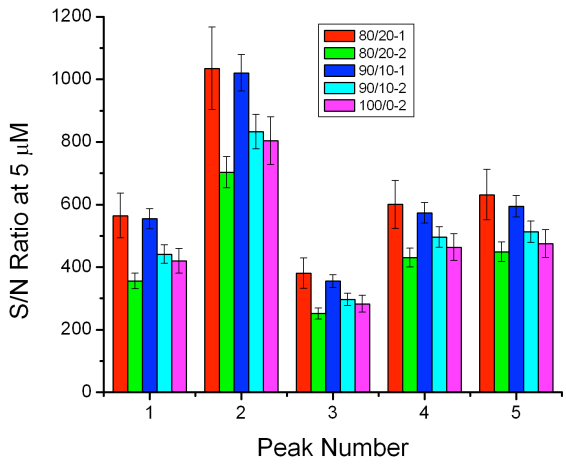

Figure 8.6. Average signal-to-noise ratio for 5-μM chloride, sulfate, nitrate, oxalate, and 1,3-propanedisulfonate (PDS) using MCE and the separation approach given in chapter 5. BGE = 17-mM picolinic acid/19-mM HEPBS/19-mM TDAPS. Separation field = –300 V cm^{-1}. Injection time = 1.4 sec. The Pt wires were 20 μm in diameter, whereas the Pt/Ir alloys had 15-μm diameters. The microchip design used for the study was the same as that employed in chapter 5.

Inadequate data quantity was collected for statistical comparisons, but the data indicate that the alloys perform similarly to pure Pt. The 90/10 alloy has a tensile strength about three times stronger than pure Pt, and the 80/20 alloy is about five times stronger than pure Pt.

To further improve the detection limits of MCE with conductivity detection, a new detector will be required. As mentioned above, the 16-bit analog output limitation of the Dionex CD20 detector was circumvented by employing the detector's baseline offset function. However, under nominal operation the detector is still the limiting component in the instrument. Specifically, the CD20 utilizes an analog-to-digital converter that limits the smallest change in conductivity detectable by the instrument. Because the MCE detection volumes are so small and the other significant sources of noise have been eliminated, this limitation of the CD20 has been reached. Offline microchip performance is not necessarily hampered by this limit because offline systems can utilize larger separation channels, increasing the signal and minimizing the impact of this limit. However, online MCE systems must use relatively small separation channels, yielding smaller signals, and therefore suffer a larger relative drop in performance because of the detector limitation. To further improve detection limits, new conductivity detectors have been pursued.

The first detector tested was one developed at the University of California at San Diego (UCSD). This detector required a change to the microchip that replaced the two-wire scheme used in chapters 3-7 with a different conductivity cell defined between one detection wire and the end buffer reservoir. The separation current then acts as the excitation current, and the potential drop between the detection wire and the end reservoir can be monitored to measure the solution conductivity in that zone. This scheme has the benefit of requiring simpler instrumentation. Specifically, no alternating current

excitation is required. A selected electropherogram from this approach is shown in Figure 8.7 (right) and compared to a separation at the same conditions using the CD20 as the detector (left).

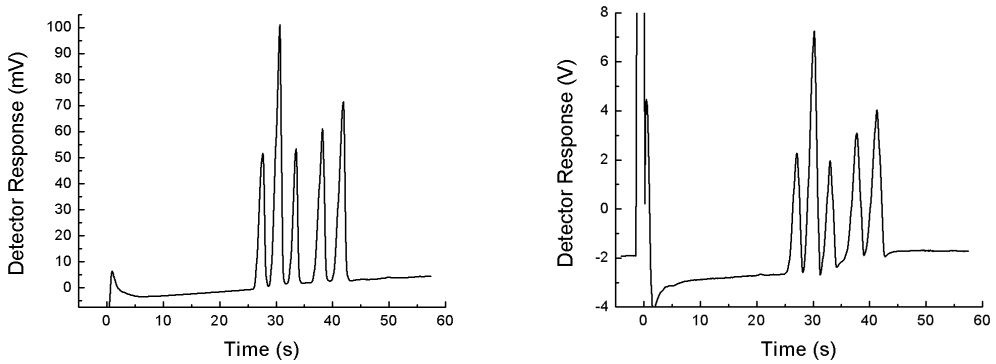

Figure 8.7. Comparison of the performance of the CD20 detector (left) and the one-wire UCSD detector (right). Analyte concentration = 50 μM. Conditions are the same as those given in Figure 8.6. Microchip used 20-μm Pt wires.

The CD20 exhibits superior signal-to-noise ratio, narrower peaks, and a flat baseline. The new detector shows broader peaks with a distorted baseline near the peaks. The majority of the peak broadening is due to the longer detection window, which is about 2.5 mm compared to the effective 480-μm window in the two-wire design. As was shown in chapter 7, the detection length can play a significant and even dominant role in peak broadening, and in this case the CD20 measures separation efficiencies 2.2-2.9 times higher than does the two-wire detector. Additional peak broadening is induced by the inclusion of a 10-Hz lowpass filter in the UCSD detector, which was included by the developers to lower the noise of the system. Despite the additional filter, the one-wire system still yields signal-to-noise values 6-8 times lower than the CD20 with the two-wire approach. The lowpass filter also distorts the baseline, specifically leading to the signal dropping below the baseline immediately after the sulfate peak. However, the

largest problem with the baseline is its step change as the peaks migrate through the detection zone. This behavior is a fundamental phenomenon of the one-wire detection and can be explained using Ohm's law. The parameter being measured is the voltage drop between the detection wire and the end reservoir, ΔV_{det}. This voltage drop is induced by the current through the separation channel (I_{sep}) and is proportional to the resistance in the detection zone (R_{dec}), as given by eq 8.2.

$$\Delta V_{\text{det}} = I_{sep} R_{\text{det}} \tag{8.2}$$

The current in the separation channel is defined by the separation voltage (ΔV_{sep}) and the total resistance in the separation channel (R_{sep}), as given by eq 8.3.

$$I_{sep} = \frac{\Delta V_{sep}}{R_{sep}} \tag{8.3}$$

Combining eqs 8.2 and 8.3 resuls in eq 8.4.

$$\Delta V_{\text{det}} = \frac{R_{\text{det}} \Delta V_{sep}}{R_{sep}} \tag{8.4}$$

Eq 8.4 shows why the baseline shift is observed in Figure 8.7. The detection voltage drop is dependent upon more than just the resistance in the detection zone, and the injection of analytes into the separation channel changes R_{sep}. As analytes migrate out of the detection zone, they simultaneously migrate out of the separation channel, changing R_{sep} and therefore the baseline signal. This is a fundamental phenomenon that limits this detection technique to samples of low concentration. Interestingly, the use of the separation current to induce a voltage difference for detection has been reported,[4-6] but this fundamental limitation of the approach has not been reported in the published literature. Given the behavior described in eq 8.4 and the poor sensitivity, I conclude that this technique should not be pursued in the future.

After the poor results for the one-wire scheme were obtained, the original two-wire method was attempted with a prototype detector developed by UCSD. Whereas the CD20 employed an 8-kHz square wave for excitation, this prototype uses a 43 kHz sine wave. Additionally, the UCSD detector operates without analog-to-digital conversion of the signal prior to amplification, avoiding the limitation encountered with the CD20. Comparisons of the signal-to-noise ratios and separation efficiencies obtained with the CD20 and the UCSD prototype during initial testing are shown in Figure 8.8.

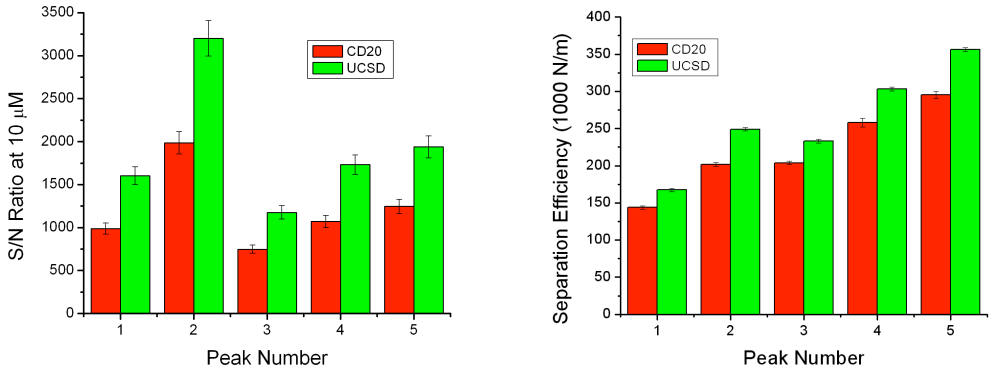

Figure 8.8. Comparison of the signal-to-noise ratio (top) and separation efficiency (bottom) observed with the CD20 and the alternating current (two-wire) UCSD detector. Analyte concentration = 10 μM. Conditions are the same as those in Figure 8.6. Microchip used 20-μm Pt wires.

On average, the UCSD detector provided signal-to-noise values 60% higher than the CD20. The separation efficiencies were also higher with the UCSD detector, on average by 16%. The improvement in separation efficiency indicates that the CD20 implements additional filtering that is not used with the UCSD detector (for example, the CD20 might use a lowpass filter to eliminate 60-Hz noise from the power source). Thus, if the separation efficiency measured by the CD20 is considered sufficiently high then additional filtration could be added to the UCSD detector to lower its separation

efficiency while improving its signal-to-noise ratio. The high separation efficiency and signal-to-noise ratio of the UCSD detector is exemplified in Figure 8.9, where a separation at –600 V cm^{-1} is shown.

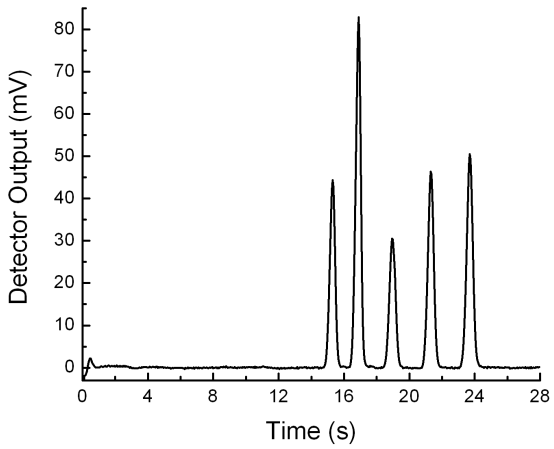

Figure 8.9. Separation of anions at –600 V cm^{-1} using the alternating current (two-wire) version of the UCSD detector, illustrating the improved separation efficiency capable with the new detector. Analyte concentration is 5 μM. Microchip used 20-μm Pt wires for detection. BGE conditions and peak order are the same as those given in Figure 8.6. The microchip used had channel widths of 40 μm with a 4x bubble cell, 25-μm channel heights, and the following channel lengths: buffer = 1.4 cm, sample = 3.0 cm, sample waste = 3.0 cm, and separation = 5.2 cm total (5.0 cm effective).

The higher field strength yields narrower peaks, increasing the relative advantage of the UCSD detector's measured separation efficiency. Currently, the primary disadvantage to the UCSD detector is its sensitivity to changes in the environment. Even movement several feet away from the detector is enough to significantly perturb the detector response. Thus, electronic shielding (Faraday cage) around the detector is needed to achieve its full potential. Improvements in the electronics and optimization of the detection parameters are still ongoing, and further refinements to the system are expected to add to the existing advantages of the UCSD detector while simultaneously reducing the sensitivity to environmental noise.

EXTENSIONS OF THE MCE TECHNOLOGY INTO OTHER FIELDS

Microchip electrophoresis is already a rapidly emerging technology in a variety of fields, particularly clinical biology, environmental monitoring, and food analysis.[7-10] The work discussed in this dissertation is only a very small part of the field of MCE, but it can potentially have a larger impact by affecting other areas of research.

Perhaps the largest impact of this work will come from the improvements in MCE contact conductivity detection through the bubble cell approach (chapter 4). Although some attempts at contact conductivity detection in MCE had been made,[4-6,11-14] these approaches have been plagued by interference from the separation electric field, leading to higher noise, fouling of electrodes, and the requirement of low separation electric fields. Consequently, contact detection has nearly been completely abandoned in MCE, and nearly all the efforts have focused on contactless conductivity detection.[15-30] Extensive modeling and testing of contactless detectors in MCE has been done for roughly a decade. Commercial options for contactless detection in MCE are available now as well. Despite this level of optimization, the best reported LODs in contactless detection are roughly 15 times worse than the values for contact detection reported in this chapter, and the average reported LODs for contactless detection in MCE are over 100 times higher than shown here. Possibly because the researchers in the field have so strongly committed to contactless detection, little adoption of the bubble cell and contact conductivity detection has taken place. The only published work (outside of my own) using my bubble cell approach also came from the Henry group and focused on

perchlorate analysis.[31] The microchip design employed in that work was identical to the one used in chapter 5,[32] which was also used for some tests in chapter 4.[33] Additionally, the BGE employed was a combination of the nicotinic acid BGE used in chapter 4 to achieve low background conductivity and the TDAPS surfactant approach for binding polarizable ions presented in chapter 5.[32,33] To lower detection limits in the perchlorate analysis, very large injection volumes and high electrophoretic stacking conditions were employed. Specifically, the estimated injection volume of perchlorate with the 10-s gated injection used for real samples is about 12% of the total capillary volume, although matrix effects may lower this value. The long injection and stacking methods are the opposite approaches to those used in my work, where I typically worked to improve the method's *mass* LOD, which would permit smaller injections, narrower peaks, and less matrix-dependent sensitivity. The advantage of smaller injections is apparent by comparing separation efficiencies. In the perchlorate analysis, a sample spiked with 1 μM perchlorate yielded a peak with a separation efficiency of about 29000 N m^{-1}, whereas 10-μM 1,3-propanedisulfonate (PDS, chosen because its migration time is similar to perchlorate in the comparison separation) yields a peak with 350000 N m^{-1} in Figure 8.6, about 12 times higher. Because the perchlorate separation is done at higher field strength and perchlorate is monovalent and present at lower concentration (thus, experiencing less electromigratory dispersion), its peak should actually be narrower than the PDS peak, so this example clearly demonstrates the advantage of smaller injection volumes. Additionally, any analysis can increase the injected sample mass through longer injections or stacking, so those measures can usually be taken after the original separation development if lower detection limits are required.

The improvements in MCE conductivity detection in chapter 4 and the methodological issues addressed in chapters 5-7 should combine to greatly improve environmental monitoring of ions with MCE. Achievable detection limits have dropped by over an order of magnitude, and the elucidation of the importance of highly selective separations and the methods to achieve them make MCE more attractive than in the past. Long-term, high-resolution, interferent-free monitoring is now possible with this technology. As an example of the speed and peak-resolving ability of MCE, a separation of 15 anions in roughly 1 min is shown with my instrument and separation chemistry in Figure 8.10.

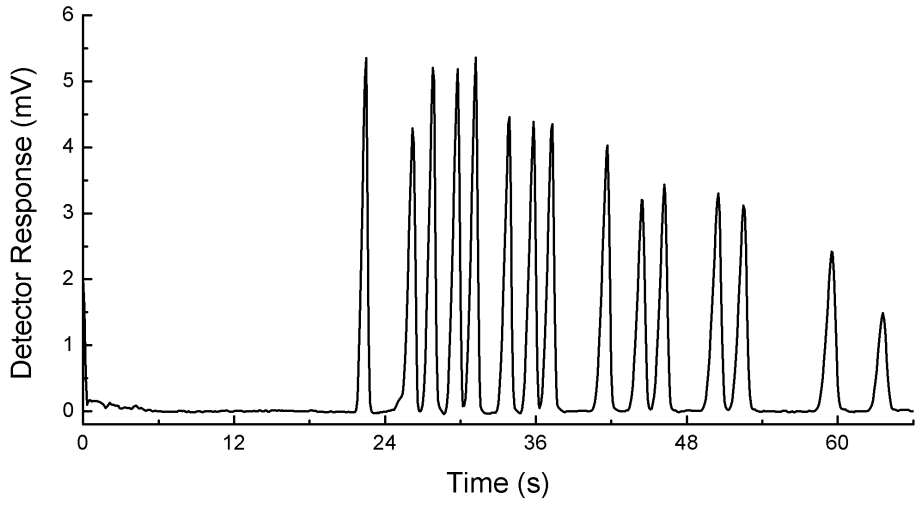

Figure 8.10. Separation of 15 anions in about 1 min using MCE. Separation channel = 7.5 cm; field = –400 V cm^{-1}; injection = 0.5 s; BGE = 10 mM nicotinic acid with 0.1-wt% poly(ethylene oxide) (MW = 10^5). Analyte (25 μN) order = dithionate, chloride, nitrate, perchlorate, chlorate, hexafluorophosphate, 1,2-benzenedisulfonate, perrhenate, sulfamate, methanesulfonate, trifluoromethanesulfonate, iodate, ethanesulfonate, benzenesulfonate, and tribromoacetate.

Another straightforward extension of my work is the development of a system for online MCE of flowing solutions. The majority of the difficulty in designing these systems, the detection and separation chemistry, were already developed in chapters 4 and 5. The final hurdle is the engineering of a microchip device specifically designed to perform injections from a flowing solution. In cooperation with Prof. Charles S. Henry, I arrived at such a microchip scheme. The general approach is shown in Figure 8.11 for both separation ("normal") operation and operation during injection.

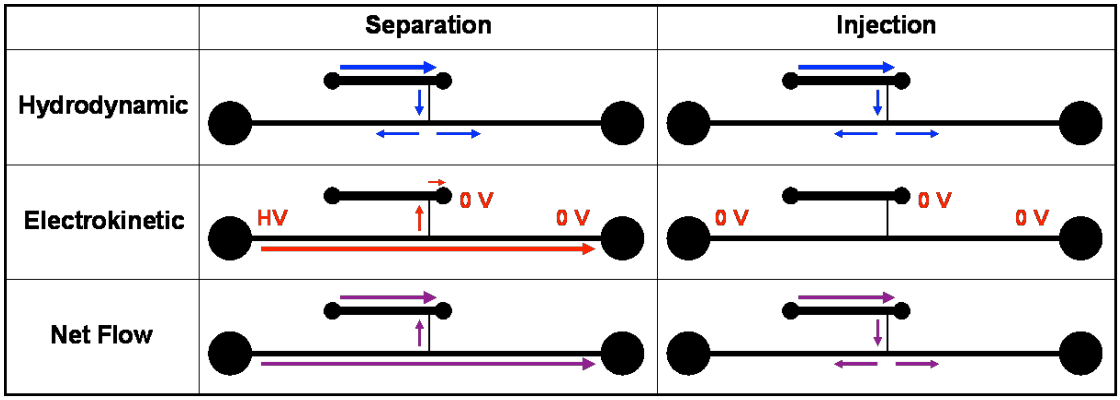

Figure 8.11. Schematic of the continuous flow microchip device for online MCE monitoring of a continuously flowing solution. Hydrodynamic, electrokinetic, and net flows for the species of interest are shown for both separation and injection mode. The continuous solution flow sample enters from the left in the wider, top channel. Part of this sample is forced through a narrow connecting channel to the separation (bottom) channel, which is intermediate in size between the sample and injection channels. The detection occurs at the far right side of the separation channel.

Because I worked on other projects, I was unable to pursue this design further. However, this design may be developed in the future and would be applicable to a wide array of analyses in several fields.

REFERENCES

1. Evanoski, A. R. Atmospheric Science Department, Colorado State University, Fort Collins, CO. Personal communication, October 5, 2010
2. Roberts, G. C.; Nenes, A., *Aerosol Sci. Technol.* **2005,** *39*, 206-221.
3. Zelenyuk, A.; Imre, D.; Earle, M.; Easter, R.; Korolev, A.; Leaitch, R.; Liu, P.; Macdonald, A. M.; Ovchinnikov, M.; Strapp, W., *Anal. Chem.* **2010,** *82*, 7943-7951.
4. Bai, X. X.; Wu, Z. Y.; Josserand, J.; Jensen, H.; Schafer, H.; Girault, H. H., *Anal. Chem.* **2004,** *76*, 3126-3131.
5. Feng, H. T.; Wei, H. P.; Li, S. F. Y., *Electrophoresis* **2004,** *25*, 909-913.
6. Tay, E. T. T.; Law, W. S.; Sim, S. P. C.; Feng, H.; Zhao, J. H.; Li, S. F. Y., *Electrophoresis* **2007,** *28*, 4620-4628.
7. Crevillen, A. G.; Hervas, M.; Lopez, M. A.; Gonzalez, M. C.; Escarpa, A., *Talanta* **2007,** *74*, 342-357.
8. Dolnik, V.; Liu, S. R., *J. Sep. Sci.* **2005,** *28*, 1994-2009.
9. Dolnik, V.; Liu, S. R.; Jovanovich, S., *Electrophoresis* **2000,** *21*, 41-54.
10. Li, S. F. Y.; Kricka, L. J., *Clin. Chem.* **2006,** *52*, 37-45.
11. Galloway, M.; Stryjewski, W.; Henry, A.; Ford, S. M.; Llopis, S.; McCarley, R. L.; Soper, S. A., *Anal. Chem.* **2002,** *74*, 2407-2415.
12. Guijt, R. M.; Baltussen, E.; van der Steen, G.; Schasfoort, R. B. M.; Schlautmann, S.; Billiet, H. A. H.; Frank, J.; van Dedem, G. W. K.; van den Berg, A., *Electrophoresis* **2001,** *22*, 235-241.
13. Schlautmann, S.; Wensink, H.; Schasfoort, R.; Elwenspoek, M.; van den Berg, A., *J. Micromech. Microeng.* **2001,** *11*, 386-389.
14. Shadpour, H.; Hupert, M. L.; Patterson, D.; Liu, C. G.; Galloway, M.; Stryjewski, W.; Goettert, J.; Soper, S. A., *Anal. Chem.* **2007,** *79*, 870-878.
15. da Silva, J. A. F.; do Lago, C. L., *Anal. Chem.* **1998,** *70*, 4339-4343.
16. Zemann, A. J.; Schnell, E.; Volgger, D.; Bonn, G. K., *Anal. Chem.* **1998,** *70*, 563-567.
17. Pumera, M.; Wang, J.; Opekar, F.; Jelinek, I.; Feldman, J.; Lowe, H.; Hardt, S., *Anal. Chem.* **2002,** *74*, 1968-1971.
18. Tanyanyiwa, J.; Hauser, P. C., *Anal. Chem.* **2002,** *74*, 6378-6382.
19. Wang, J.; Pumera, M., *Anal. Chem.* **2002,** *74*, 5919-5923.
20. Tanyanyiwa, J.; Abad-Villar, E. M.; Fernandez-Abedul, M. T.; Costa-Garcia, A.; Hoffmann, W.; Guber, A. E.; Herrmann, D.; Gerlach, A.; Gottschlich, N.; Hauser, P. C., *Analyst* **2003,** *128*, 1019-1022.
21. Guijt, R. M.; Evenhuis, C. J.; Macka, M.; Haddad, P. R., *Electrophoresis* **2004,** *25*, 4032-4057.
22. Kuban, P.; Hauser, P. C., *Electroanalysis* **2004,** *16*, 2009-2021.
23. Kuban, P.; Hauser, P. C., *Lab Chip* **2005,** *5*, 407-415.
24. Solinova, V.; Kasicka, V., *J. Sep. Sci.* **2006,** *29*, 1743-1762.
25. Kang, Q.; Shen, D. Z.; Li, Q. L.; Hu, Q.; Dong, J. F.; Du, J. G.; Tang, S., *Anal. Chem.* **2008,** *80*, 7826-7832.
26. Kuban, P.; Hauser, P. C., *Lab Chip* **2008,** *8*, 1829-1836.
27. Kuban, P.; Hauser, P. C., *Anal. Chim. Acta* **2008,** *607*, 15-29.
28. Kuban, P.; Hauser, P. C., *Electrophoresis* **2009,** *30*, 176-188.

29. Fercher, G.; Haller, A.; Smetana, W.; Vellekoopt, M. J., *Anal. Chem.* **2010,** *82*, 3270-3275.
30. Mahabadi, K. A.; Rodriguez, I.; Lim, C. Y.; Maurya, D. K.; Hauser, P. C.; de Rooij, N. F., *Electrophoresis* **2010,** *31*, 1063-1070.
31. Gertsch, J. C.; Noblitt, S. D.; Cropek, D. M.; Henry, C. S., *Anal. Chem.* **2010,** *82*, 3426-3429.
32. Noblitt, S. D.; Schwandner, F. M.; Hering, S. V.; Collett, J. L.; Henry, C. S., *J. Chromatogr. A* **2009,** *1216*, 1503-1510.
33. Noblitt, S. D.; Henry, C. S., *Anal. Chem.* **2008,** *80*, 7624-7630.

APPENDIX 1. SIMPLE FLOW MODELING OF MICROCHIP ELECTROPHORESIS SYSTEMS

Knowledge of the flow magnitudes present in microchip electrophoresis is of critical importance. Knowing the strength of the electric field in the separation channel permits the calculation of the electrophoretic and electroosmotic mobilities, which help in method development and in transferring methods to alternative microchip designs. Proper design of injection schemes in microchip electrophoresis requires calculation of all electrokinetic flows and also any present hydrodynamic flows. This section illustrates a straightforward way to calculate the electric fields (which determine the electrokinetic flow magnitudes) in microfluidic networks. The same method can be used to calculate hydrodynamic flows in these systems.

The electric field is equal to the gradient of electric potential. For a one-dimensional system, this is given by eq A1.1, where E is the electric field (V m^{-1}), V is the potential (V), and L is the length (m) that dimension of interest.

$$E = \frac{dV}{dL} \tag{A1.1}$$

For a linear system with an applied potential (ΔV) at a set distance with a constant electrical resistance per unit length, E is constant in the system and given by eq A1.2.

$$E = \frac{\Delta V}{L} \tag{A1.2}$$

In a microchip, L is determined by the physical channel layout. ΔV is applied by the operator. However, calculation of the electric field is not as straightforward because a capillary network is used and the potential at the capillary intersection(s) (V_i) determines ΔV, and this potential is determined by a combination of the applied potentials and the electrical resistances in the capillary network. Thus, this potential must be calculated. To do so, Ohm's Law (eq A1.3) is employed. Here, I (A) is the electrical current and R (Ω) is the electrical resistance.

$$\Delta V = IR \tag{A1.3}$$

Also required is the use of Kirchoff's current law, eq A1.4. This law states that the sum of the currents at an electrical intersection equals zero.

$$\sum I = 0 \tag{A1.4}$$

In microchip electrophoresis, the capillary network is often comprised of four straight channels that meet a single intersection for the injection point. This configuration can be seen in Figures 3.1 and 4.1. Additionally, the approach used here is still valid even if the capillaries contain angles, for instance as shown in Figure 6.1. Combining eqs A1.3 and A1.4 and applying them to a four-channel microchip with a single intersection point permits five equations with five unknowns (V_i and I in each of the four capillaries) to be written. Solving these equations for V_i results in eq A1.5, where the subscripts 1-4 denote the four channels in the microchip.

$$V_i = \frac{V_1R_2R_3R_4 + V_2R_1R_3R_4 + V_3R_1R_2R_4 + V_4R_1R_2R_3}{R_1R_2R_3 + R_1R_2R_4 + R_1R_3R_4 + R_2R_3R_4} \tag{A1.5}$$

The resistance in a channel can be calculated from the capillary length, the channel cross-sectional area (A, m^2), and the resistivity of the solution in the channel (ρ, Ω m), eq A1.6.

$$R = \frac{\rho L}{A} \tag{A1.6}$$

Note that this equation assumes that the channel is of uniform cross-section and contains a solution of uniform resistivity. Otherwise, the resistance can be calculated with the integral shown in eq A1.7, where ρ and A are given as functions of L.

$$R = \int \frac{\rho(L)dL}{A(L)} \tag{A1.7}$$

For rigorous electrical calculations, the approach used in A1.7 is required for systems utilizing the bubble cell detection scheme described in chapter 4. However, because the channel is not described by a continuous function, it is easiest to compute the resistance of the channel by applying eq A1.7 to individual lengths of the channel that can be described with continuous functions. The computed resistance values can than be summed with the knowledge that resistances in series are additive, eq A1.8.

$$R_{total} = \sum_i R_i \tag{A1.8}$$

Typically, capillary zone electrophoresis applications can utilize eq A1.2 because the capillary is filled with a buffer continuum of equal resistivity in a channel of constant cross-section. In this system, no integration is necessary, knowledge of the solution resistance is unnecessary, and the electrical resistance in the capillary is proportional to L and eq A1.5 can be rewritten as eq A1.9.

$$V_i = \frac{V_1 L_2 L_3 L_4 + V_2 L_1 L_3 L_4 + V_3 L_1 L_2 L_4 + V_4 L_1 L_2 L_3}{L_1 L_2 L_3 + L_1 L_2 L_4 + L_1 L_3 L_4 + L_2 L_3 L_4} \tag{A1.9}$$

Eq A1.9 is valid for many microchip electrophoresis applications. However, this simplification fails when the solutions in each channel possess different resistivities. This can often happen when the sample solution resistivity varies significantly from that

of the background electrolyte. Not only can the resisitance in the sample channel be different than expected, but the resistance in the separation channel can also be altered once sample is injected into it. Not only does this make channel A1.9 in error and requires use of eq A1.7 (which can be difficult or impossible and requires a time-dependent analysis), but it also invalidates eq A1.2, leading to non-uniform separation fields and distorted peak shapes in the electropherogram. The operator needs to be aware of the potential for these phenomena to appear and take measures to avoid them during sample preparation.

The same approach used above in the calculation of electrokinetic behavior can be used to predict hydrodynamic flows in systems with pressure differentials. Here, the applied pressure (P, kg m^{-1} s^{-2}) is analogous to applied potential, volumetric flow (Q, m^3 s^{-1}) corresponds to electrical current, and hydrodynamic resistance (R_h, kg s^{-1} m^{-4}) is akin to electrical resistance, so eq A1.10 is analogous to eq 1.3.

$$\Delta P = QR_h \tag{A1.10}$$

For rectangular capillaries, R_h is calculated using eq A1.11, where F is the form factor, w is the half-width of the channel, d is the half-depth of the channel, and η is the solution viscosity (kg s^{-1} m^{-1}).

$$R_h = \frac{4\eta L}{w^2 d^2 F} \tag{A1.11}$$

The form factor is calculated using eq A1.12.

$$F = \frac{w}{3d} - \frac{64w^2}{\pi^5 d^2} \sum_{n=0}^{\infty} \frac{\tanh\left[\frac{(2n+1)\pi d}{2w}\right]}{(2n+1)^5} \tag{A1.12}$$

APPENDIX 2. CALIBRATION RESULTS FOR THE AEROSOL ANION SEPARATION

Proper calibration of microchip electrophoresis separations is required for proper quantitative analysis. In the work described in this dissertation, an internal standard was also used to adjust for injection volume differences due to uncertainty in the injection time and differences in sample matrix composition. This appendix summarizes the results from 27 calibrations using "separation 1" from chapter 5. These calibrations took place over roughly 1 yr of time, used a range of analyte concentrations, operated with varying injection times and stacking factors (sample dilution ratios), used differing internal standard (1,3-propanedisulfonate, PDS) concentrations, were performed on different microchip designs (both from chapter 5 and chapter 6), used varying numbers of concentration calibration points (3-7), and were done using a different number of replicates per injection (3-5). The relative response factor (analyte area/PDS area multiplied by the PDS concentration is expected to remain relatively constant for a given separation, even when using different chip design or injection volumes, and this factor was measured for each calibration. Early in the testing of this separation, the solution vial material was changed from glass to polyethylene (PE) to reduce contamination. Later in the development, the calibration procedure was changed from using the displayed pipette volume to measuring each dispensed volume gravimetrically, greatly improving the calibration quality and reproducibility.

Table A1 shows the 27 calibrations that were tested. Included in the table are the date the test was performed, the standard preparation method (pipette or gravimetric), the number of calibration points used and the number of repeat injections for each point, the chip design (chapter 5 or 6), the stacking factor (sample buffer dilution ratio), the PDS concentration employed, and the analyte concentration range. Note that the 07/16/08 calibration was performed using samples prepared in glass vials, whereas polyethylene vials were used for all other calibrations. Table A2 provides the correlation coefficient (R^2) values for each analyte in each calibration. The improved correlation coefficients observed in Table A2 when using gravimetric sample preparation methods indicates the superiority of using this method. Additionally, the improved reproducibility of the gravimetric method is seen in Table A1 in the form of lower standard deviations of the calibration slopes. In general, the precision of the calibration resulting from pipette preparation heavily depends on the pipettes employed. For best results, gravimetric preparation is recommended.

Table A1 – Relative Response Factor for Calibrations

						Range (μM)		Relative Response Factor			
Date	**Prep**	**Pts, Rep**	**Chp**	**Stk**	**PDS (μM)**	**SO_4^{2-}/ NO_3^-**	**Cl^-/ $C_2O_4^{2-}$**	**Cl^-**	**SO_4^{2-}**	**NO_3^-**	**$C_2O_4^{2-}$**
07/16/08	Pipet	3, 4	5	1	25	5-50	2.5-25[1]	0.640	1.413	0.671	0.593
09/09/08	Pipet	6, 4	5	1	25	0.5-300	0.5-300	0.590	1.259	0.519	0.830
09/09/08	Pipet	7, 5	5	10	3	0.04-90	0.04-90[2]	0.583	1.329	0.569	0.844
09/20/08	Pipet	5, 5	5	1	20	3-50	0.5-6	0.548	1.254	0.567	0.841
10/02/08	Pipet	7, 4	5	1	20	6-130	1-14[3]	0.685	1.334	0.614	0.885
10/07/08	Pipet	5, 4	5	1	14.3	3-65	0.5-15[4]	0.684	1.348	0.616	0.788
11/03/08	Pipet	4, 4	6	4	9.6	3-26	0.5-5	0.625	1.567	0.638	0.760
02/10/09	Pipet	5, 4	6	4	15	1-45	0.3-14	0.600	1.332	0.525	0.741
02/16/09	Pipet	4, 4	6	4	12	2-30	1-10	0.525	1.424	0.616	0.710
02/16/09	Pipet	4, 4	6	4	12	2-30	1-10	0.536	1.423	0.609	0.725
02/17/09	Pipet	4, 4	6	4	12	2-30	1-10	0.548	1.437	0.563	0.698
03/02/09	Pipet	5, 4	6	4	9	0.9-32	0.3-11	0.597	1.391	0.573	0.739
03/03/09	Pipet	5, 4	6	4	9	0.9-32	0.3-11	0.615	1.403	0.573	0.764
03/03/09	Pipet	5, 4	6	4	9	0.9-32	0.3-11	0.656	1.366	0.559	0.760
04/28/09	Grav.	5, 4	6	1	20	1-49	1-49	0.702	1.308	0.605	0.999
05/19/09	Grav.	4, 5	6	1	15	1-53	1-53	0.703	1.398	0.594	0.915
05/25/09	Grav.	5, 5	6	1	15	1-49	1-49	0.643	1.386	0.568	0.893
05/25/09	Grav.	5, 5	6	1	15	1-49	1-49	0.684	1.408	0.590	0.888
05/28/09	Grav.	5, 4	6	1	15	1-48	1-48	0.716	1.421	0.594	0.884
06/02/09	Grav.	5, 4	6	1	15	1-54	1-54	0.725	1.403	0.598	0.859
06/09/09	Grav.	5, 3	6	1	15	1-50	1-50	0.707	1.372	0.580	0.854
06/10/09	Grav.	5, 3	6	1	15	1-35	1-35	0.712	1.372	0.588	0.875
06/15/09	Grav.	5, 3	6	1	15	1-46	1-46	0.617	1.311	0.556	0.781
06/16/09	Grav.	5, 3	6	1	15	1-46	1-46	0.696	1.359	0.573	0.864
06/16/09	Grav.	5, 3	6	1	15	1-46	1-46	0.651	1.351	0.572	0.806
06/19/09	Grav.	5, 3	6	1	15	1-35	1-35	0.655	1.317	0.569	0.806
06/30/09	Grav.	5, 3	6	1	15	1-29	0.3-7	0.702	1.424	0.588	0.911
Using all calibration data: (n = 27)						Average =		0.642	1.374	0.585	0.815
						Standard Dev =		0.061	0.063	0.032	0.074
						RSD (%) =		9.42	4.56	5.41	9.12
Using pipette calibration data: (n = 14)						Average =		0.602	1.377	0.587	0.776
						Standard Dev =		0.052	0.080	0.043	0.058
						RSD (%) =		8.64	5.78	7.25	7.45
Using gravimetric calibration data: (n = 13)						Average =		0.686	1.372	0.583	0.872
						Standard Dev =		0.033	0.041	0.014	0.056
						RSD (%) =		4.84	2.96	2.45	6.45

[1]The chloride concentration was twice that of the oxalate for this trial. Also, the oxalate result for this calibration was not included in the average because it was believed that some of the oxalate was lost to the surface of the glass sample vial.
[2]Oxalate was only calibrated to 30 μM and only used 5 calibration points.
[3]Chloride was calibrated in the 6-130 μM range. Oxalate used 5 calibration points.
[4]Chloride was calibrated in the 20-65 μM range.

Table A2 – Correlation Coefficients (R^2) for Calibrations

				Correlation Coefficient (R^2)			
Date	**PDS (μM)**	**Prep**		**Cl^-**	**SO_4^{2-}**	**NO_3^-**	**$C_2O_4^{2-}$**
07/16/08	25	Pipet		0.9821	0.9996	0.9991	0.9993
09/09/08	25	Pipet		0.9996	0.9997	0.9998	0.9997
09/09/08	3	Pipet		0.9997	0.9995	0.9997	0.9998
09/20/08	20	Pipet		0.9979	1.0000	0.9999	0.9996
10/02/08	20	Pipet		0.9975	0.9994	0.9979	0.9997
10/07/08	14.3	Pipet		0.9982	0.9995	0.9994	0.9999
11/03/08	9.6	Pipet		0.9887	0.9986	0.9992	0.9994
02/10/09	15	Pipet		0.9958	0.9950	0.9953	0.9988
02/16/09	12	Pipet		0.9937	0.9993	0.9982	0.9995
02/16/09	12	Pipet		0.9906	0.9983	0.9974	0.9993
02/17/09	12	Pipet		0.9900	0.9985	0.9953	0.9988
03/02/09	9	Pipet		0.9997	0.9997	0.9996	0.9999
03/03/09	9	Pipet		0.9989	0.9996	0.9993	1.0000
03/03/09	9	Pipet		0.9918	0.9992	0.9978	0.9996
04/28/09	20	Grav.		0.9998	0.9999	0.9998	1.0000
05/19/09	15	Grav.		0.9994	0.9999	1.0000	0.9998
05/25/09	15	Grav.		0.9995	1.0000	0.9995	1.0000
05/25/09	15	Grav.		0.9997	0.9998	0.9997	0.9999
05/28/09	15	Grav.		0.9998	0.9999	0.9999	0.9999
06/02/09	15	Grav.		0.9997	0.9997	0.9998	0.9986
06/09/09	15	Grav.		0.9998	1.0000	0.9999	1.0000
06/10/09	15	Grav.		0.9999	0.9999	0.9999	0.9997
06/15/09	15	Grav.		0.9999	0.9999	1.0000	1.0000
06/16/09	15	Grav.		0.9997	0.9999	0.9999	1.0000
06/16/09	15	Grav.		0.9997	0.9999	0.9999	0.9999
06/19/09	15	Grav.		0.9997	0.9997	0.9996	0.9997
06/30/09	15	Grav.		0.9997	0.9999	0.9999	0.9999
Using all calibration data: (n = 27)		Average =		0.9976	0.9994	0.9991	0.9997
		Standard Dev =		0.0046	0.0010	0.0013	0.0004
Using pipette calibration data: (n = 14)		Average =		0.9946	0.9990	0.9984	0.9995
		Standard Dev =		0.0053	0.0013	0.0015	0.0004
Using grav. calibration data: (n = 13)		Average =		0.9997	0.9999	0.9998	0.9998
		Standard Dev =		0.0001	0.0001	0.0001	0.0004